Zeolite based micro-mesoporous composites: synthesis, characterization and catalytic performance as heterogeneous catalyst for valorization of sugar

Thesis Submitted to AcSIR for the Award of
The Degree of

DOCTOR OF PHILOSOPHY
In Chemical Sciences

By

Mr. Nilesh Pandurang Tangale

(Enrollment No.10CC15J26026)

Under the guidance of
Dr. P. L. Dhepe

Catalysis and Inorganic Chemistry Division,
CSIR-National Chemical Laboratory,
Pune 411008, India

September, 2018

सीएसआईआर - राष्ट्रीय रासायनिक प्रयोगशाला
(वैज्ञानिक तथा औद्योगिक अनुसंधान परिषद)
डॉ. होमी भाभा मार्ग, पुणे - 411 008, भारत
CSIR - NATIONAL CHEMICAL LABORATORY
(Council of Scientific & Industrial Research)
Dr. Homi Bhabha Road, Pune - 411 008, India

CERTIFICATE

This is to certify that the work incorporated in this Ph.D thesis entitled "***Zeolite based micro-mesoporous composites: synthesis, characterization and catalytic performance as heterogeneous catalyst for valorization of sugar***" submitted by **Mr. Nilesh Pandurang Tangale** to Academy of Scientific and Innovative Research (AcSIR) in fulfillment of the requirements for the award of the Degree of **Doctor of Philosophy in Chemistry,** embodies original research work under my supervision/guidance. I further certify that this work has not been submitted to any other University or Institution in part or full for the award of any degree or diploma. Research material obtained from other sources has been duly acknowledged in the thesis. Any text, illustration, table etc., used in the thesis from other sources, have been duly cited and acknowledged.

September 2018

Ph.D. Student

Mr. Nilesh Pandurang Tangale

Supervisor

Dr. Paresh Laxmikant Dhepe

Senior Scientist, CSIR-NCL, Pune, India
Assistant Professor, AcSIR, New Delhi, India

Communication Channels
NCL Level DID : 2590
NCL Board No. : +91-20-25902000
EPABX : +91-20-25893300
: +91-20-25893400
FAX
Director's Office : +91-20-25902601
COA's Office : +91-20-25902660
SPO's Office : +91-20-25902664
WEBSITE
www.ncl-india.org

DECLARATION BY CANDIDATE

*I hereby declare that the thesis entitled "**Zeolite based micro-mesoporous composites: synthesis, characterization and catalytic performance as heterogeneous catalyst for valorization of sugar**" submitted for the award of the **Degree of Doctor of Philosophy in Chemistry** to the **Academy of Scientific & Innovative research (AcSIR)**, New Delhi, has been carried out by me at Catalysis and Inorganic Chemistry Division, CSIR-National Chemical Laboratory, Pune-411008, India, under the supervision of Dr. Paresh L. Dhepe. The work is original and has not been submitted as a part or full by me for any other degree or diploma to this or any other University.*

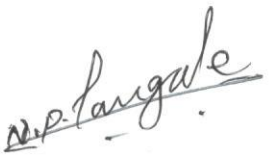

September, 2018

Nilesh P. Tangale

(Enrollment No.10CC15J26026)

Dedicated to .....

My Parents and Sister

ACKNOWLEDGEMENTS

First and foremost, I would like to express my heartfelt and sincere gratitude to my Ph.D. supervisor, Dr. Paresh L. Dhepe, for his guidance, encouragement, constructive criticism, and unconditional support throughout the year. I am deeply grateful to Dr. Praphulla N. Joshi, for his excellent guidance, advice, patience and continuous inspiration. I am highly obliged, without guidance and supervision of both, this work would not have been successful.

I would like to thanks to Dr. C.S. Gopinath, Head of Catalysis and Inorganic Chemistry Division, Dr. D. Shrinivas, and Dr. A.P. Singh (former HOD's) for providing all the divisional facilities and their continuous support throughout the course of the research.

My thanks also belong to Dr. Thirumalaiswami Raja, Dr. R. Nandini Devi and Dr. Shafeek R. Mulla for being my doctoral advisory committee for their valuable advices, discussions and constructive comments to improve the quality of my thesis time to time.

I would like to deeply grateful to Dr. Prashant S. Niphadkar, for his guidance and support during my PhD work and scientific discussion to improve the quality of the thesis.

I am also deeply grateful to Dr. R. N. Devi and Ms. S. Violet for XRD analysis, Dr. T. Raja for H_2-TPR analysis, Dr. R.S. Gholap for SEM and TEM analysis, Dr. S.S. Deo and Dr. K.R. Patil for XPS analysis, Dr. R.K. Zha for nitrogen adsorption/desorption analysis and chemisorption analysis, Dr. S.B. Umbarkar for FTIR analysis, Dr. S.S. Deshpande for UV-Vis analysis and CO_2/NH_3 TPD analysis, Dr. P.R. Rajamohanan for the solid and liquid state NMR analysis.

I would also like to thanks to all other scientific staff Dr. S. Awate, Dr. R.N. Devi, Dr. S.B. Umbarkar, Dr. T. Raja, Dr. S.B. Umbarkar, Dr. E. Balaraman, Dr. S.S. Deshpande, Dr. V.V. Bokade, Dr. C.V. Rode and non-scientific staff members Ms. Samuel Violet, Mr. A.A. Maulavi, Mr. Purushottaman, Mr. S.R. Kadam, Mr. Madhu, Mr. Jagtap and Administration, Accounts, Stores & Purchase sections, and Engineering sections for their technical help and cooperation during my research journey.

I would like to express my gratitude to my past and present group members, Dr. Anup, Dr. Babasaheb, Dr. Sandip, Dr. Richa, Dr. Manisha, Dr. Shilpa, Neha, Dhirendra, Priya, Jyoti, Shiv, Manoj, Lavanya, Tufeil, Neethu, Yayati, Kalyani, Shankar, Prajakta, Aishwarya, Mona, Shinzu, Sheethal, Shyam, Camey, and Sainath for making comfortable and cooperative

atmosphere all the time in lab during the work. I would also like to express my sincere gratitude to my friends Shilpa, Tanushree, Sonali, Shunottara, Dhananjay, Reshma, Manoj, Vinod, Shiba, Jagannath, Garima, Sourik, Anish, Sagar, Pawan, Priyanka, Shibin, Anurag, Dr. Jijl, Dr. Rajesh, Dr. Leena, Dr. Atul, Dr. Hanmant, Dr. Unni, for providing me joyful company during my stay at CSIR-NCL.

I gratefully acknowledge CSIR-NCL XII five year plan project (Project Code: CSC-0125) entitled 'Catalysts for Specialty Chemicals' for financial support and Academy of Scientific & Innovative Research (AcSIR) for registering me for the Ph.D. degree. I would like to acknowledge director, CSIR-NCL for providing me with research facilities and allowing me to carry out research work in this prestigious institute, CSIR-National Chemical Laboratory, Pune.

Finally, the acknowledgment list would not be completed without support of my family members that was always a source of inspiration for me and without them it would not have been conceptualized and accomplished. I would like to thank my parents, Mr. Pandurang Tangale and Mrs. Shakuntala Tangale and my sister, Miss. Piyusha Tangale for immense love, encouragement, support, patience, and trust. I also thank everybody who was important to the successful realization of this thesis work, and apologize that I could not mention personally everybody one by one. Above all, I owe it all to Almighty God for granting the wisdom, health and belief to undertake research work for my thesis and enabling me to its completion.

Nilesh Pandurang Tangale

CONTENTS

Chapter 1: Introduction and literature survey

Chapter 2:Experimental methods and characterization techniques

Chapter 5: Synthesis and characterization of zeolite K/LTL based micro-mesoporous composites by post-synthesis modification, seeding method, and two-step crystallization method, and their catalytic activity in the hydrogenation of xylose to sugar alcohols

Chapter 6: Dehydration of Fructose to 5-Hydroxymethylfurfural Over Micro-mesoporous H/BEA-SBA-15 Composite

List of schemes

List of Figures

Chapter 3

Chapter 6

List of Tables

List of Abbreviations

2D	One dimensional
3D	Three dimensional
12MR	Twelve membered ring
BET	Braunauer-Emmett-Teller
C-HT	Calcined Hydrotalcite
CTMABr	Cetyltrimethylammonium Bromide
DMSO-d6	Deuterated Dimethyl Sulfoxide
EDAX	Energy Dispersive X-Ray Analysis
FAU	Faujasite
FID	Flame ionization detector
FTIR	Fourier Transform Infrared
GC	Gas Chromatography
H/BEA	Beta Zeolite (H-form)
H/MOR	Mordenite (H-form)
H/USY	Ultra Stable Zeolite Y (H-form)
H/ZSM	Zeolite Socony Mobil (H-form)
HMF	5-hydroxymethylfurfural
HPLC	High Performance Liquid Chromatography
HR-TEM	High-Resolution Transmission Electron Microscopy
HT	Hydrotalcite
ICP-OES	Inductively Coupled Plasma-Optical Emission Spectrometry
JCPDS	Joint Committee on Powder Diffraction Standards
MCM	Mobil Composition of Matter
MMT	Million Metric Tons
JCPDS	Joint Committee on Powder Diffraction Standards
LTL	Linde type L zeolite
MAS NMR	Magic angle spinning Nuclear Magnetic Resonance Spectroscopy

MIBK	Methyl *iso*-butyl ketone
MMT	Million Metric Ton
MT	Metric Ton
MPa	Mega Pascal
PXRD	Powder X-Ray Diffraction
RT	Room Temperature
RPM	Rotation per Minute
SBA	Santa Barbara Amorphous
SDA	Structure Directing Agent
SEM	Scanning Electron Microscopy
TEM	Transmission Electron Microscopy
TEOS	Tetraethyl orthosilicate
THF	Tetrahydrofuran
TOF	Turn Over Frequency
NH_3/CO_2-TPD	Temperature Programmed Desorption of am
TGA-DTA	Thermo Gravimetric Analysis-Differential Thermal Analysis
UV-Vis	Ultra violet- Visible
US DOE	United States Department of Energy
XPS	X-ray Photoelectron Spectroscopy

Abstract of thesis

Introduction

The structured metallosilicate molecular sieves such as zeolites, an ordered and rigid microporous materials with unique physico-chemical properties showing excellent molecular sieving effect which led to exceptional shape selective heterogeneous catalyst for several important biomass conversions and in petroleum industries.[1-6] However, the sole presences of microspores also impose a significant limitation on the range of reactions and the performance as a catalyst would be limited by intracrystalline diffusion and stemming from the relatively smaller micropores, loss in selectivity and a reduction in the catalyst lifetime.[3, 6, 7] To overcome the constraint of micropore nature, substantial effort has been focused on increasing the pore size of the microporous material. It has been found that novel synthetic strategies have been applied for the synthesis of micro-mesoporous composites wherein the various components are present in desired molar ratios that combine the advantages of these two kinds of porosity as shown in Fig. 1.[6-10]

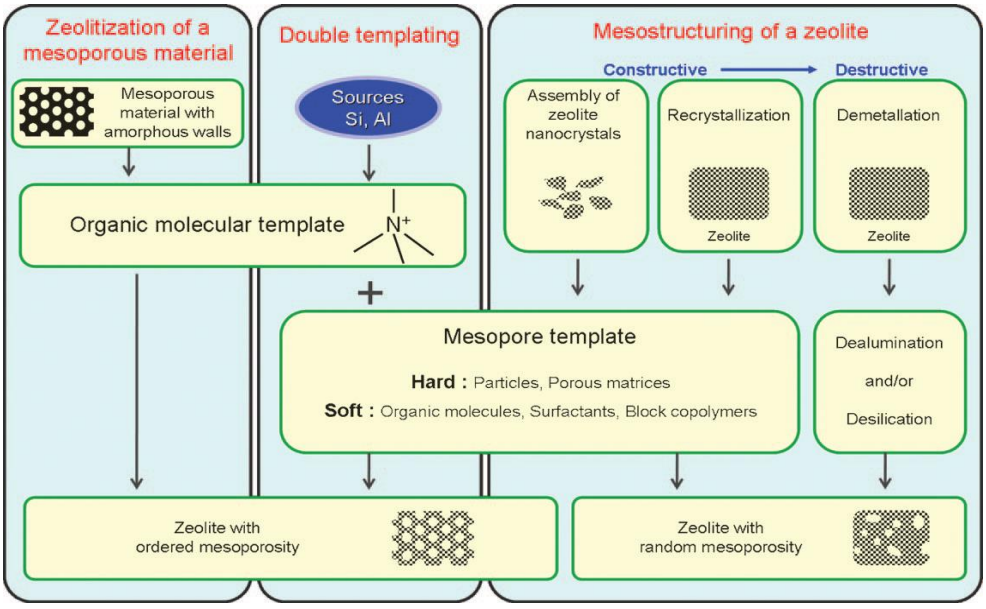

Figure 1. Synthesis of zeolite-based micro-mesoporous composites by different methods of preparations[7]

Today, with the necessity for biomass conversion based industry to treat heavier feedstock; the optimization of the accessibility of zeolite-based micro-mesoporous composites for large reactant molecules is of paramount importance. Although biomass is important but especially lignocellulosic biomass (cellulose and hemicelluloses) can be hydrolyzed to yield sugars which can undergo hydrogenation, oxidation, dehydration, etc.[11, 12] However, the catalytic performance is limited, mainly due to substrate diffusion through catalyst micropores. Therefore, the aim of the thesis is the synthesis of zeolite-based micro-mesoporous composite to enhance the accessibility of the active catalytic sites, the effective mass diffusion through the pores and the shape selective catalysis.

Statement of the problem

Methodologies to minimize diffusion limitation and enhance catalyst effectiveness of zeolites can be achieved by the synthesis of zeolites with larger micropores, the enhancement of the anti-coking ability and hydrothermal stability, as well as the reduction of the intracrystalline diffusion path length by decreasing the crystal size. The general applied strategy to obtain materials with sufficient molecular transport properties is the creation of a secondary pore system consisting of mesopores (2–50 nm) inside the microporous zeolite crystals. With this regards, various kinds of micro/mesoporous MSMs with MFI, FAU, ZSM, LTL, BEA types of topological structures have synthesized with superior structural integrity, acidity (both Brønsted and Lewis acid sites and/or redox property) using surfactant micelles as the structure-directing agent. [6-10] It is expecting that the catalytic activity results would be relevant for the synthesis of other MSM composites, which opens a new avenue for designing new catalysts and green processes in fine renewable chemistry.

Aims and objectives

The main aim of present research work is to design a zeolite (K/LTL and H/BEA) based micro-mesoporous composites that have interconnected micropores and mesopores by different methods of preparation, mainly, 1) Post-synthesis modification (Alkali treatment), 2) Seeding method and 3) Two-step crystallization method. One of the major

objectives of this study is the optimization of synthesis variables of zeolite-based micro-mesoporous composites to enhance molecular mass diffusion and thermal/ hydrothermal stability. One of the objectives of this study is to develop the qualitative and quantitative approach based on the physico-chemical characterization that correlates the catalytic performance with micro-mesoporous properties of the composites. Finally, two catalytic systems were studied mainly to evaluate the structure-activity correlations of micro-mesoporous composites in valorization of sugars, 1) Solid base promoted supported metal catalyzed hydrogenation of xylose to sugar alcohols and 2) Brønsted acidic dehydration of fructose to 5-hydroxymethylfurfural.

Methodology used

The present thesis involves the synthesis of solid basic and acidic zeolite based micro-mesoporous composites.

A. The zeolite (K/LTL, Linde type L) based micro-mesoporous composites were synthesized by different methods of preparation as follows,

1. Post-synthesis modification (alkali treatment): Micro-mesoporous K/LTL zeolites were prepared by varying molar $Si_{(K/LTL\ zeolite)}/OH^-_{(aq.\ KOH)}$ ratio by changing the concentration of aq. KOH solution per gram of zeolite.
2. Seeding method by utilizing waste mother liquor: K/LTL-MCM-41 micro-mesoporous composites were synthesized by seeding method and various synthesis parameters were optimized.
3. Two-step crystallization method: K/LTL-MCM-41 micro-mesoporous composite was also synthesized by two-step crystallization method
4. All the aforementioned micro-mesoporous composites were studied for solid base promoted metal support catalyzed hydrogenation of xylose to sugar alcohols.

B. In another set of experiments, zeolite H/BEA based micro-mesoporous composite viz, BEA-SBA-15 was prepared by seeding method. The catalytic performance of BEA-SBA-15 composite was examined as a solid acid catalyst in the dehydration of fructose to 5-hydroxymethylfurfural (HMF) reaction in the biphasic medium.

C. The physico-chemical properties of all zeolite based micro-mesoporous composites were thoroughly characterized by using ICP-OES, PXRD, N_2 adsorption-desorption measurements, NH_3-TPD, CO_2-TPD, FTIR, XPS, NMR, SEM, TEM and HR-TEM techniques in detail. In both the systems several reaction parameters and influence of method of composite preparation were investigated.

Sample results

The zeolite-based micro-mesoporous materials by various methods of preparation were implemented for the conversion of sugars into value-added chemicals. Zeolite (K/LTL and H/BEA) based micro-mesoporous composites were prepared by the different method of preparation. The thesis mainly divided into two parts. First part involves the synthesis of basic micro-mesoporous composites using K/LTL as a microporous phase. Another part contains the synthesis of acidic micro-mesoporous composites using H/BEA as a microporous phase.

A. Basic micro-mesoporous composites

Synthesis of zeolite K/LTL based micro-mesoporous composites by post-synthesis modification (aq. alkali treatment)

The post-synthesis modification by alkali treatment was employed for the synthesis of zeolite K/LTL based micro-mesoporous composites varying molar $Si_{(K/LTL\ zeolite)}/OH^-_{(aq.\ KOH)}$ ratio. Variation in molar $Si_{(K/LTL\ zeolite)}/OH^-_{(aq.\ KOH)}$ ratio parameter was found to control the degree of preferential desilication with the preserved structural fingerprint of LTL zeolite, resulting in the generation of mesoporosity in zeolite crystals as shown in Figure 1. The influence of the molar $Si_{(K/LTL\ zeolite)}/OH^-_{(aq.\ KOH)}$ ratio on the chemical composition, powder XRD crystallinity, morphology, basicity, and the textural properties of resultant micro-mesoporous composites were investigated.

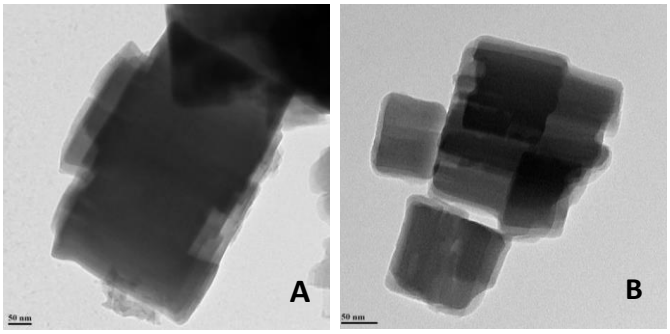

Figure 1. TEM images of K/LTL zeolite and post-synthesis modified sample with optimum molar $Si_{(K/LTL\ zeolite)}/OH^-_{(aq.\ KOH)}$ ratio of 0.265

The micro-mesoporous composites were assessed by different analytical techniques such as PXRD, ICP-OES, FTIR, N_2 adsorption/desorption analysis, CO_2-TPD, ^{29}Si, and ^{27}Al NMR, SEM and TEM. The result concluded that the generation of mesoporosity was observed along with 1) the decrease in the Si/Al ratio and percentage relative crystallinity, and 2) an increase in BET surface area and mesopore volume.[13] The catalytic activity of the composites was studied for solid base promoted metal catalyzed hydrogenation of xylose to sugar alcohols (xylitol and arabitol). Among all composites, the improved catalytic performance was demonstrated by the zeolite K/LTL based micro-mesoporous composite with molar $Si_{(K/LTL\ zeolite)}/OH^-_{(aq.\ KOH)}$ ratio of 0.265, when it is used along with 3.5 *wt%* platinum loaded γ-Al_2O_3 catalyst. The optimum activity may be attributed to the higher surface area, accessible basic sites, dispersion of Pt on γ-Al_2O_3, and the development of substantial intracrystalline mesoporosity for the enhanced molecular diffusion of open chain xylose to and from the hierarchical zeolite with better-preserved crystallinity. Influence of reaction parameters such as temperature, H2 pressure, reaction time, etc. was optimized to enhance the yield of sugar alcohols.

Synthesis of K/LTL-MCM-41 micro-mesoporous composites

An approach to the synthesis of LTL/MCM-41 micro-mesoporous composites varying molar SiO_2/Al_2O_3 ratio (20-8) was originated by following the green technology. The synthesis was based on recycling of waste mother liquor containing preformed LTL zeolite crystals and unutilized reagents. The micro-mesoporous composites consist of preformed K/LTL zeolite crystals through hydrothermal treatment. Further, the siliceous

mother liquor was transformed into the mesoporous MCM-41 (Figure 2). The various characterization results suggested that the mesoporous properties of K/LTL-MCM-41 composites were depended on molar SiO_2/Al_2O_3 ratio and accounted the following conclusions with decreasing SiO_2/Al_2O_3 molar ratio: 1) lowering the orderliness of mesophase, 2) decreasing the wall thickness of mesopores, and 3) decreasing BET surface area and pore volume.

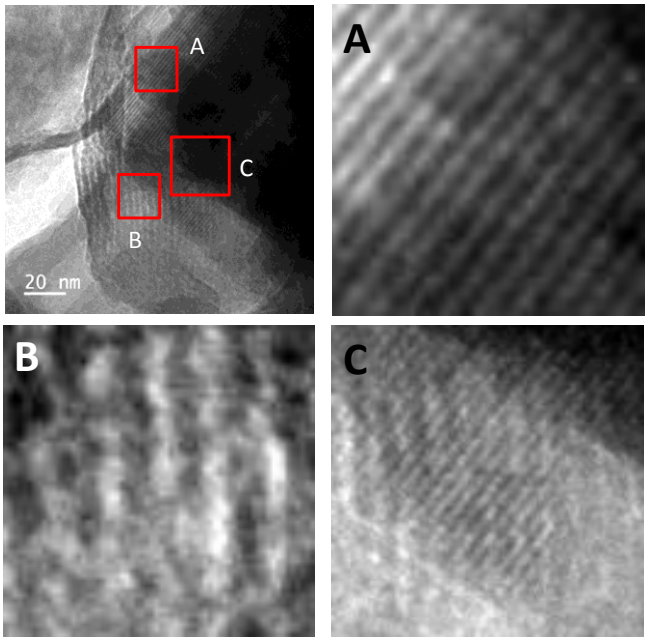

Figure 2. HR-TEM images of 8 MMC micro-mesoporous composite

Synthesis of zeolite K/LTL based micro-mesoporous composites by different methods of preparation

Micro-mesoporous LTL/MCM-41 composites were prepared by different methods of preparation viz. 1) seeding method, (K/**LTL-MCM-41-seed**), and 2) two-step crystallization method, (K/**LTL-MCM-41-Two-step**). The physico-chemical properties of the aforementioned composites (constructive strategy) were compared with the zeolite K/LTL micro-mesoporous composite prepared by the post-synthesis modification (destructive strategy). In the seeding method, fully grown K/LTL zeolite crystals were used

as seed and unused silica from the mother liquor was used for the synthesis of MCM-41 mesophase.

In two-step crystallization method, the first step involves the synthesis of partially crystallized K/LTL zeolite crystals, whereas, in the second step, surfactant template was added for the synthesis of MCM-41. The post-synthesis modification method involves the treatment of 1.5M aqueous KOH solution to the parent K/LTL zeolite at 70 ^{o}C for 1h. PXRD, TEM analysis and nitrogen sorption results indicating that both K/LTL-MCM-41-seed and K/LTL-MCM-41-Two step composites showed the interconnected mesopores of hexagonal MCM-41 mesophase and micropores of K/LTL zeolite. In the micro-mesoporous composite prepared by post-synthesis modification, the presence of non-uniform mesopores was evidenced by the TEM and nitrogen sorption analysis. However, the BET surface area, mesopore volume, and mesoporous surface area were lower as compared to the K/LTL-MCM-41 composites. The thermal and hydrothermal stability of the micro-mesoporous composites were tested and showed that K/LTL-MCM-41 composites prepared by two-step crystallization method showed higher stability.

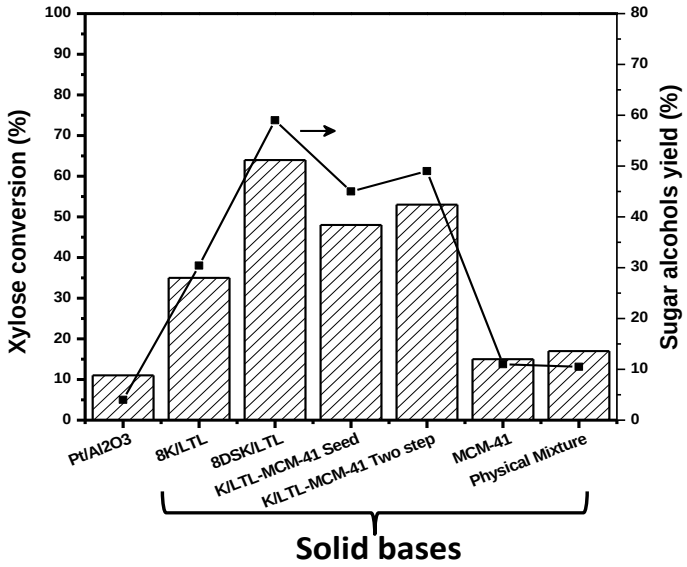

Figure 3. Catalytic activity of hydrogenation of xylose to sugar alcohols over 3.5 wt.% Pt-Al_2O_3 catalyst and micro-mesoporous composites as solid bases (Reaction conditions: xylose 0.15g, catalyst 0.075g, solid base 0.075g, water 35ml, temperature 60 ^{o}C, time 12 h, 16 bar H_2 pressure at R.T., RPM 900)

All the micro-mesoporous composites were tested for the hydrogenation of xylose to xylitol as a solid base with 3.5 *wt%* platinum loaded γ-Al_2O_3 catalyst (Figure 3) and base-catalyzed transesterification of soybean oil to biodiesel with bulkier molecules. The structural-activity correlations of micro-mesoporous composites were established with respect to the methodical characterization such as basicity, porous properties, and thermal/hydrothermal stability.

B. Acidic micro-mesoporous composites

Synthesis of H/BEA-SBA-15 micro-mesoporous composites

Brønsted acidic H/BEA-SBA-15 micro-mesoporous composite was prepared by constructive strategy using Pluronic P123 as a mesoporous template in an acidic medium. The protonic form of the zeolites (H/BEA) was used as a seed for the synthesis of micro-mesoporous composites. The composite showed the presence of SBA-15 mesophase with the wall of SBA-15 was made of crystalline H/BEA zeolite. The conscious characterization suggested that H/BEA zeolite crystals were present in the pore wall of mesoporous SBA-15 in H/BEA-SBA-15 micro-mesoporous composite. It also revealed that the composite proved to form interconnected micropores of H/BEA with mesoporous channels of SBA-15 which are beneficial to improve the catalytic performance (Figure 4).

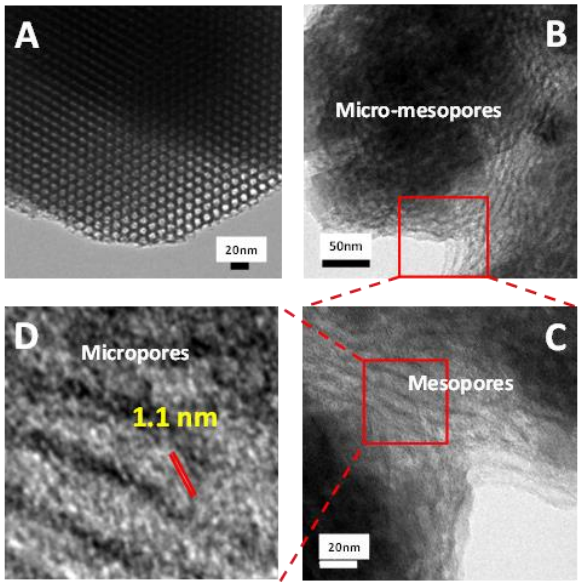

Figure 4. TEM (A) and HR-TEM images (B-D) of micro-mesoporous H/BEA-SBA-15 composite

The catalytic activity of micro-mesoporous H/BEA-SBA-15 composite was investigated for dehydration of fructose to the 5-hydroxymethylfurfural reaction in a biphasic system. Under optimum reaction conditions (MIBK 25mL, water 5mL, 1h, 165^{o}C), Brønsted acidic micro-mesoporous H/BEA-SBA-15 composites synthesized by seeding method showed enhanced catalytic activity owing to a micro-mesoporous structure which allowed diffusion of reactant/product molecules to and from active catalytic sites located in mesopores.

References

1. E. Taarning, C. M. Osmundsen, X. Yang, B. Voss, S. I. Andersen and C. H. Christensen, *Energy & Environmental Science*, 2011, **4**, 793-804.
2. A. Primo and H. Garcia, *Chemical Society Reviews*, 2014, **43**, 7548-7561.
3. I. I. Ivanova and E. E. Knyazeva, *Chemical Society Reviews*, 2013, **42**, 3671-3688.
4. H. Xiong, H. N. Pham, and A. K. Datye, *Green Chemistry*, 2014, **16**, 4627-4643.
5. J. Zhu, X. Meng, and F. Xiao, *Frontiers of Chemical Science and Engineering*, 2013, **7**, 233-248.
6. K. Moller and T. Bein, *Chemical Society Reviews*, 2013, **42**, 3689-3707.
7. J. Č. S. Mintova, *Catalysis Reviews*, 2007, **49**, 457-509.
8. V. Valtchev, G. Majano, S. Mintova and J. Pérez-Ramírez, *Chemical Society Reviews*, 2013, **42**, 263-290.
9. D. P. Serrano, J. M. Escola, and P. Pizarro, *Chemical Society Reviews*, 2013, **42**, 4004-4035.
10. C. Robin, G. Corine, B. Metin and v. D. Sander, *ChemCatChem*, 2011, **3**, 67-81.
11. A. Kumar, N. Kumar, P. Baredar and A. Shukla, *Renewable and Sustainable Energy Reviews*, 2015, **45**, 530-539.
12. R. Saidur, E. A. Abdelaziz, A. Demirbas, M. S. Hossain and S. Mekhilef, *Renewable and Sustainable Energy Reviews*, 2011, **15**, 2262-2289.
13. N. P. Tangale, S. K. Sonar, P. S. Niphadkar, and P. N. Joshi, *Journal of Industrial and Engineering Chemistry*, 2016, **40**, 128-136.

Chapter 1

Introduction and literature survey

1.1 Porous materials

"Molecular sieve", the term referred to solid a porous material, was firstly defined by J.W. Mcbain in 1932, when a mineral, Chabazite was found to have a tendency to adsorb the molecules with the pore dimensions less than 5 Å, selectively.[1] These molecular sieves have the ability to distinguish the component of the mixtures on the basis of molecular size and shape. However, the molecular sieve was first discovered in 1756 by Swedish mineralogist Alex Fredrik Cronstedt, which was termed as 'Zeolite', a boiling stone. After the tremendous success of molecular sieves as catalysts, catalysts supports, adsorbent and ion exchangers in the field of petroleum industries, catalysis, medicine, synthesis of fine chemicals and environmental protection, these porous materials have been popular to the scientific community and ultimately new, efficient and effective molecular sieves have been synthesized. [2-7]

Since last few decades, several molecular sieves with the excellent textural properties have been developed with cost-effective, alternate synthesis route and can tune the physico-chemical properties for potential applications. It also finds numerous applications in emerging fields such as microelectronics, bioengineering, nanotechnology, and photonics. Therefore, the engineering of tuning pore size, composition, structure, and other advantages properties is of paramount importance to construct the new porous materials.[2, 8-10]

Several solid porous materials have been reported extensively such as carbonaceous materials (carbon nanotubes, porous carbon, carbon foam, carbon spheres, carbon foams), metallosilicates (zeolites and zeotype materials, M41S family), metal oxides (TiO_2, Al_2O_3, etc.), and others porous materials such as metal organic framework, clay, etc. The classification and the characteristics of various porous materials on the basis of their chemical compositions are shown in Figure 1.1

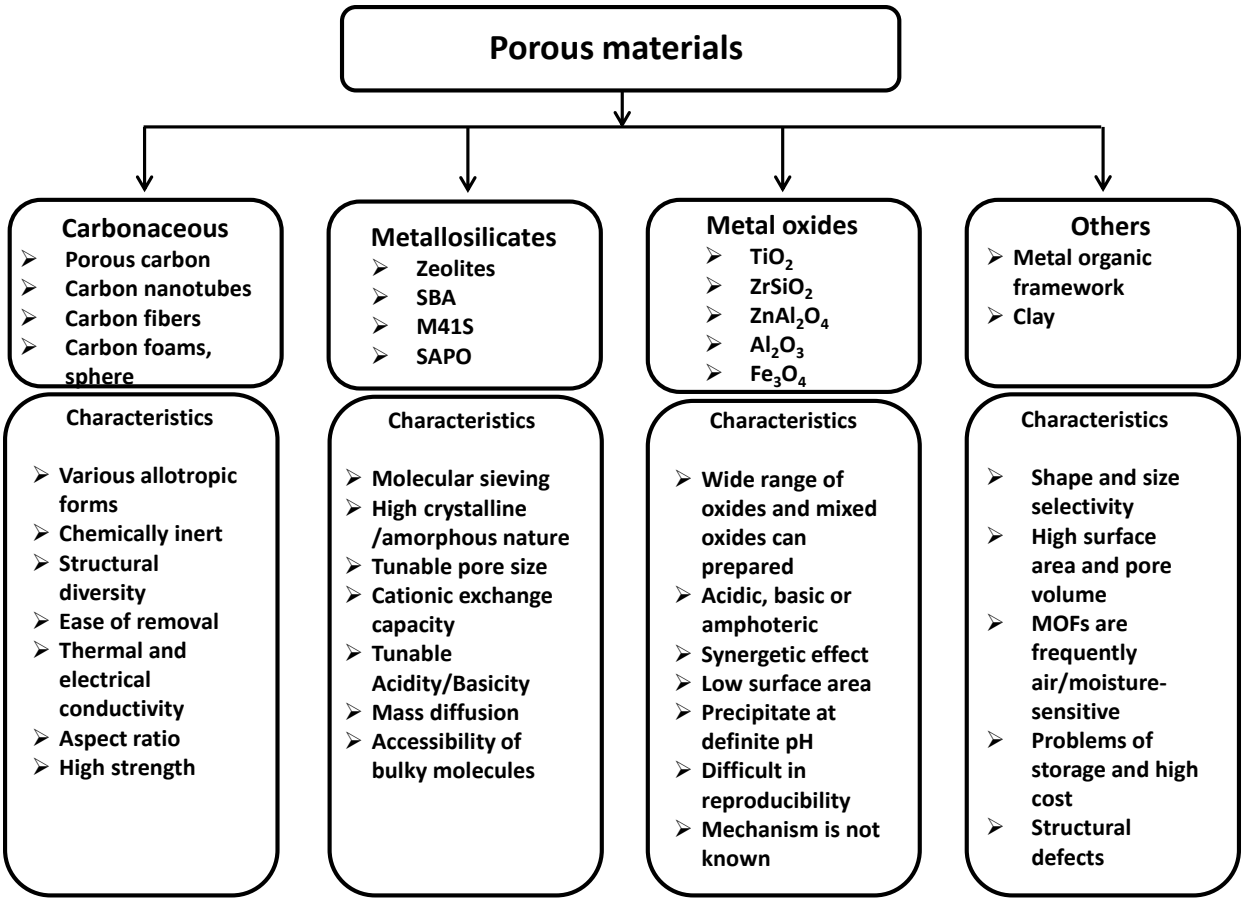

Figure 1.1. Classification and the characteristics of the porous materials on the basis of their chemical compositions

International Union of Pure and Applied Chemistry (IUPAC) have classified the porous materials on the basis of their pore diameter *(d)*. According to IUPAC rules, molecular sieves with the pores less than 2 nm were recognized as micropores materials, 2 nm < d < 50 nm termed as mesoporous materials whereas, pore diameter d > 50 nm are called macroporous materials. The classification of molecular sieves are shown in Figure 1.2.[11] These porous materials possess higher pore volume, specific surface area, acidity/basicity, thermal stability, and variable chemical compositions.

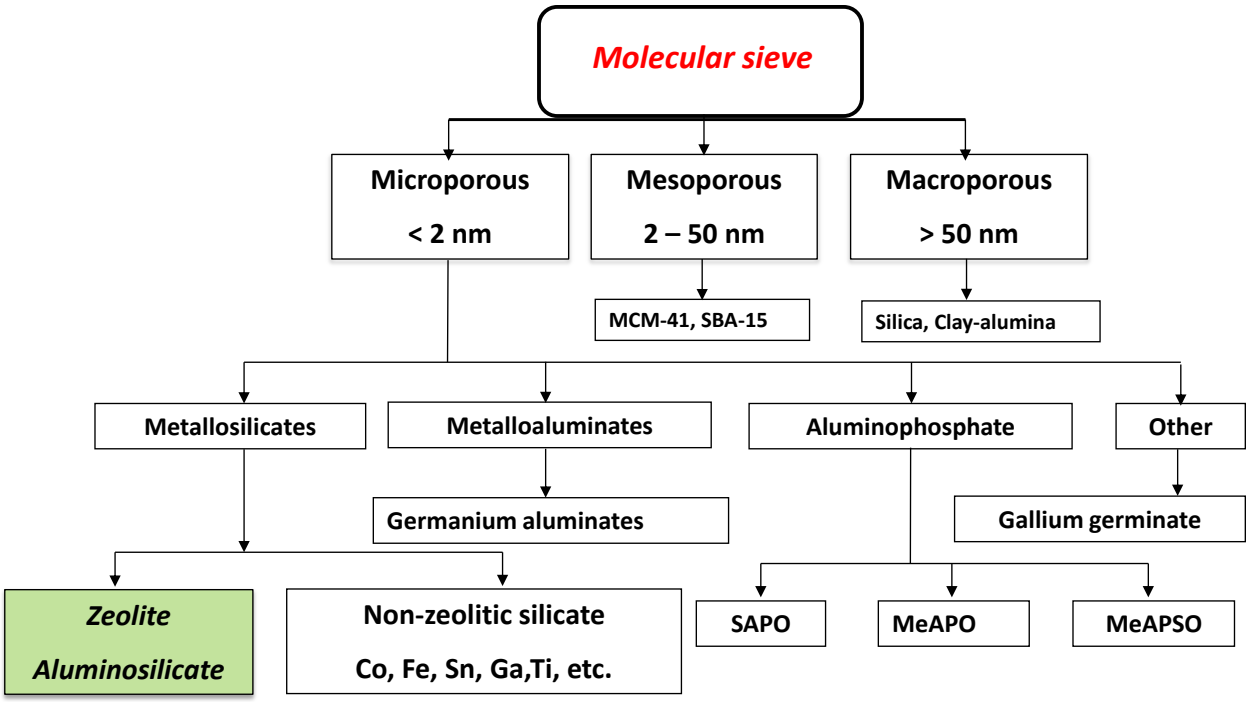

Figure 1.2. Classification of molecular sieves on the basis of pore dimensions

1.2 Microporous materials

Zeolites, a class of molecular sieves, are crystalline, microporous, hydrated aluminosilicates characterized by intracrystalline channels and cages of molecular dimensions. The three-dimensional regular frameworks of the zeolites are formed by the elementary building units of [SiO_4] and [AlO_4] tetrahedra that are linked together by oxygen bridges. The primary building units so formed are connected to form secondary building units (three, four, six-membered rings) etc. Finally, the three-dimensional channels have been formed by the connecting the secondary building units in a regular arrangement. However, according to Lowenstein's rule, the tetrahedra containing aluminium atoms adjacent to each other (Al-O-Al) are forbidden, whereas those of silicon (Si-O-Si) are allowed.[12] The crystallographic unit cell of the zeolites may be represented as:

$$\mathbf{Mx/n\ [(AlO_2)x\ (SiO_2)y]\ zH_2O}$$

Where M referred to the charge compensating cation with the valence 'n', and x, y, and z are the integers. Silica tetrahedra are electrically neutral. But, when tetravalent

silicon, Si(IV) is substituted by trivalent aluminium, Al(III), the electrically imbalanced is developed in the zeolite crystal structure, which is neutralized by an exchangeable cation (alkali metals or proton).

The characteristic properties of the zeolites are determined by the molar Si/Al ratio. Zeolite particularly attractive as catalysts for a wide variety of the chemical reactions owing to their unique physico-chemical properties, which are summarized as follows[5, 6, 13]

(1) Uniform pore size distribution in the microporous range

(2) Higher void volume providing a high surface area

(3) Well defined crystalline structure

(4) Tailorable chemical compositions

(5) Tunable acidity or basicity

(6) The ability of mass transformation through zeolite inner voids

(7) The possibility of isomorphous substitution of silicon for several tetravalent (Ti, Sn, Nb, Zr) and trivalent cations (Al, Fe, Ga, In, B) in the frameworks

(8) Relatively higher thermal and hydrothermal stabilities

(9) ion exchange and high adsorption capacities

(10) Shape-selectivity related to the kinetic diameters of the reactants, intermediates, and products with respect to the dimensions of channels and cavities

Barrer et al. have studied the separation of nitrogen and oxygen through several porous materials and reported that the zeolite can separate the components on the basis of their molecular dimensions.[14] By knowing the key results, since, then several zeolite syntheses have been beginning for the molecular separation. Berk et al. have synthesized type A (LTA), X and Y (FAU)[15] on large scale and first commercially used for gas drying purpose.[16] After the discovery and the catalytic application of ZSM-5 (Zeolite Soconyl Mobile-5), zeolites were recognized as a vital catalyst in hydrocarbon transformation. Further, aiming at the several industrial demands such as heavy metal ion separation, adsorption, and separation, etc., several zeolites and zeotype materials have been synthesized by tuning the pore dimensions in comparison with conventional zeolites. As on date, more than 215 different zeolite and zeotype frameworks have been reported,[17] which indicates the practical synthesis approach of the pore engineering of materials for its applications in chemical reactions.

Despite having aforementioned advantages, the important drawback of zeolites is often encountered diffusion limitations and restriction to the accessibility of active sites by the sole presence of micropores on the internal surfaces; restrict large-scale catalytic applications of the conventional zeolites.[2, 18, 19] Only small dimension molecules can pass through the micropores excluding bulkier molecules. Thus, the only the external surface area of the zeolite is available as a catalytic site. The slower molecular mass transport may lead to the secondary reaction or the coke formation which indirectly decreases the lifetime of the catalyst. The comparison of the advantages and disadvantages of zeolites is shown in Table 1.1.

Table 1.1 Advantages and disadvantages of zeolites

Advantages	Disadvantages
Molecular sieving and shape selective catalysis	Low accessible surface area and pore volume
High crystalline nature	Lower availability of active sites
Tunable chemical composition (isomorphous substitution trivalent cations (Al, Fe, Ga, In, B) or tetravalent cations (Ti, Sn, Nb, Zr))	Diffusion limitations
Pores properties (High surface area, tunable pore size, etc.)	Limited access to bulky molecules
Tunable Acidity/Basicity (Cationic exchange capacity)	Limited catalytic activity
High thermal and hydrothermal stability relative to MCM, SBA materials	

To circumvent the diffusion limitations, several strategies have been reported that enhance the catalytic performance of the zeolites, such as reducing the size of zeolite crystals,[20, 21] and direct synthesis of the micro-mesoporous composite by templating

methods.[22] Considering the indispensable drawbacks of the microporous materials, the scientific communities have initiated to find the alternative approach for the synthesis of mesoporous materials which could overcome the diffusion limitations and active sites accessibility in confined micropores of zeolites. With this regards, new microporous materials with the large pore such as VPI-5,[23] UTD-1,[24] and ECR-34[25] have been synthesized. But they often undergo lower hydrothermal stability and acidity, and one directional pore system. Further, ITQ-15,[26] ITQ-21,[27] and ITQ-33[28] with multimodal channels have been prepared. Catalytic upgrading of biomass over metal or metal oxides supported ordered mesoporous silica such as MCM, SBA and microporous aluminosilicates such as zeolites HY, MFI, BEA etc. supported catalysts exhibited enhanced activity in heterogeneous catalysis.[29-34] During the past few decades, a new family of crystalline zeolitic materials has been reported to encounter diffusion drawback featuring the interconnected secondary mesoporous network in the microporous zeolite matrix. Recently, the synthesis of well-organized zeolitic nanocrystals interconnected hierarchically micro/meso/macro porous system has been reported.[21, 35, 36]

1.2.1 Acidity and basicity of zeolites

Acidity of zeolites

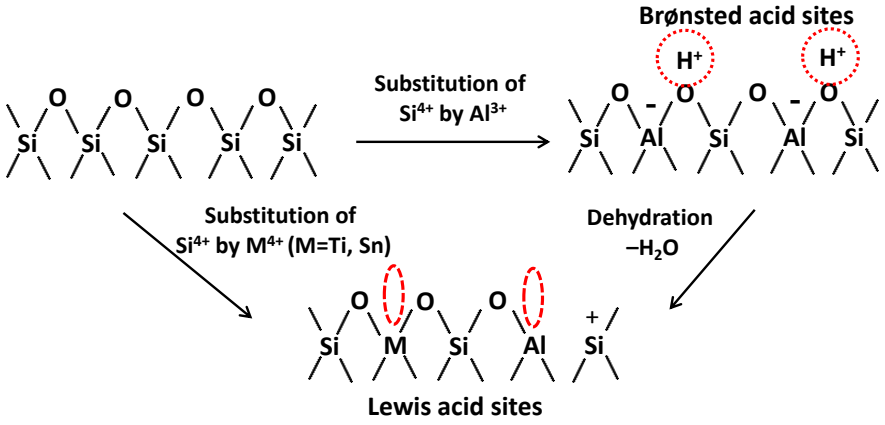

Figure 1.3. Brønsted and Lewis acidic sites in zeolites

As discussed in section 1.2, the substitution of tetrahedral Si^{4+} in the electrically neutral silica framework by aluminium Al^{3+} creates imbalance in the framework therefore,

the total charge of the framework becomes negative. This negative charge is balanced by the charge compensating cations like alkali or alkaline earth metals (Na^+, K^+, Ca^{2+}) or organic cations (H^+, NH_4^+). The nature of the heteroatom present in the framework decides the nature of the acidity. The acid sites in the zeolites may be of Lewis or Brønsted character which may be interconvertible as shown in Figure 1.3. These cations can be exchanged by several other cations, which may alter the acidity of zeolites. If the charge compensating cation is proton, it exhibit Brønsted acidity. In zeolite framework, the proton is associated with the bridging oxygen of a Si-O-Al bond acting as a strong Brønsted acidic site.[37, 38] This can be achieved by the exchange of compensating cation by NH_4^+ followed by calcination. Moreover, the Brønsted acidity is depend on the amount and strength of the acid sites present in local structure of the zeolites. On other hand, aluminium with no charge compensating cation mainly endows Lewis acidic centers, owing to electron acceptor property.[39] These acidic sites are the clusters of positively charged ions or oxides in zeolite framework, which may be formed by the dehydration of Brønsted sites.[40] The aluminium may be present in octahedral coordination.[41] Several factors are responsible for the tuning acidity of zeolites such as Si/Al ratio, distribution of aluminium, nature of charge compensating cation, and the structure of zeolite.[42]

Basicity of zeolites

In zeolites, though all thee oxygen atoms are electron rich centers, but according to Barthomeuf,[43] only those oxygen atoms (intrinsic basicity) belonging to the aluminate anions have sufficient basicity for catalytic activity. The negatively charged [AlO_4] present in the framework resulted in the intrinsic basicity.[43] However, the isolated [AlO_4] tetrahedra lead to the weak basicity of oxygen. The strength of zeolite is depending on the T site occupied by aluminium. The basicity of the zeolites can be tuned by exchange of change compensating cations. In this case, the negative charge density of the oxygen atoms adjacent to the charge compensating cations alters on the basis of electropositivity of the cations.[44] It depends on 1) alkali metal electropositive character (decreased in the order of $Cs^+ > Rb^+ > K^+ > Na^+ > Li^+$) and 2) aluminium content in framework site, (Si/Al ratio of the zeolites). Recently, we have demonstrated the alteration of basicity using X-ray photoelectron spectroscopy (XPS) technique. The trend in basicity of the samples under

investigation was further confirmed using XPS. The binding energy (E_b) of an electron with oxygen provides information of its basic strength. The basicity depends upon the availability of electrons with oxygen, the higher availability of electrons leads to the decrease E_b of O1s and hence greater Lewis basicity of oxygen.[45]

1.3 Mesoporous Materials

In the 1990's, the limitation of microporous zeolite for the large molecules coined the discovery of the mesoporous materials for the industrial applications. Yanagisawa et al. in 1990 have described the synthesis of mesoporous materials with the characteristics of the MCM-41 type of mesoporous material using alkyltrimethylammonium cations.[46] However, due to lack of characterization, the Yanagisawa et al. works have been ignored. Further, the foundation of true mesoporous materials was done by Mobil researchers in 1992 by the discovery of M41S family of mesoporous silicate/aluminosilicate molecular sieves with exceptionally uniform pore size have suggested the self-assembly mechanism of mesopore surfactant molecules. [47, 48]

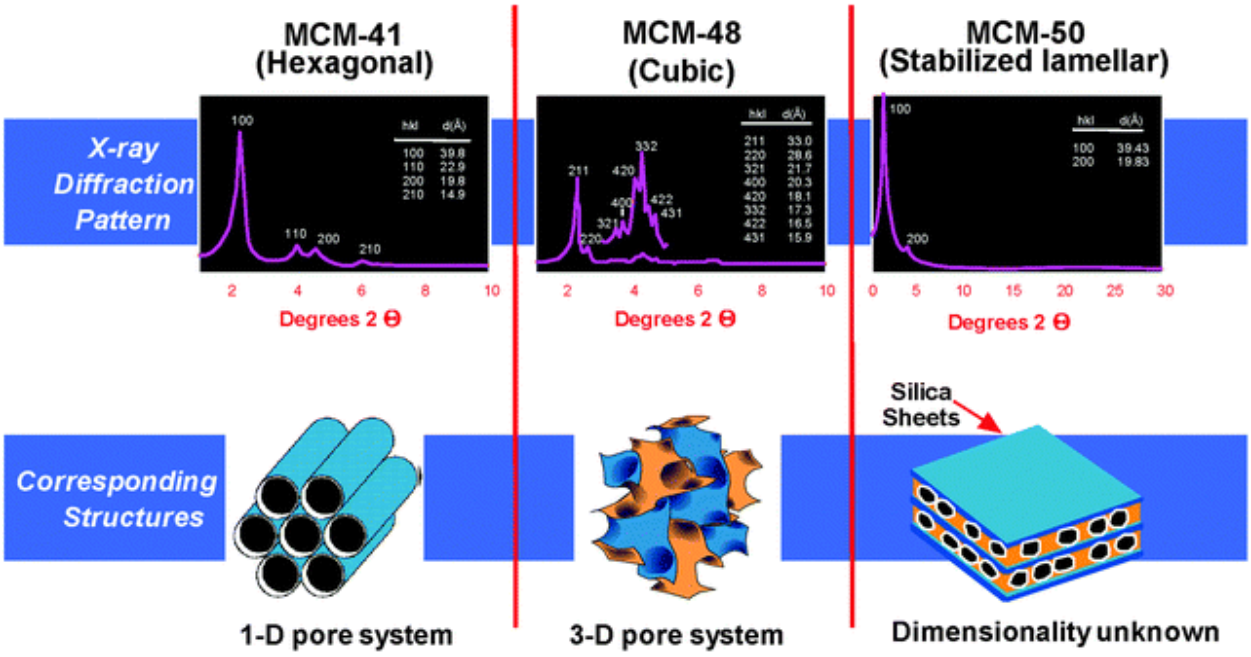

Figure 1.4. X-ray diffraction patterns and schematic representations of mesoporous materials

Table 1.2. Advantages and disadvantages of mesoporous materials

Advantages	Disadvantages
High surface area and pore volume	Low crystallinity
Tunable pore size	Amorphous wall
Requires lower synthesis temperature	Low hydrothermal stability
Hydrophilic surface area	Lower number of acidic sites
Accessibility for bulky molecules	Low shape selectivity for small dimension molecules

During this decade, three mesoporous phases were synthesized viz. hexagonal,[47] lamellar,[49] and cubic phases[50] as shown in Figure 1.4. These materials with uniform pore dimensions were applied in the field of catalysis adsorption and separation. Among these three mesoporous materials, MCM-41 mesophase with 3D hexagonal array showed pore dimensions from 2-10 nm depending on the synthesis conditions have investigated widely as other mesoporous materials were either difficult to synthesize or comparatively thermally unstable.[50] Further, in 1998, another mesoporous material has been synthesized with the hexagonal arrays with uniform pore dimensions namely Santa Barbara Amorphous no. 15 (SBA-15). Its pore dimensions can vary from 4 to 30 nm synthesized using Pluronic P123, an amphiphilic triblock copolymer in acidic media.[51-53] The choice of SBA-15 mesoporous material as catalysts or catalyst support could be due to higher chemical resistance, thermal and mechanical stability as compared to MCM-41 materials.

Despite having large pore structures of mesoporous materials for molecular diffusion, these materials have their own disadvantages such as an amorphous wall and lower hydrothermal/thermal stability causing lower catalytic performance as described in Table 1.2. The zeolites with solely microporous structures imposed the restriction to the accessibility of active sites and the molecular diffusion of reactant/product through zeolite pores. In addition to this, short-term deactivation in various catalytic reactions by the coke formation, which deposited on inner walls of pore channels,[54] is limited to their catalytic applications. The deactivation effect by micropore blockage can be overcome by the development of mesoporosity in the microporous zeolite.[5] Therefore, it is assumed that

micro-mesoporous composites with intrinsic bimodal porous properties can enhance the catalytic activity in the valorization of biomass.[55]

1.4 Micro-mesoporous composites

Aiming at the enhancement of molecular diffusion with accessible active sites, micro-mesoporous composites with interconnected porosity have been proposed and it is attracted by the researchers worldwide.

A zeolite having pore dimensions in the micropore range imposed diffusion limitations of molecules with greater dimensions as compared to the mesoporous materials and eventually difficulties in the accessibility of active sites. However, though mesoporous materials overcome the diffusion constraints, the amorphous nature of the pore wall, and importantly lower hydrothermal stability are still challenging. Micro-mesoporous composites comprising micropores and mesopores captivated enormous attention in recent years owing to the hierarchical porous network which facilitates the efficient mass transport leading to excellent shape/size selective heterogeneous catalysis.[2, 5] The micro-mesoporous composites possesses numerous advantages properties over microporous and mesoporous materials as follows.

- ✓ Contains both micro and mesopores
- ✓ High accessible external surface area
- ✓ Accessibility of active sites
- ✓ Intermediate crystallinity
- ✓ Overcome steric/diffusion limitations
- ✓ Hydrothermal stability
- ✓ Mesoporosity offers space for the deposition of active phases and functionalization with organic moieties
- ✓ Enhanced catalytic activity

The micro-mesoporous composites are characterized by enhanced diffusion properties, tunable acid/basic properties, high surface area, thermal stability, and the pore size distribution in the microporous and mesoporous region, that enable effective shape selective catalysis inside the pore channel.[56, 57] Several reviews are documented in the

synthesis strategies for the development of mesoporosity in microporous zeolites such as hard/soft templating, zeolitization of preformed solids, dual templating, demetallization and combination thereof.[2, 5, 6, 57-61]

1.5 Synthesis of micro-mesoporous materials

Several strategies have been applied in last few decades for the improvement of constraints of zeolites and stability of mesoporous materials. The synthesis of micro-mesoporous composites by different routes have been extensively studied and are schematically shown in Figure 1.5. The synthesis is mainly divided into two strategies, 1) constructive, and 2) destructive.

1.5.1 Constructive strategy

In this approach, the zeolite-based micro-mesoporous composites were synthesized by a constructive strategy using different methods of preparation. It mainly includes zeolitization of preformed mesoporous materials and use of several hard and soft templates as a mesopore directing agent have been explored.

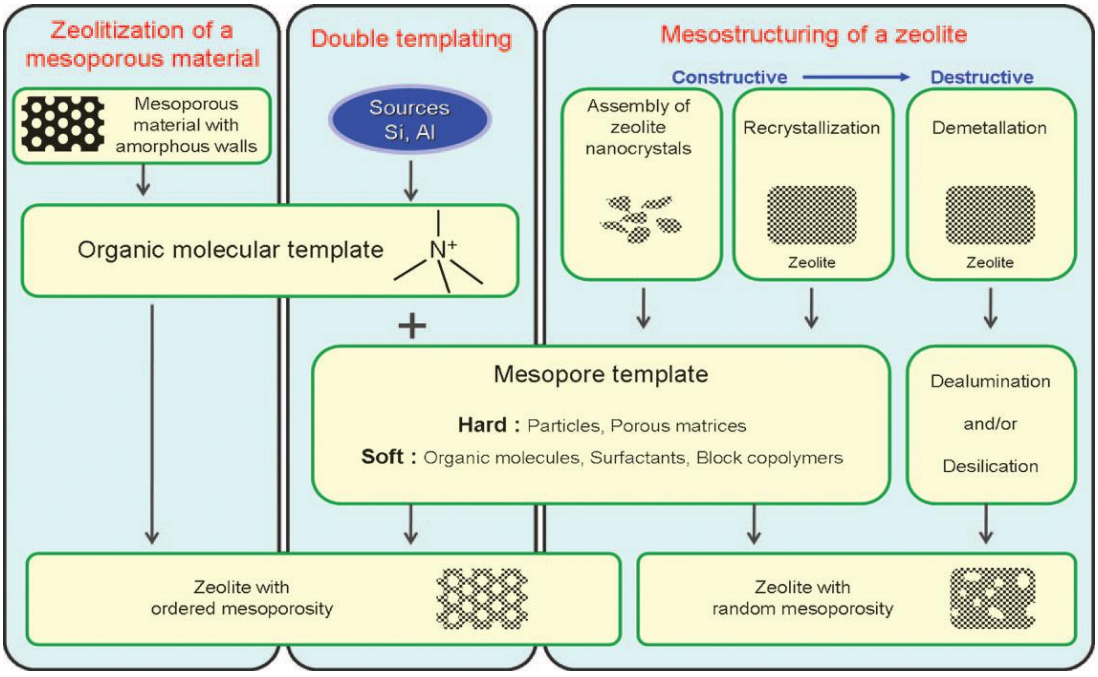

Figure 1.5. Different strategies implemented for the synthesis of micro-mesoporous composites[62]

1.5.1.1 Zeolitization of preformed mesoporous materials

In this approach, an amorphous wall of ordered mesoporous silica or aluminosilicate is converted into partially crystalline mesopore wall with zeolite nanocrystals either in the mesopores, may embed in the mesopore wall or on the pore surface.[62] Several studies have been focused on the synthesis of micro-mesoporous composites involving, particularly, mesoporous MCM-41 and SBA-15 material.[63, 64] However, this method generates solely intercrystalline mesoporosity with partially crystalline mesopore wall.[65] For example, the synthesis of TUD-M and TUD-C was carried out using tetrapropylammonium hydroxide as a micropore as well as mesopore template for the preparation of ZSM-5 zeolite nanocrystals.[66, 67]

Xu et al. have prepared micro-mesoporous materials from the dry gel of aluminosilicate by crystallization with water vapors and amines, leading to the formation of ZSM-5 zeolite.[68] After this strategy, two methods namely, Vapor Phase Transport and Steam-Assisted Conversion have been put forth for the synthesis of zeolite-based micro-mesoporous composites.[69] The prior method involves the direct contact of water and structure directing agent in vapor state with the aluminosilicate dry gel, whereas, later involves direct contact of water vapors with the dry gel containing aluminosilicate sources and the structure directing agent. Several solid precursors are reported for the synthesis of micro-mesoporous composites by this method.[70] Zhou et al. synthesized mesoporous TS-1 with the mesopore centered at 11.2 nm following a steam assisted method by crystallization of TS-1 precursors.[70] Other researchers have synthesized micro-mesoporous beta zeolite by steam assisted treatment to the dry gel containing the beta zeolite precursors including structure directing agent.[71] The mesopores thus obtained with the average diameter of 13 nm. The authors also reported that the optimum water content is crucial for the synthesis of beta zeolite within few hours. Similarly, Li et al. have obtained micro-mesoporous MFI nano-crystals by steam assisted treatment.[72]

In another methodology, the micro-mesoporous composites were obtained in which a mesoporous wall with semicrystalline zeolitic materials was formed by utilizing zeolite seeds.[62] This method possesses advantages over conventional zeolite synthesis such as identical Si/Al ratio, faster crystallization, and the lesser utilization structure directing

agents. However, the zeolitization of mesoporous materials have several disadvantages such as; sever synthesis conditions, distortion of mesopores, and the collapse of the mesopore wall after a long treatment.

1.5.1.2 Templating

The synthesis of zeolite-based micro-mesoporous composites has been achieved by the addition of mesoporous structure directing agent during the crystallization of zeolite. In the templating method, silica-alumina precursors along with the templates are subjected for the hydrothermal crystallization at elevated temperature. The silica-alumina precursors were converted into the zeolite using micropore directing agent, while the hard/soft templates generate micelles leading to the formation of mesopores which may be incorporated with zeolite pores. Finally, upon calcination, the removal of templates opens up the micropores and mesopores cavities leading to the formation of micro-mesoporous composites.

1.5.1.2.1 Hard templating

Synthesis of micro-mesoporous composites with the addition of a hard template is one of the simple and versatile procedures for the development of mesopores. Hard templates used as mesopore templates which are the solid materials with the rigid structure. Several rigid materials as hard templates such as carbonaceous materials, inorganic materials, biological materials, and polymers have been reported in the last few decades as summarized in Table 1.3. Among various hard templates, carbonaceous templates were extensively studied for the synthesis of micro-mesoporous composites. These rigid materials are chemically inert and can be easily removed by the combustion. Various carbons based hard templates such as carbon black, carbon nanotubes, carbon fibers, colloidal impregnated carbon, aerogels and mesoporous carbon with ordered structure have been extensively investigated for the synthesis of micro-mesoporous composites.

The pioneering work on the synthesis of micro-mesoporous composites using carbonaceous templates was done by Jacobson et al. The research group employed porous

carbons, carbon black pearls, and carbon fibers as hard templates.[73] Jacobsen et al. investigated carbon nanoparticles as a hard template and was found that the carbon nanoparticles were embedded into the zeolite crystals during hydrothermal crystallization.[73] In this case, mesoporous zeolite crystals were obtained with the pore size distribution in the mesopore range from 5 to 50 nm. With this approach, several micro-mesoporous composites with different zeolite or zeotype frameworks were reported such as TS-1, ZSM-11, ZSM-12, BEA, AlPO-34, and Silicalite-1.[74-77] However, the main disadvantage of the carbon hard templates frequently occurred is the inhomogeneous mixture of microphase and the mesophase completion of synthesis.

Table 1.3. Types of hard templates

Type of hard template	Pore size/ pore volume	Reference
Carbon black	2-25 nm	73
Carbon fibers	-	61, 78
Carbon nanotubes	2-10 nm	79
Colloidal imprinted carbon	10-85 nm	80
Mesoporous carbon	2-12 nm	81
Carbon aerogel	2-10 nm	82
Aerogel/polymer/resin		
Polystyrene, polyurethane	~250 ± 30 nm	83
Resorcinol-formaldehyde aerogel	9-25 nm	84
organic gel		85
Biological		
Starch, bacteria, wood cell	0.17 ml/g	86
Inorganic		
Silica	2-250 nm	87
$CaCO_3$	50-100 nm	88

Although, these micro-mesoporous composites showed excellent mass diffusion and catalytic properties, a very broad pore size distribution was obtained in the mesopore region. In another experiment, Schmidt et al. have used carbon nanotubes with the 1-20 nm diameters for the synthesis of silicalite-1.[79] The synthesized single zeolite crystal showed mesopore channels. Janssen et al. have studied the synthesis of the micro-mesoporous composite using carbon nanofibers as hard template constructing the cylindrical mesopores.[78] Another group of researchers has used carbon aerogel for the synthesis of zeolite Y and A based micro-mesoporous composites with interconnected pores.[82, 89] Further, ordered mesoporous structural carbon material (CMK-1 and CMK-3) have been synthesized from a relatively cheap precursor such as sugars and employed as hard template for the synthesis of MCM-48 or SBA-15 type of micro-mesoporous composites.[90-93] Several other materials such as polymers, resins, silica, $CaCO_3$ and biological materials such as starch, bacteria, wood cells etc. have been studied as hard templates as described in Table 1.3.

1.5.1.2.2 Soft templating

In the case of the synthesis of micro-mesoporous composites by the soft templating method, relatively soft or no rigid surfactants have been used, where intre and intracrystalline mesopores can be developed. The mesopore surfactants used may be flexible long carbon chain molecules or the polymers as described in Table 1.4. The problems associated with the hard templates have overcome by the use of soft templates such as amphiphilic surfactants, organosilane, silylated zeolite seeds or surfactants or polymers, cationic amphiphilic polymer, Polyquaternary ammonium surfactants, and random grafted polymers have been reported. The main function of the long chain soft templates is to anchor the exposed surface of the zeolite nanocrystals which inhibits the growth of zeolites into bigger crystals.

Kloetstra et al. was synthesized micro-mesoporous Y-MCM-41 composite using both the templates for the synthesis of Y zeolite and the MCM-41 mesophase and reported the importance of the sodium content during the NaY crystallization.[94] In this context, Ryoo et al. have synthesized micro-mesoporous ZSM-5 using an amphiphilic organosilane in a single step.[95] In amphiphilic surfactant templates, a strong interaction of positive end of

surfactant and the silanol groups of aluminosilicate precursors via formation of the covalent bond. By altering the hydrothermal conditions and the molecular structure of the amphiphilic soft surfactants, the tuning of the mesopores in the range of 2-8 nm could be achieved. The soft templating method has been employed for the synthesis of micro-mesoporous LTA, SOD, ALPO, FAU and SALPO frameworks with the aid of alkylphosphonic acid or amphiphilic organosilanes mesostructural directing agents.[96-100]

Table 1.4. Types of soft templates

Type of soft templates	Pore size/ pore volume	References
(Amphiphilic) surfactants	0.7 ml/g	101
Organosilanes	2-10 nm	95
Silylated seed: PHAPTMS	2-8 nm	102
Silylated surfactant: TPHAC	2-20 nm	95
Silylated polymer: PEI	2-5 nm	103
Cationic amphiphilic copolymer: C-PSt-co-P4VP	6-60 nm	104
polydiallyldimethylammonium chloride (PDADMAC)	5-30 nm	105
Polyquaternary ammonium surfactants: C22-6-6 C22-4-4	5-30 nm	106
Polyquaternary ammonium surfactants: C18–N3–C18	2-5 nm	107
Random-graft polymer: linear polystyrene-N3-SDA	2-10 nm	108

PHAPTMS :phenylaminopropyltrimethoxysilane, TPHAC: 3-(trimethoxysilyl)propyl hexadecyl dimethyl ammonium chloride, PEI: polyethyleneimine, C-PSt-co-P4VP: polystyrene-co-4 – polyvinylpyridine, C22-6-6: $C_{22}H_{45}$-$N^+(CH_3)_2$-C_6H_{12}-$N^+(CH_3)_2$-C_6H_{13}, C18–N3–C18: $C_{18}H_{37}$–N^+ $(CH_3)_2$–C_6H_{12}–N^+ $(CH_3)_2$–C_6H_{12}–N^+ $(CH_3)_2$–$C_{18}H_{37}(Br^-)_3$, C22-4-4: $C_{22}H_{45}$–$N^+(CH_3)_2$–$(CH_2)_4$– $N^+(CH_3)_2$–$C_4H_9(Br^-)_2$

In addition to this several cationic polymers have been investigated as a soft template for the synthesis of micro-mesoporous composites due to efficient interaction with aluminosilicate precursors and the stability under hydrothermal reaction conditions. In the first report, zeolite beta based micro-mesoporous composites have been synthesized using tetraethylammonium hydroxide and polydiallyldimethylammonium chloride (PDADMAC) with the mesopore size ranging from 5 to 40 nm.[105] The synthesized micro-mesoporous composite showed enhanced catalytic activity as compared to the pristine beta zeolite in alkylation reaction due to efficient diffusion of reactants and products. By following the similar procedure, zeolite ZSM-5 based micro-mesoporous composite was prepared by using tetrapropylamine hydroxide and dimethyldiallyl ammonium chloride acrylamide copolymer (Polyquaternium-7).[104] Considering advantages of the surfactant polymers as mesopore directing agents, some researchers reported the use of polyquaternary ammonium surfactants which functions as micropore as well as mesopore templates as shown in Table 1.4.

1.5.1.3 Zeolite Recrystallization

Another approach for the synthesis of zeolite-based micro-mesoporous composites is zeolite recrystallization. Zeolite recrystallization refers to the development of mesoporosity by coupling of zeolite assembly and the demetallation methods. In this method, the zeolite is subjected for the dissolution in acidic or alkaline media followed by the recrystallization using surfactants as a mesopore directing agent (often used CTMABr) under basic media. Most frequently, the base leaching (NaOH, TMAOH, NH_3, etc.) of zeolites has been carried out to form primary and/or secondary building units. Several factors govern the quality of micro and mesoporosity in the composites such as alkali concentration, treatment temperature and the treatment time.[109] Further, the ordered mesoporosity is developed by the recrystallization of the zeolite framework. Several zeolites such as MOR, MFI, FER, LTA, FAU, BEA, MTW, MEL, and MAZ were thoroughly studied for the synthesis of micro-mesoporous composites as reviewed. [109]

Ivanova et al. have carried out the base leaching treatment to the mordenite using NaOH and cetyltrimethylammonium bromide (CTMABr) to get the MCM-41 type of

mesoporous material.[110] It was observed that the mesopore volume increased with increasing the concentration of alkali at the expense of micropore volume. They have also found the optimum concentration of alkali and recrystallization treatment conditions where the truly interconnected micro-mesoporosity was developed with mesopores ranging between 3-20 nm. The author tested the micro-mesoporous composite for the cracking of 1,3,5-triisopropyl benzene and transalkylation of biphenyl and p-diisopropyl benzene. It was found that the catalytic activity mainly depended on the recrystallization conditions and on the concentration of NaOH solution. It showed improved activity as a result of diffusion of bulky reactants and products through mesopores and the acidity of the materials exhibited by the zeolite crystals.

These observations were also confirmed by the Wang et al. during the synthesis of micro-mesoporous MOR-MCM-41 composite materials by desilication followed by recrystallization approach.[111] The higher catalytic activity was ascribed to the secondary building units present in the walls of the mesopores. These materials also exhibited good hydrothermal stability because of the partial crystalline wall. Further, ZSM-5 based micro-mesoporous composites with the MCM-41 type of the materials were reported by the Inagaki et al. by recrystallization rout.[112] The materials showed improved catalytic activity in cumene cracking as compared to the Al-MCM-41 due to stronger acidic sites. Ying et al. reported the mesostructured zeolites (Y, mordenite, and ZSM-5) with retained zeolite crystallinity.[113] The better catalytic activity was observed for the cracking of 1,3,5-triisopropylbenzene as compared to Al-MCM-41.

Further, Tsapatsis et al. have reported the duel mesoporosity for mesoporous ZSM-5 zeolites, in which the ZSM-5 was subjected for the desilication followed by recrystallization process.[114] Garcia-Martinez et al. proposed the formation of a mesoporous Y zeolite by the hydrothermal treatment of surfactant CTMABr and NH_4OH solution.[115] The mesoporous Y zeolite showed enhanced catalytic activity as compared to the USY catalyst with less coke formation. Another researcher has reported the mesoporous ferrierite zeolite by alkali treatment followed by recrystallization in presence of CTMABr as a surfactant.[116] The micro-mesoporous ferrierite showed enhanced catalytic activity in the isomerization of n-butene.

One of the advantages of the zeolite recrystallization methods is that it does not involve the loss of silica or the severe damage of zeolite crystal structure which is mainly observed in the case of desilication. However, due to use of costly surfactant for the synthesis of micro-mesoporous composites, very less number of papers was devoted for the aforementioned strategy as it was a major issue in an industrial point of view.

1.5.1.4 Assembly of zeolite nanocrystals

Another approach for the synthesis of micro-mesoporous composites is an assembly of zeolite nanocrystals. It comprises the synthesis of preformed zeolite nanocrystals, or zeolite seeds or protozeolitic nanocrystals in the preliminary stage and subsequently utilized for the synthesis of micro-mesoporous aluminosilicates using mesoporous surfactant template.[117] These zeolite nanocrystals were condensed around the surfactant. This approach was first reported by the Liu et al. which involve the assembly of zeolite Y nanocrystals with CTMABr as a surfactant at 100 ^{o}C for 20 h.[118] The hydrothermally stable micro-mesoporous composite was denoted as MSU-S. Pinnavaia et al. synthesized protozeolitic units initially and further subjected for the zeolite assembly using a surfactant template for mesopore generation showing better stability and catalytic performance.[119] However, it showed amorphous nature as determined by wide-angle X-ray analysis.

Considering the aforementioned problem with the assembly of zeolite nanocrystals method, Moller et al. have improved synthesis strategy during the zeolite beta nanocrystals by using the polydiallyldimethylammonium chloride cationic polymer.[120] The flocculation of beta nanocrystals caused by the cationic polymer led to the formation of interparticle mesopores or macropores ranging from 40 to 400 nm. The size of the pores depends on the concentration of the polymer used for the synthesis. Van Oers et al. have reported the zeolite beta particles embedded into the mesoporous wall by two-step synthesis process.[121] Fang et al. have synthesized micro-mesoporous composite by the assembly of zeolite nanocrystals without using any secondary template.[122] In addition, Lam et al. have synthesized micro-mesoporous zeolite thin film by the surfactant-mediated assembly of zeolite nanocrystals.[123]

1.5.2 Destructive strategy (Post-synthesis modification)

Another approach for the synthesis of micro-mesoporous composites is a destructive strategy, wherein the framework atom is selectively removed by the post-synthesis modification, such as dealumination, desilication, calcination, and combination thereof. Removal of framework T=Si or Al atom, commonly termed as demetallation, is the common approaches for the development of mesoporosity in the zeolite. The demetallation process consists of removal of Silicon (desilication) or Aluminium (dealumination) metal atoms from the zeolite framework by the different technique such as using steam, acids, bases, etc. leading to the appearance of mesoporosity. Demetallation technique has several advantages such as 1) simple and ease of operation, 2) high zeolitic character, 3) applicable to different zeolites, 4) cost-effective, and 5) possibility to scale-up the process. However, the demetallation has several disadvantages like, 1) uncontrolled mesopore development, 2) Loss of significant amount of zeolite mass, 3) destruction of zeolite crystal, 3) may alter the Si/Al ratio of the parent zeolite, 4) tuning of the additional porosity is still a challenge, and 5) expensive when organic templates/acids are involved. But, the features of the micro-mesoporous structure created in the zeolite are depending on the application of the post-synthesis method.

1.5.2.1 Dealumination

Dealumination is one of the conventional post-synthesis treatment techniques involve the selective removal of aluminium from the zeolite framework. One of the reasons for applying the dealumination method was to synthesize the zeolite with high Si/Al ratio with higher thermal and hydrothermal stability.[124] The dealumination can be accomplished by several post-synthesis treatments. Outmost, the steam treatment at a higher temperature ranging between 500 ^{o}C and 600 ^{o}C could be one of the primary techniques used for the development of mesopores. This method leads to the development to about 5-50 nm defects in the faujasites (Y zeolite).[125] However, the steaming generally causes the mobility of silicon and aluminium species inside zeolite pores.[126] The steaming has been mainly implemented for the stabilization of Y zeolite in fluid catalytic cracking (FCC) reactions which involve the heating of zeolite under a steam atmosphere at 600–800 ^{o}C.[127]

The steaming method causes the removals of framework aluminium from the zeolitic by the hydrolysis of Al–O–Si linkages using steam at high temperatures which generate mesopores. In the steaming process, the aluminium atoms were extracted from the zeolite framework and get deposited on the external or internals surface of pores. The extra-framework aluminium can be removed by the milder acid treatment that can enhance the porous properties of the zeolites.[128] The steaming treatment not only resulted in the dealumination but also causes desilication which was reported by Malola et al.[129] Some other zeolites such as ZSM-5,[130] Ferrierite,[131] Mazzite,[132] Beta,[133] and Mordenite[134] have been investigated.

Another process by which aluminium can be leached out is chemical treatment, e.g. inorganic acids (nitric or hydrochloric acid) and organic acids, oxalate, can be used.[124] The removal of aluminium in the framework accompanied by the generation of mesopores in the zeolite crystals at the expense of the partial zeolite structural collapse. Since the acidity depends on the presence of aluminium in the zeolite framework, the acidity can be greatly affected by the dealumination post-synthesis treatment.[61] Several dealumination agents were reported for the development of mesopores such as oxalic or methanesulfonic acid, ammonium hexafluorosilicate, $SiCl_4$, acetic, or tartaric acid.[135,136] In one report, ethylenediaminetetraacetic acid (EDTA) was used for dealumination which removes surface aluminium ions leading to the material with heterogeneous distributions of aluminium in the zeolite framework.[137] Van Oers et al. have reported the dealumination treatment to the BEA zeolite using HCl followed by the hydrothermal treatment.[121] It reported that the subsequential treatments leading to the formation of the materials with the better zeolite properties with the development of mesoporosity. Due to the detrimental effects of dealumination on the acidity of the zeolites, several researchers were focused on the various coupling routes such as dealumination and desilication, which improves the porous properties of the zeolites.[138] Besides the aforementioned conventional dealumination methods, calcination at higher temperature or treatment with silicon tetrachloride and ammonium hexafluorosilicate has also been reported in the literature.[62]

1.5.2.2 Calcination

In addition to the aforementioned dealumination methods, the aluminium can also be removed from the framework by calcination in presence of oxygen to impart stability to the zeolite. The removal of the aluminium, however, depends on the type of the zeolite and the calcination conditions. This aluminium dislodged from the zeolite framework and lead to the formation of extra-framework aluminum.[18, 126, 139] Though, the bulk molar Si/Al ratio does not change with the calcination, but the framework molar Si/Al ratio increases. Further, the extra-framework aluminium can be removed by mild acidic treatment to form interconnected micro and mesoporosity. [140, 141]

1.5.2.3 Desilication

The zeolite-based micro-mesoporous composites prepared by yet another versatile demetallation technique viz. desilication or base leaching is one of the promising post-synthesis modification techniques by which the hierarchically structured zeolites coupled with micro-mesoporosity can be synthesized owing to its versatile, effective, scalable and green synthetic approach. The desilication with alkaline solution primarily concerned with the development of intracrystalline mesoporosity by the controlled extraction of silicon atoms from the zeolitic framework with the partial deterioration of the crystalline structure. The post-synthetic treatment parameters such as the Si/Al ratio, concentration, and volume of alkali solution, exposure time and temperature were found to influence the nature of secondary mesoporous network in the microporous zeolite. Thus, the viability of the zeolite catalyzed reactions can be enhanced distinctly by the application of hierarchically structured zeolites in the catalysis. The micropores provide the reactive sites for the catalytic conversion and the interconnected mesopores resulted in the enhanced molecular transport on account of improved diffusion rate. The desilication method was first patented by Young D.A. in 1960, wherein the Mordenite zeolite was treated with base preserving its crystallinity and enhanced sorption capacity.[142] The desilication have found to be an efficient, simple and scalable technique for the generation of mesopores in the zeolite crystal. The amorphous silica fragments generated during desilication can be leached out by the alkali solution, thus opening the mesopores of zeolites.[143] The

mesoporous zeolite thus formed showed excellent adoption, catalytic properties and catalyst support[143, 144] The mesoporous ZSM-5 zeolite was synthesized by Rutkowska et al. by the alkali treatment and employed as a catalyst in the conversion of methanol to dimethyl ether.[146] The mesoporosity generation by alkaline treatment resulted in the improved catalytic performance. Furthermore, the mesoporous acidic ZSM-5 was used as novel solid support for cobalt catalyst in the Fischer–Tropsch synthesis.[145] In comparison to the conventional Co/SiO_2 catalyst, the cobalt loaded mesoporous ZSM-5 decreased the wax production and suppressed the hydrocarbon cracking. The mesoporosity also enhanced the selectivity to the $C_{5–18}$ fractions. Parez Ramirez et al have investigated the desilication of various zeolites varying Si/Al ratio.[61] Under the given post-synthesis conditions, the silicon is preferentially removed leaving an atomic vacancy in the zeolite framework as shown in Figure 1.6.

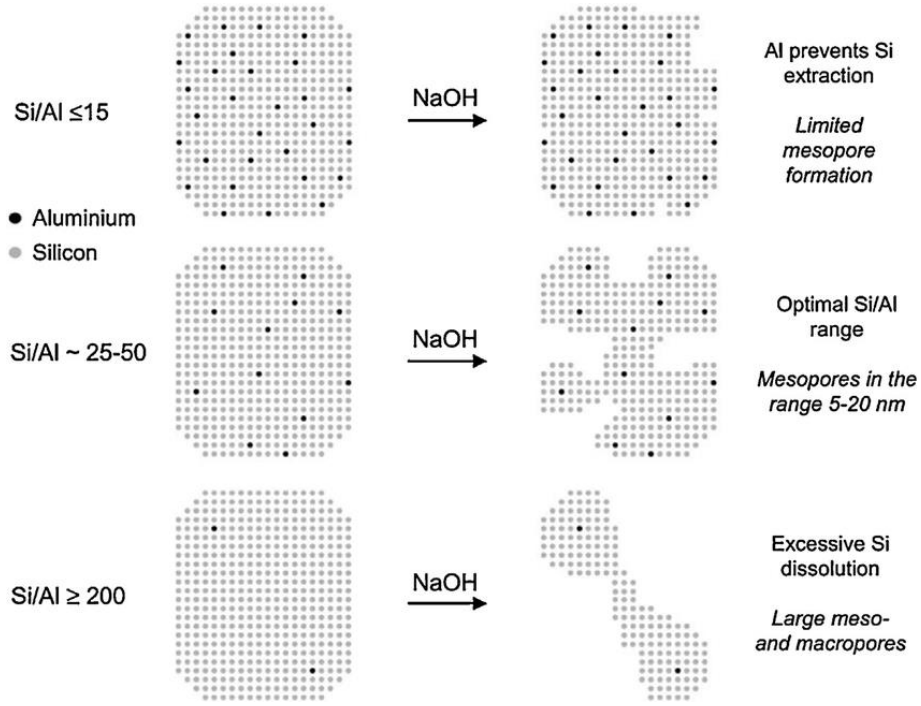

Figure 1.6. Desilication and the mesopore formation mechanism of ZSM-5 zeolite with different Si/Al ratio

This also lowers the Si/Al ratio of the zeolite. They reported that the molar Si/Al ratio of 50-100 for ZSM-5 could be optimal for the mesoporosity formation with preserved acidity and crystallinity.[20] A thorough study suggested that silicon removal from the

aluminium rich silicon zeolites could be less susceptible which might be associated with higher stabilization by neighboring Al-rich environment.[61] Recently, they have introduced the concept of organic and inorganic 'pore-directing agent' such as $Al(OH)_4$, $Ga(OH)_4$, tetrapropyl ammonium and tetrabutyl ammonium and it was studied for the Beta and USY zeolites.[146-148]

Several chemicals were reported for the desilication process such as NaOH, KOH and LiOH, Na_2CO_3, $NaAlO_2$, tetraalkylammonium hydroxides (tetrapropylammonium and tetrabutylammonium hydroxide), tetraalkylammonium salts (cetyltrimethylammonium bromide, tetrabutylammonium bromides, benzyltriethylammonium bromide).[109, 148-151] Being less reactive, the tetraalkylammonium hydroxides require higher treatment temperature and/or longer treatment time. Further, using organic hydroxides, a protonic form of zeolite can be prepared after calcination which eliminates the ion exchange procedure. Zeolites such as MOR (mordenite),[150] ZSM-12,[152] BEA,[150] FAU (faujasite),[153] and FER (ferrierite)[154]have been investigated for alkali post-synthesis treatment. Several other zeolites CHA, TUN, ZSM-22, ZSM-12, ITQ-4, SSZ-35 have also been studied which are well compiled in the review.[155]

1.6 Zeolite used in the present study

In the present study, two zeolites namely, LTL and BEA have been extensively studying for the synthesis of zeolite-based micro-mesoporous composites discussed as follows. Chemical composition and porous structures of zeolites are tabulated in Table 1.5.

1.6.1 LTL zeolite

Linde type L zeolite (LTL) is a member of large pore 12-membered ring zeolite family with unique one-dimensional pore (1-D) pore structure.[156] Structurally, it comprises cancrinite cages and doubles six-membered rings to form columns in c-direction leading the pore diameter of 7.1 Å.[17] Compositionally, its framework is defined by the Si/Al ratio of about 3.05±0.45. Zeolite LTL with K^+ as an extra framework charge balancing cation (K/LTL) is conventionally prepared by hydrothermal crystallization of $K_2O–Al_2O_3–SiO_2–H_2O$ gel system.[157] Zeolite LTL showed excellent sorption properties and heterogeneous base catalysis due to ordered porous structure and confined void spaces.[156-159] The catalytic activity comparison and sulfur tolerance are reported over platinum supported

acidic and alkaline LTL zeolite.[160] Recently, a low Si/Al ratio containing LTL zeolite is reported as a host material for the supramolecular organization of molecules, complexes, and clusters.[161] Furthermore, the application of Pt supported LTL zeolite is also reported for the various chemical reactions.[162, 163]

1.6.2 BEA type Zeolite

Zeolite beta (BEA) is a crystalline aluminosilicate belongs to large pore family with a three-dimensional network of 12-membered rings. Beta zeolite has two mutually perpendicular channels with the pore diameter of 0.76 x 0.64 nm directed along the a-axis and b-axis, and helical channels with the pore diameter of 0.55 X 0.55 nm along c-axis. The crystal structures of beta zeolite are well documented in the IZC website[17] and are shown in Table 1.5. It is synthesized in the molar Si/Al range from 10 to 30. The zeolite beta comprises an intergrowth of two structures entitled polymorph A (P4122, a = 12.632 Å and c = 26.186 Å) and polymorph B (C2/c, a = 17.896 Å, b = 17.920 Å, c = 14.328 Å, and β = 114.8°) as shown in Figure 1.7. Corma et al. have proposed the structure of beta zeolite with Polymorph C (P42/mmc, a = 12.769 Å, and c = 12.977 Å).[164] Wadlinger *et al.* first synthesized the beta zeolite. These polymorphs are built by stacking of 12-membered ring in a different manner.[165]

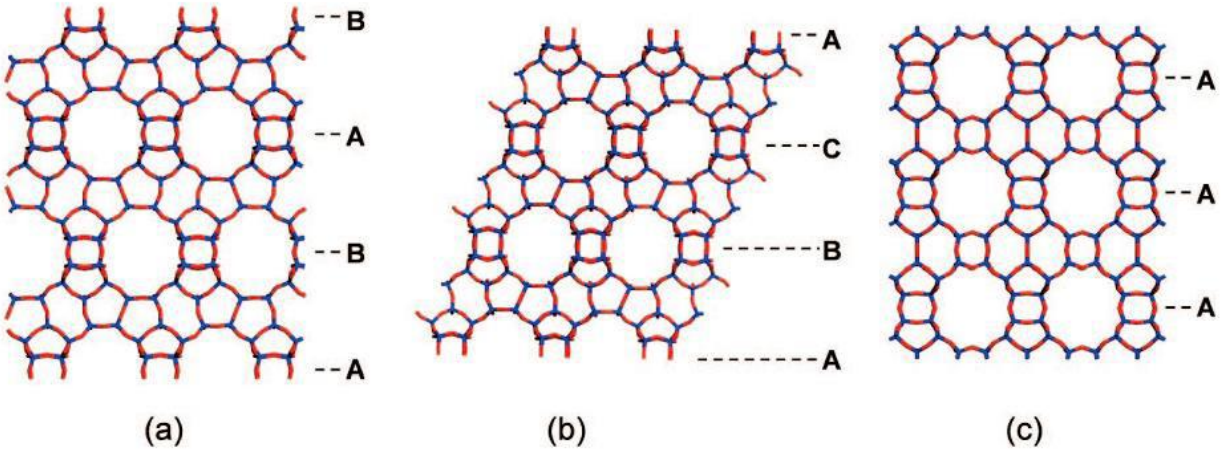

Figure 1.7. Zeolite Beta framework structures with different polymorphs: a) Polymorph A (ABAB), b) Polymorph B (ABCABC) and (c) Polymorph C (AA), parenthesis indicating the stacking of 12-membered rings

Table 1.5. Chemical composition and porous properties of zeolites studied in the present thesis

Zeolite Code	**BEA**	**LTL**
Pore Structure	Large-pore, 12 membered ring	Large-pore, 12 membered ring
Chemical Composition	Na^{+}_{7}| **[**$Al_7Si_{57}O_{128}$**]**	$K^{+}_{6}Na^{+}_{3}(H_2O)_{21}$| **[**$Al_9Si_{27}O_{72}$**]**
Pore dimension	6.6 x 6.7 Å 5.6 x 5.6 Å	7.1 x 7.1 Å
Ring structure	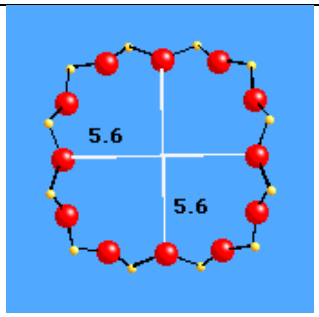 12-ring viewed along [001]	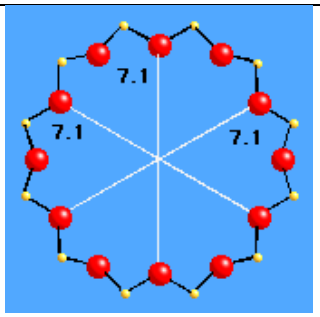 12-ring viewed along [001]
Ring structure	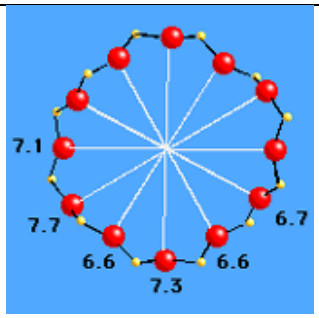 12-ring viewed along <100>	
3D Structure	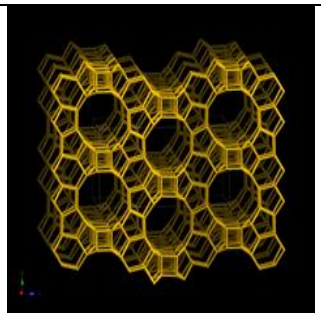 Viewed along [100]	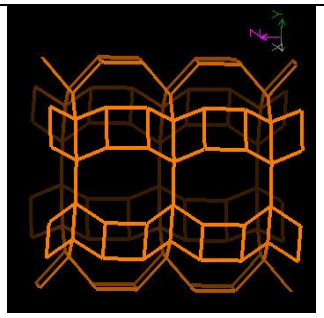 12-channel viewed [001]

The remarkable chemical and structural properties of beta zeolite make it vital catalytic material for solid acid-catalyzed reactions, because of their advantageous catalytic properties such as high surface area, micropores with molecular dimensions, desirable acidic properties, and importantly stability under thermal and chemical conditions.[166, 167] It is used as a catalyst for several reactions namely cracking,[168] isomerization,[169] alkylations,[170] and dehydration reactions. The catalytic activity of beta zeolite has been reported for various industrially important reactions such as Baeyer Villiger (BV) reaction, phenol hydroxylation, intramolecular carbonyl-ene reactions, and Meerwein–Ponndorf–Verley (MPV) reactions.

Table 1.6. Strengths and limitations of different preparative routes for hierarchical zeolites

Route	Advantages	Limitations
Hard templating	High zeolitic character Variation of Si/Al possible Applicable to different zeolites High degree of additional porosity	Pore connectivity High production costs Tuning of the additional porosity is still a challenge
Soft templating	Tunable mesoporosity Variation of Si/Al possible Applicable to different zeolites High degree of additional porosity Good pore connectivity is possible	High production costs Low to medium zeolitic character Most templates are not available commercially
Demetallation	High zeolitic character Applicable to different zeolites Applicable to wide Si/Al ratios Cost-effective High pore connectivity possible with desilication Scale-up possible	Low pore interconnectivity Dealumination is applicable to Al-rich zeolites only Expensive when organic templates/acids are involved May alter the Si/Al ratio of the parent zeolite Tuning of the additional porosity is still a challenge

Though several hard and soft templates have been used for the synthesis of micro-mesoporous composites, several advantages and disadvantages have observed during the synthesis of composites, which are discussed in brief in Table 1.6.

1.7 Biomass

The rapid growth of urban and industrial sectors with the development of the high living standards resulted in the depletion of fossil fuels and the global warming due to the generation of greenhouse gases. It is expected that the world energy consumption and petroleum demand will be increased by over 30% in the next two decades.[171] Therefore it is necessary to find a cheap alternative carbon source which is widely available and energy efficient. In conjunction with these facts, biomass is considered a promising candidate for the production of liquid fuels and chemicals.

The biomass, in general, refers to the organic materials obtained from mainly dead plants and animals. The lignocellulosic materials are non-edible oxygenated biomass to human which is nowadays a keen interest of academic and industrial researchers worldwide. The non-edible biomass is abundant, renewable and inexpensive. The use of biomass instead of petroleum product decreases the negative impact on the environment caused by the use of fossil fuel as energy resources and provides a clean and renewable energy source. Biomass is mainly comprised agricultural wastes (crops), forest waste, aquatic plants, industrial, organic part of municipal solid garbage, animal-derived organic matter as shown in Figure 1.8 that can improve our environment and economy.[172]

Among several biomass sources, the agricultural crop waste is the major source of lignocellulosic biomass for the synthesis of value-added chemicals. These biomass sources are carbon neutral, non-edible to humans, cost-effective and importantly abundantly available in the world. Annual production of renewable lignocellulosic bio-feedstocks available in India is about 700 MT.[173-176]

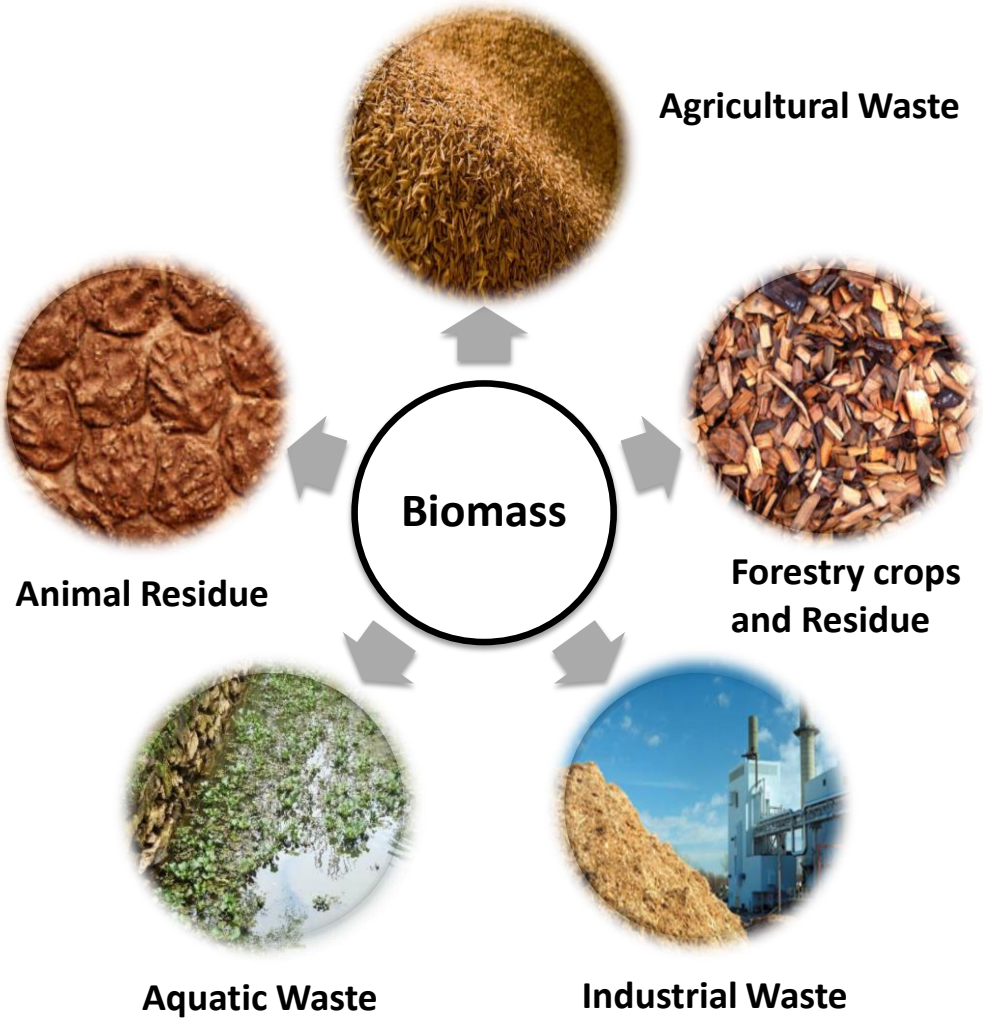

Figure 1.8. Classification of biomass

1.7.1 Chemical composition and structure of lignocellulosic biomass

The chemical composition of lignocellulosic biomass mainly depends on the type of source. The lignocellulosic biomass comprises 40-50% of cellulose (polysaccharide of glucose units), 25-35% of hemicellulose (heteropolymer of C5 and C6 sugars), and 10-25% of lignin (aromatic polymer) and, in addition to this, it consists of a lesser amount of nutrients, proteins, and wax.[177, 178]

Cellulose, an abundantly available polysaccharide, comprises about 40-50% of lignocellulosic biomass. It is a linear chain polymer of β–D–glucopyranose monosaccharide units which are linked together by β-(1→4) glycosidic linkage (Figure 1.9).[179] Owing to the

intra and inter-molecular hydrogen bonds, cellulose processes crystalline nature.[180, 181] Due to lack of an enzyme required for cellulose hydrolysis, humans can be digested easily. But it has many applications in industries like paper and garments industries.

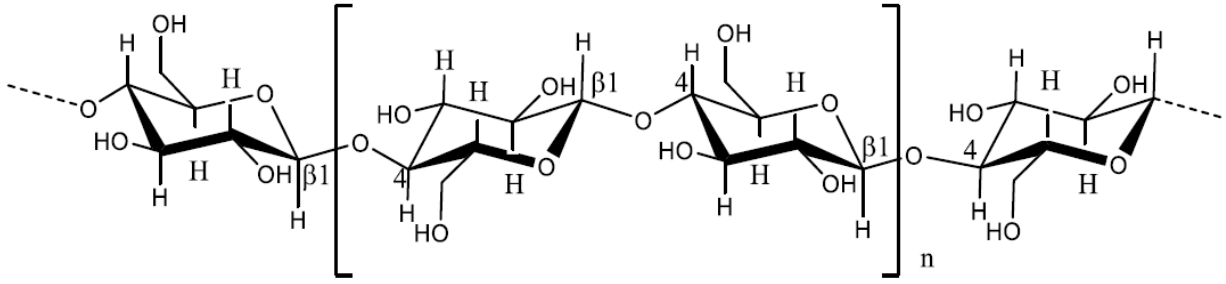

Figure 1.9. Structure of cellulose

Hemicellulose, a second most abundant polysaccharide, comprises about 15–30% of lignocellulosic biomass. Depending on the source of the plant, the hemicellulose can be made up of polysaccharide or homo-polysaccharide of C5 or C6 sugars. On the basis of chemical composition, the hemicellulose can be referred as xylan (polysaccharide of xylose), arabinan (arabinose), glucomannan (glucose and mannose), arabinogalactan (arabinose and galactose), etc. Structurally, the hemicelluloses (xylan) are a polymer of D-xylopyranose units which are joined by β-(1→4) linkage (Figure 1.10). In hardwood hemicellulose, the xylan is the major constituent whereas, in softwood hemicellulose the major component is glucomannan. [182, 183]

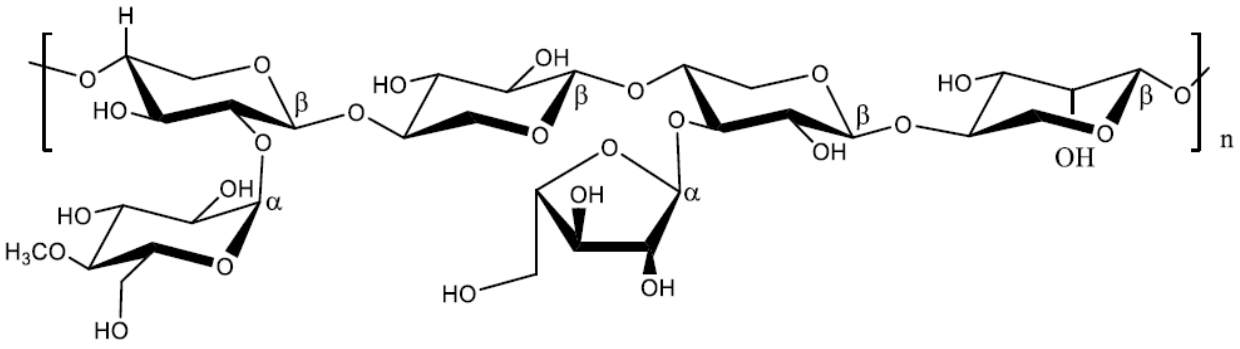

Figure 1.10. Structure of hemicellulose

Lignin is a three dimensional, complex polymer of aromatic compounds and constitutes about 15-30% of lignocellulosic biomass.[183, 184] The phenyl propane monomers are the fundamental building units present in the lignin including, coniferyl alcohol, sinapyl

alcohol, and coumaryl alcohol) (Figure 1.11). These building units are bonded by either carbon-oxygen or carbon-carbon linkages. However, the precise structure of the lignin is not predicted clearly. Since, its structure development is depended on the several geological factors such as age, location, and type of plants. Another important factor governing the structure of lignin is isolation method. It has been reported that the lignin undergoes some structural changes during extraction.[185] Considering the importance of building units, lignin has wide applications in the synthesis of fine chemicals and biofuels.

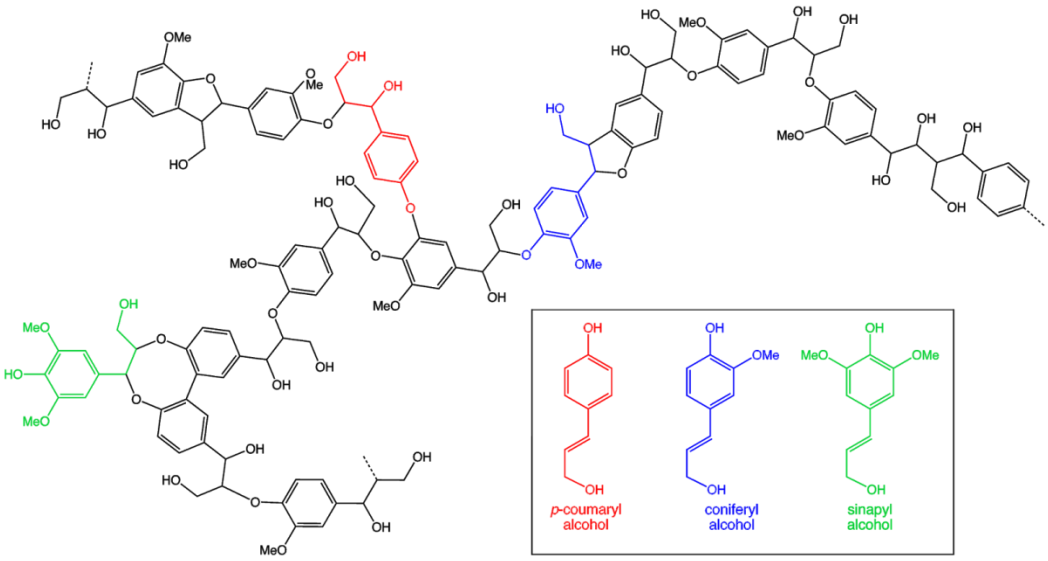

Figure 1.11. Structure of lignin

1.7.2 Valorization of sugars

The catalytic conversion of non-edible lignocellulosic biomass, comprising mainly cellulose, hemicelluloses, and lignin to the value-added chemicals and transportation fuels has intensely investigated in recent years.[186-188] Out of which the polysaccharides, viz. cellulose and hemicelluloses are made up of linking of several monosaccharide units, sugars. The hydrolysis of cellulose and hemicellulose can yield fundamental monosaccharide units, C5, and C6 sugars. These sugars can be further converted into value-added chemicals using a wide variety of the catalysts. U.S. Department of Energy has recognized several Top values added chemicals as shown below [Top Value Added Chemicals From Biomass, Vol. 1: Results of Screening for Potential Candidates from Sugars and Synthesis Gas, 2004].

Top value added chemicals from biomass

C3- glycerol, 3-hydroxypropionic acid

C4- succinic acid, fumaric acid, malic acid, aspartic acid, 3-hydroxybutyrolactone

C5- glutamic acid, itaconic acid, levulinic acid, xylitol

C6- 2,5-furan dicarboxylic acid, glucaric acid, sorbitol

Cellulose is a polymer of glucose units which on the hydrolysis yields glucose. Similarly, hemicelluloses are made up of several C5 sugars (xylose, arabinose) and C6 sugars (glucose, galactose, mannose). Depending on the compositions of the hemicelluloses, the hydrolysis will yield different types of sugars. These sugars acting as a fundamental building unit and undergo several transformations reactions to give value-added chemicals, such as sugar alcohols, e.g. xylitol, and arabitol (hydrogenation products), and furans, 5- hydroxymethylfurfural (dehydration product).

In the present thesis, two reactions namely, hydrogenation of xylose to sugar alcohols and the dehydration of fructose to HMF were studied.

1.7.2.1 Sugar alcohols

Sugar alcohols are a class of polyols or polyhydroxy alcohols, which is obtained by the hydrogenation of sugars. These sugars are further classified as aldoses (having aldehyde as a functional group) and ketoses (having ketone as a functional group). The carbonyl group of aldehyde or ketone of sugars in presence of active metal and hydrogen yields the sugar alcohols. The general formula of sugar alcohol is $HOCH_2(CHOH)nCH_2OH$. The names of most of the sugar alcohols are derived from their respective sugars. The sugar alcohol, Xylitol, is the named from the sugar, xylose, from which it is obtained. In sugar alcohols, each carbon atom in the chain has one –OH group attached and differentiated according to the orientation of the –OH group with the similar molecular formula. For example, the xylitol and arabitol are the epimers of each other with the same molecular formula, but they have a different orientation of one –OH group in space as shown in Figure 1.12.

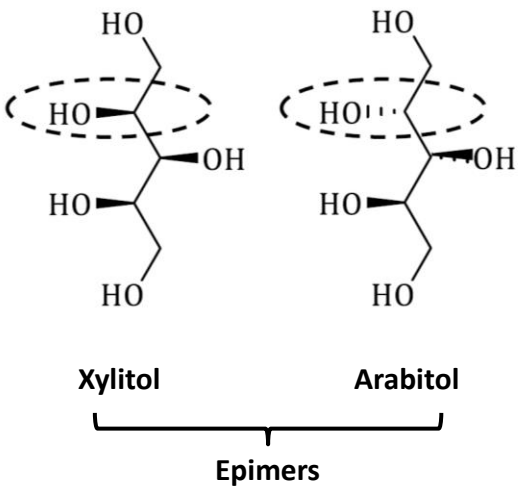

Figure 1.12. Structures if xylitol and sorbitol

These sugar alcohols are crystalline, water-soluble, sweet in the test, thermally and chemically stable, chemical stability at a wide range of pH, excellent moisture stabilizing effect, preserving effect and importantly, high microbial stability. Owing to these properties, sugar alcohols have several applications in pharmaceuticals, chemicals synthesis, food additives, cosmetic, oral and personal care.[189] For example, xylitol, mannitol, sorbitol, and erythritol.

1.7.2.1.1 Xylitol

Xylitol is a pentacarbon sugar alcohol naturally occurring in fruits and vegetables and mainly derived industrially by the hydrogenation of xylose (Scheme 1.1). It has verities of applications in pharmaceutical, food, cosmetics and polymer industry. Xylitol is used as a low-calorie sweetener, having anti-caries and non-diabetes properties. Xylitol is also used in the pharmaceutical, food and cosmetic industries. The world worldwide production of xylitol is about 2.4 x 104 TPA (tons per annum).[190] Owing to the several applications of the sugar alcohols, a demand for sugar alcohols is continuously increasing. Therefore, the researchers are seeking to develop a new efficient catalytic system for the conversion of sugars and sugar alcohols under amenable reaction conditions.

Xylitol can be prepared by different processes such as enzymatic, microbial and chemical process.[191-195] The enzymatic process produces almost 96% xylitol yield from xylose without any issue regards to the recycling, environment, energy consumption.

However, due to the preparation of coenzyme regeneration, the process becomes costlier. The microbial process involves the conversion of xylose into xylitol using wild-type of yeast and recombinant yeast. The 65-85% yield of xylitol can be obtained using wild-type yeast, whereas 86-100% xylitol yield can be achieved using recombinant yeast. Though a microbial process is cost effective and environmentally benign, it is associated with the limitations such as time-consuming process, and recyclability issue. [191-196]

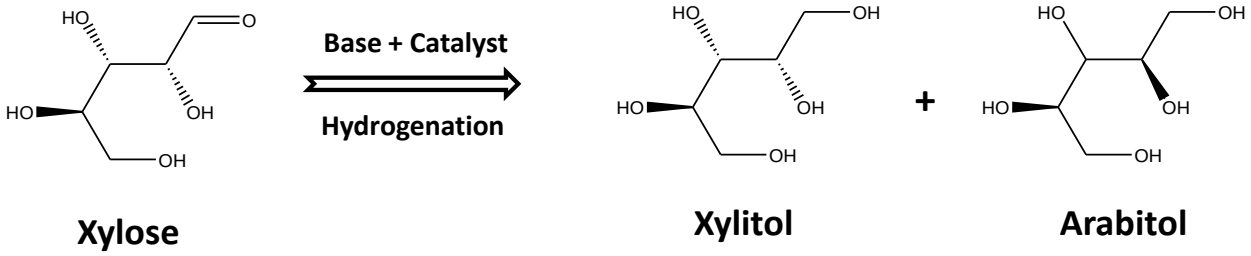

Scheme 1.1. Hydrogenation of xylose to sugar alcohols

The xylose hydrogenation is conventionally carried out in presence of Raney-nickel® and other noble metal (Pt, Pd, Ru) catalysts.[197, 198, 199] Bae et al. have reported the conversion of xylan to yield 50-60% of xylitol.[200] However, secondary processes such as catalyst and products separation and the purification are the major limitations of the mentioned process. The leaching of active metal, fouling of the catalyst with high reaction temperature and hydrogen pressure led to finding a new catalytic system which would operate under simple reaction conditions.[201-203] Considering the above drawbacks, several heterogeneous noble metals loaded on supports have been studied extensively. The noble metals like Pt and Pd on metal oxides, e.g. NiO, TiO_2, Al_2O_3, zeolites, e.g. HYZ, have been recently studied for the hydrogenation of xylose to xylitol.[204-207] Barbaro et al. have reported the Ru supported NiO-TiO_2 showing higher catalytic activity and showing a 99% yield of xylitol with 100% product selectivity.[208] The xylose conversion was achieved at a reactant concentration of 20 *wt%* at 120 °C and 5.5 MPa H_2 pressure. Moreover, Hernandez-Mejia reported the Ru@Dowex-H catalyst showing a 99.7% conversion of xylose with 99.3% xylitol yield at 120 °C and 3 MPa H_2.[199] However, the higher reaction temperature, hydrogen pressure and longer time required for the complete xylose conversion are the major drawbacks of the currently reported literature. Previous

literature from our group has reported that Pt impregnated on γ-Al_2O_3 catalyst showed enhanced hydrogenation of xylose to sugar alcohols in presence of hydrotalcite as a solid base at a lower temperature of 60 ^oC.[209] The detailed characterization showed that in alkaline media, the higher fraction of sugars were present in the open chain by undergoing Lobry de Bruyn-Albeda van Ekenstein transformation (discussed discussion in a later chapter). This open chain sugars were easily subjected for the hydrogenation by using Pt/γ-Al_2O_3 catalyst.

1.7.2.2 5-Hydroxymethylfurfural (HMF)

According to the US-DOE, the HMF is one of the top biobased versatile intermediate used as a precursor for production of various value-added chemicals, furan-based polymers, and bio-fuels.[210-212] HMF is low-melting solid and it is soluble in water and organic solvents, for example, MIBK, DMF, etc. The molecule contains both aldehyde and alcohol, functional groups. HMF is produced by the heating or cooking of sugar-containing foods. Industrially, it is mainly obtained from glucose or fructose. Glucose can be isomerized into fructose, which is dehydrated further in presence of an acid catalyst to give HMF. It is used as a food improvement agent, flavoring agent, biomarker in food industries and treated as a platform chemical for the production of value-added chemicals and fuels as shown in scheme 1.2.

HMF is conveniently produced by the dehydration of monosaccharide feedstock, fructose, in the presence of acid catalyst (Brønsted acid sites are desirable). Several homogeneous and heterogeneous acid catalysts such as mineral acids[211-213], supported hetropolyacids,[214] ionic liquids,[215] oxides,[216, 217] phosphates,[218, 219] and acidic ion-exchange resins[220, 221] have been reported. Considering the industrial demand of sustainable fuel resource, the designing of catalytic process benign, simple, efficient, and non-toxic catalyst for fructose dehydration into HMF is challenging. The heterogeneous Brønsted acid catalyst, for instance, a protonic form of the zeolite may offer potential advantages of avoiding corrosion, ease of separation and recyclability.

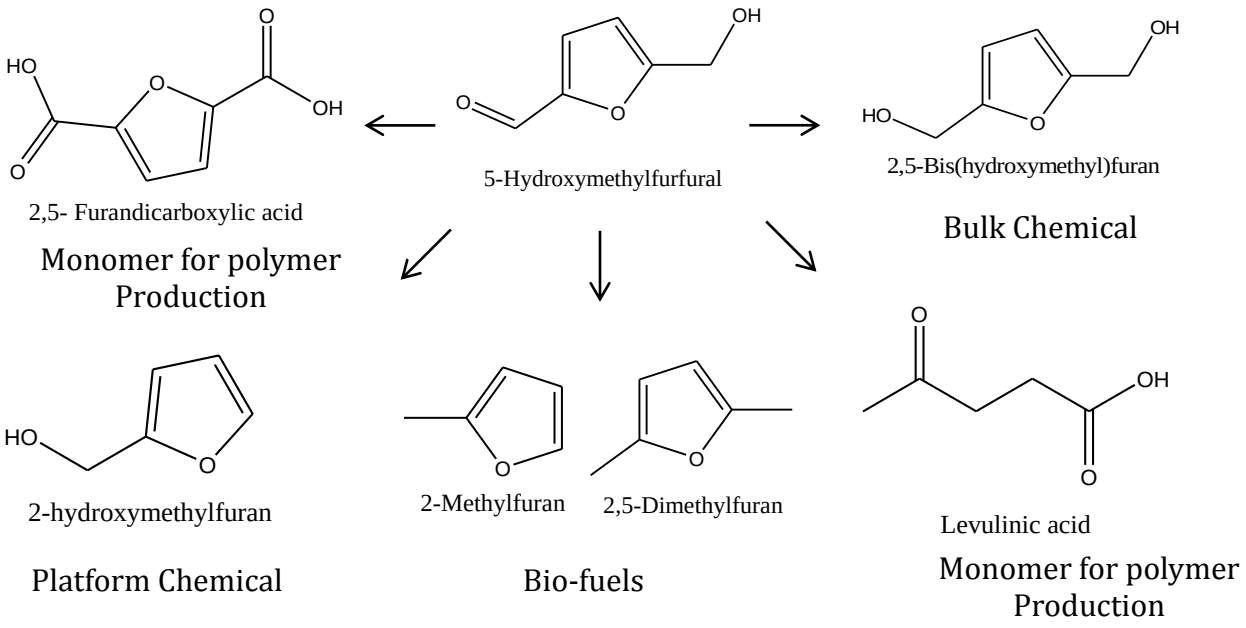

Scheme 1.2. Various applications of HMF

1.8 Scope and objectives of the thesis

By considering the several methods of preparation as discussed in above sections, the thesis focused on the development of an efficient interconnection of micropores and mesopores within the single system to enhance the accessibility of active sites and shorter diffusion path lengths for reactants and products. The ultimate goal is the synthesis, characterization and the catalytic applications of micro-mesoporous composites to advance existing knowledge in the area of heterogeneous catalysis by micro-mesoporous composites study.

Following are the objectives of my research work:

1. To develop efficient methods for the synthesis of zeolite (K/LTL or H/BEA) based micro-mesoporous composites with interconnected micropores and mesopores. To achieve this objective, the following methods of preparation were taken into consideration.
    a. Post-synthesis modification: In this method, the micro-mesoporous K/LTL zeolites were prepared by treating zeolite varying alkali concentration with different molar $Si_{(K/LTL\ zeolite)}/OH^-_{(aq.\ KOH)}$ ratio.
    b. Two-step crystallization method: In this method, the controlled synthesis of zeolite nanocrystals, primary and/or secondary building units was accomplished and subsequently subjected for the further hydrothermal crystallization to achieve mesophase.
    c. Seeding method: In the seeding method, fully grown zeolite crystals were utilized as a seed for the synthesis of micro-mesoporous composites.
2. Optimization of synthesis variables of zeolite-based micro-mesoporous composites to enhance molecular mass diffusion and thermal/hydrothermal stability.
    a. Explore the effects of various synthesis parameters and their optimization
    b. To study the physico-chemical properties, several analytical techniques were used such as PXRD, FTIR, TG/DTG, TPD, XPS, N_2 adsorption, and desorption measurements, SEM, TEM, HR-TEM, UV-Vis spectroscopy, and elemental analysis.
3. Catalytic evaluation of micro-mesoporous composites in the valorization of sugars
    a. Solid base promoted supported metal catalyzed hydrogenation of xylose to sugar alcohols

b. Brønsted acidic dehydration of fructose to HMF in a biphasic system

c. To develop a qualitative and quantitative approach based on the physico-chemical characterization useful to correlate the catalytic performance.

4. Structure-activity correlation of interconnected micro-mesoporous composites

a. A comprehensive understanding of the catalytic activity over synthesized micro-mesoporous composites was carried out and importantly, the interconnected micro-mesopores of the composites were studied to demonstrate the effective mass diffusion. Moreover, the factors governing the catalytic activity were also investigated. The thesis attempts to furnish insights into the synthesis of zeolite-based micro-mesoporous composites for the valorization of sugars.

b. To design new pathways for the synthesis of catalysts and green processes in fine renewable chemistry.

1.9 Outline of the thesis

The thesis is divided into seven chapters. Chapter 1 provides a brief introduction of the topic and overview of microporous, mesoporous and micro-mesoporous composites molecular sieves. Further details on the methods of preparation of micro-mesoporous composites to overcome the drawbacks of conventional zeolites are described. A brief introduction to the biomass and the applications of composites in the valorization of sugars is discussed. Finally, the scope and objective of the research work are outlined briefly.

Chapter 2 describes the synthesis and characterization of micro-mesoporous composites by different methods of preparation. Moreover, it also includes the synthesis of 3.5 *wt%* Pt-Al_2O_3 catalyst for the hydrogenation reactions. The detailed experimental details and the characterization techniques such as PXRD, ICP-OES, FTIR, NH_3/CO_2 TPD, ^{29}Si and ^{27}Al MAS-NMR, SEM, TEM, HR-TEM, TGA, N_2 adsorption-desorption measurements, and UV-Vis analysis are also discussed in brief. The detailed experimental procedure and methods for analysis of reaction mixture have been explained.

Chapter 3 deals with the results of synthesis and the characterization of micro-mesoporous K/LTL zeolites with varying degree of mesoporosity by post-synthesis modification (demetallation) are described. The influence of the alkali concentration on the chemical composition, powder XRD crystallinity, morphology, basicity, and the textural properties of resultant micro-mesoporous K/LTL zeolites are explained. The catalytic performance of the synthesized materials was assessed for hydrogenation of xylose to sugar alcohols. The different process parameters were evaluated in order to maximize the hydrogenation activity.

Chapter 4 describes the synthesis and characterization of micro-mesoporous K/LTL-MCM-41 composites varying molar SiO_2/Al_2O_3 ratio by recycling of waste mother liquor containing preformed LTL zeolite crystals and unutilized reagents (Soft templating). The synthesis parameters such as crystallization time, water content and molar SiO_2/Al_2O_3 ratio for the optimization of composites are discussed. The influence of the molar SiO_2/Al_2O_3 ratio on the porous properties and the morphology of the composites are discussed. The catalytic activity of micro-mesoporous K/LTL-MCM-41 composites was

correlated with the accessibility of basic sites and the interconnected micro-mesopores is assessed as a solid base in the hydrogenation of xylose to sugar alcohols.

Chapter 5 deals with the synthesis and characterization of zeolite K/LTL based micro-mesoporous composites were prepared by different methods of preparation, namely, post-synthesis modification, seeding method, and two-step crystallization method. The influence of the methods of preparation on the structure of composites and their activity has been thoroughly discussed in the hydrogenation of xylose to xylitol as a solid base. Moreover, the basicity of the composites was tested using a Knoevenagel condensation reaction. The zeolite K/LTL based micro-mesoporous composites were also tested as catalysts in the transesterification of soybean oil with methanol to biodiesel.

In chapter 6, the results of synthesis and characterization of Brønsted acidic zeolite H/BEA based micro-mesoporous composites were prepared by seeding method (Soft templating). The catalytic activity of the synthesized composites was performed in the Brønsted acid catalyzed fructose to HMF dehydration reaction.

Chapter 7 summarizes the conclusions of the thesis and novelty of the work and conclusive remarks for future research.

1.10 References

1. J. W. McBain, *The Sorption of Gases and Vapors by Solids; Routledge and Sons: London, UK,*, 1932, 169.
2. A. Corma, *Chemical Reviews*, 1997, **97**, 2373-2420.
3. A. Corma, V. Fornes, S. B. Pergher, T. L. M. Maesen and J. G. Buglass, *Nature*, 1998, **396**, 353.
4. G. W. Huber and A. Corma, *Angewandte Chemie International Edition*, 2007, **46**, 7184-7201.
5. K. Moller and T. Bein, *Chemical Society Reviews*, 2013, **42**, 3689-3707.
6. J. Č. a. S. Mintova, *Catalysis Reviews*, 2007, **49**, 457-509.
7. Z. ALOthman, *Materials*, 2012, **5**, 2874.
8. M. E. Davis, *Nature*, 1993, **364**, 391.
9. M. Tsapatsis, *AIChE Journal*, 2002, **48**, 654-660.
10. A. Stein, *Advanced Materials*, 2003, **15**, 763-775.
11. J. Rouquerol, D. Avnir, C. Fairbridge, D. H. Everett, J. M. Haynes, N. Pernicone, J. D. F. Ramsay, K. Sing and K. Unger, *Recommendations for the Characterization of Porous Solids*, 1994.
12. E. M. Flanigen, in *Studies in Surface Science and Catalysis*, eds. H. van Bekkum, E. M. Flanigen and J. C. Jansen, Elsevier, 1991, vol. 58, pp. 13-34.
13. A. E. W. Beers, J. A. van Bokhoven, K. M. de Lathouder, F. Kapteijn and J. A. Moulijn, *Journal of Catalysis*, 2003, **218**, 239-248.
14. R. M. Barrer and D. W. Brook, *Transactions of the Faraday Society*, 1953, **49**, 1049-1059.
15. D. W. Breck, W. G. Eversole and R. M. Milton, *Journal of the American Chemical Society*, 1956, **78**, 2338-2339.
16. D. W. Breck, W. G. Eversole, R. M. Milton, T. B. Reed and T. L. Thomas, *Journal of the American Chemical Society*, 1956, **78**, 5963-5972.
17. http://www.iza-online.org/.
18. M. Müller, G. Harvey and R. Prins, *Microporous and Mesoporous Materials*, 2000, **34**, 135-147.

19. J. Kärger and D. Freude, *Chemical Engineering & Technology*, 2002, **25**, 769-778.
20. J. C. Groen, J. C. Jansen, J. A. Moulijn and J. Pérez-Ramírez, *The Journal of Physical Chemistry B*, 2004, **108**, 13062-13065.
21. D. Verboekend, T. C. Keller, M. Milina, R. Hauert and J. Pérez-Ramírez, *Chemistry of Materials*, 2013, **25**, 1947-1959.
22. S. Kulawong, S. Prayoonpokarach, A. Neramittagapong and J. Wittayakun, *Journal of Industrial and Engineering Chemistry*, 2011, **17**, 346-351.
23. M. E. Davis, C. Saldarriaga, C. Montes, J. Garces and C. Crowdert, *Nature*, 1988, **331**, 698.
24. C. C. Freyhardt, M. Tsapatsis, R. F. Lobo, K. J. Balkus Jr and M. E. Davis, *Nature*, 1996, **381**, 295.
25. K. G. Strohmaier and D. E. W. Vaughan, *Journal of the American Chemical Society*, 2003, **125**, 16035-16039.
26. A. Corma, M. J. Díaz-Cabañas, F. Rey, S. Nicolopoulus and K. Boulahya, *Chemical Communications*, 2004, DOI: 10.1039/B406572G, 1356-1357.
27. A. Corma, M. J. Díaz-Cabañas, J. Martínez-Triguero, F. Rey and J. Rius, *Nature*, 2002, **418**, 514.
28. A. Corma, M. J. Díaz-Cabañas, J. L. Jordá, C. Martínez and M. Moliner, *Nature*, 2006, **443**, 842.
29. D. K. Mishra, A. A. Dabbawala and J.-S. Hwang, *Journal of Molecular Catalysis A: Chemical*, 2013, **376**, 63-70.
30. Y. Kathiraser, J. Ashok and S. Kawi, *Catalysis Science & Technology*, 2016, **6**, 4327-4336.
31. L. B. Malihan, G. M. Nisola, N. Mittal, S.-P. Lee, J. G. Seo, H. Kim and W.-J. Chung, *RSC Advances*, 2016, **6**, 33901-33909.
32. S. Srivastava, P. Mohanty, J. K. Parikh, A. K. Dalai, S. S. Amritphale and A. K. Khare, *Chinese Journal of Catalysis*, 2015, **36**, 933-942.
33. H. I. Lee, H. J. Park, Y.-K. Park, J. Y. Hur, J.-K. Jeon and J. M. Kim, *Catalysis Today*, 2008, **132**, 68-74.
34. M. Käldström, N. Kumar and D. Y. Murzin, *Catalysis Today*, 2011, **167**, 91-95.

35. K. Hao, B. Shen, Y. Wang and J. Ren, *Journal of Industrial and Engineering Chemistry*, 2012, **18**, 1736-1740.
36. S. K. Saxena, N. Viswanadham and M. O. Garg, *Journal of Industrial and Engineering Chemistry*, 2014, **20**, 3875-3883.
37. R. C. Hansford, *Industrial & Engineering Chemistry*, 1947, **39**, 849-852.
38. D. Barthomeuf, *Materials Chemistry and Physics*, 1987, **17**, 49-71.
39. D. Barthomeuf∗, *Catalysis Reviews*, 1996, **38**, 521-612.
40. A. P. Bolton and M. A. Lanewala, *Journal of Catalysis*, 1970, **18**, 1-11.
41. J. Gałuszka, A. Barański and S. Cęckiewicz, *Journal of the Chemical Society, Faraday Transactions 1: Physical Chemistry in Condensed Phases*, 1978, **74**, 146-152.
42. E. G. Derouane, J. C. Védrine, R. R. Pinto, P. M. Borges, L. Costa, M. A. N. D. A. Lemos, F. Lemos and F. R. Ribeiro, *Catalysis Reviews*, 2013, **55**, 454-515.
43. D. Barthomeuf, *Microporous and Mesoporous Materials*, 2003, **66**, 1-14.
44. D. Barthomeuf, in *Studies in Surface Science and Catalysis*, eds. H. Chon, S.-K. Ihm and Y. S. Uh, Elsevier, 1997, vol. 105, pp. 1677-1706.
45. N. P. Tangale, S. K. Sonar, P. S. Niphadkar and P. N. Joshi, *Journal of Industrial and Engineering Chemistry*, 2016, **40**, 128-136.
46. T. S. a. K. K. a. C. K. T. Yanagisawa, *Bulletin of the Chemical Society of Japan*, 1990, **63**, 988-992.
47. J. S. Beck, J. C. Vartuli, W. J. Roth, M. E. Leonowicz, C. T. Kresge, K. D. Schmitt, C. T. W. Chu, D. H. Olson, E. W. Sheppard, S. B. McCullen, J. B. Higgins and J. L. Schlenker, *Journal of the American Chemical Society*, 1992, **114**, 10834-10843.
48. C. T. Kresge, M. E. Leonowicz, W. J. Roth, J. C. Vartuli and J. S. Beck, *Nature*, 1992, **359**, 710.
49. M. Dubois, T. Gulik-Krzywicki and B. Cabane, *Langmuir*, 1993, **9**, 673-680.
50. J. C. Vartuli, K. D. Schmitt, C. T. Kresge, W. J. Roth, M. E. Leonowicz, S. B. McCullen, S. D. Hellring, J. S. Beck and J. L. Schlenker, *Chemistry of Materials*, 1994, **6**, 2317-2326.
51. D. Zhao, J. Sun, Q. Li and G. D. Stucky, *Chemistry of Materials*, 2000, **12**, 275-279.
52. M. Colilla, F. Balas, M. Manzano and M. Vallet-Regí, *Chemistry of Materials*, 2007, **19**, 3099-3101.

53. J. Puputti, H. Jin, J. Rosenholm, H. Jiang and M. Lindén, *Microporous and Mesoporous Materials*, 2009, **126**, 272-275.

54. L. M. Chua, T. Vazhnova, T. J. Mays, D. B. Lukyanov and S. P. Rigby, *Journal of Catalysis*, 2010, **271**, 401-412.

55. K. Y. Nandiwale, S. K. Sonar, P. S. Niphadkar, P. N. Joshi, S. S. Deshpande, V. S. Patil and V. V. Bokade, *Applied Catalysis A: General*, 2013, **460–461**, 90-98.

56. J. C. Groen, W. Zhu, S. Brouwer, S. J. Huynink, F. Kapteijn, J. A. Moulijn and J. Pérez-Ramírez, *Journal of the American Chemical Society*, 2007, **129**, 355-360.

57. D. P. Serrano, J. M. Escola and P. Pizarro, *Chemical Society Reviews*, 2013, **42**, 4004-4035.

58. D. Verboekend and J. Perez-Ramirez, *Catalysis Science & Technology*, 2011, **1**, 879-890.

59. Y. Wei, T. E. Parmentier, K. P. de Jong and J. Zecevic, *Chemical Society Reviews*, 2015, **44**, 7234-7261.

60. L.-H. Chen, X.-Y. Li, J. C. Rooke, Y.-H. Zhang, X.-Y. Yang, Y. Tang, F.-S. Xiao and B.-L. Su, *Journal of Materials Chemistry*, 2012, **22**, 17381-17403.

61. V. Valtchev, G. Majano, S. Mintova and J. Pérez-Ramírez, *Chemical Society Reviews*, 2013, **42**, 263-290.

62. C. Robin, G. Corine, B. Metin and v. D. Sander, *ChemCatChem*, 2011, **3**, 67-81.

63. D. Trong On, D. Lutic and S. Kaliaguine, *Microporous and Mesoporous Materials*, 2001, **44-45**, 435-444.

64. D. Trong On and S. Kaliaguine, *Angewandte Chemie International Edition*, 2001, **40**, 3248-3251.

65. K. Li, J. Valla and J. Garcia-Martinez, *ChemCatChem*, 2014, **6**, 46-66.

66. J. Wang, J. C. Groen, W. Yue, W. Zhou and M.-O. Coppens, *Chemical Communications*, 2007, DOI: 10.1039/B708822A, 4653-4655.

67. J. Wang, W. Yue, W. Zhou and M.-O. Coppens, *Microporous and Mesoporous Materials*, 2009, **120**, 19-28.

68. W. Xu, J. Dong, J. Li, J. Li and F. Wu, *Journal of the Chemical Society, Chemical Communications*, 1990, DOI: 10.1039/C39900000755, 755-756.

69. M. Matsukata, M. Ogura, T. Osaki, P. R. Hari Prasad Rao, M. Nomura and E. Kikuchi, *Topics in Catalysis*, 1999, **9**, 77-92.

70. J. Zhou, Z. Hua, X. Cui, Z. Ye, F. Cui and J. Shi, *Chemical Communications*, 2010, **46**, 4994-4996.

71. K. Möller, B. Yilmaz, R. M. Jacubinas, U. Müller and T. Bein, *Journal of the American Chemical Society*, 2011, **133**, 5284-5295.

72. C. Li, Y. Wang, B. Shi, J. Ren, X. Liu, Y. Wang, Y. Guo, Y. Guo and G. Lu, *Microporous and Mesoporous Materials*, 2009, **117**, 104-110.

73. C. J. H. Jacobsen, C. Madsen, J. Houzvicka, I. Schmidt and A. Carlsson, *Journal of the American Chemical Society*, 2000, **122**, 7116-7117.

74. I. Schmidt, A. Krogh, K. Wienberg, A. Carlsson, M. Brorson and C. J. H. Jacobsen, *Chemical Communications*, 2000, DOI: 10.1039/B006460M, 2157-2158.

75. M. Y. Kustova, P. Hasselriis and C. H. Christensen, *Catalysis Letters*, 2004, **96**, 205-211.

76. X. Wei and P. G. Smirniotis, *Microporous and Mesoporous Materials*, 2006, **89**, 170-178.

77. K. Egeblad, M. Kustova, S. K. Klitgaard, K. Zhu and C. H. Christensen, *Microporous and Mesoporous Materials*, 2007, **101**, 214-223.

78. A. H. Janssen, I. Schmidt, C. J. H. Jacobsen, A. J. Koster and K. P. de Jong, *Microporous and Mesoporous Materials*, 2003, **65**, 59-75.

79. I. Schmidt, A. Boisen, E. Gustavsson, K. Ståhl, S. Pehrson, S. Dahl, A. Carlsson and C. J. H. Jacobsen, *Chemistry of Materials*, 2001, **13**, 4416-4418.

80. S.-S. Kim, J. Shah and T. J. Pinnavaia, *Chemistry of Materials*, 2003, **15**, 1664-1668.

81. Z. X. Yang, Y. D. Xia and R. Mokaya, *Advanced Materials*, 2004, **16**, 727-732.

82. Y. Tao, H. Kanoh and K. Kaneko, *The Journal of Physical Chemistry B*, 2003, **107**, 10974-10976.

83. B. T. Holland, L. Abrams and A. Stein, *Journal of the American Chemical Society*, 1999, **121**, 4308-4309.

84. Y. Tao, Y. Hattori, A. Matumoto, H. Kanoh and K. Kaneko, *The Journal of Physical Chemistry B*, 2005, **109**, 194-199.

85. W.-C. Li, A.-H. Lu, R. Palkovits, W. Schmidt, B. Spliethoff and F. Schüth, *Journal of the American Chemical Society*, 2005, **127**, 12595-12600.

86. A. Dong, Y. Wang, Y. Tang, N. Ren, Y. Zhang, Y. Yue and Z. Gao, *Advanced Materials*, 2002, **14**, 926-929.

87. A. G. Machoke, A. M. Beltrán, A. Inayat, B. Winter, T. Weissenberger, N. Kruse, R. Güttel, E. Spiecker and W. Schwieger, *Advanced Materials*, 2015, **27**, 1066-1070.

88. H. Zhu, Z. Liu, Y. Wang, D. Kong, X. Yuan and Z. Xie, *Chemistry of Materials*, 2008, **20**, 1134-1139.

89. Y. Tao, H. Kanoh and K. Kaneko, *Langmuir*, 2005, **21**, 504-507.

90. M. Kustova, K. Egeblad, K. Zhu and C. H. Christensen, *Chemistry of Materials*, 2007, **19**, 2915-2917.

91. X. Wang, G. Li, W. Wang, C. Jin and Y. Chen, *Microporous and Mesoporous Materials*, 2011, **142**, 494-502.

92. Y. Fang and H. Hu, *Journal of the American Chemical Society*, 2006, **128**, 10636-10637.

93. A. Sakthivel, S.-J. Huang, W.-H. Chen, Z.-H. Lan, K.-H. Chen, T.-W. Kim, R. Ryoo, A. S. T. Chiang and S.-B. Liu, *Chemistry of Materials*, 2004, **16**, 3168-3175.

94. K. R. Kloetstra, H. W. Zandbergen, J. C. Jansen and H. van Bekkum, *Microporous Materials*, 1996, **6**, 287-293.

95. M. Choi, H. S. Cho, R. Srivastava, C. Venkatesan, D.-H. Choi and R. Ryoo, *Nature Materials*, 2006, **5**, 718.

96. G. V. Shanbhag, M. Choi, J. Kim and R. Ryoo, *Journal of Catalysis*, 2009, **264**, 88-92.

97. M. Choi, R. Srivastava and R. Ryoo, *Chemical Communications*, 2006, DOI: 10.1039/B612265E, 4380-4382.

98. K. Cho, H. S. Cho, L.-C. de Ménorval and R. Ryoo, *Chemistry of Materials*, 2009, **21**, 5664-5673.

99. Y. Fan, H. Xiao, G. Shi, H. Liu and X. Bao, *Journal of Catalysis*, 2012, **285**, 251-259.

100. A. Inayat, I. Knoke, E. Spiecker and W. Schwieger, *Angewandte Chemie International Edition*, 2012, **51**, 1962-1965.

101. W. Park, D. Yu, K. Na, K. E. Jelfs, B. Slater, Y. Sakamoto and R. Ryoo, *Chemistry of Materials*, 2011, **23**, 5131-5137.

102. D. P. Serrano, J. Aguado, J. M. Escola, J. M. Rodríguez and Á. Peral, *Chemistry of Materials*, 2006, **18**, 2462-2464.

103. H. Wang and T. J. Pinnavaia, *Angewandte Chemie International Edition*, 2006, **45**, 7603-7606.

104. F. Liu, T. Willhammar, L. Wang, L. Zhu, Q. Sun, X. Meng, W. Carrillo-Cabrera, X. Zou and F.-S. Xiao, *Journal of the American Chemical Society*, 2012, **134**, 4557-4560.

105. F.-S. Xiao, L. Wang, C. Yin, K. Lin, Y. Di, J. Li, R. Xu, D. S. Su, R. Schlögl, T. Yokoi and T. Tatsumi, *Angewandte Chemie International Edition*, 2006, **45**, 3090-3093.

106. M. Choi, K. Na, J. Kim, Y. Sakamoto, O. Terasaki and R. Ryoo, *Nature*, 2009, **461**, 246.

107. K. Na, C. Jo, J. Kim, K. Cho, J. Jung, Y. Seo, R. J. Messinger, B. F. Chmelka and R. Ryoo, *Science*, 2011, **333**, 328-332.

108. C. Jo, Y. Seo, K. Cho, J. Kim, H. S. Shin, M. Lee, J.-C. Kim, S. O. Kim, J. Y. Lee, H. Ihee and R. Ryoo, *Angewandte Chemie International Edition*, 2014, **53**, 5117-5121.

109. I. I. Ivanova and E. E. Knyazeva, *Chemical Society Reviews*, 2013, **42**, 3671-3688.

110. I. I. Ivanova, A. S. Kuznetsov, V. V. Yuschenko and E. E. Knyazeva, *Journal*, 2004, **76**, 1647.

111. S. Wang, T. Dou, Y. Li, Y. Zhang, X. Li and Z. Yan, *Catalysis Communications*, 2005, **6**, 87-91.

112. S. Inagaki, M. Ogura, T. Inami, Y. Sasaki, E. Kikuchi and M. Matsukata, *Microporous and Mesoporous Materials*, 2004, **74**, 163-170.

113. J. Y. Y. a. J. Garcia-Martinez, *U.S. Patent, 7,589,041,assigned to Massachusetts Institute of Technology*, 2009.

114. W. C. Yoo, X. Zhang, M. Tsapatsis and A. Stein, *Microporous and Mesoporous Materials*, 2012, **149**, 147-157.

115. J. García-Martínez, M. Johnson, J. Valla, K. Li and J. Y. Ying, *Catalysis Science & Technology*, 2012, **2**, 987-994.

116. Y. P. Khitev, Y. G. Kolyagin, I. I. Ivanova, O. A. Ponomareva, F. Thibault-Starzyk, J. P. Gilson, C. Fernandez and F. Fajula, *Microporous and Mesoporous Materials*, 2011, **146**, 201-207.

117. L. Tosheva and V. P. Valtchev, *Chemistry of Materials*, 2005, **17**, 2494-2513.

118. Y. Liu and T. J. Pinnavaia, *Journal of Materials Chemistry*, 2002, **12**, 3179-3190.

119. Y. Liu, W. Zhang and T. J. Pinnavaia, *Journal of the American Chemical Society*, 2000, **122**, 8791-8792.

120. K. Möller, B. Yilmaz, U. Müller and T. Bein, *Chemistry of Materials*, 2011, **23**, 4301-4310.

121. C. J. Van Oers, W. J. J. Stevens, E. Bruijn, M. Mertens, O. I. Lebedev, G. Van Tendeloo, V. Meynen and P. Cool, *Microporous and Mesoporous Materials*, 2009, **120**, 29-34.

122. Y. Fang, H. Hu and G. Chen, *Chemistry of Materials*, 2008, **20**, 1670-1672.

123. C. H. Lam, H.-Y. Chi, S.-M. Hsu, Y.-S. Li, W.-Y. Lee, I. C. Cheng and D.-Y. Kang, *RSC Advances*, 2017, **7**, 49048-49055.

124. A. Zukal, V. Patzelová and U. Lohse, *Zeolites*, 1986, **6**, 133-136.

125. J. Lynch, F. Raatz and P. Dufresne, *Zeolites*, 1987, **7**, 333-340.

126. S. Moreno and G. Poncelet, *Microporous Materials*, 1997, **12**, 197-222.

127. R. Szostak, in *Studies in Surface Science and Catalysis*, eds. H. van Bekkum, E. M. Flanigen, P. A. Jacobs and J. C. Jansen, Elsevier, 2001, vol. 137, pp. 261-297.

128. S. van Donk, A. H. Janssen, J. H. Bitter and K. P. de Jong, *Catalysis Reviews*, 2003, **45**, 297-319.

129. S. Malola, S. Svelle, F. L. Bleken and O. Swang, *Angewandte Chemie International Edition*, 2012, **51**, 652-655.

130. R. M. Lago, W. O. Haag, R. J. Mikovsky, D. H. Olson, S. D. Hellring, K. D. Schmitt and G. T. Kerr, in *Studies in Surface Science and Catalysis*, eds. Y. Murakami, A. Iijima and J. W. Ward, Elsevier, 1986, vol. 28, pp. 677-684.

131. R. J. Pellet, D. G. Casey, H. M. Huang, R. V. Kessler, E. J. Kuhlman, C. L. Oyoung, R. A. Sawicki and J. R. Ugolini, *Journal of Catalysis*, 1995, **157**, 423-435.

132. R. Dutartre, L. C. de Ménorval, F. Di Renzo, D. McQueen, F. Fajula and P. Schulz, *Microporous Materials*, 1996, **6**, 311-320.

133. M. M. L. Ribeiro Carrott, P. A. Russo, C. Carvalhal, P. J. M. Carrott, J. P. Marques, J. M. Lopes, I. Gener, M. Guisnet and F. Ramôa Ribeiro, *Microporous and Mesoporous Materials*, 2005, **81**, 259-267.

134. J. A. van Bokhoven, M. Tromp, D. C. Koningsberger, J. T. Miller, J. A. Z. Pieterse, J. A. Lercher, B. A. Williams and H. H. Kung, *Journal of Catalysis*, 2001, **202**, 129-140.

135. I. I. Ivanova, Kuznetsov, A.S., Yuschenko, V.V., and Knyazeva, E.E., *Pure Appl. Chem.*, 2004, **76**, 1647-1658.
136. G. Garralón, V. Fornés and A. Corma, *Zeolites*, 1988, **8**, 268-272.
137. B. Sulikowski, *The Journal of Physical Chemistry*, 1993, **97**, 1420-1425.
138. A. Boréave, A. Auroux and C. Guimon, *Microporous Materials*, 1997, **11**, 275-291.
139. Y. Hong and J. J. Fripiat, *Microporous Materials*, 1995, **4**, 323-334.
140. J. P. Marques, I. Gener, P. Ayrault, J. M. Lopes, F. R. Ribeiro and M. Guisnet, *Chemical Communications*, 2004, DOI: 10.1039/B409964H, 2290-2291.
141. S. van Donk, J. H. Bitter, A. Verberckmoes, M. Versluijs-Helder, A. Broersma and K. P. de Jong, *Angewandte Chemie*, 2005, **117**, 1384-1387.
142. D. A. Young, *US3326797*, 1967.
143. M.-H. Sun, S.-Z. Huang, L.-H. Chen, Y. Li, X.-Y. Yang, Z.-Y. Yuan and B.-L. Su, *Chemical Society Reviews*, 2016, **45**, 3479-3563.
144. M. Rutkowska, D. Macina, N. Mirocha-Kubień, Z. Piwowarska and L. Chmielarz, *Applied Catalysis B: Environmental*, 2015, **174-175**, 336-343.
145. Y. Wang, W. Zhao, Z. Li, H. Wang, J. Wu, M. Li, Z. Hu, Y. Wang, J. Huang and Y. Zhao, *Journal of Porous Materials*, 2015, **22**, 339-345.
146. D. Verboekend and J. Pérez-Ramírez, *Chemistry – A European Journal*, 2011, **17**, 1137-1147.
147. J. Pérez-Ramírez, D. Verboekend, A. Bonilla and S. Abelló, *Advanced Functional Materials*, 2009, **19**, 3972-3979.
148. S. Abelló, A. Bonilla and J. Pérez-Ramírez, *Applied Catalysis A: General*, 2009, **364**, 191-198.
149. J. C. Groen, J. A. Moulijn and J. Pérez-Ramírez, *Industrial & Engineering Chemistry Research*, 2007, **46**, 4193-4201.
150. J. C. Groen, S. Abelló, L. A. Villaescusa and J. Pérez-Ramírez, *Microporous and Mesoporous Materials*, 2008, **114**, 93-102.
151. A. Čižmek, B. Subotić, R. Aiello, F. Crea, A. Nastro and C. Tuoto, *Microporous Materials*, 1995, **4**, 159-168.
152. X. Wei and P. G. Smirniotis, *Microporous and Mesoporous Materials*, 2006, **97**, 97-106.

153. V. Danny, K. T. C., M. Sharon and P. R. Javier, *Advanced Functional Materials*, 2013, **23**, 1923-1934.
154. A. Bonilla, D. Baudouin and J. Pérez-Ramírez, *Journal of Catalysis*, 2009, **265**, 170-180.
155. K. M. a. T. Bein, *Comprehensive Inorganic Chemistry II, ed.Elsevier*, 2013, **7.16**.
156. H. V. R.M. Barrer, *Z. Krostallogr.* , 1969, **128**, 352-370.
157. S. D. Bhat, P. S. Niphadkar, T. R. Gaydhankar, S. V. Awate, A. A. Belhekar and P. N. Joshi, *Microporous and Mesoporous Materials*, 2004, **76**, 81-89.
158. L. J. Garces, V. D. Makwana, B. Hincapie, A. Sacco and S. L. Suib, *Journal of Catalysis*, 2003, **217**, 107-116.
159. W. Insuwan and K. Rangsriwatananon, *Journal of Porous Materials*, 2014, **21**, 345-354.
160. J. T. Miller and D. C. Koningsberger, *Journal of Catalysis*, 1996, **162**, 209-219.
161. D. Bruhwiler, G. Calzaferri, T. Torres, J. H. Ramm, N. Gartmann, L.-Q. Dieu, I. Lopez-Duarte and M. V. Martinez-Diaz, *Journal of Materials Chemistry*, 2009, **19**, 8040-8067.
162. J. Song, H. Ma, Z. Tian, L. Yan, Z. Xu, Q. Liu and W. Qu, *Applied Catalysis A: General*, 2015, **492**, 31-37.
163. P. L. De Cola, R. Gläser and J. Weitkamp, *Applied Catalysis A: General*, 2006, **306**, 85-97.
164. A. Corma, M. T. Navarro, F. Rey, J. Rius and S. Valencia, *Angewandte Chemie*, 2001, **113**, 2337-2340.
165. G. T. K. R.L. Wadlinger, E.J. Rosinski, , *US Patent 33080691*, 1967.
166. M. M. J. T. J.M. Newsam, W.T. Koetsier, C.B. de Gruyter, *Proceedings of the Royal Society of London. A. Mathematical and Physical Sciences*, 1988, **420**, 375-405.
167. J. B. Higgins, R. B. LaPierre, J. L. Schlenker, A. C. Rohrman, J. D. Wood, G. T. Kerr and W. J. Rohrbaugh, *Zeolites*, 1988, **8**, 446-452.
168. K. Smith, M. D. Ajarim, G. A. El-Hiti and C. Peters, *Topics in Catalysis*, 2009, **52**, 1696-1700.
169. K. Smith, M. D. Ajarim and G. A. El-Hiti, *Catalysis Letters*, 2010, **134**, 270-278.

170. B. M. Choudary, M. Sateesh, M. Lakshmi Kantam, K. Koteswara Rao, K. V. Ram Prasad, K. V. Raghavan and J. A. R. P. Sarma, *Chemical Communications*, 2000, DOI: 10.1039/A908011B, 25-26.

171. J. A. Geboers, S. Van de Vyver, R. Ooms, B. Op de Beeck, P. A. Jacobs and B. F. Sels, *Catalysis Science & Technology*, 2011, **1**, 714-726.

172. G. W. Huber, S. Iborra and A. Corma, *Chemical Reviews*, 2006, **106**, 4044-4098.

173. A. Kumar, N. Kumar, P. Baredar and A. Shukla, *Renewable and Sustainable Energy Reviews*, 2015, **45**, 530-539.

174. C. Somerville, H. Youngs, C. Taylor, S. C. Davis and S. P. Long, *Science*, 2010, **329**, 790-792.

175. E. Taarning, C. M. Osmundsen, X. Yang, B. Voss, S. I. Andersen and C. H. Christensen, *Energy & Environmental Science*, 2011, **4**, 793-804.

176. M. Hiloidhari, D. Das and D. C. Baruah, *Renewable and Sustainable Energy Reviews*, 2014, **32**, 504-512.

177. H. Kobayashi and A. Fukuoka, *Green Chemistry*, 2013, **15**, 1740-1763.

178. P. Mäki-Arvela, T. Salmi, B. Holmbom, S. Willför and D. Y. Murzin, *Chemical Reviews*, 2011, **111**, 5638-5666.

179. J. H. M. Berchel, S. p. S. Le Corre, J.P. Haelters, P.A. Jaffras, *Tetrahedron Letters*, 2015, **56**, 2345-2348.

180. A. Demirbas, *Energy conversion and Management*, 2000, **41**, 633-646.

181. P. B. M. Hall, J. H. Lee, M. J. Realff, A. S. Bommarius, *FEBS Journal*, 2010, **277**, 1571-1582.

182. G. W. D. Fengel, *Wood. Chemistry, Ultrastructure, Reactions, Walter de Gruyter, Berlin, Germany*, 1989.

183. E. Sjöström, *Wood Chemistry. Fundamentals and Applications, 2nd edition, Academic Press, San Diego, CA, USA*, 1993.

184. A. V. Bridgwater, *Thermal Science* 2004, **8**, 21-49.

185. P. C. A. B. J. Zakzeski, A. L. Jongerius, B. M. Weckhuysen, *Chemical Reviews*, 2010,, **110**, 3552-3599,.

186. L. D. Schmidt and P. J. Dauenhauer, *Nature*, 2007, **447**, 914.

187. X. Tong, Y. Ma and Y. Li, *Applied Catalysis A: General*, 2010, **385**, 1-13.

188. D. M. Alonso, J. Q. Bond and J. A. Dumesic, *Green Chemistry*, 2010, **12**, 1493-1513.

189. R. J. M.M. Silveira *Appl Microbiol Biotechnol*, 2002, **59**, 400-408.

190. M. G. Leisola, Tom; Izumori, Ken., *APPLIED MICROBIOLOGY AND BIOTECHNOLOGY*, 2007, **74**, 273-276.

191. P. Nigam and D. Singh, *Process Biochemistry*, 1995, **30**, 117-124.

192. H. Horitsu, Y. Yahashi, K. Takamizawa, K. Kawai, T. Suzuki and N. Watanabe, *Biotechnology and Bioengineering*, 1992, **40**, 1085-1091.

193. T.-B. Kim, Y.-J. Lee, P. Kim, C. S. Kim and D.-K. Oh, *Biotechnology Letters*, 2004, **26**, 623-627.

194. R. Govinden, B. Pillay, W. H. van Zyl and D. Pillay, *Applied Microbiology and Biotechnology*, 2001, **55**, 76-80.

195. B. Nidetzky, W. Neuhauser, D. Haltrich and K. D. Kulbe, *Biotechnology and Bioengineering*, 1996, **52**, 387-396.

196. M. Herskowitz, *Chemical Engineering Science*, 1985, **40**, 1309-1311.

197. T. B. Granström, K. Izumori and M. Leisola, *Applied Microbiology and Biotechnology*, 2007, **74**, 273.

198. P. Barbaro, F. Liguori and C. Moreno-Marrodan, *Green Chemistry*, 2016, **18**, 2935-2940.

199. C. Hernandez-Mejia, E. S. Gnanakumar, A. Olivos-Suarez, J. Gascon, H. F. Greer, W. Zhou, G. Rothenberg and N. Raveendran Shiju, *Catalysis Science & Technology*, 2016, **6**, 577-582.

200. S.-M. Bae, Y.-C. Park, T.-H. Lee, D.-H. Kweon, J.-H. Choi, S.-K. Kim, Y.-W. Ryu and J.-H. Seo, *Enzyme and Microbial Technology*, 2004, **35**, 545-549.

201. M. Yadav, D. K. Mishra and J.-S. Hwang, *Applied Catalysis A: General*, 2012, **425–426**, 110-116.

202. J. P. Mikkola and T. Salmi, *Catalysis Today*, 2001, **64**, 271-277.

203. J.-P. Mikkola, D. Kubicka, J. Kuusisto, N. Granholm, T. Salmi and B. Holmbom, *Journal of Chemical Technology & Biotechnology*, 2003, **78**, 203-207.

204. D. K. M. Mithilesh Yadav, Jin-Soo Hwang, *App.Catal.A general.*, 2012 **425-426** 110-116

205. T. S. a. R. S. Jyri-Pekka Mikkola, *J.Chem.Technol.Biotechnol.*, 1999, **74**, 655-662.

206. A. A. D. Dinesh Kumar Mishra, Jin-Soo Hwang, *J. Mol.Cata.A Chem.*, 2013, **376**, 63-70.
207. T. K. Anup Tathod, E.S. Sanil, Paresh L. Dhepe, *J.Mol.Catal.A:Chem.*, 2014, **388-389**, 90-99.
208. J.-P. Mikkola, T. Salmi and R. Sjöholm, *Journal of Chemical Technology & Biotechnology*, 1999, **74**, 655-662.
209. A. Tathod, T. Kane, E. S. Sanil and P. L. Dhepe, *Journal of Molecular Catalysis A: Chemical*, 2014, **388–389**, 90-99.
210. P. Bhaumik and P. L. Dhepe, *Catalysis Reviews*, 2016, **58**, 36-112.
211. Y. Román-Leshkov, C. J. Barrett, Z. Y. Liu and J. A. Dumesic, *Nature*, 2007, **447**, 982.
212. Y. Román-Leshkov, J. N. Chheda and J. A. Dumesic, *Science*, 2006, **312**, 1933-1937.
213. H. Kazuhiko, Y. Hiroshi and S. Gohfu, *Chemistry Letters*, 1982, **11**, 617-618.
214. M. A. Schwegler, P. Vinke, M. van der Eijk and H. van Bekkum, *Applied Catalysis A: General*, 1992, **80**, 41-57.
215. B. M. Matsagar and P. L. Dhepe, *Catalysis Science & Technology*, 2015, **5**, 531-539.
216. M. Watanabe, Y. Aizawa, T. Iida, R. Nishimura and H. Inomata, *Applied Catalysis A: General*, 2005, **295**, 150-156.
217. H. Yan, Y. Yang, D. Tong, X. Xiang and C. Hu, *Catalysis Communications*, 2009, **10**, 1558-1563.
218. F. Benvenuti, C. Carlini, P. Patrono, A. M. Raspolli Galletti, G. Sbrana, M. A. Massucci and P. Galli, *Applied Catalysis A: General*, 2000, **193**, 147-153.
219. P. Carniti, A. Gervasini, S. Biella and A. Auroux, *Catalysis Today*, 2006, **118**, 373-378.
220. M. Daniel, R. Luc, G. Antoine and G. Jean-Pierre, *Journal of Chemical Technology and Biotechnology*, 1981, **31**, 497-502.
221. G. A. Halliday, R. J. Young and V. V. Grushin, *Organic Letters*, 2003, **5**, 2003-2005.

Chapter 2

Experimental Methods and Characterization Techniques

2.1 Introduction

As described in chapter 1, several methods can be employed for the synthesis of zeolite-based micro-mesoporous composites with interconnected micro and mesoporosity. The present chapter describes the synthesis of various zeolite (K/LTL and H/BEA) based micro-mesoporous composites as solid base/acid, and the noble metal (Pt) supported a catalyst for the execution of present work, as tabulated in Table 2.1. The zeolite K/LTL based micro-mesoporous composites were, employed as solid bases, prepared mainly by three methods as, 1) Post-synthesis modification (alkali treatment), where effect of molar $Si_{(K/LTL\ zeolite)}/OH^-_{(aq.\ KOH)}$ ratio was studied, 2) Seeding method, in which K/LTL-MCM-41 composites were synthesized with varying SiO_2/Al_2O_3 ratios (8, 10, 15, 20) by recycling of waste mother liquor, and 3) Two-step crystallization method implemented for the synthesis of K/LTL-MCM-41 composite. The noble metal (Pt) supported on the γ-Al_2O_3 catalyst was prepared by wet impregnation method which is used as a catalyst. In addition to this, the zeolite H/BEA based micro-mesoporous composite, H/BEA-SBA-15 was prepared by the seeding method and it was used as a solid acid catalyst. The chapter also deals with the different characterization techniques implemented to assay physico-chemical properties of the synthesized materials, such as identification of phase and purity, composition, crystallinity, textural properties, morphology, nature of acid/basic sites, etc. The structure-property-activity correlation was discussed with various characterization techniques. The activity of zeolite K/LTL based micro-mesoporous composites were tested as solid bases for the hydrogenation of xylose to sugar alcohols using Pt/γ-Al_2O_3 catalyst in the aqueous phase. Moreover, the catalytic performance of zeolite H/BEA based micro-mesoporous H/BEA-SBA-15 composite was studied as a solid acid catalyst in dehydration of fructose to 5-hydroxymethylfurfural (HMF) in a biphasic system.

The above-mentioned zeolite based micro-mesoporous composites were characterized by various analytical techniques, such as, inductively coupled plasma-optical emission spectroscopy (ICP-OES), powder X-ray diffraction (PXRD), nitrogen adsorption-desorption measurement, fourier transform infrared spectroscopy (FTIR and Pyridine adsorbed IR), temperature programmed desorption of CO_2/NH_3 (CO_2/NH_3-

TPD), temperature-programmed reduction of H_2 (H_2-TPR), thermogravimetric analysis (TGA), X-ray photoelectron spectroscopy (XPS), scanning electron microscopy (SEM), transmission electron microscopy (TEM and HR-TEM), energy dispersive X-ray analysis (EDAX) and ^{27}Al and ^{29}Si magic angle spinning nuclear magnetic resonance (MAS NMR).

Table 2.1. Zeolite-based micro-mesoporous composites and a noble metal supported catalyst synthesized in current work

Sr. No.	Micro-mesoporous composites	Method of preparation
	Solid bases	
1	**Micro-mesoporous K/LTL zeolite** KL(X) Where, X = $Si_{(K/LTL\ zeolite)}/OH^-_{(aq.\ KOH)}$ ratio	Post-synthesis modification (aq. KOH treatment varying molar $Si_{(K/LTL\ zeolite)}/OH^-_{(aq.\ KOH)}$ ratio = 1.128-0.142 mol/mol)
2	K/LTL-MCM-41 XMMC Where, X = SiO_2/Al_2O_3 ratio	Seeding method (Utilizing waste mother liquor, SiO_2/Al_2O_3 ratio = 8- 20 mol/mol)
3	K/LTL-MCM-41	Two-step crystallization method (SiO_2/Al_2O_3 ratio = 8 mol/mol)
	Solid acid	
4	H/BEA-SBA-15	Seeding method (SiO_2/Al_2O_3 ratio = 57 mol/mol)
	Noble metal supported catalyst	
1	Pt/γ-Al_2O_3	Wet impregnation method (3.5 *wt%* Pt on γ-Al_2O_3 support)

2.2 Synthesis of micro-mesoporous composites and a noble metal supported catalyst

2.2.1 Synthesis of zeolite K/LTL based micro-mesoporous composites: Solid bases

2.2.1.1 Chemicals

The chemicals used in the synthesis of zeolite K/LTL based micro-mesoporous composites were silica sol (40%, V.P. Chemical, India), pseudoboehmite (70%, Condea, Germany), potassium hydroxide (85%, Merck, India) and cetyltrimethylammonium bromide (98%, CTMABr, Dishman, India) and sulfuric acid (98%, Merck, India). For the synthesis of Pt/γ-Al_2O_3 catalyst, aluminium oxide (γ-Al_2O_3, 99%, Aldrich Chemicals, USA) and tetraamineplatinum nitrate (99.99%, Alfa Aesar, UK) were used. All the materials synthesized using millipore water as a solvent. The chemicals were used as received without further purification.

2.2.1.2 Synthesis of K/LTL zeolite

The K/LTL zeolite was with molar Si/Al ratio = 2.86 was used to study the post-synthesis modification and synthesized by hydrothermal crystallization with the molar gel composition of 20SiO_2: Al_2O_3: 8K_2O: 200H_2O at 170 ^oC for 8 h. The overall synthesis procedure was reported elsewhere.[1] In a typical procedure, the homogeneous solution was prepared by dissolving 2.56 g of pseudoboehmite and 15.84 g of potassium hydroxide in 28.52 g millipore (the reaction mixture was heated to achieve a clear solution). The reaction mixture was allowed to cool to room temperature and water loss due to heating was compensated by the addition of a requisite amount of millipore water. Further, clear potassium aluminate solution was added to the 54 g silica sol under vigorous stirring to form a white colored homogeneous gel. After stirring for 1 h, the homogeneous gel was transferred to the 300 mL stainless steel autoclave, sealed and then placed in a preheated oven for hydrothermal crystallization at 170 ^oC. After completion of the time interval of 8 h, the autoclave was quenched to room temperature. The solid product was separated by filtration, followed by the washing with a copious amount of milipore water till the effluent showed pH value about ~7. Finally, the solid mass was dried at 100 ^oC for 12 h. The final product was designated as K/LTL.

2.2.1.3 Post-synthesis modification (alkali treatment)

The micro-mesoporous K/LTL zeolites with varying degree of mesoporosity were synthesized by post-synthesis modification using alkali treatment (aq. KOH), by following the procedure reported elsewhere.[2] The post-synthesis modification was carried out with different molar $Si_{(K/LTL\ zeolite)}/OH^-_{(aq.\ KOH)}$ ratio (1.128-0.142 mol/mol) by treating pre-synthesized K/LTL (described in Section 2.2.1.2) with aqueous KOH solutions with different concentrations keeping all other parameters constant. Briefly, 10 g K/LTL zeolite was dispersed in 300 mL of aqueous KOH solution (0.3/0.6/0.9/1.5/1.8/2.1/2.8 M) (alkali volume to K/LTL zeolite ratio 30 mL/g) and heated at a temperature of 70 ^oC for 1 h with constant stirring. The aqueous KOH solution was chosen in order to overcome the pronounced effect of other cations such as Na^+ in NaOH, over catalysis process. The resultant solution was cooled to room temperature and solid was recovered by vacuum filtration, washed thoroughly with of millipore water till the pH of the filtrate ~7. Finally, the solid was dried in an oven at 100 ^oC for 12 h. The micro-mesoporous K/LTL zeolites thus obtained were designated as KL(X), where X indicates the molar $Si_{(K/LTL\ zeolite)}/OH^-_{(aq.\ KOH)}$ ratio.

2.2.1.4 Synthesis of micro-mesoporous K/LTL-MCM-41 composite by the seeding method

The micro-mesoporous K/LTL-MCM-41 composites varying molar SiO_2/Al_2O_3 ratio (8, 10, 15, 20) were synthesized by seeding method following the experimental procedure reported elsewhere with little modification.[1, 3] The optimum initial molar gel composition, molar gel composition of mother liquor, and synthesis conditions for zeolite and the composite phase are tabulated in Table 2.2.

In the present study, the mother liquor present along with crystalline K/LTL zeolite was used to employ unutilized sources including water for the syntheses of K/LTL-MCM-41 composites. In syntheses procedure of micro-mesoporous K/LTL-MCM-41 composites, in the first step, the hydrogel of K/LTL zeolite with molar composition of xK_2O: Al_2O_3: $ySiO_2$: zH_2O was prepared and subjected to hydrothermal crystallization at 170 ^oC at a different time interval. The reaction mixture was allowed to cool.

Table 2.2. Initial molar gel composition and synthesis conditions of K/LTL and micro-mesoporous K/LTL-MCM-41 composites composite

Composites	Molar gel composition									Synthesis conditions			
	Initial				Mother liquor*			MCM-41 phase		Zeolite phase		Composite phase	
	SiO_2	Al_2O_3	K_2O	H_2O	SiO_2	K_2O	H_2O	CTMABr	H_2O	Time[a] h	t_C ^oC	Time[b] h	t_{CM} ^oC
20 MMC	20	1	8	200	14.3	7.0	187	4.8	460	8	170	24	110
15 MMC	15	1	6	150	9.5	4.8	135	3.6	330	12	170	24	110
10 MMC	10	1	4	100	4.6	2.9	86	2.4	220	16	170	24	110
8 MMC	8	1	3.2	80	2.8	1.9	69	1.9	176	24	170	24	110

a = Time required for the synthesis of K/LTL zeolite, t_C = Crystallization temperature for K/LTL zeolite, b = Time required for the synthesis of K/LTL-MCM-41 composite, t_{CM} = Crystallization temperature for K/LTL-MCM-41 composite, * ±5% Handling loss, (determined by ICP-OES analysis)

The synthesized K/LTL zeolite crystals were used as a seed. The synthesized colloidal suspension contains preformed K/LTL zeolite crystals and mother liquor with unutilized reagents. In the second stage, with no any correction to mother liquor composition, the colloidal suspension was added dropwise to an aqueous solution containing the requisite amount of cetyltrimethylammonium bromide (CTAMABr) as templates under vigorous stirring at room temperature. The resulting reaction mixture was stirred for 2 h at room temperature. The pH of reaction mixture was adjusted to 8-9 by a dropwise addition of 2 M sulfuric acid under vigorous stirring. A homogeneous gel obtained further aged for 5 h at room temperature. The final reaction mixture was then transferred to stainless steel autoclave and subjected to hydrothermal crystallization statically at 110 ^{o}C for 24 h at autogenous pressure. After quenching, the solid product was separated by filtration, washed thoroughly with a copious amount of millipore water and dried in air at 110 ^{o}C for 12 h. Finally, the surfactant template was removed by calcination at 550 ^{o}C for 6 h by following the calcination program as shown in Figure 2.1. The calcined samples were designated as XMMC, where X= initial molar SiO_2/Al_2O_3 ratio of the hydrogel as sown in Table 2.1.

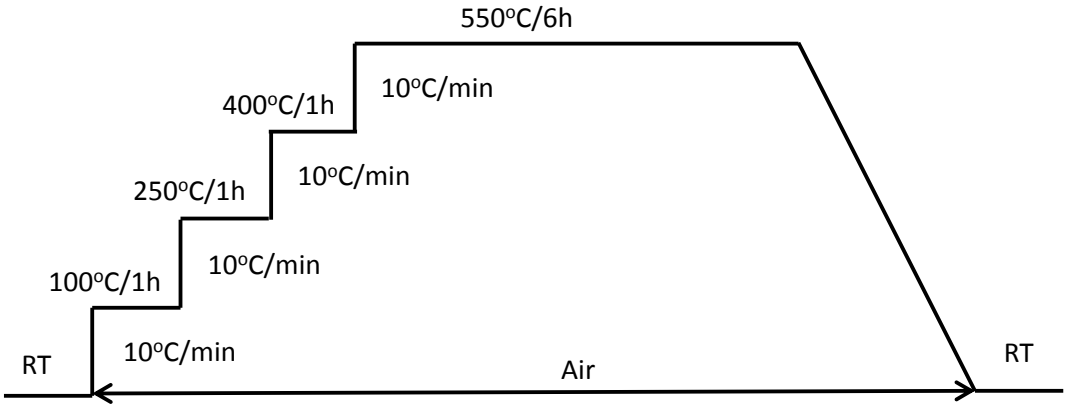

Figure 2.1. Calcination program for micro-mesoporous K/LTL-MCM-41 composites

2.2.1.5 Synthesis of micro-mesoporous K/LTL-MCM-41 composite by two-step crystallization method

In present studies, micro-mesoporous K/LTL-MCM-41 composite was synthesized by two-step crystallization method, by following the procedure described in Section 2.2.1.4 with the modification. Aiming at the synthesis of K/LTL-MCM-41 composite with initial molar gel composition $8SiO_2$: Al_2O_3: $3.2K_2O$: $80H_2O$, first step, a solution A was prepared by adding 6.27 g of pseudoboehmite and 15.42 g of potassium hydroxide in 26.63 g millipore water to get a clear solution. The solution was heated for 4 h to dissolve pseudoboehmite in an aqueous KOH solution. Further, a homogeneous hydrogel was prepared by adding clear solution A to the 51.66 g silica sol under vigorous stirring. After the continuous stirring of solution for 1 h, the synthesized gel was transferred into 300 mL stainless steel autoclave and subjected for the hydrothermal crystallization at 170 ^oC for 10 h only. The crystallization time for K/LTL zeolite was chosen in such a way that only zeolite nano-crystals were developed. After quenching of reaction mixture to room temperature, the colloidal suspension was added dropwise to the aqueous solution containing 15.14 g of cetyltrimethylammonium bromide (CTAMBr) in 292 g of millipore water under vigorous stirring at room temperature. After stirring the solution for 2 h, the pH of reaction mixture was adjusted to 8-9 by a dropwise addition of 2 M sulfuric acid. The solution was stirred vigorously and aged for 5 h at room temperature. Finally, the homogeneous mixture was transferred to stainless steel autoclave and subjected to hydrothermal crystallization statically at 110 ^oC for 24 h at autogenous pressure. The solid product was separated by filtration, washed thoroughly with a copious amount of millipore water and dried in air at 110 ^oC for 12 h. The surfactant template was removed by calcination at 550 ^oC for 6 h by following the calcination program as shown in Figure 2.1.

2.2.1.6 Synthesis of 3.5 *wt%* platinum loaded γ-Al_2O_3 catalyst by wet impregnation method

The platinum supported on the γ-Al_2O_3 catalyst was synthesized by wet impregnation method by following the procedure reported elsewhere.[4] Prior to metal

loading, γ-Al_2O_3 solid support was evacuated under vacuum (10^{-4} MPa) at 150 °C for 3 h. In a typical synthesis of 3.5 *wt%* Pt/γ-Al_2O_3 catalyst, 1 g γ-Al_2O_3 solid support was dispersed in 3.5 mL millipore water under stirring for half an hour. Further, the 1.5 mL of an aqueous salt solution of tetraamineplatinum nitrate ($Pt(NH_3)_4(NO_3)_2$) of known concentration (12 mg per mL) was added dropwise to the above solution. The resulting suspension was stirred for 16 h at room temperature. The powder thus obtained was separated by vacuum evaporation and dried in an oven at 60 °C for 16 h.

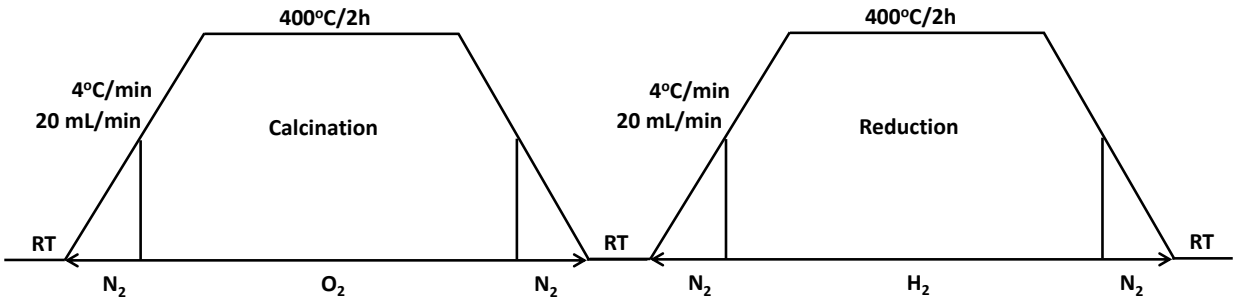

Figure 2.2. Calcination and reduction program for 3.5 *wt%* Pt/γ-Al_2O_3 catalyst

The platinum loaded γ-Al_2O_3 further dried under vacuum (10^{-4} MPa) at 150 °C for 3 h. Finally, 3.5 *wt%* Pt/ γ-Al_2O_3 was subjected for calcination in the air flow of 20 mL/min and reduced in hydrogen flow 20 mL/min at 400 °C for 2 h each. The calcination and reduction program are depicted in Figure 2.2.

2.2.2 Synthesis of zeolite H/BEA based micro-mesoporous composites: Solid acid

2.2.2.1 Chemicals

The chemicals used for synthesis of zeolite H/BEA based micro-mesoporous composite were sodium aluminate (43.8% Al_2O_3, 39.0% Na_2O, Aldrich, USA), silica sol (40%, SiO_2, V.P. Chemicals, India), tetraethylammonium hydroxide (TEAOH, aqueous 30% *wt/wt* solution, Aldrich, USA), sodium hydroxide (99%, LOBA Chemie, India), ammonium chloride (99.8%, Thomas Baker, India), tetraethyl orthosilicate (TEOS, 99%, Aldrich, USA), triblock copolymer Pluronic P123 ($EO_{20}PO_{70}EO_{20}$, Aldrich, USA), hydrochloric acid (HCl, 37%, Merck, India), aluminium isopropoxide (98%, LOBA Chemie, India) and millipore water.

2.2.2.2 Synthesis of Na/BEA zeolite

Beta zeolite (Na/BEA) was prepared by following the literature reported elsewhere.[5] The Na/BEA zeolite was prepared by the hydrothermal crystallization from the aluminosilicate with the molar gel composition $6(TEA)_2O$: $2.4Na_2O$: $30SiO_2$: Al_2O_3: $840H_2O$. The homogeneous gel was then transferred in stainless-steel autoclave and kept in a preheated oven maintained at 140 ^oC. After completion of the crystallization period of 72 h, the reaction mixture was quenched to room temperature. The solid product was recovered by the centrifugation, washed thoroughly with millipore water and dried in an oven at 120 ^oC for 12 h. Finally, the dried sample was calcined at 550 ^oC for 10 h under static conditions.

2.2.2.3 Synthesis of H/BEA zeolite by ammonium ion exchange method

To prepare BEA zeolite in protonic form (H/BEA), the calcined sample was subjected to ion exchange using 1M ammonium chloride solution with the ratio of 25 mL per gram of zeolite for 3 times at 70 ^oC for 3 h. After completion of ion exchange, the solution was allowed to cool to room temperature and excess salt was washed with an excess of millipore water. The solid was dried at 120 ^oC for 12 h. Finally, the ammonium form of BEA zeolite was converted into protonic form by calcination at 500 ^oC for 6 h under continuous air flow with the rate of 5 ^oC/min. The protonic form of BEA zeolite was designated as H/BEA.

2.2.2.4 Synthesis of micro-mesoporous H/BEA-SBA-15 composite

The micro-mesoporous H/BEA-SBA-15 composite was synthesized by seeding method by following the reported literature with little modification.[6] In a typical synthesis, firstly, a solution A was prepared by dissolving 4.0 g of Pluronic P123, a structure directing template, in 30 mL of water for 4 h at room temperature in a glass beaker. The solution was stirred for 4 h to get the clear solution. Then, 100 mL of 0.29 M HCl was added to the above solution and the resultant solution was stirred for another 2 h. The solution A was then transferred to a round bottom flask which maintained at 40 ^oC in an oil bath for another 2 h. Further, 12 g TEOS as a silica source for SBA-15 synthesis

was added dropwise to the above-prepared solution with constant stirring for 2 h. In another glass beaker, a solution B (slurry) was prepared by a dispersing pre-crystallized 3 g of H/BEA zeolite in 30 mL millipore water for 2 h. Further, the solution B was transferred into the solution A dropwise with vigorous stirring to get a white colored solution, followed by aging at 40 ^{o}C for 24 h. Finally, the resulting solution was transferred into a Teflon-lined autoclave followed by aging at 100 ^{o}C for 24 h for further silica condensation. The solid product was filtered, washed with copious amount of millipore water, and dried in an oven at 100 ^{o}C for 16 h. The as-synthesized product obtained was calcined at 550 ^{o}C for 6 h under static air with a heating rate of 2 ^{o}C/min, in order to remove the organic template. The catalyst was denoted as H/BEA-SBA-15. For comparison purpose, Al-SBA-15 and Si-SBA-15 were prepared with/without aluminium isopropoxide by following the same procedure described above without the addition of H/BEA zeolite under the same synthesis condition.

2.3 Hydrothermal stability test

The hydrothermal stability of zeolite-based micro-mesoporous composites was evaluated by refluxing the composite in boiling water for a time period of 8 h by following the reported literature.[7, 8] In a typical procedure, 1 g of the composite was dispersed in 10 mL of millipore water (solid to water ratio 0.1 g/mL). The solution was placed in round bottom flask attached with condenser and reflux for 8 h. After hydrothermal treatment, the solid was separated by centrifugation and washed with an adequate amount of millipore water and dried at 110 ^{o}C for 12 h.

2.4 Characterization techniques and sample preparation

All the synthesized composites/catalysts were thoroughly characterized by using various characterization techniques like ICP-OES, PXRD, FTIR, Py-IR, N_2 adsorption-desorption measurement, TPD, H_2-TPR, solid MAS NMR, SEM, TEM, HR-TEM, XPS, and TGA. The present section described details of the principle of instruments, sample preparation and the operational conditions used in for the current study.

2.4.1 Inductively coupled plasma-optical emission spectrometry (ICP-OES)

'Inductively coupled plasma-optical emission spectroscopy' (ICP-OES) is the most popular and powerful analytical technique and most frequently used for the qualitative and quantitative analysis of elements in trace amount (in PPM level). It is an atomic emission type of spectroscopy in which the inductively coupled plasma was used to produce excited atoms and ions which emitted radiations of a particular wavelength. Every element has the characteristics wavelength of the emitted radiation. The concentration of the element present in the sample was detected by the intensity of the emitted photons. The liquid samples may inject directly into the instrument, whereas the solid samples were extracted in the solution by treatment with acid digestion of definite concentration. The instrument was calibrated by using standard solutions of various elements.

The elemental compositions of samples were determined by 'SPECTRO ARCOS Germany, FHS 12' inductive coupled plasma-optical emission spectroscopy (ICP-OES) instrument. The sample preparation procedure for ICP-OES analysis is described as follows; 0.1 g of solid sample was weighed in the polypropylene bottle. About 2-3 mL of hydrofluoric acid (40% solution, HF) was added to above bottle. The reaction mixture was evaporated to dryness by heating at 60-70 °C to remove the excess HF. The sample was allowed to cool and weighed. The HF treatment removes silicon in the form of SiF_4 as shown in following reactions.

$$SiO_2 + 4HF \longrightarrow SiF_4\,(g) + 2H_2O$$
$$SiO_2 + 6HF \longrightarrow H_2SiF_6 + 2H_2O$$
$$H_2SiF_6 \longrightarrow SiF_4\,(g) + 2HF$$

For micro-mesoporous composites, a white colored solid residue mainly contains Al, K and the traces of Na. The solid residue thus obtained was dissolved in 3 mL of freshly prepared aqua-regia (a mixture of nitric acid and hydrochloric acid, in a molar ratio of 1:3). Finally, the solution was diluted with 7 mL of millipore water. Before sample analysis, the solution was filtered through a 0.22 micron filter, in order to remove any suspended particles.

2.4.2 Powder X-ray diffraction (PXRD)

Powder X-ray diffraction (PXRD) is one of the fundamental, important, and imperative characterization techniques employed to determine the crystallinity phase(s), phase purity, crystallographic structure, and crystallite size of long-range ordered solid materials.[9] The PXRD involves the interaction of incident monochromatic X-ray (CuK_α or MoK_α) with the atoms of periodic crystal lattices and scattered to a definite angle. Bragg's equation is used to calculate the inter-planner distance between two lattice planes (hkl miller indices) which is the characteristic feature of the crystalline material.[10] Bragg's equation is represented as shown below;

$$\mathbf{n\lambda = 2d\ (Sin\ \theta)}$$

where d is the inter-planner distance between two lattice planes, theta θ is the angle between the incident X-ray and the normal to reflecting lattice plane, λ is the wavelength of X-ray and n = 1, 2, 3 ..., is the integer commonly known as the order of plane. The finely ground powder sample was placed as a thin layer on a glass plate having sample holding pit and sample was pressed gently with another glass slab. The powder XRD patterns were recorded on X'pert Pro Philips diffractometer working under 40 kV and 30 mA with Ni-filtered monochromatic Cu Kα (1.5418 Å) radiations. The samples were scanned in the 2 theta range from 0.5 to 5^o for low angle PXRD patterns and from 5 to 90^o for wide PXRD patterns with the scanning rate of 2^o/min.

2.4.3 Fourier transformed infrared spectroscopic (FTIR)

Fourier transformed infrared spectroscopic (FTIR) is recognized as a diverse molecular spectroscopy technique where several functional groups existing in the molecule can be detected. Irrespective of the physical nature of the sample, the FTIR provides the information about the geometry, structure, and orientation of all molecules present in the sample. FTIR has various advantages over other techniques like sensitivity, accuracy, faster analysis speed, simple operating instrument, and internal calibration. Fourier transform infrared spectroscopic (FTIR) analysis of the composites was carried out using Perkin Elmer Spectrum-1 spectrometer at ambient conditions. The composites were well dispersed in KBr, pelletized and the spectra were recorded in the 4000-450

/cm spectral range. In this technique, the spectra were recorded by simply placing thin self-supporting discs of about 0.1 g mixture of powdered sample and KBr on the holder.

2.4.4 N_2 adsorption-desorption measurement

For porous materials, the N_2 adsorption-desorption measurement is a profound analytical technique that measures the porous properties of the materials such as total surface area, total pore volume, pore sizes, etc. by gas adsorption method. The most well-known method for determining the surface area was developed by Brunauer, Emmett, and Teller in 1938 considering the multilayer adsorption. Typically N_2 gas is used for the determination of surface area because at -196 °C, the cross-sectional area σ for nitrogen is 16.2 Å assuming the hexagonal close-packed nitrogen monolayer formation. The known volume of inert gas, adsorbate, was allowed to adsorb on the surface of the porous sample at a lower temperature and the volume of adsorbed gas is calculated at relatively lower pressure (p/p_0). An Adsorption is obtained by plotting of volume of gas adsorbed across a wide range of relative pressures at a constant temperature against relative pressure. The Brunauer-Emmett-Teller (BET) equation for the determination of surface area is given as,[11]

$$\mathbf{P/V(P_0-P) = 1/CVm+ [(C-1)/CVm] (P/P_0)}$$

where P is adsorption equilibrium pressure, P_0 is saturation vapor pressure of the adsorbate at experimental temperature, Vm is the volume of adsorbate required for monolayer coverage, V is the volume of gas adsorbed at pressure P, and C is a constant related to the heat of adsorption and liquefaction.

Moreover, the surface area of the materials is related to Vm by the equation as,

$$\mathbf{S_{BET} = (Vm/22414)\ Na\ \sigma}$$

where Na is Avogadro number and σ is mean cross-sectional area covered by one adsorbate molecule.

The nitrogen adsorption and desorption studies were performed at -196 ^oC on the Autosorb-1-Quantachrome instrument, USA. Prior to measurement, the sample was degassed in-situ at 200 ^oC for 3 h under vacuum. The total surface area was estimated by

the nitrogen adsorption data at a relative pressure (p/p_0) ranging from 0.05 to 0.25 using BET method. The pore size was determined by the Barrett–Joyner–Halenda (BJH) method and pore volume using the t-plot method. The total pore volume was calculated from the volume of nitrogen adsorbed by the relative pressure of 0.976. The mesopore size distribution was calculated by (BJH) method.

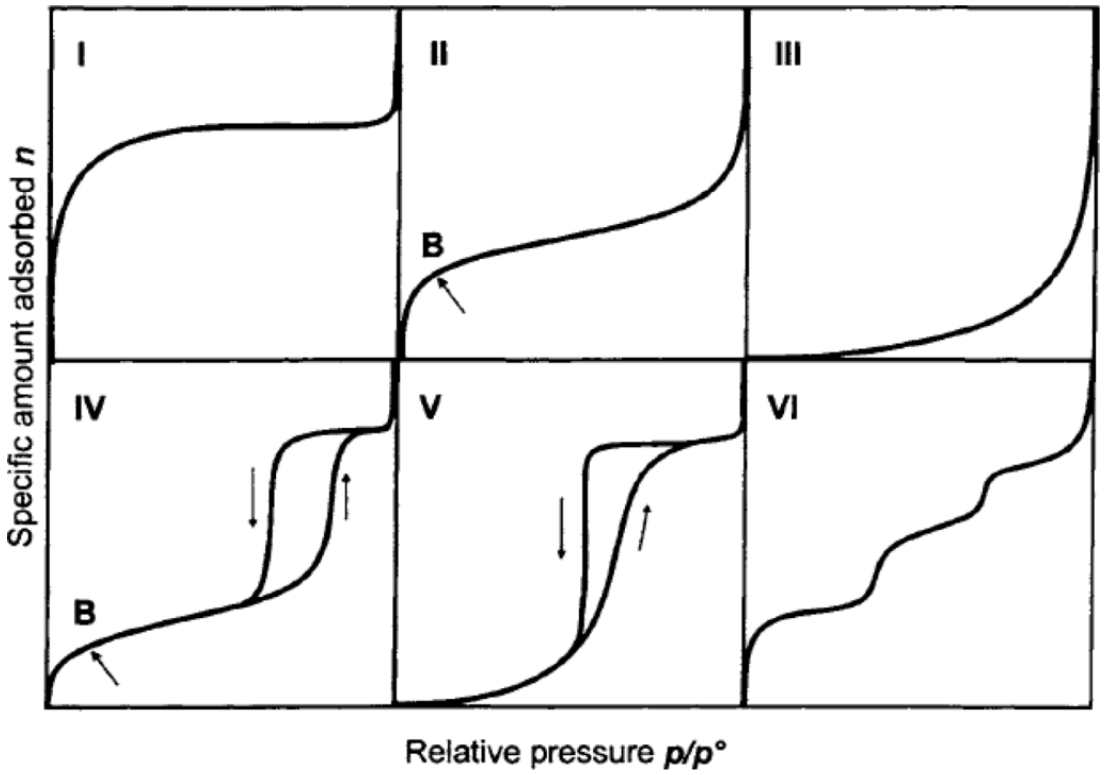

Figure 2.3 Types of adsorption isotherms[12]

The materials exhibited commonly six types of adsorption isotherms as shown in Figure 2.3.[12] Materials can show any one of the types of adsorption isotherm depending on the porous properties like porosity, pore size distribution, and surface area. The microporous materials such as zeolites and metal oxides with little external surface area shown by Type I adsorption isotherm. The adsorption of hydrogen or nitrogen on the charcoal is an example of Type I isotherm. Type II adsorption isotherm is shown when the adsorption occurs over nonporous or macroporous solids, for example, the adsorption of nitrogen on iron Fe catalyst at -195 ^{o}C. The materials in which the interaction of adsorbate with an adsorbate is greater than the interaction with the adsorbent surface shod Type III

isotherm. In Type III the lateral interactions between the adsorbent molecules are stronger as compared to the adsorbent surface and adsorbate. The mesoporous materials such as MCM-41, SBA-15 exhibited Type IV adsorption isotherm. It also showed the hysteresis loop which is associated with the capillary condensation carried out in mesopores. Type V isotherm is observed where the adsorbate-adsorbent interaction is very small. Type VI isotherm shows a stepwise increase and the sharpness of the steps depends on the system and the temperature. it represents the stepwise multilayer adsorption on a uniform non-porous surface.

2.4.5 ^{29}Si and ^{27}Al magic angle spinning nuclear magnetic resonance spectroscopy (^{29}Si and ^{27}Al MAS NMR)

The ^{29}Si and ^{27}Al magic angle spinning nuclear magnetic resonance spectroscopy (^{29}Si and ^{27}Al MAS NMR) spectra are performed in order to investigate the silicon and aluminium environment in samples. ^{29}Si and ^{27}Al MAS NMR spectra were recorded on a JEOL ECX-400 spectrometer at resonance frequencies of 79.5 and 104.3 MHz for ^{29}Si and ^{27}Al, respectively. This technique is used to acquire high-resolution data from the solid materials. It is a versatile method for establishing the structural features of the ordered materials. The ^{29}Si MAS NMR spectra used to determined distinct Si(OAl)n(OSi)4-n (n= 0, 1, 2, 3, 4) structural groups quantitatively from the zeolite framework of first tetrahedral coordination shell of a silicon atom.[13] The ^{27}Al MAS NMR spectra provide the information about the octahedral or tetrahedral coordination environment of aluminium present in the zeolite structure. ^{29}Si and ^{27}Al MAS NMR used as a powerful device for studying the several solid-state processes.

It should be noted that irrespective of the structure of the zeolite, ^{29}Si MAS NMR can be an impressive tool to determine the molar Si/Al ratio of the framework of zeolite by using the following formula as,

$$\left(\frac{\mathrm{Si}}{\mathrm{Al}}\right)_{\mathrm{framework}} = \frac{\left(\sum_{n=0}^{4} I_{\mathrm{Si}(n\mathrm{Al})}\right)}{\left(\sum_{n=0}^{4} 0.25 n I_{\mathrm{Si}(n\mathrm{Al})}\right)}$$

where, I is the intensity n^{th} peak, and n = 0,1,2,3,4.

2.4.6 Temperature programmed desorption of NH_3/CO_2 (NH_3/CO_2 -TPD)

Temperature programmed desorption of NH_3/CO_2 (NH_3/CO_2–TPD) analysis is one of the widely employed bulk technique used to determine total acidity or basicity of catalysts. The strength and the number of acid sites are determined by NH_3 (basic probe), while that of basic sites are determined by CO_2 (acidic probe). The acidity or the basicity of the catalysts is the critical parameters that explain the catalytic activity of a catalyst. The acidity or the basicity of samples is determined by measuring the conductivity of the gas stream passing through the sample by TCD. Moreover, the various species evolved during the measurement can be identified by coupling the TPD with Mass Spectrometer. When analyzed gas (probe molecules NH_3 or CO_2) is allowed to pass through the catalysts, the probe molecules interact with the acidic or basic sites in the catalysts and undergo either physisorption or chemisorption at a lower temperature. As the temperature of the sample increases with precise ramping rate, the adsorbed gas starts desorbing from the catalyst surface. The major drawback of this method is that we cannot differentiate Brønsted sites or Lewis sites as there is no specific adsorption of a gas on the catalytically active sites. But this problem can be overcome by using other molecules like alkyl amines.

Temperature programmed desorption of NH_3/CO_2 (NH_3/CO_2 -TPD) was carried out on Micromeritics, AutoChem 2910 instrument in the range of 100–600 ^oC with a thermal conductivity detector (TCD). Prior to analysis, all the samples were activated at 550 °C for 30 min in helium flow (30 mL/min) in order to remove adsorbed gases/moisture. Further, the sample was allowed to cool to a temperature of 50 ^oC. At this temperature, NH_3/CO_2 gas was allowed to adsorb under helium gas flow and the temperature increased to 100 °C for 30 min to remove the physisorbed gases. Finally, the temperature was increased to 100 °C to 700 °C in helium flow (30 mL/min) at the rate of 10 °C/min and the TCD profile was recorded. The number of acidic or basic sites present in the catalysts is directly proportional to the amount of NH_3/CO_2 gas adsorbed.

2.4.7 Electron microscopy

The electron microscopy is well known and widely used spectroscopic techniques used to obtained high-resolution images of the catalysts as well as biological specimens. It is used to investigate the detailed structural and morphological features of the materials. In this section, two main types of electron microscopes are studied namely, the transmission electron microscope (TEM) and the scanning electron microscope (SEM). The TEM provides the thin images of the materials where the electrons with high energy can pass through the materials resulting in the generation of a projectile image. In the SEM technique, the secondary electrons with low energy have been deployed to find the surface morphological features like size and shape of materials.

2.4.7.1 Transmission electron microscopy (TEM) and High resolution-transmission electron microscopy (HR-TEM)

Transmission electron microscopy (TEM) and high-resolution transmission electron microscopy (HR-TEM) are an interesting and indispensable tool used for high resolution imaging the thin film of a solid sample in order to assess the microstructure and composition. This is been widely used in the field of heterogeneous catalysis, nanotechnology, development of photonics and semiconductors etc. This technique involves the irradiation of a thin layer of the sample with high energy electron beam emitted by a cathode (200-300 eV). The partially transmitted electron beam through the thin sample specimen is diffracted through the lattice planes of the crystalline or the semi-crystalline materials and is propagated in different directions. The image is formed by a refracted beam which gives the information about the structure of the sample. A very small object can be clearly magnified with the high resolution because of the small wavelength of electrons. Transmission electron microscopy (TEM) measurements carried out on the FEI Technai T-20 electron microscopes operating at 200 kV. Similarly, high-resolution transmission electron microscopic analysis (HR-TEM) was performed on FEI Technai G2, F-30 electron microscopes operating at 300 kV. In both the cases, the sample was prepared by placing a droplet of suspension solution, prepared by ultrasonicating the

catalysts in isopropyl alcohol on a carbon-coated copper grid (mesh 200). The sample was allowed to dry at room temperature.

2.4.7.2 Scanning electron microscopy (SEM)

Scanning electron microscopy (SEM) focused on the sample surface by scanning it with a high-energy beam of electrons. It examined directly the external morphological features of samples. The SEM is performed by scanning the external surface of the materials with a beam of electrons (5-50 eV). The SEM images were recorded by secondary electrons or back-scattered electrons with respect to the position of the primary beam. The external structural morphology and the composition of the samples were obtained in detained by the interaction of the electron beam and the sample surface. The SEM micrographs of the samples were performed on a Leo Leica Cambridge UK Model Stereoscan 440 scanning electron microscope with an electron beam of 5-50 eV. For SEM imaging, the sample was placed on the carbon tape followed by sputtering with the gold film. The elemental composition of the sample was carried out using EDAX attached with SEM instrument. The powdered samples were loaded on the stubs and sputtered with the thin gold film to prevent surface charging and also protect from degradation by thermal energy by the electron beam.

2.4.8 Thermal gravimetric analysis (TGA)

The thermal gravimetric analysis (TGA) involves the measurements of the response of physical and chemical changes occurred during the thermal treatment as a function of rising temperature (or time) and/or mass loss when it is heated in a definite manner. This technique can be employed for the micro-mesoporous composites to assess the mass loss during the calcination with regards to the surfactant, loss of moisture, etc. it is also useful to predict the volatile matter content, thermal stability reaction kinetics and the degradation of the materials under study. The TGA of the composite was carried out under the air atmosphere by using Mettler Toledo TGA/SDTA 851 series, USA instrument under an air atmosphere with a heating rate of 10^{o} min^{-1} in a range of 25-1000 ^{o}C using about 10 mg of sample in a platinum pan.

2.4.9 X-ray photoelectron spectroscopy (XPS)

X-ray photoelectron spectroscopy (XPS), which is also termed as electron spectroscopy for chemical analysis (ESCA), is a classical surface sensitive spectroscopic technique used for the qualitative and quantitative analysis of surface including chemical composition, chemical state and the electronic state of the elements. The principle of the XPS is founded on the photoelectric effect, which involves the irradiation of the sample with a beam of X-ray which resulted in the emission of electron following excitation of core level electrons by photons. The kinetic energy and the number of the photoelectrons were recorded. The kinetic energy of ejected photoelectron can be measured if the energy of the incident X-ray is known. The electron binding energy of an element in a particular state is calculated by using the following equation.

$$\textbf{Binding energy} = E_{X\text{-}ray} - (E_{kinetic} + \phi)$$

where $E_{X\text{-}ray}$ is the energy of incident X-ray, $E_{kinetic}$ is the kinetic energy of ejected photoelectron, and Φ is the work function depends on spectrometer and material. The XPS was performed on ESCA-3000 (V.G. Scientific Ltd., UK) with the pressure of 1.3×10^{-7} Pa. The Mg Ka radiation (1253.6 eV) was used as an X-ray source and operated at 150 W. For the analysis of the XPS peaks, the charging effects were corrected by setting the positions of the C1s at a binding energy of 284.6 eV.

2.4.10 Temperature programmed reduction of H_2 (H_2-TPR)

Temperature programmed reduction of H_2 (H_2-TPR) study was carried out on Micromeritics Autochem-2920 instrument in the temperature range of 50-800 °C using 5% H_2 in He gas and the consumed hydrogen was measured by the thermal conductivity detector (TCD).

2.4.11 Pyridine adsorbed IR (Pyridine-IR) analysis

Pyridine Infrared (Pyridine-IR) spectra were taken on a spectrometer (Perkin Elmer Spectrum-1) in the range of 2000–400 cm^{-1}. Catalyst was dried at 100°C for 1 h before making contact with pyridine then subjected to directly with pyridine. Pyridine

adsorbed catalyst was subjected to oven at 120°C for 1 h to remove physisorbed pyridine. The spectrum was recorded when catalyst cooled at room temperature.

2.5 Catalytic activity for the valorization of sugars

In present work, two valorization reactions of sugars are studied, namely, 1) Solid base promoted noble metal catalyzed hydrogenation of sugar to sugar alcohols and 2) Brønsted acid catalyzed dehydration of fructose to 5-hydroxymethylfurfural (HMF). The detailed experimental procedure, analysis, and the calculation methods are described as follows.

2.5.1 Solid base promoted noble metal catalyzed hydrogenation of sugar to sugar alcohols

2.5.1.1 Chemicals

D-xylose (99%) was purchased from Loba Chemicals, India. Xylitol (99%), Arabitol (99%) and Arabinose (99%), glycerol (98%), ethylene glycol (99%), and 1,2-propanediol (99.5%) were procured from s.d. Fine Chemicals Ltd., India. All the chemicals were used without any further purification. For activity testing and HPLC standardization, millipore water was used as a solvent.

2.5.1.2 Experimental procedure

The catalytic activity of zeolite K/LTL based micro-mesoporous composites was tested for the liquid phase hydrogenation of xylose to sugar alcohols (xylitol and arabitol) as a solid base and 3.5 *wt%* Pt/γ-Al_2O_3 as a catalyst. All the catalytic and non-catalytic activity runs were carried out in a batch process. The hydrogenation reactions were conducted in a 50 mL batch reactor (Amar equipment's, India). In a typical experiment, 0.15 g xylose, 0.075 g of 3.5 *wt%* Pt/γ-Al_2O_3 catalyst (substrate/catalyst ratio= 2 *wt/wt*) , 0.075 g solid base (catalyst/solid base ratio= 1 *wt/wt*) and 35 mL millipore water was charged in the reactor. The hydrogen gas was purged into the reactor with the pressure of 8-20 bar at room temperature. The reactions were carried out at the desired temperature of 40-80 °C. The reaction mixture was allowed to stir initially at 150 RPM until the required temperature and once the temperature reached, the stirring speed was

increased to 900 RPM. After completion of the reaction, the reaction mixture was allowed to cool to room temperature. The reaction mixture at different time intervals was collected and centrifuged for catalyst separation. The samples were filtered through 0.22 µm syringe filter and analyzed using HPLC.

2.5.1.3 Analysis and Calculations

2.5.1.3.1 Kinetic diameter

The kinetic diameter of fructose, glucose, and HMF was calculated based on their molecular weights as discussed in the reported literature,[14] as shown below,

$$\textbf{Kinetic diameter } (\sigma) = 1.234 \times (MW)^{1/3}$$

Where MW is the molecular weight in g/mol. The kinetic diameter calculations were based on the assumption that the molecules are spherical and hence the correlation between the critical mass and the size of the sphere can be established. In sugars, these values may change according to the structure (open or closed chain) and the orientation as well as the number of hydroxyl groups present.

2.5.1.3.2 Analysis of the reaction mixture

The reaction mixture after completion of the reaction was filtered through 0.22 µm syringe filter analyzed using HPLC (Agilent Technologies, 1200 infinite series, USA) equipped with Rezex RPM-Monosaccharide Pb^{2+} (dimensions 7.8 mm x 300 mm, particle size 8 µm) column with refractive index detector maintained at 40 ^{o}C. The conversion of the substrate and yield of sugar alcohols were determined on mole basic. For the calculation of conversion and sugar alcohols yield, the calibration curves of the commercially available substrate and the products were drawn. The slope of the calibration curves was calculated and further used for the calculation of sugar conversion and sugar alcohol product yield, by using the following formulae.

2.5.1.3.3 Calculations

The conversion of the sugar was calculated on moles basis by using the following formula.

$$\% \textbf{ Conversion} = \frac{[\textbf{Initial mole of xylose} - \textbf{ Unconverted mole of xylose }]}{[\textbf{Initial mole of xylose}]} \times \textbf{100}$$

Similarly, the yields of sugar alcohols were calculated on moles basis by using the following formula.

$$\% \textbf{ Yield of sugar alcohols} = \frac{[\textbf{Mole of sugar alcohol formed }]}{[\textbf{Theoretical moles of sugar alcohol}]} \times \textbf{100}$$

2.5.2 Brønsted acid catalyzed dehydration of fructose to 5-hydroxymethylfurfural (HMF)

2.5.2.1 Chemicals

Fructose dehydration reactions were carried out using fructose (99%), glucose (99%), and methyl isobutyl ketone (MIBK, 99%) were purchased from LOBA Chemie, India. The toluene (99%) and 5-hydroxymethylfurfural (HMF, 99%) were procured from Merck, India, and Aldrich chemicals, USA, respectively. All the reagents were used as received without further purification. The dehydration reactions and the HPLC analysis was carried out using millipore water as a solvent.

2.5.2.2 Experimental procedure

The dehydration of fructose to HMF reactions was carried out in a 50 mL batch reactor (Amar equipment's, India). Prior to use, the micro-mesoporous H/BEA-SBA-15 composite was activated at 550 °C for 16 h in static air. In a typical reaction, 0.5 g of fructose and 0.143 g catalyst in 5 mL millipore water (10% *wt/wt* with respect to water) and 25 mL organic solvent as charged in an autoclave (water + organic solvent ratio= 1:5 *v/v*). The solution was heated at a desired temperature under stirring of 700 rpm. After completion of the reaction under autogenous pressure, the reactor was allowed to cool to room temperature. The reactions were carried out at various temperature (150-175 ^{o}C) and reaction time (0.5-2 h). The reaction mixture was subjected for centrifugation and the catalyst was separated from the reaction mixture. Further, an aqueous layer was separated from the organic layer and analyzed by HPLC and GC instruments, respectively.

2.5.2.3 Analysis of the reaction mixture

The aqueous layer was analyzed using high-pressure liquid chromatography, HPLC (Agilent Technologies, 1200 infinity series, USA) equipped with HC-75 Pb^{2+} column (dimensions 7.8 mm x 300 mm, particle size 8 μm) maintained at a column temperature of 80 ^{o}C and refractor index detector maintained at 40 ^{o}C. The millipore water was used as the mobile phase with a flow rate of 0.5 mL/min. The organic layer was analyzed by Agilent gas chromatograph, equipped with BPX-5 column (50 m x 0.22 mm ID) and refractive index detector. For each analysis, the sample was filtered through 0.22 μm syringe and 10 μL sample was injected.

2.5.2.4 Calculations

All the conversion and yield were calculated by GC and HPLC by plotting the calibration curves using standards of definite concentrations. Details on the calculations are given below,

$$\% \textbf{ Conversion} = \frac{[\textbf{Initial moles of fructose} - \textbf{ Unconverted moles of fructose (HPLC)}]}{[\textbf{Initial moles of fructose}]} \times \textbf{100}$$

$$\% \textbf{ Yield} = \frac{[\textbf{Moles of product formed (HPLC water} + \textbf{GC org)}]}{[\textbf{Theoretical moles of product}]} \times \textbf{100}$$

The turn over frequency (TOF) was calculated based on the number of moles of the reactant converted and the moles of acidic sites present on the zeolite as follows.

$$\textbf{TOF} = \frac{[\textbf{Moles of product formed}]}{[\textbf{Moles of acidic sites on zeolite/g}] \times [\textbf{Reaction time in h}]}$$

2.6 References

1. S. D. Bhat, P. S. Niphadkar, T. R. Gaydhankar, S. V. Awate, A. A. Belhekar and P. N. Joshi, *Microporous and Mesoporous Materials*, 2004, **76**, 81-89.
2. N. P. Tangale, S. K. Sonar, P. S. Niphadkar, and P. N. Joshi, *Journal of Industrial and Engineering Chemistry*, 2016, **40**, 128-136.

3. Y.-S. Ooi, R. Zakaria, A. R. Mohamed and S. Bhatia, *Applied Catalysis A: General*, 2004, **274**, 15-23.
4. A. Tathod, T. Kane, E. S. Sanil and P. L. Dhepe, *Journal of Molecular Catalysis A: Chemical*, 2014, **388–389**, 90-99.
5. M. W. Kasture, P. S. Niphadkar, N. Sharanappa, S. P. Mirajkar, V. V. Bokade, and P. N. Joshi, *Journal of Catalysis*, 2004, **227**, 375-383.
6. D. Zhang, A. Duan, Z. Zhao, X. Wang, G. Jiang, J. Liu, C. Wang and M. Jin, *Catalysis Today*, 2011, **175**, 477-484.
7. F. Carniato, C. Bisio, G. Paul, G. Gatti, L. Bertinetti, S. Coluccia and L. Marchese, *Journal of Materials Chemistry*, 2010, **20**, 5504-5509.
8. L. Wang, J. Zhang, F. Chen and M. Anpo, *The Journal of Physical Chemistry C*, 2007, **111**, 13648-13651.
9. J. W. Niemantsverdriet, 1993.
10. S. R. S. B.D. Cullity *Elements of X-ray Diffraction, Prentice Hall, 3rd ed.*, 2001.
11. S. Brunauer, P. H. Emmett and E. Teller, *Journal of the American Chemical Society*, 1938, **60**, 309-319.
12. D. H. E. K. S. W. Sing, R. A. W. Haul, L. Moscou, R. A. Pierotti, J. Rouquerol, T. Siemieniewska, *Pure Appl. Chem.*, 1985, **57**, 603-619.
13. F. C. A., T. J. M., K. Jacek, and G. G. C., *Angewandte Chemie International Edition in English*, 1983, **22**, 259-275.
14. P. Bhaumik and P. L. Dhepe, *Catalysis Today*, 2015, **251**, 66-72.

Chapter 3

Synthesis of zeolite K/LTL based micro-mesoporous composite by post-synthesis modification (Alkali treatment) and their catalytic activity in the hydrogenation of xylose to sugar alcohols

3.1 Introduction

As discussed in Chapter 1, the zeolite-based micro-mesoporous composites combining micro-mesoporosity captivated enormous attention in recent years owing to the hierarchical porous network which facilitates the efficient mass transport leading to excellent shape/size selective heterogeneous catalysis.[1, 2] Among the several synthesis strategies, the alkali treatment is an elegant technique to develop intracrystalline mesoporosity in the zeolites, consist of selective removal of framework silicon atoms, commonly referred as desilication.[3-6] The post-synthesis modification via desilication has gain attention in the past few decades due to simplicity and controlled mesoporosity generation.[4, 6] The introduction of mesoporosity in the microporous zeolite matrix depends on the alkali concentration, treatment time, temperature, zeolite topology, and its chemical composition.

From Chapter 1, it is anticipated that platinum loading on γ-Al_2O_3 with the addition of a solid base may explore the possibility of bi-functionality for catalytic reactions in one-pot synthesis strategy.[7] It has been reported that in an aqueous sugar solution contains almost 98 % sugar molecules in cyclic form and very less amount of sugar molecules are present in open chain form at equilibrium under neutral conditions.[8] Therefore, in order to enhance the sugar conversion into sugar alcohols, more amount of sugar molecules should present in the open chain. The thorough literature study suggested that under alkaline condition, sugar molecules undergo Lobry de Bruyn-Alberda van Ekenstein isomerization reaction.[9] This isomerization carried out via the formation of open chain intermediates. Therefore, in presence of active metal and hydrogen, the catalytic performance in the hydrogenation of sugar to sugar alcohols may enhance by open-chain sugar molecules under alkaline condition. Hence, the present study was focused on the hydrogenation reactions of xylose in the alkaline reaction medium. Considering the advantages of the heterogeneous nature of the solid base, in the present study, the solid base was used as a promoter in the hydrogenation of xylose to sugar alcohols.

The present chapter emphasized on the synthesis and characterization of zeolite K/LTL based micro-mesoporous composites and their catalytic activity was evaluated in solid base promoted hydrogenation of xylose to sugar alcohols in the aqueous phase with 3.5 *wt%* Pt/γ-Al_2O_3 as a catalyst.

3.2 Experimental

3.2.1 Chemicals

The chemicals used for the synthesis of zeolite K/LTL based micro-mesoporous composites and Pt/γ-Al_2O_3 catalyst are summarized in Chapter 2, Section 2.2.1.1, whereas, the chemicals used in the hydrogenation of xylose to sugar alcohols and the standardization for HPLC are summarized in Chapter 2, Section 2.5.1.1.

3.2.2 Synthesis of zeolites K/LTL based micro-mesoporous composites

The synthesis of K/LTL zeolite by hydrothermal crystallization is explained in Chapter 2, Section 2.2.1.2. The micro-mesoporous K/LTL zeolites synthesized, with varying molar $Si_{(K/LTL\ zeolite)}/OH^-_{(aq.\ KOH)}$ ratio (1.128-0.142 mol/mol), by post-synthesis modification using aqueous KOH treatment to pre-synthesized K/LTL zeolite is described in Chapter 2, Section 2.2.1.3. The obtained composites were designated as KL(X), where X indicates the concentration of the aqueous KOH solution used in the post-synthesis modification by alkali treatment.

3.2.3 Synthesis of 3.5 *wt%* platinum loading on the γ-Al_2O_3 catalyst

3.5 *wt%* Pt/γ-Al_2O_3 catalyst was synthesized by the impregnation method. The detailed procedure for the synthesis of 3.5 *wt%* Pt/γ-Al_2O_3 catalyst is discussed in Chapter 2, Section 2.2.1.6.

3.2.4 Characterization of micro-mesoporous composites and catalyst

A parent K/LTL zeolite, micro-mesoporous composites, and 3.5 *wt%* Pt/γ-Al_2O_3 catalyst are characterized using several analytical techniques such as ICP-OES, PXRD, N_2 adsorption-desorption measurement, FTIR, TEM, CO_2-TPD, ^{29}Si, and ^{27}Al MAS NMR, H_2-TPR are discussed in detail in Chapter 2, Section 2.4.

3.2.5 Catalytic activity

All the micro-mesoporous composites were tested as a solid base in the hydrogenation of xylose to sugar alcohols. The detailed about the solid base promoted hydrogenation of xylose to sugar alcohols over 3.5 *wt%* Pt/γ-Al_2O_3 catalyst in the aqueous phase is described in Chapter 2, Section 2.5.1.2.

3.2.6 Analysis of products and calculations

The reactants and the products formed during the hydrogenation reactions were analyzed by HPLC. The conversion and the products yields were calculated is given in Chapter 2, Section 2.5.1.3. This section also showed the calculations of kinetic diameter of the reactants and products.

3.3 Results and discussions

3.3.1 Characterization micro-mesoporous composite

3.3.1.1 Powder X-ray diffraction (PXRD)

The variation in the molar $Si_{(K/LTL\ zeolite)}/OH^-_{(aq.\ KOH)}$ ratio was accompanied by the changes in the structural features of the micro-mesoporous composites. The phase purity and the crystallinity of the composites were studied by PXRD as shown in Figure 3.1. One can see that, after undergoing the post-synthesis treatment, the intensity of diffraction peaks corresponding to K/LTL phase decreases with the decrease in molar $Si_{(K/LTL\ zeolite)}/OH^-_{(aq.\ KOH)}$ ratio without a change in the peak position from KL (0.3) to KL (2.8).

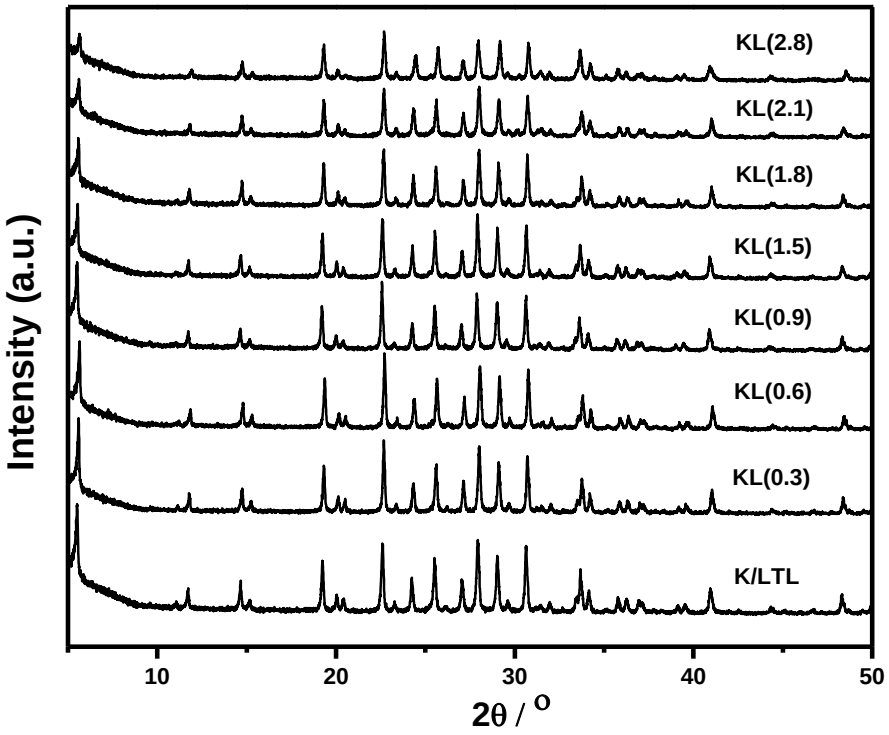

Figure 3.1. Powder X-ray diffraction patterns of parent K/LTL and micro-mesoporous composites

The concentration of alkali solution, molar $Si_{(K/LTL\ zeolite)}/OH^-_{(aq.\ KOH)}$ ratio and the % relative crystallinity values of all micro-mesoporous composites are tabulated in Table 3.1. KL(0.3) analogue has shown the minimal decrease in crystallinity (96 %) indicating no perceptible structural damage. The values of % relative crystallinity were found to decrease as molar $Si_{(K/LTL\ zeolite)}/OH^-_{(aq.\ KOH)}$ ratio was decreased indicating the progressive structural damage. KL(2.8) has exhibited the lowest value of % crystallinity (67) which can be associated with maximum structural damage due to the higher alkali concentration used for the treatment. Thus, the extent of the drop in % crystallinity was found to depend on the molar $Si_{(K/LTL\ zeolite)}/OH^-_{(aq.\ KOH)}$ ratio as it introduces the substantial mesoporosity on account of the preferential removal of framework (T= Si^{4+} and/or Al^{3+}) atoms from the zeolite crystal domain.[3] One of the possibilities of the decreasing PXRD crystallinity is the presence of amorphous zeolitic fragments on post-synthesis modification.

Table 3.1. Chemical composition and the crystallinity of the micro-mesoporous composites

Catalyst	C_{KOH} [a] (mol/L)	Molar $Si_{(K/LTL\ zeolite)}/OH^-_{(aq.\ KOH)}$ ratio	Crys.[b] (%)	(Si/Al)[c] Bulk	(Si/Al)[d] surf
K/LTL	-		100	2.86	2.84
KL(0.3)	0.3	1.128	96	2.76	2.69
KL(0.6)	0.6	0.664	92	2.64	2.55
KL(0.9)	0.9	0.442	89	2.65	2.51
KL(1.5)	1.5	0.265	86	2.63	2.46
KL(1.8)	1.8	0.221	81	2.57	2.40
KL(2.1)	2.1	0.189	77	2.48	2.37
KL(2.8)	2.8	0.142	67	2.35	2.23

a-Concentration of aqueous KOH solution used per gram of zeolite, b- PXRD, c-ICP-OES analysis, d-XPS

These observations demonstrated that in post-synthesis modification by alkali treatment, the molar $Si_{(K/LTL\ zeolite)}/OH^-_{(aq.\ KOH)}$ ratio played a crucial role in the formation of hierarchically structured micro-mesoporous composites.

3.3.1.2 Inductively coupled plasma-optical emission spectrometry (ICP-OES)

In order to investigate the influence of molar $Si_{(K/LTL\ zeolite),}$ $/OH^-_{(aq.\ KOH)}$ ratio on the elemental composition of KL(X) samples, the $(Si/Al)_{bulk}$ ratio was determined by ICP-OES analysis and is presented in Table 3.1. The molar $(Si/Al)_{bulk}$ ratio of parent K/LTL was 2.86. Upon aqueous KOH treatment, the molar $(Si/Al)_{bulk}$ ratio of the micro-mesoporous KL(X) composites was decreased from 2.76 to 2.35 with the decreasing the molar $Si_{(K/LTL\ zeolite)}/OH^-_{(aq.\ KOH)}$ ratio from 1.128 to 0.142. Nevertheless, the filtrate analysis showed that the aqueous KOH solution treatment resulted in the leaching of aluminum. Indeed, the amount of leached aluminum was negligible as compared to the amount of silicon in the filtrate. Thus, the decrease in $(Si/Al)_{bulk}$ ratio of micro-mesoporous KL(X) composites suggested the preferential extraction of silicon from the K/LTL zeolitic framework.

3.3.1.3 X-ray photoelectron spectroscopy (XPS)

The surface composition of the samples in terms of $(Si/Al)_{surf}$ ratio was also quantified by the XPS measurements and values are tabulated in Table 3.1. Similar to bulk $(Si/Al)_{bulk}$ ratio, the surface $(Si/Al)_{surf}$ ratio of the entire samples also found to decrease with the decrease in molar $Si_{(K/LTL\ zeolite)}/OH^-_{(aq.\ KOH)}$ ratio. When compared with the $(Si/Al)_{bulk}$ ratio, all samples have shown lower values for $(Si/Al)_{surf}$ indicating the relatively high amount of Al was present on the surface. Moreover, the % decrease in the $(Si/Al)_{surf}$ was found to be higher than $(Si/Al)_{surf}$ ratio in case of all the KL(X) composites. The formation of an aluminium rich surface in all alkali treated samples can be considered as an evidence for the preferential removal of silicon atoms and for the enhanced accessibility or population of sites associated with the Al-species.

3.3.1.4 N_2 adsorption-desorption measurement

In order to investigate the structural changes, the nitrogen adsorption and desorption measurement were carried out and the isotherms of representative micro-mesoporous samples viz. K/LTL, KL(0.3), KL(0.6), KL(1.5), KL(2.8) are shown in Figure 3.2. The K/LTL zeolite exhibited a type I isotherm with higher N_2 uptake at lower relative pressures corresponding to the microporous molecular sieves. The hysteresis loop at the relative pressure of 0.3 indicates the presence of mesoporosity on account of intercrystalline porosity formed by of the accumulation of the zeolite crystals.[10] The hierarchical KL(X) samples exhibited a combination of both type I and type IV isotherms.[11] The alkali treatment resulted in the steady enhancement in the nitrogen uptake up to the concentration 1.8 M in the order of: K/LTL < KL(2.8) < KL(0.3) < KL(0.6) < KL(1.5).

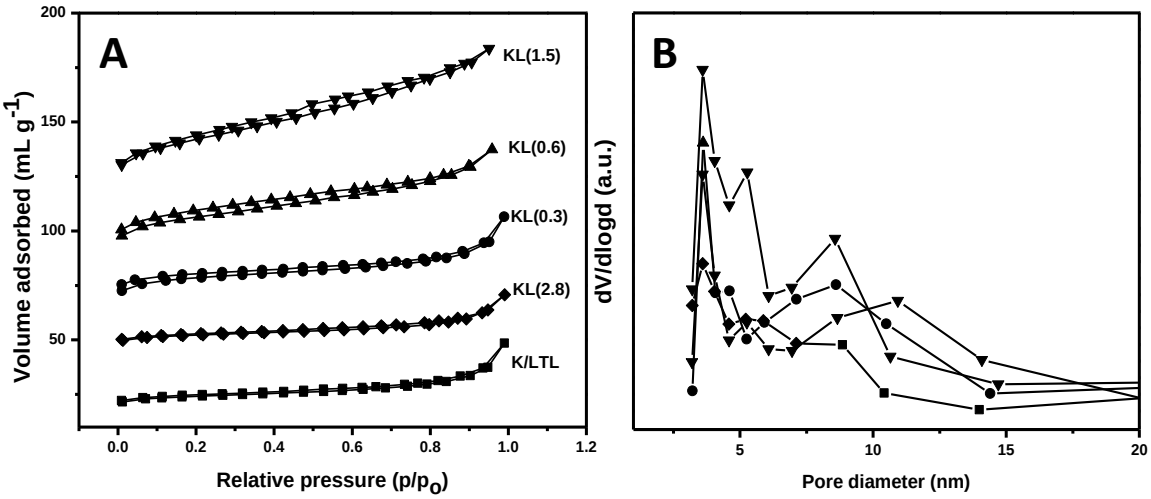

Figure 3.2. Nitrogen adsorption-desorption isotherm of parent and micro-mesoporous KL(X) composites (A) and corresponded BJH pore size distribution (B)

The values for BET surface area, mesoporous surface area, total pore volume, the pore volumes from microporous and mesoporous regions of all the samples are summarized in Table 3.2. The BET surface area and the mesoporous surface area for micro-mesoporous composites were increased with decreasing molar $Si_{(K/LTL\ zeolite)}/OH^-_{(aq.\ KOH)}$ ratio from K/LTL to KL(1.8). In addition, the total pore volume and the pore volume in the mesopore region were also increased in a similar fashion. This increase in porous properties indicating the alkali treatment led to the formation of pores in the mesoporous region at the expense of micropores as micropore volume was decreased with decrease in molar $Si_{(K/LTL\ zeolite)}/OH^-_{(aq.\ KOH)}$ ratio. Further, the decline in the nitrogen uptake for KL(2.1) and KL(2.8), may be partly due to the severe structural damage as indicated by a considerable % relative crystallinity loss by the severe alkali treatment. Another possibility for a decrease in the BET surface area and the total pore volume which cannot be denied is that, upon sever alkali treatment, amorphous debris formed may also block the pores leading to lower nitrogen uptake.

Table 3.2. Physico-chemical properties of the micro-mesoporous composites

Catalyst	S_{BET}[a] (m^2/g)	S_{meso}[b] (m^2/g)	V_{Pore}[c] (cm^3/g)	V_{Meso}[d] (cm^3/g)	V_{Micro}[e] (cm^3/g)	Basicity[f] (mmol/g)
K/LTL	220	-	0.13	0.010	0.120	0.159
KL(0.3)	240	185	0.21	0.103	0.107	0.172
KL(0.6)	241	188	0.22	0.115	0.105	0.186
KL(0.9)	242	192	0.23	0.125	0.106	0.203
KL(1.5)	245	194	0.24	0.138	0.102	0.209
KL(1.8)	248	208	0.38	0.290	0.090	0.219
KL(2.1)	230	189	0.15	0.120	0.030	0.227
KL(2.8)	225	176	0.16	0.098	0.062	0.254

a-BET surface area, b-mesopore surface area by the t-plot method, c- Total pore volume by Langmuir method, d- Pore volume from the mesoporous region by BJH method, e- Pore volume from the microporous region by HK method, f- by CO_2-TPD

In conclusion, molar $Si_{(K/LTL\ zeolite)}/OH^-_{(aq.\ KOH)}$ ratio of 0.265 was found to be an optimum ratio for micro-mesoporous composites with improved textural properties without significant loss of pronounced crystallinity was achieved. The preferential removal of silicon atoms from the framework confirming the aqueous KOH treatment resulted in the formation of secondary mesopores with higher mesoporous volume.

3.3.1.5 Temperature programmed desorption of CO_2 (CO_2-TPD)

The influence of molar $Si_{(K/LTL\ zeolite)}/OH^-_{(aq.\ KOH)}$ ratio on the basicity of micro-mesoporous composites was evaluated by CO_2-TPD technique and the corresponding basicity is tabulated in Table 3.2. It was revealed that, upon alkali treatment, the total basicity was increased with the decrease in the molar $Si_{(K/LTL\ zeolite)}/OH^-_{(aq.\ KOH)}$ ratio. The basicity trend observed in the order of: KL(2.8) > KL(2.1) > KL(1.8) > KL(1.5) > KL(0.9) > KL(0.6) > KL(0.3) > K/LTL. The enhancement in basic sites could be ascribed to the decrease in molar Si/Al ratio and the higher aluminate anion content that are bounded to the potassium ions as charge compensating cations per gram of sample.[11]

3.3.1.6 Fourier transform infrared spectroscopic analysis (FTIR)

The FTIR spectra of all the samples are shown in Figure 3.3. The absorption bands appeared at 608 and 643 /cm could be assigned to the double six-membered ring vibration from the external linkage.[12] Moreover, the absorption bands appeared at 725 and 768 /cm were attributed to the symmetric T-O (T= Si or Al) stretching vibrations due to the external tetrahedral linkage.[12] The intensities of absorption bands related to symmetric T-O stretching vibrations and double ring vibration were sensitive to molar Si/Al composition of the zeolite.[13] The frequency of these bands was found to vary with the variation in molar Si/Al ratios. The frequency shifting to the higher or lower values is believed to be due the dealumination or desilication, respectively.[13]

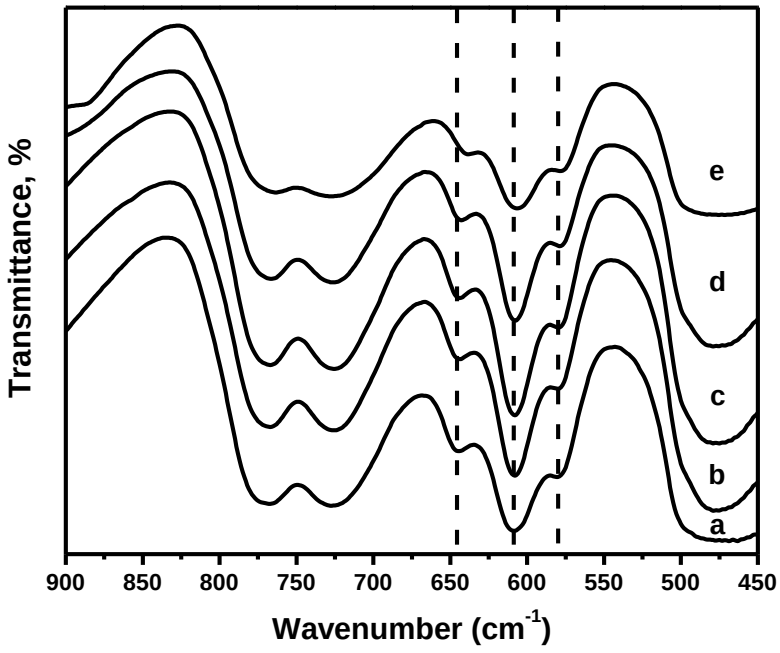

Figure 3.3. FTIR spectra of parent and micro-mesoporous composites a) K/LTL, b) KL(0.3), b) KL(0.6), d) KL(1.5), e) KL(2.8)

Table 3.3. FTIR frequencies of parent and hierarchical K/LTL zeolites

Catalysts	Double six-member ring vibration (/cm)		Symmetric T-O stretching vibrations (/cm)	
K/LTL	608.1	643.7	725.3	768.5
KL(0.3)	607.9	642.9	725.0	767.3
KL(0.6)	607.6	642.1	724.2	765.8
KL(1.5)	607.3	640.2	723.0	765.2
KL(2.8)	606.3	639.2	721.5	763.2

The FTIR results implied that the frequencies of symmetric T-O stretching vibrations and double ring vibration gradually shifted to lower wavenumbers with decrease in the molar $Si_{(K/LTL\ zeolite)}/OH^-_{(aq.\ KOH)}$ ratio (Table 3.3). The shifting of wavenumber could be ascribed to the preferential extraction of the silicon from the zeolite framework in an alkaline medium.[13, 14] The results were consistent with Si/Al_{bulk} ratios estimated by ICP-OES analysis.

3.3.1.7 ^{29}Si and ^{27}Al solid-state magic angle spinning nuclear magnetic resonance spectroscopy (^{29}Si and ^{27}Al MAS NMR)

The silicon and aluminium environment in the parent and micro-mesoporous KL(X) composite frameworks were studied by ^{29}Si and ^{27}Al MAS NMR spectra, respectively, and are presented in Figure 3.4. In ^{29}Si MAS-NMR spectra (Figure 3.4 A), all samples showed two distinct resonance peaks at -97.1 and -101.5 ppm corresponding to Si (2Al) and Si (1Al), respectively, while a weak resonance peak at -107.5 ppm attributed to the Si (0Al).[15, 16] It clearly exhibited from Figure 3.4 A that, the relative integrated area under the peak associated with Si (0Al) and Si (1Al) units apparently decreased with the decrease in the molar $Si_{(K/LTL\ zeolite)}/OH^-_{(aq.\ KOH)}$ ratio. Whereas the relative integrated area under the peak corresponding Si (2Al) was found to increase gradually with the decrease in the molar $Si_{(K/LTL\ zeolite)}/OH^-_{(aq.\ KOH)}$ ratio. The decrease in silicon-rich units by alkaline treatment resulted in an increase in the population of the aluminium rich silicon units. It has been reported that the aluminium rich zeolites with lower Si/Al ratio face the difficulties in the

silicon removal by the attack of OH^- ions, due to negatively charged AlO^{4-} that prevents the hydrolysis of the Si-O-Al bond.[6] Based on the above discussion, it can be inferred that the decrease in the molar $Si_{(K/LTL\ zeolite)}/OH^-_{(aq.\ KOH)}$ ratio leads to the preferential removal of the silicon atoms.

Figure 3.4 B shows the ^{27}Al MAS NMR spectra of the parent and micro-mesoporous composites. All samples showed a strong resonance peak centered at 54.1 ppm originating from tetrahedrally coordinated aluminium sites, whereas the octahedrally coordinated Al (signal at 0 ppm) was found to be absent.[11] Thus all samples possess no extra-framework aluminium on account of post-synthesis alkali treatment irrespective of its molar $Si_{(K/LTL\ zeolite)}/OH^-_{(aq.\ KOH)}$ ratio. Nevertheless, the intensity of the signal was found to increase slightly with the increase in the concentration of alkali suggesting an increase in the relative content of tetrahedral Al species.

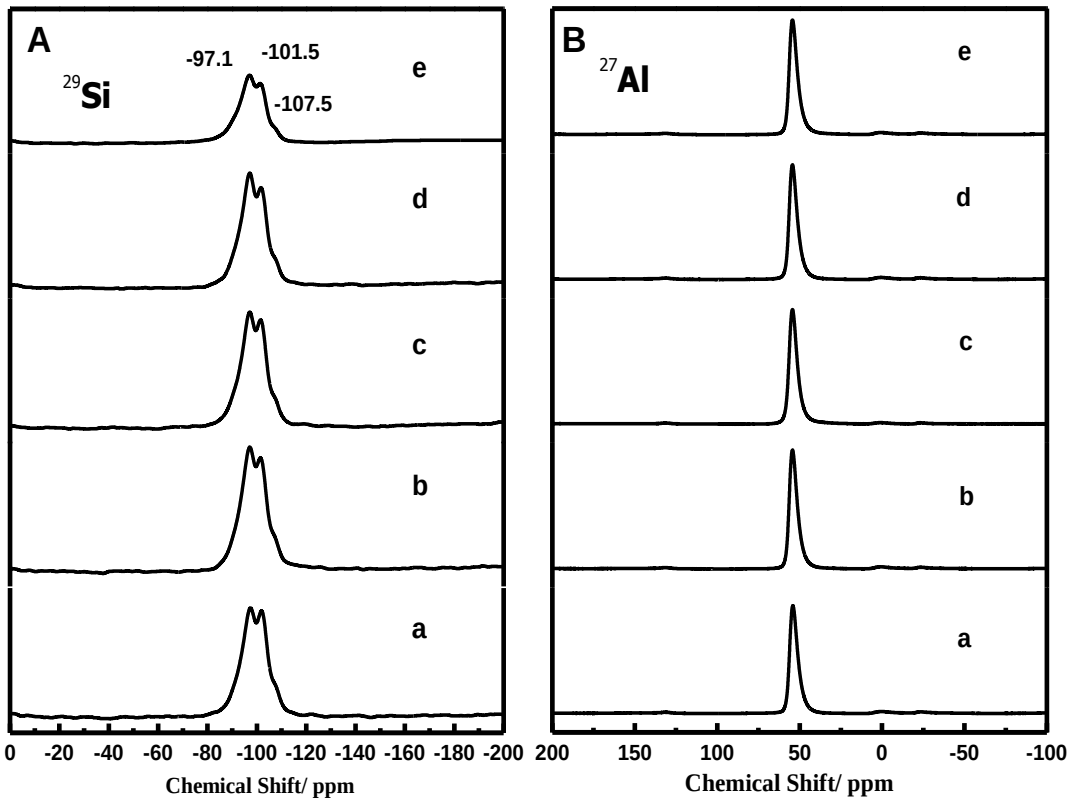

Figure 3.4. ^{29}Si and ^{27}Al MAS-NMR spectra of parent and hierarchical zeolites, a) K/LTL, b) KL(0.3), b) KL(0.6), d) KL(1.5), e) KL(2.8)

Table 3.4. Relative content of Si(nAl) units (n = 0-2) and Si/Al ratio determined by ^{29}Si MAS NMR spectra of parent K/LTL zeolite and micro-mesoporous composites

Composites	Si/Al_{NMR}	% Relative content of Si(nAl) units		
		Si (0Al)	Si (1Al)	Si (2Al)
K/LTL	2.89	12	38	50
KL(0.3)	2.77	10	36	54
KL(0.6)	2.70	9	34	57
KL(1.5)	2.63	7	34	59
KL(2.8)	2.50	5	30	65

Further, the Si/Al_{NMR} ratios of micro-mesoporous composites were determined by ^{29}Si MAS NMR and the relative content of Si(nAl) units of parent and their analogues are tabulated in Table 3.4. As can be seen, the Si/Al_{NMR} ratio was decreased with the decrease in the molar $Si_{(K/LTL\ zeolite)}/OH^-_{(aq.\ KOH)}$ ratio studied for the post-synthesis treatment of parent K/LTL. These results are also supported ICP-OES and XPS analysis, suggesting a preferential removal of silicon from the framework. The lesser susceptibility towards silicon removal from the aluminium rich silicon units might be associated with higher stabilization by neighboring Al-rich environment.[17]

3.3.1.8 Scanning electron microscopy (SEM)

The uniformity of prepared samples was checked by SEM images of K/LTL and micro-mesoporous composites as provided in Figure 3.5. The SEM image of the parent K/LTL zeolite showed the cylindrically shaped morphology of K/LTL zeolite (Figure 3.5 A). The SEM image of the KL(1.5) showed that the cylindrical shape of most of the zeolite crystals was maintained, but the edges of the zeolite crystals were damaged as clearly seen in Figure 3.5 B. This could be observed as a result of mass loss by the desilication on post-synthesis modification. Further, severe alkali treatment to K/LTL zeolite with 2.8 M KOH solution resulted in the formation of a substantial amount of amorphous debris/ aggregates of zeolite crystals (Figure 3.5 C).

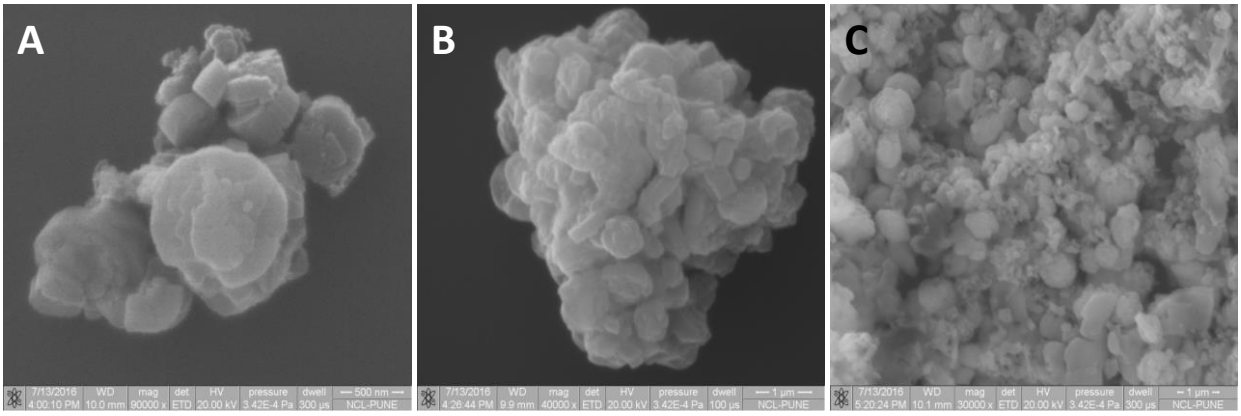

Figure 3.5. SEM images of A) K/LTL, B) KL(1.5) and C) KL(2.8)

3.3.1.9 Transmission electron microscopy (TEM)

Further, the structural features of the micro-mesoporous composite were studied by TEM analysis. Figure 3.6 shows the TEM images of the parent K/LTL, revealed cylindrical rod shape aggregates of fully grown parent K/LTL zeolite crystals. The TEM image of the micro-mesoporous KL(1.5) composite (Figure 3.6 B) showed the alkali treatment caused the structural destruction witnessed at the edges of the crystals. This could be attributed to the preferential removal of silicon atoms from the zeolite framework. As a result, the non-uniform intra-crystalline mesopores appeared with higher mesoporous volume. The TEM image also explains why the percentage crystallinity calculated by PXRD drastically reduced by the treatment of higher concentration of aqueous KOH solution.

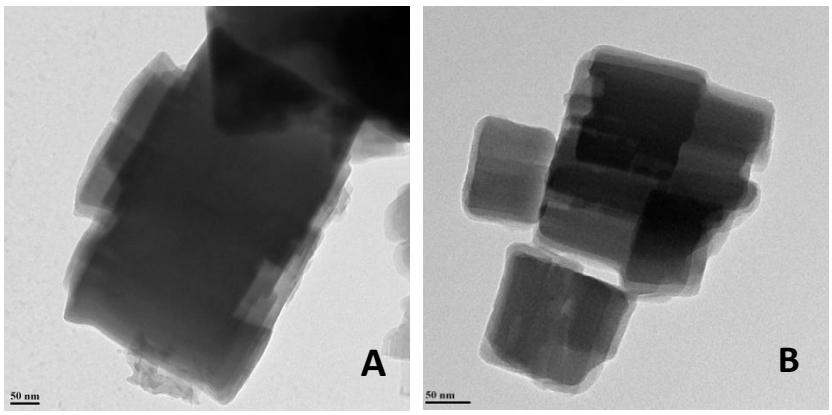

Figure 3.6. TEM images of A) K/LTL and B) KL(1.5)

3.4 Hydrogenation of xylose over micro-mesoporous composites as a solid base

3.4.1 Initial screening of micro-mesoporous composites

Typically, the catalytic hydrogenation of xylose to xylitol is accompanied by the formation of a small number of undesirable side products such as arabitol, xylulose, glycerol, ethylene glycol, 1, 2-propanediol, etc. These side products are formed during, 1) isomerization of xylose to xylulose, and, 2) the subsequent secondary reduction/ cracking/ hydrogenolysis reactions. Considering this, it was interesting to study the effect of synthesized materials on the formations of these products.

The influence of microporous parent K/LTL and micro-mesoporous composites with combined micro-mesoporosity as solid bases in xylose hydrogenation over 3.5 *wt%* Pt/γ-Al_2O_3 was investigated as shown in Figure 3.7. The catalytic activity over 3.5 *wt%* Pt/γ-Al_2O_3 catalyst at 60 ^oC showed 10.5% xylose conversion with only 4% sugar alcohols (xylitol and arabitol) yield at 4 h. The noticeable effect of a solid base on the hydrogenation of xylose over Pt/γ-Al_2O_3 catalyst under above-mentioned reaction conditions was observed after the addition of an equal quantity of K/LTL zeolite to the reaction mixture. The parent K/LTL zeolite as a solid base showed 16% xylose conversion and 7% sugar alcohols yield. In order to check the effect of Pt/γ-Al_2O_3 catalyst, the control experiment under the similar conditions (60 ^oC and 16 bar H_2 pressure for 4 h) was carried out solely with a solid base (KL(1.5)) but sugar alcohols formation was not observed in this reaction. Thus, for the formation of sugar alcohols, the presence of Pt/γ-Al_2O_3 catalyst along with a solid base is required.

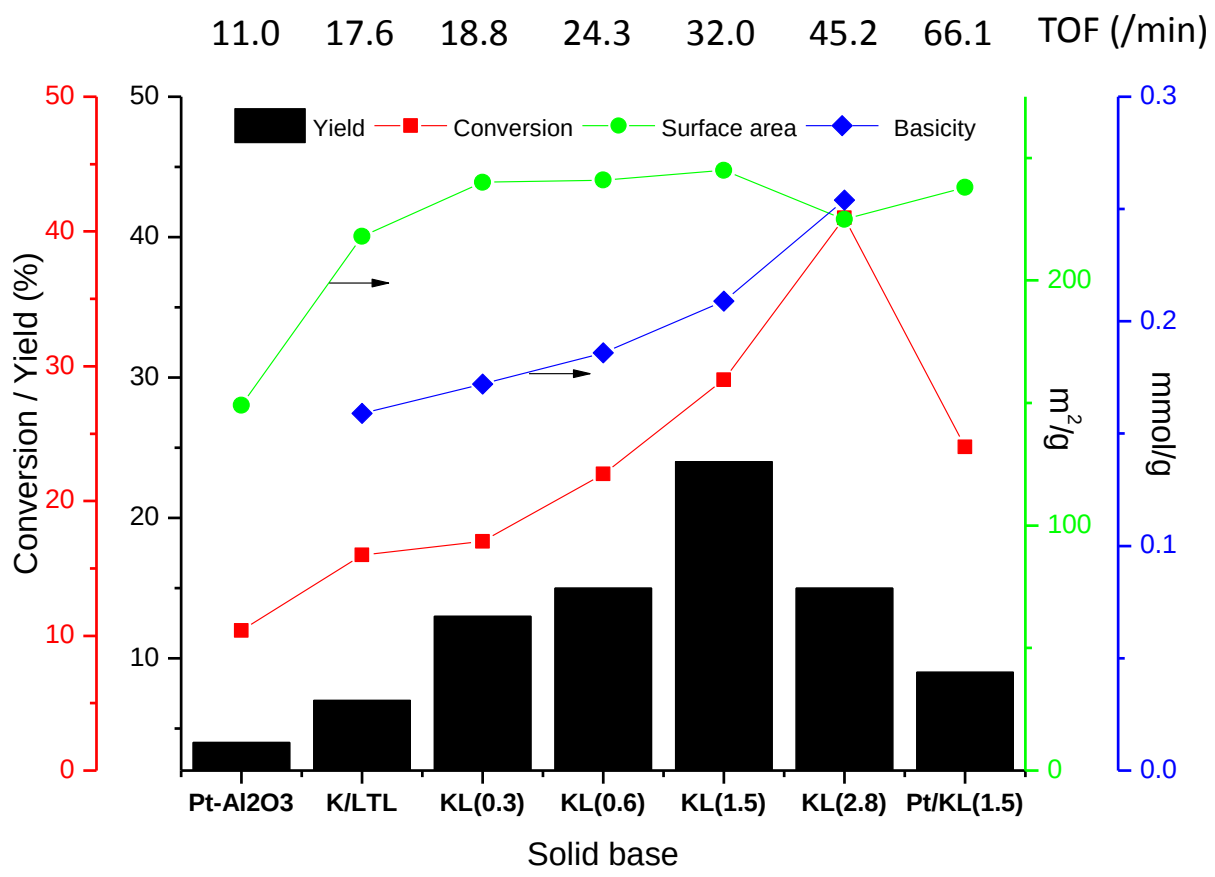

Figure 3.7 The influence of micro-mesoporous KL(X) composites solid base as an additive in xylose hydrogenation over 3.5 *wt%* Pt/γ-Al_2O_3 catalyst
(Reaction condition: Xylose: 0.15 g, Catalyst: 0.075 g, Solid base: 0.075 g, Volume of H_2O: 35 mL, Temperature: 60 °C, Pressure: 16 bar H_2 at room temperature, Time: 4 h, 900 RPM)

The micro-mesoporous KL(X) composites were synthesized varying molar $Si_{(K/LTL\ zeolite)}/OH^-_{(aq.\ KOH)}$ ratio and these samples showed a pronounced effect in catalytic hydrogenation of xylose carried out at 60 °C for 4 h over Pt/γ-Al_2O_3 catalyst. With the addition of KL(0.3) (17%), KL(0.6) (22%) and KL(1.5) (29%) composites as a solid base, the enhancement in xylose conversion was observed compared to hydrogenation carried out with only Pt/γ-Al_2O_3 catalyst (10.5 %). A similar trend of improvement in yield of sugar alcohol was also observed after addition of K/LTL treated with increasing concentration of KOH treatment (13% with KL(0.3), 15% with KL(0.6), and 24% with KL(1.5).

The trend of sugar alcohols yield was observed to be in line with the basicity of the micro-mesoporous KL(X) composites in aqueous solution. The pH of the reaction mixture was increased in the following order: KL(0.3) (pH, 8.6) < KL(0.6) (pH, 8.7) < KL(1.5) (pH, 9.1). However, under identical reaction conditions, the KL(2.8) sample showed 41% xylose conversion and 15% sugar alcohols yield. Although the pH of KL(2.8) reaction mixture was 9.5, the catalytic activity of KL(2.8) was lower as compared to KL(1.5) with lower pH value (pH, 9.1). In order to confirm the catalytic activity, the adsorption study of xylose and xylitol on the catalyst system was studied and it showed that only 7 *wt%* xylose and 4 *wt%* xylitol were adsorbed on the catalyst surface.

It is reported in the literature that the basic sites are active for ring opening of sugar molecules, which in turn improve the yield of sugar alcohols.[7, 9] The formation of the open chain form of xylose in the basic medium was confirmed by UV-Vis spectroscopic analysis, as shown in Figure 3.8. The detailed experimental procedure for UV-Vis analysis is discussed as follows. UV-Vis analysis of the aqueous solution of xylose in presence of solid base was performed to check the possibility of the ring chain opening phenomenon of xylose in alkaline media. The sugar solution A was prepared by dissolving of 0.2 g of xylose in 10 mL millipore water (pH =6.23). Another solution B was prepared by the mixing of 0.2 g of xylose and 0.1 g base in 10 mL millipore water (pH = 9.52). Finally, sugar solutions were subjected to UV-Vis analysis.

Since the CHO group of sugar (glucose/xylose) is UV active, therefore, if the xylose is present in the open chain, it should show the peak maxima at about λ_{max} = 270 nm.[7] In the present study, the small absorbance peak with lower intensity at λ_{max} = 268.3 nm was observed in xylose solution (Figure 3.8 a, pH = 6.23) which is corresponded to the presence of CHO group in the open chain of xylose molecules. Further, the addition of solid base to the xylose solution resulted in enhancement in the absorbance peak of CHO group (λ_{max} = 272.2 nm) by many folds (Figure 3.8 b, pH = 9.23). The UV-Vis study clearly showed that, in alkaline conditions, the cyclic form xylose is converted into an open chain form which will be promoting the hydrogenation reactions.

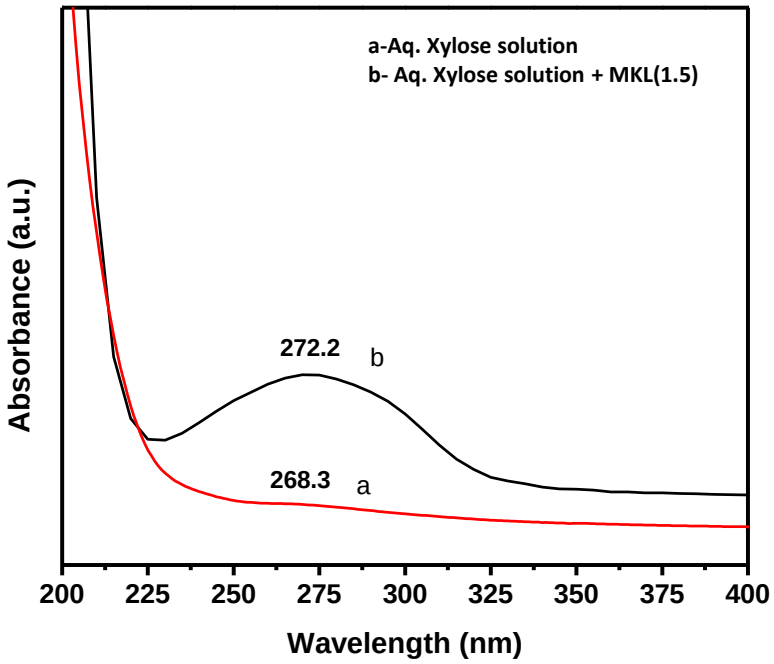

Figure 3.8. UV absorbance spectra of xylose

In addition to this, the kinetic diameters of xylose and xylitol are 6.55 Å and 6.58 Å, respectively as calculated based on the molecular weight of the molecules as reported in the literature.[18] The pore dimensions of parent K/LTL zeolite (pore dimensions 7.1 Å x 7.1 Å) and the kinetic diameter of the sugar and sugar alcohol are thus very much comparable. Hence, xylose molecules may experience restriction in accessing the basic sites in K/LTL zeolite pores. Further, it was assumed that due to the increase in the pore size of K/LTL zeolite after treatment with KOH would provide higher accessibility of the basic sites and this would eventually increase the catalytic performance.

With regards to the micro-mesoporous analoges, the catalytic activity of alkali treated zeolites was increased with increasing severity of alkali treatment. It appears that the pronounced effect of desilication was observed for KL(1.5) composite prepared by treating K/LTL with aqueous 1.5 M KOH solution per gram of zeolite. As shown in Table 3.1, the desilication resulted in the decrease in the Si/Al ratio, which enhanced the basicity of micro-mesoporous composites. Therefore, the KL(1.5) analogue showed higher catalytic performance in the hydrogenation of xylose. Further, KL(1.8) showed almost similar activity as that KL(1.5).

The catalytic activity results of micro-mesoporous KL(X) composites as compared to the parent K/LTL anticipated that, in addition to the basicity, the effective mass transfer through mesopores is responsible for the enhanced catalytic activity for xylose hydrogenation carried out with Pt/γ-Al_2O_3 catalyst at 60 ^oC for 4 h along with solid base. The catalytic activity increased in the order: K/LTL (7%) < KL(0.3) (13%) < KL(0.6) (15%) < KL(1.5) (24%), which was in accordance with the increasing trend of BET surface area and total pore volume. The probable reason for the higher activity could be the confined space of the hierarchical KL(1.5) zeolite with micro-mesoporous nature allows higher accessibility of aluminates ions to the xylose molecules and ring opening takes place. However, the significant decrease in the catalytic activity was observed for KL(2.8) which was probably due to the blocking of developed mesopores by the amorphous debris as evidenced by TEM and N_2 adsorption-desorption data.

Other crucial factors that influence the catalytic performance are the particle size and the homogeneous distribution of platinum on a solid support (γ-Al_2O_3). The PXRD pattern of 3.5 *wt%* Pt loaded on γ-Al_2O_3 solid support is shown in Figure 3.9. The PXRD pattern depicts characteristic peaks at 2θ°= 39.8, 46.3, 67.5, 81.3 and 85.8 were assigned to (111), (200), (220), (311), and (222) planes, respectively, that corresponding to the metallic platinum particles (JCPDS file no. 01-088-2343).

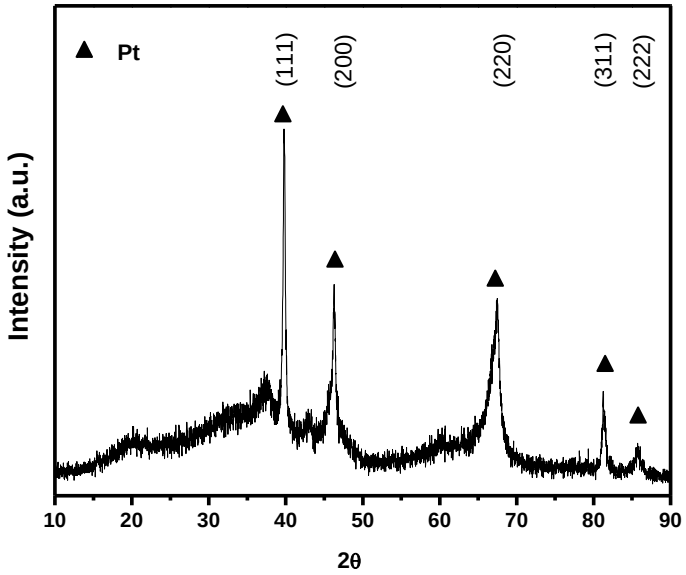

Figure 3.9. PXRD pattern of 3.5 *wt*% Pt loaded γ-Al_2O_3 catalyst

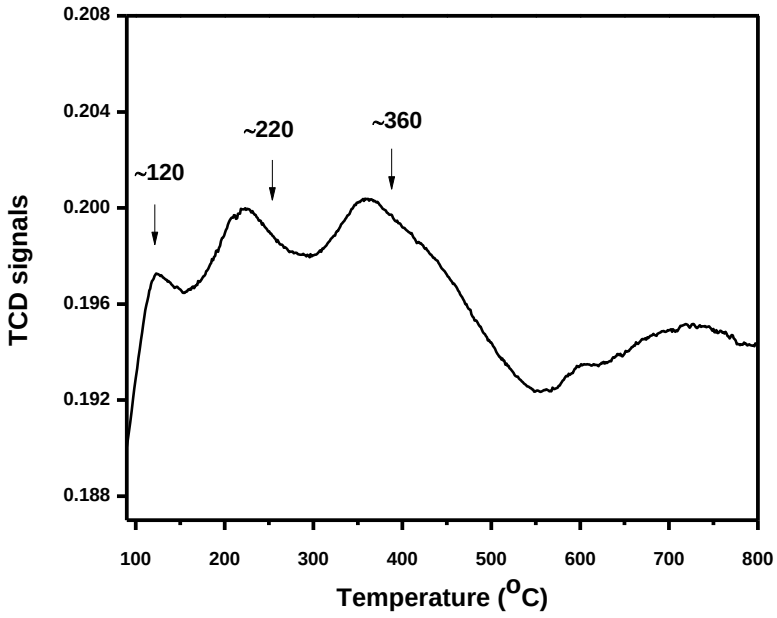

Figure 3.10. H_2-TPR profile of 3.5 *wt%* Pt/Al_2O_3 catalyst

Further, the H_2-TPR profile of 3.5 *wt%* Pt/Al_2O_3 catalyst was done to understand the interaction of Pt with alumina support as shown in Figure 3.10. The $Pt\text{-}Al_2O_3$ catalyst was primarily characterized by three hydrogen consumption peaks. The first peak centered at ~120 ^oC could be assigned to the reduction of PtO_2 particles weakly bonded to the alumina support. Another hydrogen consumption peak at ~220 ^oC could assign to the reduction of Pt^{4+} species in tiny PtO_2 particles, whereas, the pronounced hydrogen consumption at ~360 ^oC could be characteristics of reduction of isolated Pt^{2+} ions. [19] The reduction peak at higher temperature was corresponding to the strong interaction of Pt on the alumina support. These results are in line with the reported literature.[19] Aznarez et al. also showed that the noble metal and solid support interaction was governed mainly by the calcination temperature and nature of the metallic phase and solid support.[19]

The Pt metal loading on $\gamma\text{-}Al_2O_3$ solid support was evaluated by TEM analysis. It is reported in the literature that one of the reasons for improved catalytic activity was the higher dispersion of nano-sized platinum on a solid support.[20] Figure 3.11 showed the TEM image and corresponding particle size distribution of 3.5 *wt*% Pt loaded on KL(1.5) and $\gamma\text{-}Al_2O_3$ supports. The average particles size of the platinum was distributed in the range of 2-

10 nm whereas, in the case of KL(1.5) support, the particle size of the platinum was found to be 2-20 nm.

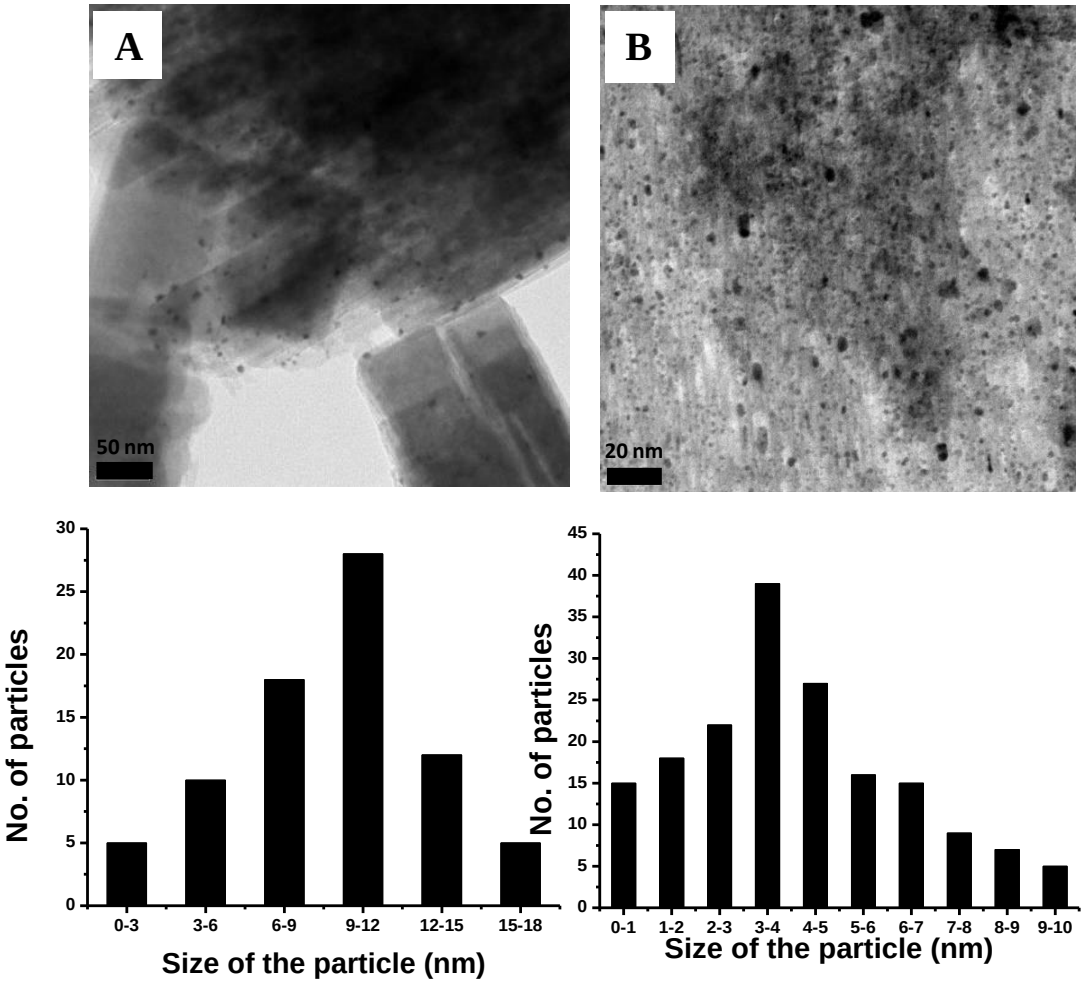

Figure 3.11. TEM images of 3.5 wt% Pt loaded on KL(1.5) and γ-Al_2O_3 supports

Considering the Pt particle size by TEM images, the TOF values for all the catalytic systems were calculated. It showed that the TOF value of Pt/γ-Al_2O_3 catalyst at 60 ^oC for 4 h for the hydrogenation of xylose was 11.0 /min. Further, the addition of a solid base to the reaction medium results in the increase in the TOF values from K/LTL (17.6 /min) to KL(2.8) (45.2 /min). In order to study the influence of the micro-mesoporous KL(X) composites as solid support and milder acidity of alumina, the hydrogenation of xylose to xylitol was evaluated with 3.5 *wt*% platinum loading on parent K/LTL and micro-mesoporous KL(1.5) composite under given reaction conditions. The 3.5 *wt*% Pt/K/LTL showed only 4% xylose conversion with 1% sugar alcohols yield. Similarly, 3.5 *wt*% Pt/

KL(1.5) gave 25% xylose conversion with 4% sugar alcohols yield. These results speculated that the milder acidity of γ-Al_2O_3 as a solid support may contribute to the catalytic activity.[7] We observe from all the data as represented in Figure 3.7 that KL (1.5) having the optimized surface area, basicity and mesopore volume is the best solid base to achieve highest sugar alcohol yield. As seen from Figure 3.7, the activity was directly correlated with surface area, and basicity only with an exception to KL (2.8). Even if KL (2.8) exhibited higher basicity than KL(1.5) but due to the limitation of accessibility of these basic sites (as is evident from the surface area and pore volume) and also may be due to higher basicity, side reactions are prominent, lower activity was observed.

In summary, the experimental results concluded that the catalytic performance of the micro-mesoporous KL(X) composites as solid base was influenced by 1) the basicity of oxygen corresponding to the aluminate ions increased with the concentration of alkali solution per gram of the zeolite, 2) the co-existence of micro-mesoporous structure, and 3) the nano-sized platinum on solid support.

3.4.2 Optimization of reaction parameters

3.4.2.1 Effect of temperature

The influence of the temperature on the xylose conversion was studied in the range of 40-80 ^{o}C under given reactions conditions (Figure 3.12). The activity of catalytic hydrogenation of xylose was increased as a function of temperature (until 60 ^{o}C) and thereafter remains constant. The xylose conversion was increased from 19% to 29% as the reaction temperature was increased from 40 to 60 ^{o}C. This suggesting that the temperature of 60 ^{o}C favored xylose conversion as the sugar alcohols yield enhanced from 14% to 24%. Whereas at a higher temperature of 80 ^{o}C, the xylose conversion was marginally increased to 31% and the sugar alcohols yield of 25% was obtained. Therefore, further optimization of reaction parameters was carried out at 60 ^{o}C temperature.

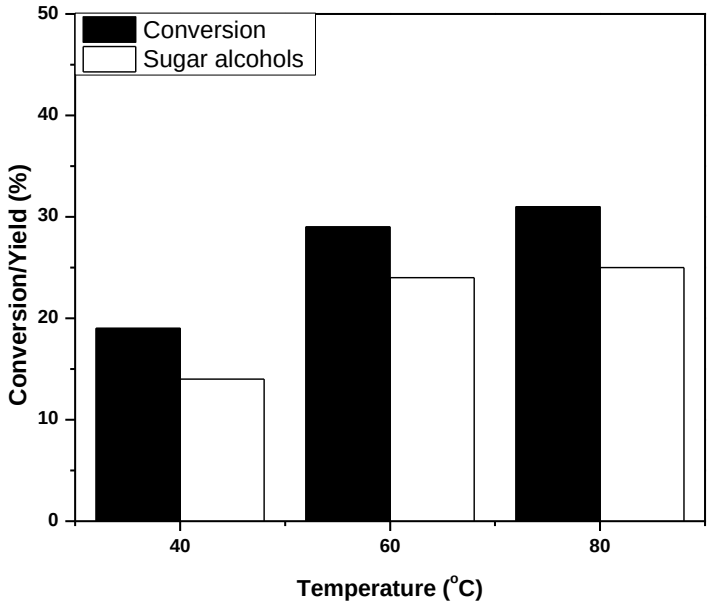

Figure 3.12. The effect of temperature on micro-mesoporous KL(1.5) composite as a solid base in xylose hydrogenation over 3.5 *wt%* Pt/γ-Al_2O_3 catalyst
(Reaction Conditions: Xylose: 0.15 g, Catalyst: 0.075 g, Solid base: 0.075 g, Volume of H_2O: 35 mL, Pressure: 16 bar H_2 at room temperature, 4 h, 900 RPM)

3.4.2.2 Effect of hydrogen pressure

The influence of hydrogen pressure on the catalytic activity was evaluated at 60 °C in a 4 h reactions and the hydrogen with a pressure from 8 to 24 bar as shown in Figure 3.13 was charged in the reactor at the beginning of the reaction. Though, the xylose hydrogenation was found to increase marginally from 28% to 35% with increasing pressure from 8 to 24 bar. But, the sugar alcohols yield was drastically increased from 12% to 30% with increasing hydrogen pressure. This indicated that the hydrogenation of xylose is directly proportional to the hydrogen pressure to obtain desired products. It is reported that the solubility of the hydrogen gas varies as a function of partial pressure of hydrogen at a given temperature.[21] At a temperature of 51.6 °C, the solubility values of hydrogen gas in the water at 8, 16 and 24 bar are approximately 0.19, 0.32, and 0.45 mL/g, respectively.[21] It is assumed that hydrogen after dissolution in the aqueous phase adsorbs on the surface of active metal sites, which in turn generates activated hydrogen. It is

suggested that with the higher dissolution of hydrogen in the solvent will enhance the pool of active hydrogen species in the solvent which in turn will influence the catalytic activity. The activated hydrogen is responsible for driving the hydrogenation of xylose to yield sugar alcohols with higher selectivity.[22] The optimum hydrogen pressure of 16 bar was used for further hydrogenation reactions.

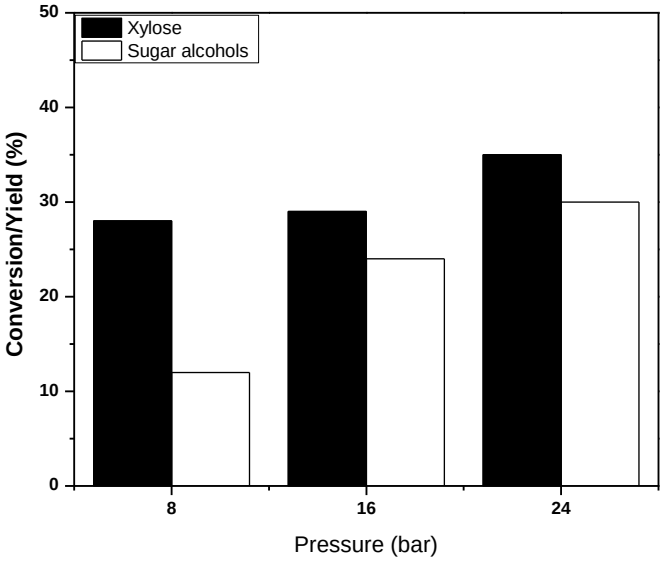

Figure 3.13. The effect of pressure on micro-mesoporous KL(1.5) composite as a solid base in xylose hydrogenation over 3.5 *wt%* Pt/γ-Al_2O_3 catalyst
(Reaction Conditions: Xylose: 0.15 g, Catalyst: 0.075 g, Solid base: 0.075 g, Volume of H_2O: 35 mL, Temperature: 60 °C, Time: 4 h, 900 RPM)

3.4.2.3 Effect of a solid base to catalyst ratio

The effect of the amount of solid base to Pt/γ-Al_2O_3 catalyst ratio towards the xylose conversion was studied and the results are summarized in Figure 3.14. The ratios of solid base, KL(1.5) to Pt/γ-Al_2O_3 used were 1:0.5 (pH, 10.2), 1:1 (pH, 9.1) and 1:2 (pH, 7.9) (*wt/wt*). The catalytic activity for xylose hydrogenation was increased from 16% to 61% with an increase in the solid base to catalyst ratio from 1:0.5 to 1:2. Similarly, the sugar alcohols yield was found to increase from 11% to 36%. Under the same reaction conditions, the maximum selectivity of sugar alcohols (83%) was observed at a ratio of 1:1 because of more Pt active sites on the γ-Al_2O_3 catalyst were available for hydrogenation. Interestingly, although higher xylose conversion and the sugar alcohols yield were

observed at a higher ratio of 1:2, the selectivity of sugar alcohols was lowered (59%). The lower activity at higher ratio could be due to the fact that the rate of hydrogenation of xylose may be faster than that of ring opening of xylose in open chain form. These results envisioned that the optimization of a solid base to the Pt/γ-Al_2O_3 catalyst ratio is important in order to achieve the higher selectivity to sugar alcohols.

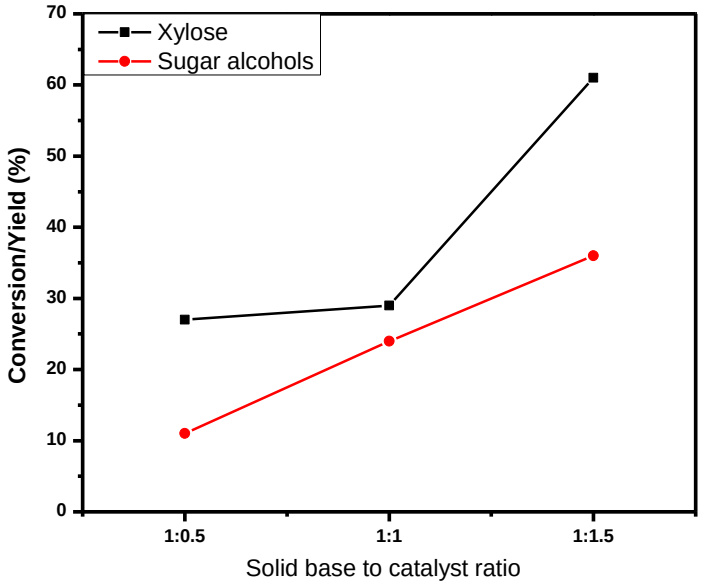

Figure 3.14. The effect of amount of solid base to catalyst ratio on micro-mesoporous KL(1.5) composite as a solid base in xylose hydrogenation over 3.5 *wt%* Pt/γ-Al_2O_3 (Reaction Condition : Xylose: 0.15 g, Catalyst: 0.035-0.15 g, Solid base: 0.075 g, Volume of H_2O: 35 mL, Temperature: 60 °C, Time 4 h)

3.4.2.4 Effect of reaction time

Figure 3.15 compares the activity of xylose hydrogenation with different reaction time at 60 °C with 16 bar hydrogen pressure. The reaction time revealed that the xylose conversion was found to increase from 29 to 82 with the increase in the contact time from 4 to 24 h. In addition, maximum sugar alcohols yield of 50% was achieved with selectivity to sugar alcohols of 79% at 12 h contact time. Nevertheless, it appeared that the extent of sugar alcohols yield was marginally declined to 47% and the sugar alcohols selectivity was significantly dropped to 57% with an increase in the contact time from 12 h to 24 h. The probable reason for fall in activity at longer reaction time could be the formation of by-

products by side reactions such as condensation, hydrogenolysis etc. The product analysis suggested that the lowering in the activity could be due to the presence of glycols (ethylene glycol, glycerol) in 24 h reaction time. To check the stability of the product, the catalytic reaction of sugar alcohol viz. xylitol under the reaction conditions of 12 h, 60 ^{o}C and 16 bar H_2 pressure was carried out. The absence of any side products formation confirmed the stability of xylitol with Pt/γ-Al_2O_3 catalyst and solid base. It was concluded from time study that the improved catalytic activity was achieved at 12 h under the identical reaction conditions.

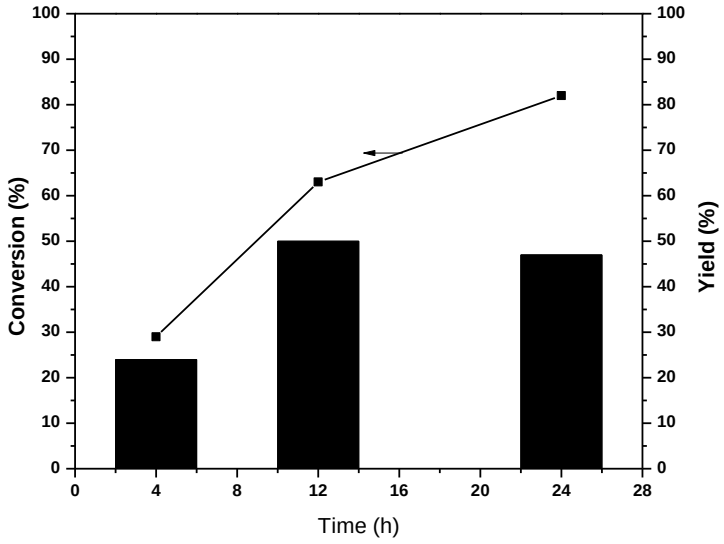

Figure 3.15 The time on stream study of micro-mesoporous KL(1.5) composite as a solid base in xylose hydrogenation over 3.5 *wt%* Pt/γ-Al_2O_3 (Reaction Condition : Xylose: 0.15 g, Catalyst: 0.075 g, Solid base: 0.075 g, Volume of H_2O: 35 mL, Temperature: 60 °C, 900 RPM)

3.5 Conclusions

In the present study, the micro-mesoporous KL(X) composites were synthesis by post-synthesis modification by changing the molar $Si_{(K/LTL\ zeolite)}/OH^-_{(aq.\ KOH)}$ ratio (1.128-0.142). The physico-chemical characterization revealed that alkaline treatment leading to the selective removal of silicon from K/LTL framework. Under given conditions (1.5 M KOH, 70 ^{o}C, 1 h), the controlled desilication promoted the generation of intracrystalline mesoporosity in micro-mesoporous KL(X) composites leading to enhance BET surface area and mesopore volume without significant alteration in microporosity, which facilitate the

accessibility of basic sites and enhanced molecular diffusion. ^{29}Si and ^{27}Al MAS NMR spectra demonstrated Si (0Al) and Si (1Al) species were leached, while the presence of all the aluminum atoms in tetrahedral configuration contributes to the higher basicity of hierarchical zeolite. The catalytic performance of micro-mesoporous KL(X) composites synthesized varying molar $Si_{(K/LTL\ zeolite)}/OH^-_{(aq.\ KOH)}$ ratio was investigated in the hydrogenation of xylose to xylitol as a solid base with 3.5 *wt%* Pt/γ-Al_2O_3 catalyst in the aqueous phase. The micro-mesoporous composite achieved with molar $Si_{(K/LTL\ zeolite)}/OH^-_{(aq.\ KOH)}$ ratio of 0.265 showed significant improvement in xylose hydrogenation, as compared with parent K/LTL zeolite. The higher catalytic performance was a coalescence of the development of mesoporosity and the improved accessibility of xylose molecules to active sites in hierarchical porosity. It also revealed that both porosity and the basicity variations of micro-mesoporous composite beneficial in xylose hydrogenation. However, extensive desilication of K/LTL zeolite with severe alkali treatment leading to blockage of mesoporosity and active sites due to amorphous debris, imparting the lower hydrogenation activity.

3.6 References

1. K. Moller and T. Bein, *Chemical Society Reviews*, 2013, **42**, 3689-3707.
2. A. Corma, *Chemical Reviews*, 1997, **97**, 2373-2420.
3. J. C. Groen, S. Abelló, L. A. Villaescusa and J. Pérez-Ramírez, *Microporous and Mesoporous Materials*, 2008, **114**, 93-102.
4. V. Valtchev, G. Majano, S. Mintova and J. Pérez-Ramírez, *Chemical Society Reviews*, 2013, **42**, 263-290.
5. D. Verboekend, T. C. Keller, M. Milina, R. Hauert, and J. Pérez-Ramírez, *Chemistry of Materials*, 2013, **25**, 1947-1959.
6. D. Verboekend and J. Perez-Ramirez, *Catalysis Science & Technology*, 2011, **1**, 879-890.
7. A. Tathod, T. Kane, E. S. Sanil and P. L. Dhepe, *Journal of Molecular Catalysis A: Chemical*, 2014, **388–389**, 90-99.
8. J. L. T. a. L. S. J. M. Berg, *Biochemistry New York: W H freeman*, 2002, **5th Edition**.

9. H. S. Singh, A. Gupta, A. K. Singh and B. Singh, *Transition Metal Chemistry*, 1998, **23**, 277-281.
10. K. Leng, Y. Wang, C. Hou, C. Lancelot, C. Lamonier, A. Rives and Y. Sun, *Journal of Catalysis*, 2013, **306**, 100-108.
11. N. P. Tangale, S. K. Sonar, P. S. Niphadkar, and P. N. Joshi, *Journal of Industrial and Engineering Chemistry*, 2016, **40**, 128-136.
12. P. N. Joshi, A. N. Kotasthane and V. P. Shiralkar, *Zeolites*, 1990, **10**, 598-602.
13. R. Devi, R. Borah, and R. C. Deka, *Applied Catalysis A: General*, 2012, **433**, 122-127.
14. R. Le Van Mao, A. Ramsaran, S. Xiao, J. Yao and V. Semmer, *Journal of Materials Chemistry*, 1995, **5**, 533-535.
15. P. Bartl and W. F. Hölderich, *Microporous and Mesoporous Materials*, 2000, **38**, 279-286.
16. P. N. Joshi, N. E. Jacob, and V. P. Shiralkar, *The Journal of Physical Chemistry*, 1995, **99**, 4225-4229.
17. A. Bonilla, D. Baudouin, and J. Pérez-Ramírez, *Journal of Catalysis*, 2009, **265**, 170-180.
18. P. Bhaumik and P. L. Dhepe, *Catalysis Today*, 2015, **251**, 66-72.
19. A. Aznarez, A. Gil and S. A. Korili, *RSC Advances*, 2015, **5**, 82296-82309.
20. B. Veldurthy, J. M. Clacens, and F. Figueras, *Advanced Synthesis & Catalysis*, 2005, **347**, 767-771.
21. H. A. Pray, C. E. Schweickert and B. H. Minnich, *Industrial & Engineering Chemistry*, 1952, **44**, 1146-1151.
22. D. K. Mishra, A. A. Dabbawala and J.-S. Hwang, *Journal of Molecular Catalysis A: Chemical*, 2013, **376**, 63-70.

Chapter 4

Micro-mesoporous K/LTL-MCM-41 composite as a solid base for hydrogenation of sugars

4.1 Introduction

As described in Chapter 1, zeolites have paramount importance as a heterogeneous catalyst due to their beneficial properties.[1, 2] However, the main drawbacks associated with the restricted diffusion of bulky reactant and product molecules to and from zeolite micropore channels limit its performance as industrial catalysts.[2-4] Therefore it is necessary to overcome molecular diffusion constraint, mass transfer, and active sites inaccessibility problems associated with conventional zeolites by the fabrication of micro-mesoporous composites with zeolite topologies by the development of potential micro-mesoporous composites.[5] It provides an effective pathway to improve the diffusion rate and accessibility of active sites which improves the catalytic performance.

The prominent features of micro-mesoporous composites in the field of catalysis are discussed elaborately in Chapter 1. Considering the advantages of bimodal porosity in a single system, several efforts have been devoted to the synthesis of zeolite-based materials with a mesoporous framework structure through different methods of preparation, such as BEA/MCM-41,[6] MOR/SBA-15,[7] MFI/MCM-48,[8] 13X/MCM-41,[9] MFI/SBA-15,[10] etc. as described earlier. In past few years, the concept of core-shell structures with zeolite materials such as MOR/ZSM-5, Y/MCM-41, H/MCM-22/MCM-41, H/ZSM-5 coated with polycrystalline silicalite crystals, has gained increasing interest due to the interconnectivity of micro and mesoporous systems.[11-15] These composites were synthesized by overgrowing siliceous shell on zeolite core crystal, which connects the micro and/or mesoporous channels.

In the present chapter, the synthesis of zeolite K/LTL based micro-mesoporous K/LTL-MCM-41 composite is discussed. The problem associated with the synthesis of K/LTL was the generation of a considerable amount of waste. After termination of the crystallization process and cooling the reaction mixture, the recovery of solid product results into large volume liquid filtrate (Mother Liquor, ML) which was generally discarded. Due to lower consumption of precursors, ML comprises unutilized sources and water. These waste materials not only cause adverse environmental effects but also make process unattractive towards cost-effectiveness and green technology. Therefore, treatment of such wastes becomes most essential to protect the environment. The physico-chemical

characteristics of K/LTL zeolite and the challenges which need a proactive approach for tackling the problems associated with the ML and environmental pollution.

Several studies have been carried out on the synthesis of micro-mesoporous composite molecular sieves containing MFI, BEA, FAU and MOR zeolitic materials. However, scanty literature is available showing the micro-mesoporous materials containing K/LTL zeolite. One of the reasons could be difficulties arises in the synthesis of meso-microporous K/LTL molecular sieves. In the present work, we have studied micro-mesoporous K/LTL-MCM-41 composites varying SiO_2/Al_2O_3 molar ratio utilizing mother liquor by efficient, economical and environmentally compatible route. The micro-mesoporous composites composed of K/LTL crystals through hydrothermal treatment. Further, the siliceous mother liquor was transformed into the mesoporous MCM-41 using cetyltrimethylammonium bromide (CTMABr) as a structure directing agent. Previously, MCM-41 type of micro-mesoporous composite molecular sieve was prepared by using the zeolite L nanocrystals as a precursor. The catalysts exhibit good catalytic performance for hydro-upgrading of FCC gasoline.[16] Moreover, the ordered mesoporous aluminosilicates of MAS-3 and MAS-8 from zeolite L precursors were synthesized by using CTMABr and Pluronic P123 as templates, showed catalytic activity for cumene cracking.[17]

As mentioned in earlier chapters, the study of the catalytic conversion of xylose to sugar alcohols using the solid base for the metal supported hydrogenation of xylose is essential, the industrial point of view. Thus, considering the importance of the hydrogenation of xylose reaction, in the present chapter, the catalytic activity of the micro-mesoporous K/LTL-MCM-41 composites were evaluated for the xylose hydrogenation to sugar alcohols (xylitol and arabitol) as a solid base and 3.5 *wt%* $Pt/\gamma\text{-}Al_2O_3$ as catalysts.

4.2 Experimental

4.2.1 Chemicals

The chemicals used for the synthesis of micro-mesoporous K/LTL-MCM-41 composites and hydrogenation reactions are discussed in Chapter 2, Section 2.2.1.1 and Section 2.2.5.1, respectively. All the chemicals were used without any further purification.

4.2.2 Synthesis of micro-mesoporous K/LTL-MCM-41 composite

Micro-mesoporous K/LTL-MCM-41 composites varying molar SiO_2/Al_2O_3 ratio were synthesized by seeding method by following the experimental procedure reported elsewhere with little modification as discussed in Chapter 2, Section 2.2.1.4,[18, 19] as shown in scheme 4.1. The initial molar gel composition (xK_2O: Al_2O_3: $ySiO_2$: zH_2O) and the synthesis conditions are tabulated in Table 4.1. It describes the optimum chemical composition and the crystallization parameters only, whereas the study of other optimization parameters is explained in detail in Section 4.3.1.1**.** In the present study, the mother liquor present along with crystalline K/LTL zeolite was used to employ unutilized sources including water for the syntheses of K/LTL-MCM-41 composites. The calcined samples were designated as XMMC, where the X= molar SiO_2/Al_2O_3 ratio of initial gel.

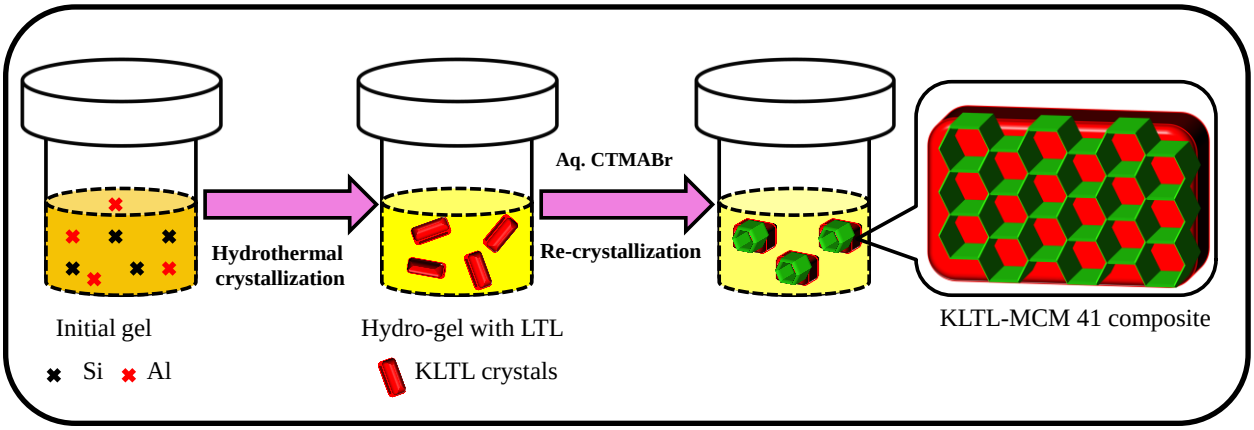

Scheme 4.1. Synthesis of micro-mesoporous K/LTL-MCM-41 composites

Table 4.1. Molar gel composition and synthesis conditions of micro-mesoporous K/LTL-MCM-41 composite

Composites	**Molar gel composition**									**Synthesis conditions**			
	Initial				**Mother liquor***			**MCM-41 phase**		**Zeolite phase**		**Composite phase**	
	SiO_2	Al_2O_3	K_2O	H_2O	SiO_2	K_2O	H_2O	CTMABr	H_2O	Time[a] h	t_C ^oC	Time[b] h	t_{CM} ^oC
20 MMC	20	1	8	200	14.3	7.0	187	4.8	460	8	170	24	110
15 MMC	15	1	6	150	9.5	4.8	135	3.6	330	12	170	24	110
10 MMC	10	1	4	100	4.6	2.9	86	2.4	220	16	170	24	110
8 MMC	8	1	3.2	80	2.8	1.9	69	1.9	176	24	170	24	110

* ±5% Handling loss (determined by ICP-OES analysis), a = Time required for the synthesis of K/LTL zeolite, t_C = Crystallization temperature for K/LTL zeolite, b = Time required for the synthesis of K/LTL-MCM-41 composite, t_{CM} = Crystallization temperature for K/LTL-MCM-41 composite,

4.2.3 Characterization

All the synthesized micro-mesoporous composites were thoroughly characterized by several analytical techniques, such as inductive coupled plasma-optical emission spectroscopy (ICP-OES), powder X-ray diffraction (PXRD), fourier transform infrared spectroscopy (FTIR), low-temperature nitrogen adsorption and desorption experiments, ^{27}Al magic angle spinning nuclear magnetic resonance spectroscopy (^{27}Al MAS-NMR), temperature programmed desorption of CO_2 (CO_2-TPD), transmission electron microscopy (TEM-EDX), high resolution transmission electron microscopy (HR-TEM) and UV-Vis spectroscopic analysis as discussed in Chapter 2, Section 2.4.

4.2.4 Experimental set-up and analysis of the reaction mixture

The catalytic activity of the micro-mesoporous K/LTL-MCM-41 composites was tested for the liquid phase hydrogenation of xylose to xylitol as a solid base and 3.5 *wt%* Pt/γ-Al_2O_3 as a catalyst. 3.5 *wt%* platinum loaded γ-Al_2O_3 catalyst was synthesized by wet impregnation method as described in Chapter 2, Section 2.2.1.6.[20] The catalytic and non-catalytic activity was conducted in the batch reactor as discussed in Chapter 2, Section 2.5.1.2. The hydrogen gas was purged into the reactor through the pressure of 8-20 bar at room temperature. The reactions were carried out at the desired temperature of 40-80 °C. The reaction mixture was allowed to stir initially at 500 rpm until the required temperature and once the temperature reached, the stirring speed was increased to 900 rpm. After completion of the reaction, the reaction mixture was allowed to cool to room temperature. The reaction mixture at different time intervals was collected and centrifuged for catalyst separation. The samples were filtered through a 0.22 μm syringe filter analyzed using HPLC (Chapter 2, Section 2.5.1.3).

4.2.5 Calculations

The xylose conversion, yield of sugar alcohols and TOF values for various runs were calculated on mole basis as discussed in Chapter 2, Section 2.5.1.3.3. For the calculation of conversion and sugar alcohols yield, the calibration curves of the commercially available substrate and the products were drawn. The slope of the calibration curves was calculated and further used for the calculation of sugar conversion and sugar alcohol product yield.

4.2.6 Hydrothermal stability test

The hydrothermal stability of the mesoporous materials was reported in boiling water/steam for a different period of time.[21, 22] In the present chapter, the calcined micro-mesoporous K/LTL-MCM-41 composites were subjected to the hydrothermal stability test as per the procedure is given in Chapter 2, Section 2.3. The hydrothermally treated powdered micro-mesoporous composites were evaluated by low angle and wide angle PXRD technique.

4.3 Results and discussion

4.3.1 Optimization of synthesis parameters of micro-mesoporous K/LTL-MCM-41 composites

The micro-mesoporous K/LTL-MCM-41 composites were synthesized successfully by seeding process by modification of the reported literature. However, it has been observed that the synthesis conditions for K/LTL zeolites with varying molar Si/Al ratios and Si-MCM-41 are different. Therefore, to achieve the optimum synthesis conditions, the study of different parameters such as molar gel composition, crystallization of time (aging time) of K/LTL zeolitic phase and MCM-41 mesophase, and the ratio of CTMABr/H_2O of composite materials are necessary. In the present study, the optimization parameters were assessed by PXRD technique, and further study was carried out by different analytical techniques.

4.3.1.1 Aging time of micro and mesophase

The PXRD is one of the preliminary analytical techniques used to evaluate the crystalline/amorphous nature and orders of micro-mesoporous materials. The influence of different synthesis parameters of micro-mesoporous K/LTL-MCM-41 composites was studied by PXRD.

In the seeding method for the syntheses of micro-mesoporous K/LTL-MCM-41 composites, initially, the synthesis of K/LTL zeolite was carried out by aging the hydrogel for a certain crystallization time. Further, without any further modification in the hydrogel, the surfactant template was added and the hydrogel was subjected for the hydrothermal crystallization to synthesize MCM-41.

In the present study, the hydrogel of 20 MMC with the molar gel composition $8K_2O$: Al_2O_3: $20SiO_2$: 4.8CTMABr: $660H_2O$ was subjected for the different aging times viz. 1) in the first step for K/LTL, 2 h, 4 h, and 8 h crystallization time at 170 ^oC and 2) in the second step for MCM-41, the crystallization times of 8 h, 12 h, 20 h, 24 h and 30 h at 110 ^oC. The micro-mesoporous K/LTL-MCM-41 composites syntheses varying different parameter study were analyzed by PXRD as shown in Figure 4.1 to Figure 4.3.

The low angle region PXRD of all the samples showed three characteristic diffraction peaks along (100), (110), and (200) planes in all the samples. This confirms the presence of ordered hexagonal MCM-41 mesoporous phase with crystallization period for 2, 4, and 8 h of K/LTL microphase in 20 MMC micro-mesoporous composites. The intensity of the MCM-41 phase in all composites increased with an increase in the crystallization time for mesophase. In addition, all the samples showed shifting of diffraction peak corresponding to (100) plane to the lower 2θ angles with increasing recrystallization time for the MCM-41 phase in the second step, suggesting the increasing orderness of the composite.

Further, wide-angle PXRD patterns showed, the entire samples exhibit the characteristic peaks of K/LTL zeolite. In comparison, 20 MMC prepared with 2 h crystallization period of K/LTL zeolite showed lower diffraction peak intensity with relatively lower crystallinity as an increase in the crystallization time of MCM-41 mesophase (Figure 4.1). Similar results were also observed for 20 MMC synthesized with the crystallization period of 4 h for K/LTL phase (Figure 4.2). It suggested that the K/LTL zeolite crystals were not grown or damaged by the increasing the crystallization time of MCM-41 mesophase. This can be attributed to the fact that the added CTMABr has an adverse effect on the crystallization of K/LTL zeolite along with the MCM-41 phase during the recrystallization in the second step. Since, the crystallization of K/LTL zeolite favors alkaline conditions (pH > 10), the lowering of pH during the synthesis of MCM-41 gel (pH= 8.9) may inhibit the crystal growth of K/LTL zeolite.

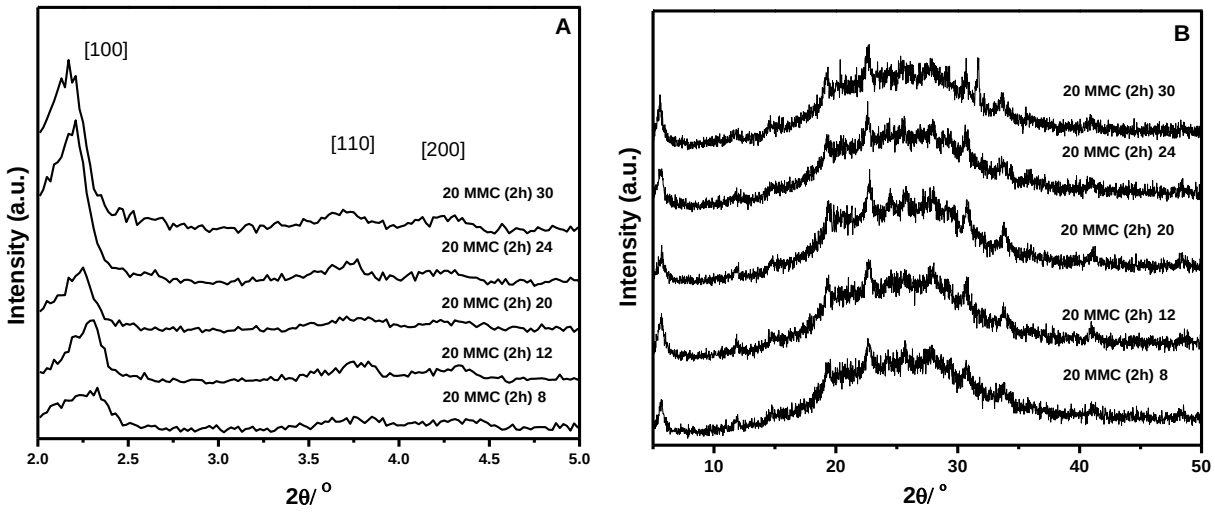

Figure 4.1. PXRD study of 20 MMC synthesized by 2 h crystallization of K/LTL zeolite, A) low angle PXRD patterns, B) wide-angle PXRD patterns of 20 MMC at different crystallization time for mesophase MCM-41

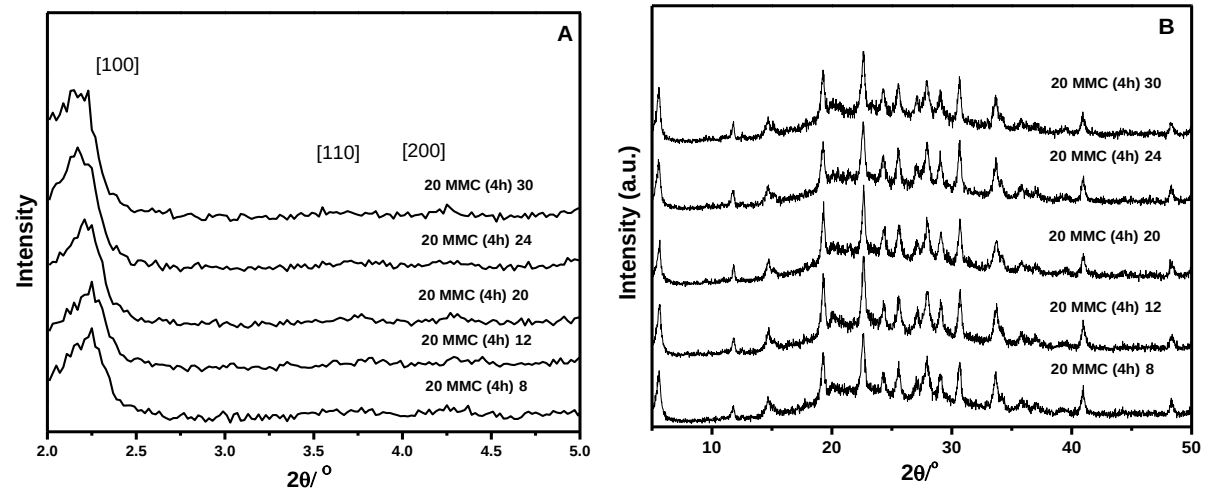

Figure 4.2. PXRD study of 20 MMC synthesized by 4 h crystallization of K/LTL zeolite, A) low angle PXRD patterns, B) wide-angle PXRD patterns of 20 MMC at different crystallization time for mesophase MCM-41

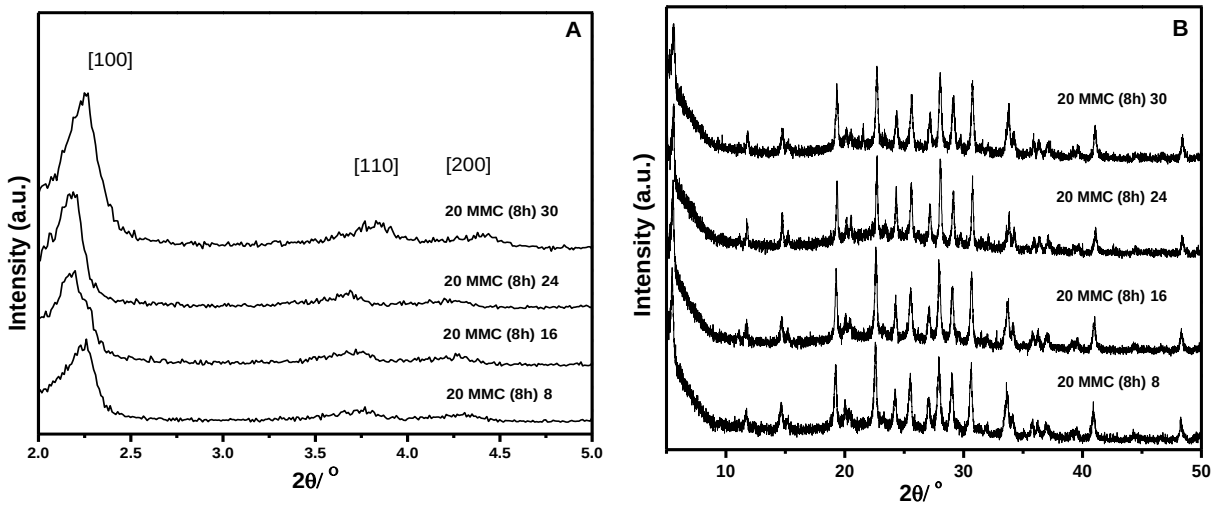

Figure 4.3. PXRD study of 20 MMC synthesized by 8 h crystallization of K/LTL zeolite, A) low angle PXRD patterns and B) wide-angle PXRD patterns of 20 MMC at different crystallization time for mesophase MCM-41

The wide-angle PXRD pattern also showed that the degree of crystallinity for K/LTL zeolite phase was increased with the increasing the crystallization period of K/LTL zeolite (2-8 h). It was noteworthy that fully grown K/LTL topological structure was formed after the crystallization period of 8 h with relatively higher crystallinity (Figure 4.3). The fully grown K/LTL zeolite crystals can only form well-ordered and interconnected porous system with micro-mesoporous K/LTL-MCM-41 composite molecular sieve. Hence, among all the 20 MMC composites, the best results were obtained for the synthesis of 20 MMC micro-mesoporous composite with the optimum crystallization period of 8 h for K/LTL zeolite phase and the recrystallization period of 24 h for ordered MCM-41 mesophase.

4.3.1.2 Molar CTMABr/H_2O ratio

Further, another important synthesis parameter which influences the characteristic porous properties is molar CTMABr/H_2O ratio. The influence of the surfactant concentration on the quality of the mesoporous phase was examined by changing the molar CTMABr/H_2O ratio of 20 MMC micro-mesoporous composite from 0.021 to 0.045. Other parameters like molar CTMABr/SiO_2 and K_2O/SiO_2 were kept constant. The optimization was carried out at 8 h crystallization time for K/LTL phase at 170 ^oC initially, and later, the

crystallization time was kept 24 h at 110 °C. The low angle (A) and wide-angle (B) PXRD patterns of 20 MMC synthesized with different molar CTMABr/H_2O ratio are shown in Figure 4.4.

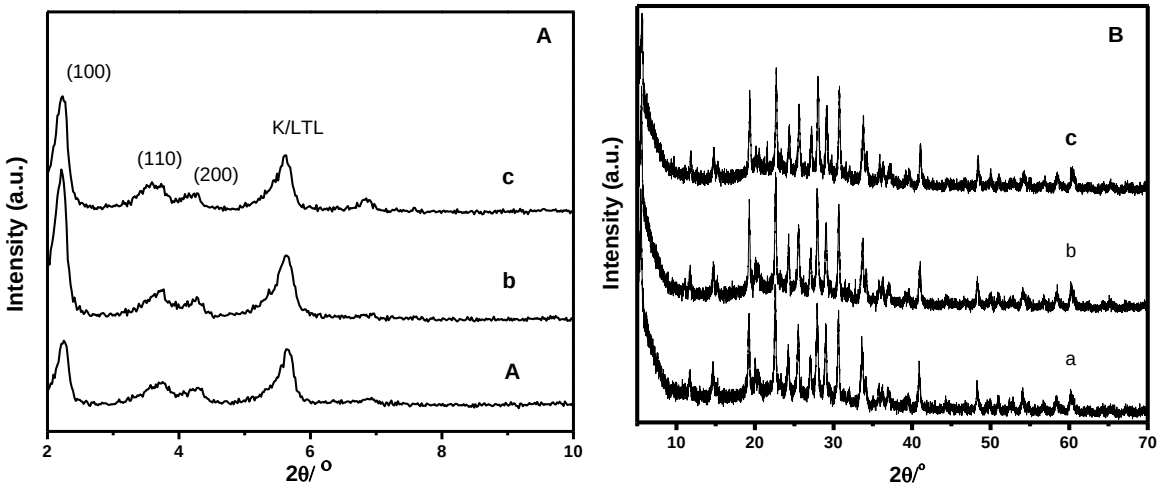

Figure 4.4. low angle (A) and wide-angle (B) PXRD patterns of 20 MMC synthesized with different molar CTMABr/H_2O ratio, a) 20 MMC(0.021), b) 20 MMC(0.031), and c) 20 MMC (0.045)

The low angle PXRD (Figure 4.4A) patterns of all the composites showed that with different molar, CTMABr/H_2O ratio, MCM-41 type mesophase with the three peaks corresponding to the (100), (110), and (200) planes appeared with varying intensity. The intensity of the composite with CTMABr/H_2O ratio 0.021 was much lower suggesting that the inadequate concentration of CTMABr for the formation of MCM-41 phase. When the molar CTMABr/H_2O ratio of the composites was increased from 0.021 to 0.045, the intensity of peaks corresponding to MCM-41 was increased. As compared to the product achieved by the molar CTMABr/H_2O ratio 0.045, the intensity basal (100) peak was much higher in the composite obtained with the molar CTMABr/H_2O ratio of 0.031. Moreover, the wide-angle PXRD patterns (Figure 4.4B) of all the composites did not show any structural changes as evidenced by almost the same intensity patterns of all the

composites. Thus, molar CTMABr/H_2O ratio of 0.031 with higher (100) peak intensity was considered the optimum ratio for 20 MMC micro-mesoporous composite.

4.3.1.3 Optimization of the molar SiO_2/Al_2O_3 ratio

The molar SiO_2/Al_2O_3 ratio is one of the crucial compositional parameters that govern the morphological features of the micro, meso, and micro-mesoporous materials. The micro-mesoporous K/LTL-MCM-41 composites synthesized by using mother liquor containing preformed K/LTL crystals with initial SiO_2/Al_2O_3 molar gel composition of 20, 15, 10 and 8 by hydrothermal crystallization. A series of experiments were conducted to investigate the crystallization period for 15 MMC, 10 MMC, and 8 MMC micro-mesoporous composites. In present work, the optimum crystallization period of 12, 16 and 24 h for K/LTL zeolite phase and the recrystallization period of 24 h for MCM-41 mesophase were chosen for the synthesis of 15 MMC, 10 MMC, and 8 MMC, respectively, as shown in Table 4.1.

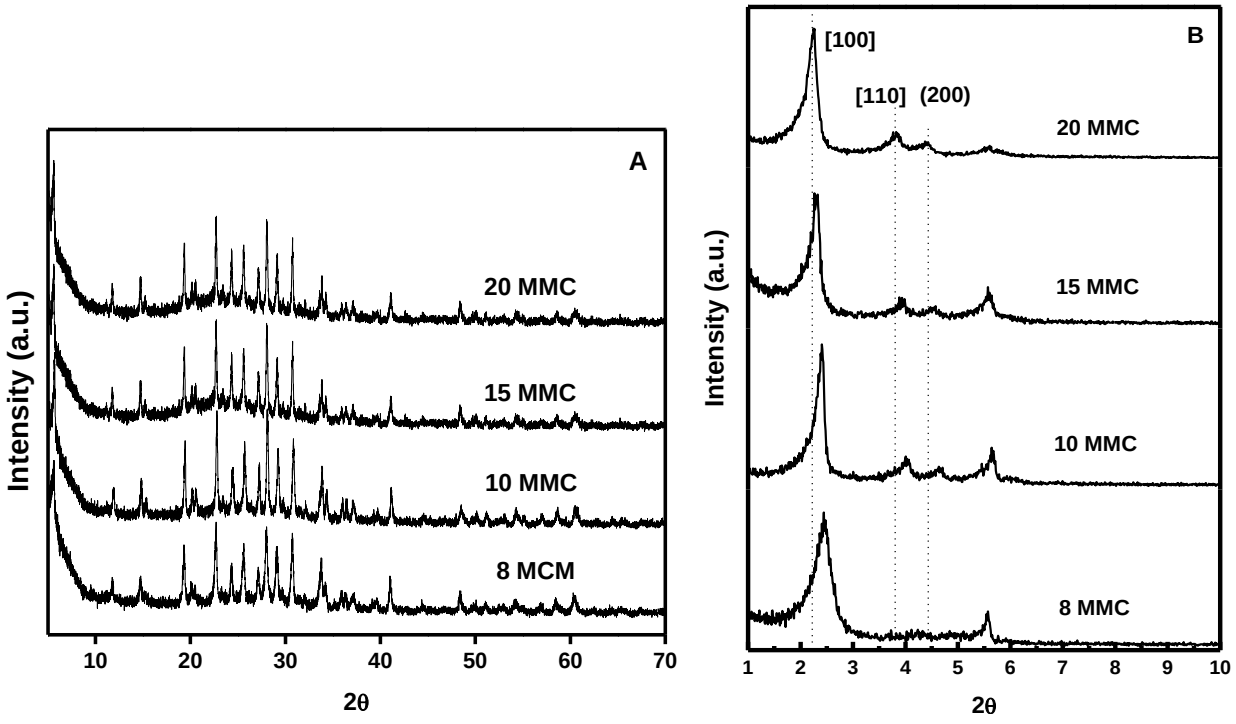

Figure 4.5. Wide-angle (A) and low angle (B) PXRD patterns of K/LTL-MCM-41 micro-mesoporous composites

Table 4.2. Physical properties of micro-mesoporous K/LTL-MCM-41 composites

Catalysts	Yield[a] (*Wt%*)	d_{100} (nm)	a_o (nm)	Crystalline phase[b] (%)
20 MMC	94.3	3.91	4.51	38
15 MMC	92.1	3.80	4.39	53
10 MMC	87.9	3.68	4.25	66
8 MMC	93.1	3.62	4.18	67

a= On dry calcined solid basis, d_{100} = spacing of (100) plane, a_o = unit cell parameter = $2d_{100}/\sqrt{3}$, b = By PXRD

It has been found that the crystallization period for K/LTL phase was delayed with lowering molar SiO_2/Al_2O_3 ratio of initial gel from 20 MMC to 8 MMC (8-24 h) at the same temperature of 170 ^oC. One of the reasons was that the lowering siliceous matter may cause a decrease in the rate of nucleation for the K/LTL crystal growth.[18] Another reason could be the increasing aluminium content in the initial gel may lower the dissolution of amorphous gel in an alkaline medium. As a result, the induction period of K/LTL crystal growth was increased with decreasing the molar SiO_2/Al_2O_3 ratio.[18]

The yield of calcined micro-mesoporous K/LTL-MCM-41 composites on dry basis was tabulated in Table 4.2, as 20 MMC (94.3 %), 15 MMC (92.1 %), 10 MMC (87.9 %), and 8 MMC (93.1 %). The low angle and wide angle PXRD patterns of calcined composites are shown in Figure 4.5. The wide-angle XRD patterns (Figure 4.5 A) of composites showed the long-range structural ordering characteristics of crystalline K/LTL type of zeolite after crystallizing for 8-24 h.[23] As can be seen, no other unidentified phases were PXRD visible, indicating the presence of pure K/LTL phase. Moreover, the alkaline condition during the synthesis of MCM-41 phase does not affect the crystalline structure of the zeolite. The low angle XRD patterns (Figure 4.5 B) exhibited a main intense peak indexed to (100) plane and the weak reflections of (110) and (200) planes revealing the highly ordered 2D hexagonal symmetry of MCM-41 mesophase with the higher molar SiO_2/Al_2O_3 ratio. It also revealed that the position of most prominent (100) diffraction peaks of the mesophases was gradually shifted to a higher angle when the molar SiO_2/Al_2O_3 ratio was decreased. The

results indicating that the orderliness of the mesophase decreases with decreasing the molar SiO_2/Al_2O_3 ratio.

On the other hand, 8 MMC displays a (100)peak broadening with weak reflections of (110)and (200)plane, suggesting poor pore symmetry and greater disorder. It is also concluded that the decreasing molar SiO_2/Al_2O_3 ratio has an adverse influence on the periodicity of the hexagonal mesoporous system of MCM-41 to a certain extent. The (100) interplanar spacing (*d*) and unit cell parameter (a_o) values are summarized in Table 4.2. It shows that *d* spacing and unit cell parameters (a_o) decreased with the decreasing molar SiO_2/Al_2O_3 ratio of micro-mesoporous composites. The PXRD pattern confirms the appearance of two distinct meso and microporous phases in K/LTL-MCM-41 composites and the synthesis parameters have considerable significance on the structural regularity. The results indicated that the mesostructure phase of the synthesized composites depended on the molar SiO_2/Al_2O_3 ratio and the micro-mesoporous composites prepared with higher silica content were more ordered than those with lower silica content. Another reason for the trend of orderness in MMC samples could be increased in $CTMABr/SiO_2$ ratio with decreasing the molar SiO_2/Al_2O_3 ratio. Since the K/LTL zeolite was synthesized in narrow phase region between the molar SiO_2/Al_2O_3 ratio of 5–7, the concentration of unreacted silica in the gel, after the first step, decreased with decreasing the molar SiO_2/Al_2O_3 ratio as can be seen from the composition of mother liquor (Table 4.1). Although, molar $CTMABr/SiO_2$ ratio of the composite was constant (Table 4.1), there was an increase in the $CTMABr/SiO_2$ ratio from 20 MMC to 8 MMC after the first step. The obtained results were similar to the reported literature in which the influence of the $CTMABr/SiO_2$ ratio on the textural properties of MCM-41 mesoporous materials was investigated.[24, 25] Further, the % crystalline microporous phase was also determined by PXRD. The low angle and wide angle PXRD of a physical mixture containing an accurately known amount of crystalline microphase and amorphous mesophase were carried out. The graph of intensity of peak corresponding to (100) plane of MCM-41 mesoporous phase and that of (100) plane of K/LTL zeolite plotted against *wt%* of crystalline and amorphous matter. The intensity of the synthesized samples was compared with the known intensity of reference with the known weight as tabulated in Table 4.2. The % of crystalline phases

present in the micro-mesoporous K/LTL-MCM-41 composites were changed with silica content as follows, 20 MMC (38 %) < 15 MMC (53 %) < 10 MMC (66 %) < 8 MMC (67 %).

4.3.2 N_2 adsorption-desorption analysis

The influence of molar SiO_2/Al_2O_3 ratio on the porous nature of K/LTL-MCM-41 composites was evaluated by N_2 adsorption-desorption analysis as shown in Figure 4.6. It can be seen that 10 MMC, 15 MMC and 20 MMC exhibit type IV isotherms with hysteresis loop. It arises due to capillary condensation; certify that the composites have the mesoporous framework. The inflection in the volume of nitrogen adsorbed at relative pressure (P/P_0) ca. 0.3 corresponded to the formation of mesopores with the large pore volume. Moreover, the nitrogen uptake in this region increased with increasing molar SiO_2/Al_2O_3 ratio in the order of 8 MMC < 10 MMC < 15 MMC < 20 MMC. In addition, 8 MMC exhibited the combination of type I and type IV isotherms with the appearance of the hysteresis loop. This was attributed to the larger contribution of the microporous phase and lower contribution of mesoporous phase as compared to other micro-mesoporous composites.

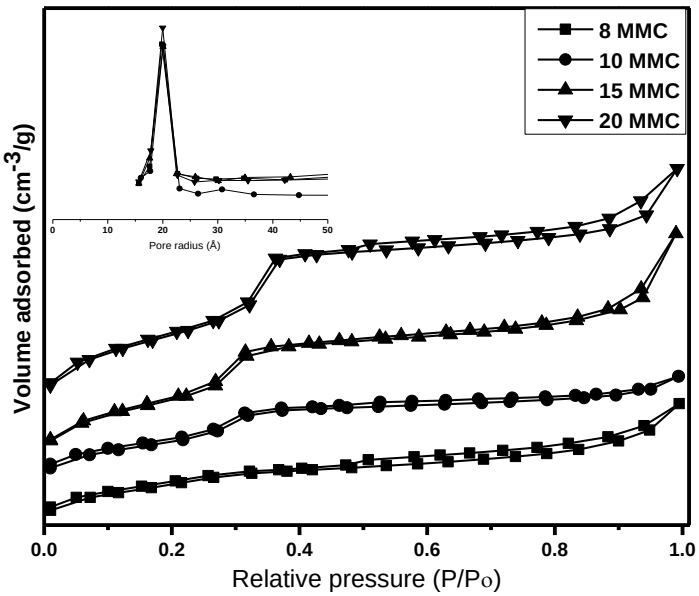

Figure 4.6. N_2 adsorption-desorption isotherms of micro-mesoporous K/LTL-MCM-41 composites and inset showing the BJH pore size distribution

The textural properties viz. BET surface area, average pore diameter, and total pore volume of all the calcined micro-mesoporous K/LTL-MCM-41 composites are tabulated in Table 4.3. It has been found that the average pore diameter of the composites was remained constant in all the micro-mesoporous composites (Figure 4.6 Inset). Moreover, all micro-mesoporous K/LTL-MCM-41 composites exhibit higher BET surface area. The BET surface areas (736 - 458 m^2/g) and the total pore volumes (0.54 - 0.38 cm^3/g) of the K/LTL-MCM-41 composites were gradually decreased with decreasing molar SiO_2/Al_2O_3 ratio. Table 4.3 showed that the wall thickness of the K/LTL-MCM-41 composites was decreased with decreasing SiO_2/Al_2O_3 molar ratio. The decrease in the BET surface area, pore volume and the wall thickness of MMC composite molecular sieves can be ascribed to the increasing $CTMABr/SiO_2$ ratio with decreasing the molar SiO_2/Al_2O_3 ratio.[32] The PXRD analysis and the nitrogen adsorption and desorption results accounted the following conclusions with decreasing SiO_2/Al_2O_3 molar ratio initial gel: 1) lowering orderliness of mesophase, 2) decreasing the wall thickness of mesopores, and 3) decreasing BET surface area and pore volume.

Table 4.3. Physico-chemical properties of micro-mesoporous K/LTL-MCM-41 composites

Catalysts	Si/Al Ratio (Input)	Si/Al ratio[a]	Si/Al ratio[b]	Dp (nm)	t (nm)	S_{BET} (m^2/g)	V_T (cm^3/g)
20 MMC	10.0	8.5	16.5	3.99	0.52	736	0.54
15 MMC	7.5	7.1	9.5	4.01	0.38	557	0.49
10 MMC	5.0	6.1	5.4	4.01	0.24	498	0.41
8 MMC	4.0	4.4	3.1	3.96	0.22	458	0.38

a = by ICP-OES, b = Determined by EDX, Dp = Average pore diameter, t= Wall thickness= a_o- Dp, S_{BET} =BET surface area, V_T =Total pore volume

4.3.3 Inductive coupled plasma-optical emission spectroscopy (ICP-OES)

The Si/Al ratios of all the micro-mesoporous composites in the initial gel and that determined by ICP-OES were tabulated in Table 4.3. The Si/Al ratios (input) of the composites in the initial gel were 10, 7.5, 5 and 4. The elemental analysis showed that the Si/Al ratios of micro-mesoporous composites were matches with the input values. In order to study the surface composition of micro-mesoporous K/LTL-MCM-41 composites, the molar Si/Al ratios of the composites were determined by EDX, and are tabulated in Table 4.3. It appears that the surface molar Si/Al ratio of all the composites decreased with decreasing the molar Si/Al ratio from 16.5 to 3.1. The experimental resulted showed that the Si/Al ratios determined by EDX were higher than those of initial gel in case of 20 MMC and 15 MMC composites. The results suggested that the surface of the K/LTL zeolite crystals in the composites was covered by the MCM-41 mesophase. However, the distribution of the mesophase on the surface of the K/LTL zeolite was non-uniform in 20 MMC and 15 MMC composite. This could be due to higher silica content remaining in the solution after complete synthesis of K/LTL crystals. Further, the decrease in the silica content may lead to the homogeneous distribution of the MCM-41 mesophase over zeolite crystals in the case of 10 MMC and 8 MMC composite.

4.3.4 Fourier transform infrared spectroscopic analysis (FTIR)

The FTIR spectra of calcined micro-mesoporous K/LTL-MCM-41 composites are shown in Figure 4.7. Most of the vibrations corresponding to the MCM-41 phase were overlap with the vibrations of K/LTL zeolite with regards to both Si-OH groups and Si-O-Al bonds vibrations. In addition to this, all the composites exhibit broad and intense vibration band appeared at 3450 /cm which was assigned to the surface silanol groups.[26] The broad adsorption band at 3450 /cm and 1640 /cm could assign to OH vibration mode of the physisorbed water content of the material. One can see that the intensity of the peak increases with increasing the SiO_2/Al_2O_3 molar ratio of the composites. Since the total physisorbed water content in all the samples remains same as evidenced by the similar area under the adsorption peak at 1640 /cm, the increase in the intensity was attributed to

the highly localized silanol groups on the surface of K/LTL-MCM-41 composite, which was a consequence of increasing molar SiO_2/Al_2O_3 ratio.

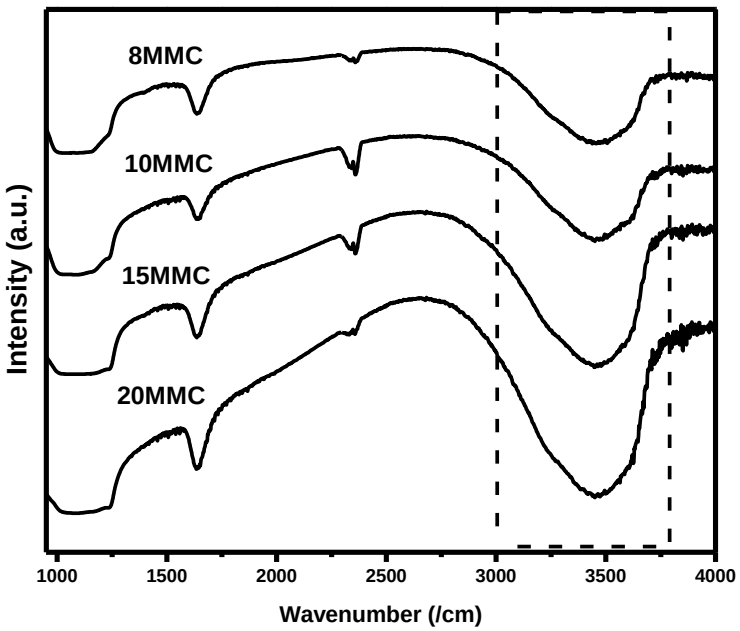

Figure 4.7. FTIR spectra of Micro-mesoporous K/LTL-MCM-41 composites

4.3.5 Solid-state ^{27}Al magic angle spinning nuclear magnetic resonance spectroscopy (^{27}Al MAS NMR)

The solid-state ^{27}Al magic angle spinning nuclear magnetic resonance (^{27}Al MAS NMR) spectra of the micro-mesoporous K/LTL-MCM-41 composites recorded to investigate the local environment of aluminum species as shown in Figure 4.8. All the micro-mesoporous K/LTL-MCM-41 composites showed typical resonance peak 55.8 ppm, which was assigned to the tetrahedrally coordinated Al encountered for zeolite K/LTL.[23] On another hand, the octahedrally coordinated Al (0 ppm) was not observed indicating the absence of extra-framework Al species. In all the K/LTL-MCM-41 composites the intensity of the tetrahedral Al remains constant suggesting that all the aluminum was incorporated into K/LTL zeolite framework in the first step. It can also be concluded that the acidic conditions (addition of H_2SO_4) during the preparation of MCM-41 did not result in the dealumination of K/LTL zeolite framework and the structure was retained.

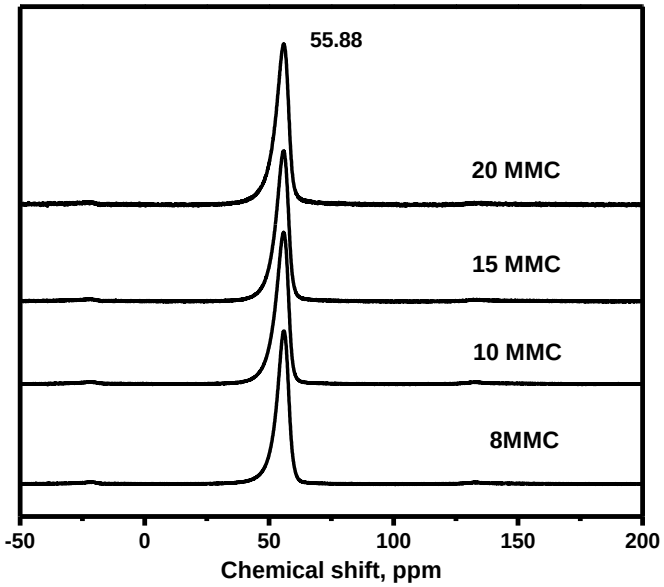

Figure 4.8. ^{27}Al MAS-NMR spectra of Micro-mesoporous K/LTL-MCM-41 composites

4.3.6 Temperature programmed desorption of CO_2 (CO_2-TPD)

The basic characteristics viz. the quantity and strength of the basic sites of micro-mesoporous K/LTL-MCM-41 composites were determined by temperature programmed desorption of CO_2 (CO_2-TPD) analysis, as shown in Figure 4.9. All the oxygen atoms were considered to be basic sites; however, the oxygen atoms belonging to the aluminate ions in the zeolites can show basicity for the catalytic activity.[27] Figure 4.9 shows that all the micro-mesoporous K/LTL-MCM-41 composites exhibited single maxima at a lower temperature in the temperature range of 100-300 ^{o}C, revealing the presence of relatively weak basic sites in K/LTL-MCM-41 composites. However, the maxima of CO_2 desorption was shifted to the higher temperature with the decreasing molar SiO_2/Al_2O_3 ratio. These results ascribed to the fact that the aluminate ions of microporous K/LTL zeolites were accessible to a lesser extent with increasing overgrowth of siliceous MCM-41 phase with enhancing SiO_2/Al_2O_3 ratio. The total amount and the strength of the basic sites of micro-mesoporous K/LTL-MCM-41 composites decreased in the order: 8 MMC (0.047 mmol/g) > 10 MMC (0.032 mmol/g) > 15 MMC (0.028 mmol/g) > 20 MMC (0.016 mmol/g).

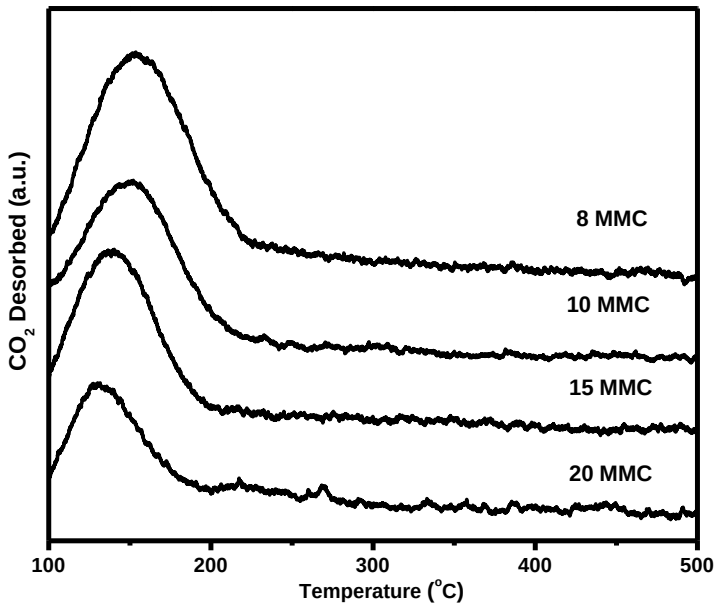

Figure 4.9. CO_2-TPD curves of KLTL-MCM-41 micro-mesoporous composites

4.3.7 Scanning electron microscopy (SEM)

The scanning electron microscopy (SEM) micrographs of optimized calcined micro-mesoporous K/LTL-MCM-41 composites are illustrated in Figure 4.10. The SEM image of MCM-41 shows the aggregates of particles in the range of 0.5-2μm. Similarly, all other composites also showed the MCM-41 type of morphology.

It was observed that the morphology of micro-mesoporous composites was depended on the SiO_2/Al_2O_3 ratio. The amorphous MCM-41 content was found to decrease with decreasing the SiO_2/Al_2O_3 ratio. As the SiO_2/Al_2O_3 ratio decreased, the K/LTL zeolite particles start appearing, and 8 MMC showed more amounts of K/LTL zeolite crystals. This could be attributed to the decreasing the silica content with decreasing the SiO_2/Al_2O_3 ratio from 20 MMC to 8 MMC, which is also supported by the amount of crystalline matter present in the composites shown in Table 4.2. But, the separate micro and mesophases were not observed in any micro-mesoporous composites.

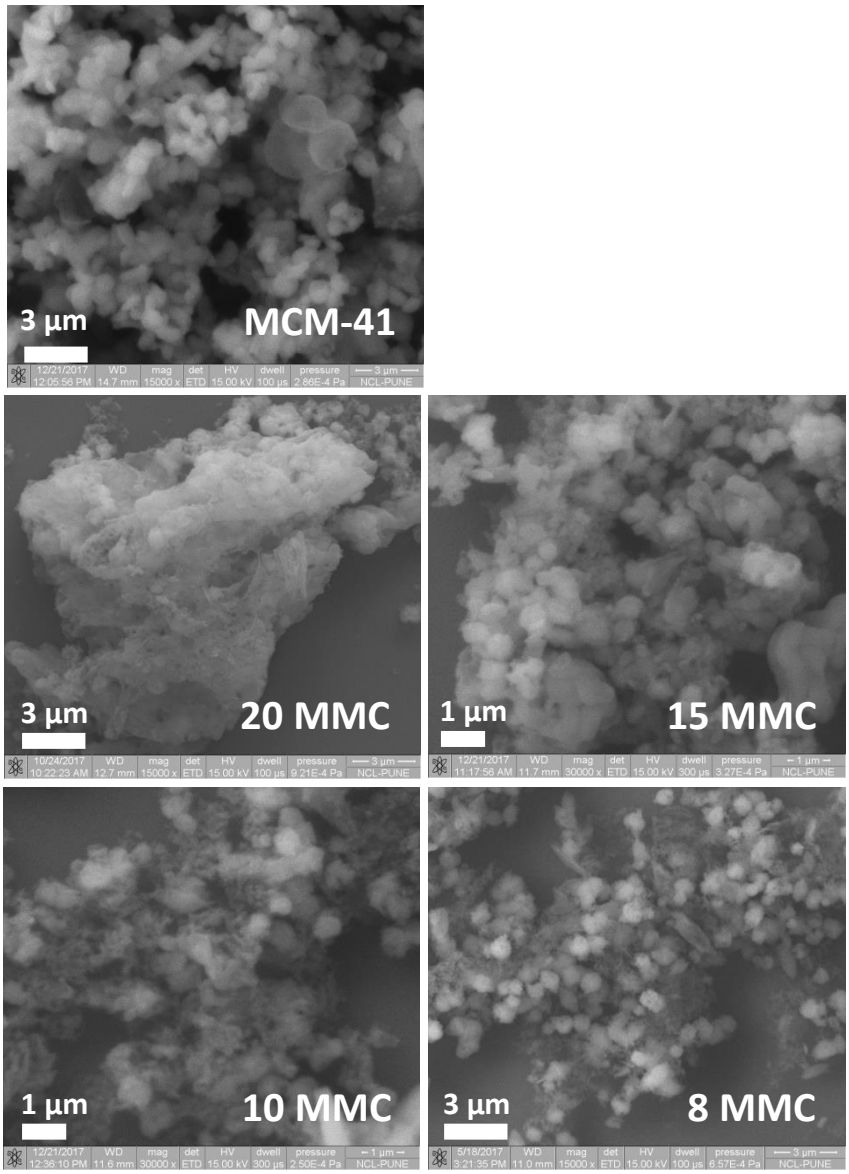

Figure 4.10. SEM images of micro-mesoporous K/LTL-MCM-41 composites

4.3.8 Transmission electron microscopy (TEM and HR-TEM)

The transmission electron microscopy (TEM) further gives information about the porous nature of composites. Figure 4.11 shows the TEM images of calcined micro-mesoporous K/LTL-MCM-41 composites. One can see that all micro-mesoporous K/LTL-MCM-41 composites exhibit two-dimensional, well-defined and ordered a hexagonal array of uniform channels corresponding to the mesoporous structure of MCM-41 materials. These results were consistent with the PXRD analysis. Moreover, the micro-mesoporous

composites with all the compositions did not show the presence of K/LTL zeolite crystals, indicating the K/LTL crystals wrapped in MCM-41 materials.

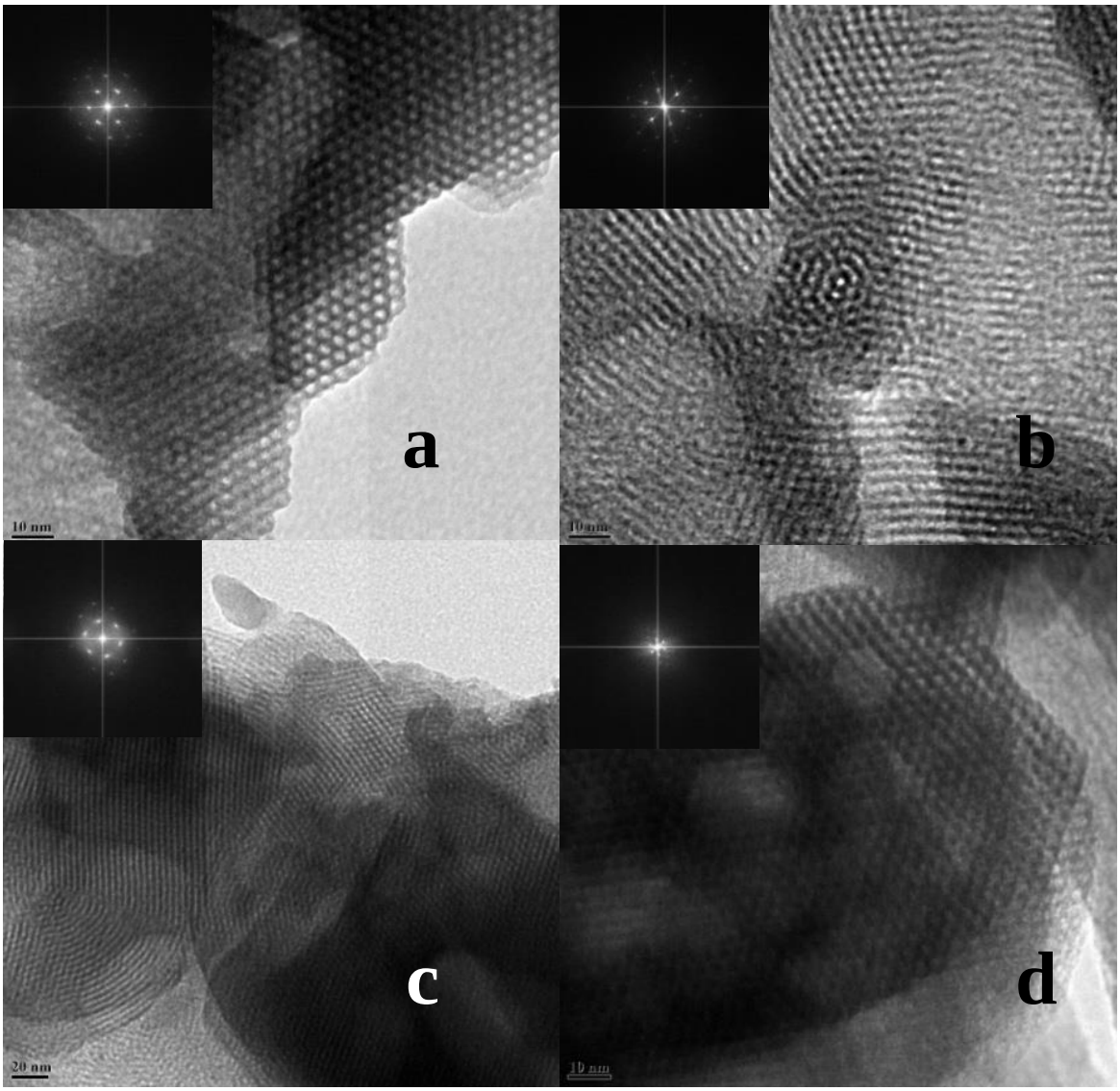

Figure 4.11. TEM images of 20 MMC (a), 15 MMC (b), 10 MMC (c) and 8 MMC (d) (inset showing corresponding SAED patterns).

Moreover, the SAED patterns (Figure 4.11 Inset) of corresponding composites showed orderness of micro and mesophases. Thus, the PXRD and TEM images revealed the appearance of fully crystallite K/LTL microporous zeolite covered with mesoporous MCM-41 phase on the surface of zeolite K/LTL crystal.

4.3.9 Hydrothermal stability test

The hydrothermal stability of the calcined micro-mesoporous K/LTL-MCM-41 composites was evaluated in a stainless steel reactor at 100 ^{o}C for 8 h and the structural changes were carefully studied by PXRD as shown in Figure 4.13. The PXRD patterns of all micro-mesoporous K/LTL-MCM-41 composites showed characteristic peaks of MCM-41 mesophase with 2D hexagonal nature (Figure 4.12 A). However, after being hydrothermally treated for 8 h, the intensity of the composite materials was considerably decreased. Thus, by comparison of the intensity of micro-mesoporous K/LTL-MCM-41 composites without hydrothermal treatment (Figure 4.5) with that of hydrothermally treated samples, the trend of hydrothermal stability of micro-mesoporous composites was decreased in the order of 20 MMC > 15 MMC > 10 MMC > 8 MMC. It was observed because of fact that the amount of silica present in the mother liquor decreased gradually with decreasing the molar SiO_2/Al_2O_3 ratio after the first K/LTL crystallization step.

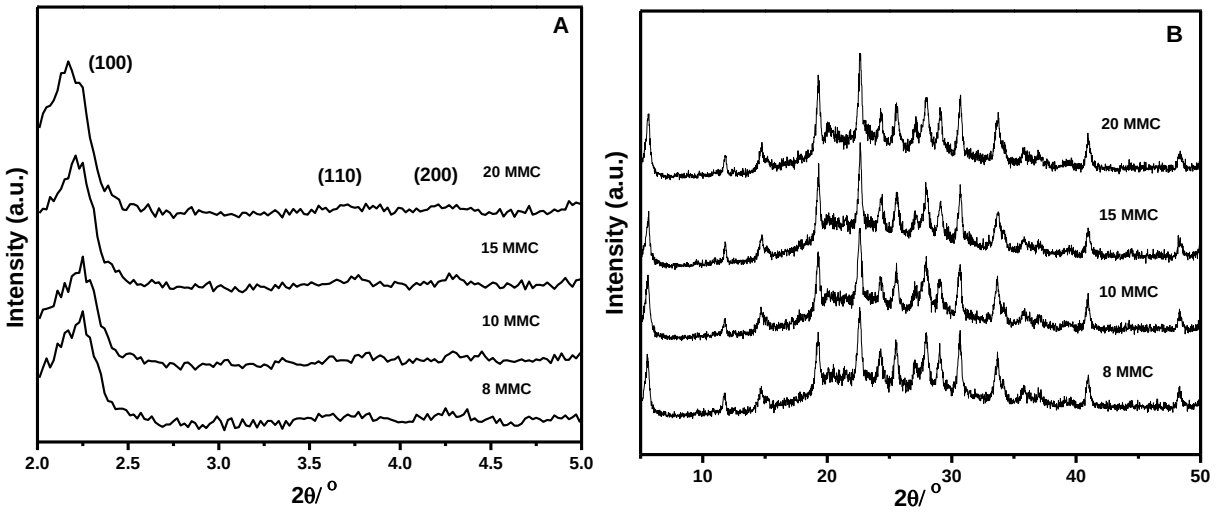

Figure 4.12. Low angle (A) and wide-angle (B) PXRD patterns of hydrothermally treated micro-mesoporous K/LTL-MCM-41 composites

In addition to this, the hydrothermal stability trend of composites was attributed to the increase in CTMABr/SiO_2 ratio with decreasing the molar SiO_2/Al_2O_3 ratio in the second crystallization step. As the molar CTMABr/SiO_2 ratio of the composite was constant, the pore wall thickness of the composite was decreased with decreasing molar SiO_2/Al_2O_3 ratio (Table 4.3). Therefore, 20 MMC micro-mesoporous composite showed highest hydrothermal stability. Moreover, the wide-angle spectra of the micro-mesoporous composites did not show any structural changes in the K/LTL zeolite framework (Figure 4.14 B). This observation indicating that the synthesis conditions of MCM-41 do not alter the structural features of the K/LTL zeolites.

4.3.10 Catalytic activity of micro-mesoporous composites as a solid base in the hydrogenation of xylose to sugar alcohols

A series of micro-mesoporous K/LTL-MCM-41 composites were evaluated as solid bases for the aqueous phase hydrogenation of xylose to sugar alcohols (xylitol and arabitol) using 3.5 *wt%* Pt/γ-Al_2O_3 as catalysts. Recently, under milder reaction conditions, the enhanced catalytic activity for the hydrogenation of xylose over Pt/γ-Al_2O_3 catalysts has been reported by the addition of a solid base, hydrotalcite.[20] The results concluded that the ring chain opening of sugar molecules favors in alkaline conditions, and the basic sites are recognized as the active sites,[20] as discussed in Chapter 3 using UV-Vis analysis. The open chain structured sugar molecules are easily hydrogenated under milder reaction conditions using Pt/γ-Al_2O_3 catalysts. Moreover, the cumulative basic property and the active metal are responsible for the effective xylose hydrogenation.[20] Therefore, in the present study, the micro-mesoporous K/LTL-MCM-41 composites were studies as solid bases and 3.5 *wt%* Pt/γ-Al_2O_3 catalyst for the hydrogenation of xylose to sugar alcohols.

The catalytic activity for hydrogenation of xylose is shown in Figure 4.13. The hydrogenation of xylose over 3.5 *wt%* Pt/γ-Al_2O_3 catalyst showed only 10.5% xylose conversion with 4.2% sugar alcohols yield. The lower xylose conversion may attribute to the acidic reaction medium (pH, 6.4), where the fraction of the open chain structured xylose molecules was lower.

The influence of the structural and basic properties of micro-mesoporous K/LTL-MCM-41 composites was clearly demonstrated by the addition of a solid base with the catalyst. In comparison with Pt/γ-Al_2O_3 catalyst, the xylose conversion was enhanced ca. two folds (19%) by the addition of 20 MMC as a solid base. The higher catalytic hydrogenation was attributed to the higher BET surface area (736 m^2/g) and basicity (0.016 mmol/g) of 20 MMC. Further, the xylose conversion was increased from 19% to 29% in the order of: 20 MMC(19%) < 15 MMC(19%) < 10 MMC(24%) < 8 MMC(29%). Among all composites, the higher xylose conversion was obtained over 8 MMC, suggesting the xylose conversion was strongly depending on porous properties and the basicity of MMC composite, and consequently, upon SiO_2/Al_2O_3 ratio. It has been observed that with the addition of micro-mesoporous K/LTL-MCM-41 composites, the pH of the solution

became basic (8 MMC, pH 8.7; 10 MMC, pH 8.6; 15 MMC, pH 8.4; 20 MMC, pH 8.3), which was acidic when reactions were performed only with Pt/γ-Al_2O_3 catalyst (pH 6.4). The pH of the solution was increased as a result of the basicity of the aluminate ions present in the zeolite. Another reason for the increase in the pH could be the presence of potassium ions in the solution which may occlude in the pores of the micro-mesoporous composites after synthesis. However, the latter possibility was ruled out as no evidence for potassium leaching was observed by ICP-OES analysis.

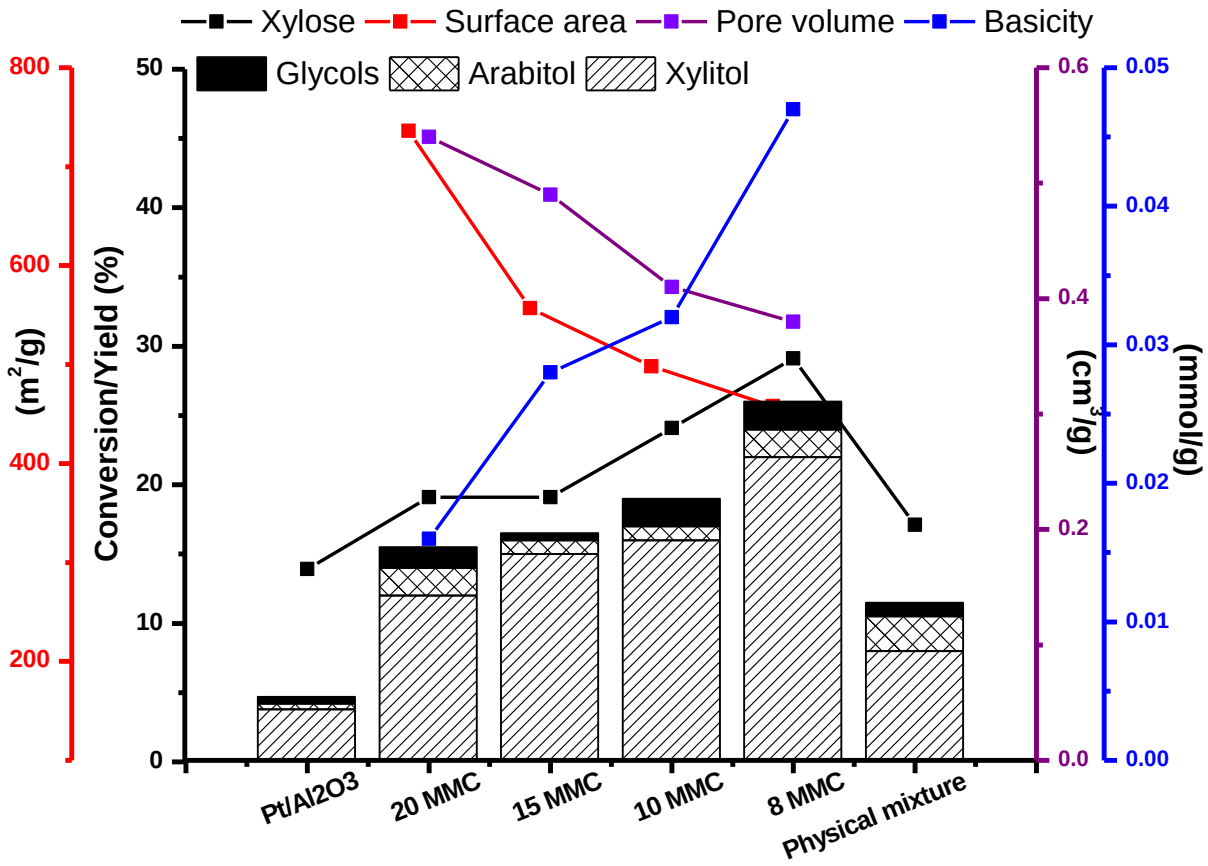

Figure 4.13. Catalytic activity of hydrogenation of xylose to sugar alcohols over micro-mesoporous K/LTL-MCM-41 composites as solid bases and 3.5 *wt*% Pt/γ-Al_2O_3 catalyst

(Reaction conditions: xylose: 0.5g, catalyst: 0.075g, solid base: 0.075g, water: 35 mL, temperature: 60 ^oC, time: 4 h, 16 bar H_2 pressure at R.T, 900 RPM)

The TOF values further give an insight into the profound activity enhancement by the addition of solid base for hydrogenation reaction. The TOF value of Pt/Al_2O_3 catalyst was found to be 15.2 /h only. The TOF value for hydrogenation of xylose over Pt/Al_2O_3 catalyst and the 20 MMC solid base was increased to 20.9 /h. Further, TOF values were increased from 20.9 /h to 32.0 /h by decreasing the SiO_2/Al_2O_3 ratio of micro-mesoporous composites. Finally, the physical mixture was also tested and showing lower TOF value of 18.7 /h, suggesting the interconnected micro and mesopores play an important role in the catalytic activity. The TOF values were increased in the order of Pt/Al_2O_3 (15.2 /h) < physical mixture (18.7 /h) < 20 MMC (20.9 /h) = 15 MMC (20.9 /h) < 10 MMC (26.5 /h) < 8 MMC (32.0 /h). It clearly showed the catalytic performance of the Pt/Al_2O_3 catalyst was significantly enhanced by the addition of micro-mesoporous K/LTL-MCM-41 composites under given conditions.

The yield of sugar alcohols (Figure 4.13) showed an increasing trend with regards to the chemical composition of micro-mesoporous K/LTL-MCM-41 composites. 20 MMC composite exhibited 14% yield to the sugar alcohols. Overall with decrease in molar gel ratio, increase in the yield of sugar alcohols was seen; 20 MMC (14%) < 15 MMC (16%) < 10 MMC (17%) < 8 MMC (24%). The composite 8 MMC exhibited the highest sugar alcohols yield of 24% as compared to other analogs. This inferred that the yield of sugar alcohols in the hydrogenation of xylose over $Pt/\gamma\text{-}Al_2O_3$ catalyst was dependent on the porosity and basicity of micro-mesoporous K/LTL-MCM-41 composites and the $Pt/\gamma\text{-}Al_2O_3$ catalyst. The higher catalytic activity over $Pt/\gamma\text{-}Al_2O_3$ catalyst using solid base micro-mesoporous K/LTL-MCM-41 composites can be attributed to the formation of higher concentration of open chain form of xylose. The ring opening of xylose was expected to appear by passing xylose molecules through the K/LTL zeolite channels and undergoes ring opening phenomenon. It also indicated that the $Pt/\gamma\text{-}Al_2O_3$ catalyst is not efficient at a low temperature of 60 ^oC in aqueous media, whereas, upon incorporation of composite material in the reaction media with the $Pt/\gamma\text{-}Al_2O_3$ catalyst, the catalytic activity becomes more prominent. In order to confirm the effectiveness of the micro-mesoporous composites in the xylose hydrogenation, the physical mixture of 8K/LTL zeolite (0.037 g) and MCM-41 (0.038 g) was also tested as a solid base. It was shown only 17% xylose conversion and 10.5% sugar alcohols yield. Contrary to this, with 8 MMC (0.075 g), 29% yield of sugar alcohols was

observed. The catalytic activity correlation of 8 MMC and the physical mixture clearly envisioned that the interconnected micro-mesoporosity plays a vital role in the chain opening of sugar molecules and hydrogenation of xylose.

In addition, the BET surface area and mesopore size of the MCM-41 provide more accessible surface area. As a result, the open chain form of xylose diffused through the K/LTL micropore channels followed by mesopores of MCM-41. A consequence of these results in the open-chain form xylose experienced higher accessibility of Pt that undergoes reduction subsequently using Pt on Al_2O_3 support. One of the reasons of improved catalytic activity was the higher dispersion of nano-sized platinum on an Al_2O_3 support. The average particles size of the platinum was distributed in the range of 2-10 nm as revealed by TEM image, which promoted the enhancement in the sugar alcohols selectivity. In summary, though, 8 MMC possessed lower BET surface area, the overall higher catalytic performance for hydrogenation of xylose over 3.5 *wt%* Pt/γ-Al_2O_3 catalysts and micro-mesoporous K/LTL-MCM-41 composite solid base was attributed to the cumulative effect of, 1) the higher basicity of micro-mesoporous K/LTL-MCM-41 composite, 2) the beneficial diffusion of open chain form xylose through the K/LTL zeolite channels, and 3) the accessibility of nano-sized Pt on Al_2O_3.

In order to enhance the catalytic performance of 8 MMC, the reaction parameters such as time on stream, reaction temperature, and hydrogen pressure were studied.

4.3.10.1 Optimization of reaction parameters

4.3.10.1.1 Effect of time

The influence of reaction time for the catalytic hydrogenation of xylose over 8 MMC as the solid base was studied at 60 ^oC at 16 bar H_2 pressure as shown in Figure 4.14. The catalytic performance of 8 MMC for the hydrogenation of xylose was increased with an increase in the reaction time up to 12 h. However, a further increase in the reaction time enhanced the catalytic activity to a lesser extent. The time study indicated that the steady state was achieved at 12 h of reaction time. At the reaction time of 12 h, the xylose conversion of 48 % and the sugar alcohols yield of 45% were achieved. Thus, 12 h reaction time was chosen for further parameter studies.

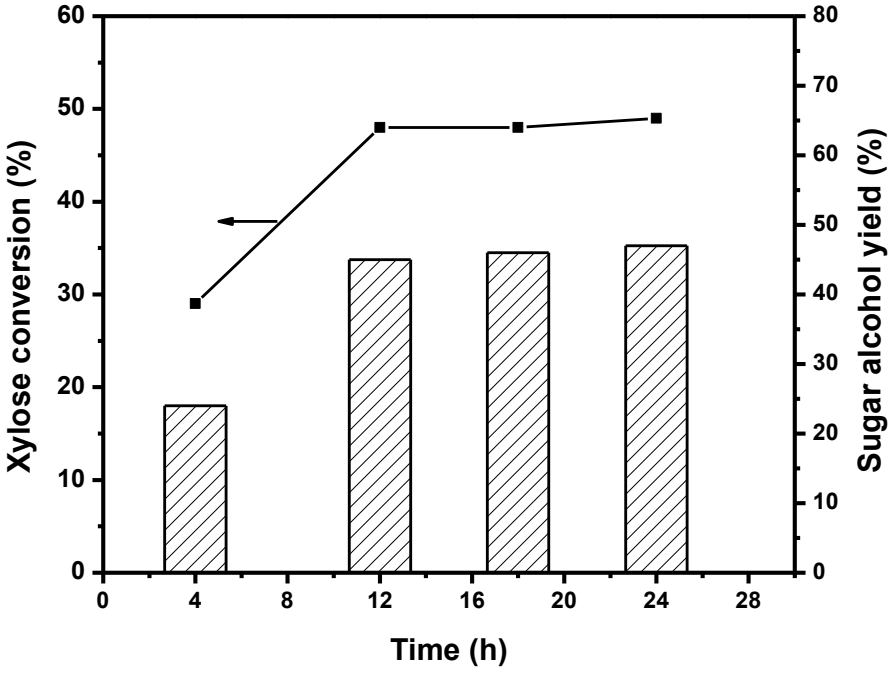

Figure 4.14. Effect of time over 3.5 *wt*% Pt/γ-Al_2O_3 catalyst and 8 MMC micro-mesoporous composites as solid bases

(Reaction conditions: xylose: 0.5g, catalyst: 0.075g, solid base: 0.075g, water: 35 mL, temperature: 60 ^oC, 16 bar H_2 pressure at R.T, 900 RPM)

4.3.10.1.2 Influence of temperature

The catalytic performance of 8 MMC as the solid base was studied as a function of reaction temperature as shown in Figure 4.15. The temperature was varied from 40 ^oC to 80 ^oC at 16 bar H_2 pressure for 12 h. At a lower temperature of 40 ^oC, merely 18% xylose conversion was observed with 9% sugar alcohols yield. However, a significant increase in the catalytic performance was observed at a higher temperature. At the higher temperature of 60 ^oC, the xylose conversion was 48% and sugar alcohols yield of 45% were observed. In addition, at 80 ^oC of reaction temperature, 8 MMC showed a slight increase in the xylose conversion of 53% with the sugar alcohols yield of 48%. The temperature study revealed that the xylose conversion to sugar alcohols can be carried out at a lower temperature with the minimum side product formation. In the present study, about 94% selectivity of sugar alcohols were obtained at 60 ^oC, therefore, the optimum reaction temperature of 60 ^oC was used to study further parameter.

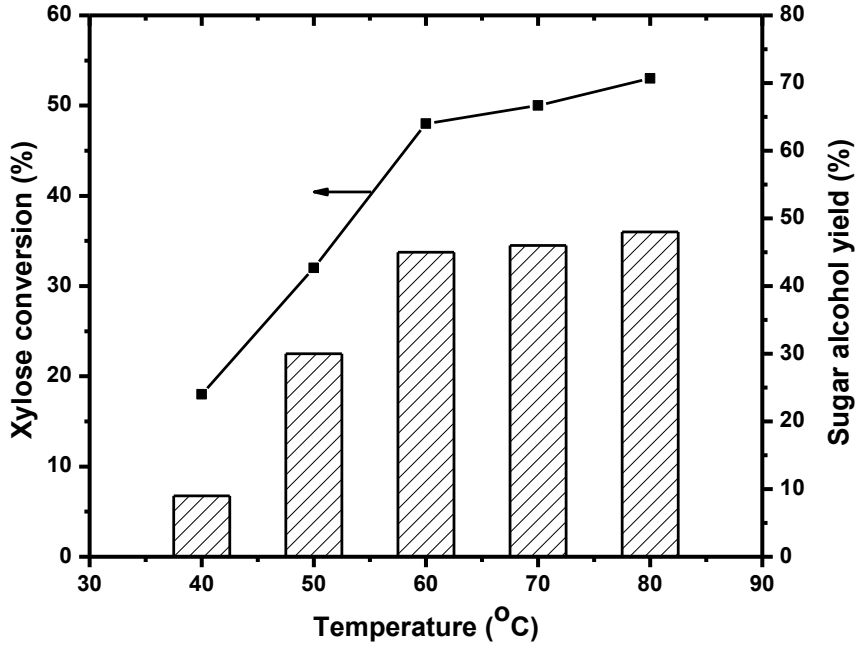

Figure 4.15. Effect of reaction temperature over 3.5 *wt*% Pt/γ-Al_2O_3 catalyst and 8 MMC micro-mesoporous composites as solid bases
(Reaction conditions: xylose 0.5g, catalyst 0.075g, solid base 0.075g, water 35mL, time 12h, 900 RPM, 16 bar H_2 pressure at R.T.)

4.3.10.1.3 Influence of hydrogen pressure

In the hydrogenation of xylose to sugar alcohols, it is well known that the hydrogen pressure played a crucial role in the catalytic performance. Thus, in the present study, the hydrogen pressure was changed from 8 bar to 20 bar at room temperature as shown in Figure 4.16. At a lower H_2 pressure of 8 bar, only 36% xylose conversion and 21% sugar alcohols yield was achieved, whereas, at 16 bar H_2 pressure, 48% xylose conversion and 45% sugar alcohols yield was achieved. At lower hydrogen pressure the solubility of hydrogen in aqueous solution was lower. As a result, the adsorption of hydrogen on the Pt catalyst was lower. However, at high H_2 pressure, the solubility of hydrogen gas increased and thereby the adsorption of hydrogen on the Pt catalyst was expected to be high. In addition to this, a further increase in the H_2 pressure to 20 bar, the xylose conversion was increased to 51% with sugar alcohols yield of 48%. The noteworthy fact is that the catalytic

performance of 8 MMC as a solid base and 3.5 *wt%* Pt/γ-Al_2O_3 catalysts did not improve significantly with H_2 pressure. One of the reasons could be, at higher pressure, hydrogen gas did not adsorb on the Pt catalyst surface linearly.

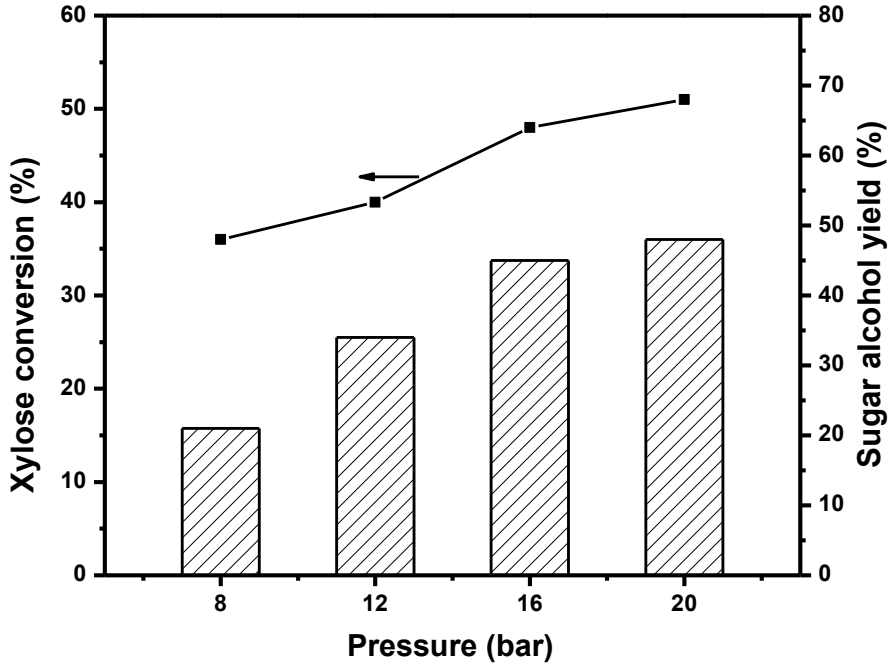

Figure 4.16. Effect of hydrogen pressure over 3.5 *wt*% Pt/γ-Al_2O_3 catalyst and 8 MMC micro-mesoporous composites as solid bases
(Reaction conditions: xylose: 0.5g, catalyst: 0.075g, solid base: 0.075g, water: 35 mL, time: 12h, 16 bar H_2 pressure at R.T., 900 RPM)

4.4 Conclusions

Micro-mesoporous K/LTL-MCM-41 composites were synthesized varying molar SiO_2/Al_2O_3 ratio (20-8) by recycling of waste mother liquor. The utilization of mother liquor with the minimal waste would allow the synthesis cost-effective and environmentally green. The micro–mesoporous K/LTL-MCM-41 composites assembled by preformed K/LTL zeolite crystals and MCM-41 mesophase. The physico-chemical properties of the micro-mesoporous K/LTL-MCM-41 composites were depending on the molar SiO_2/Al_2O_3 ratio. The micro-mesoporous K/LTL-MCM-41 composites showed

lowering the BET surface area, pore volume, orderliness of mesophase and the wall thickness of mesopores with decreasing molar SiO_2/Al_2O_3 ratio. Moreover, the total amount and the strength of the basic sites K/LTL-MCM-41 composites increased with decreasing molar SiO_2/Al_2O_3 ratio. The catalytic activity of micro-mesoporous K/LTL-MCM-41 composite was evaluated as a solid base for hydrogenation of xylose using 3.5 *wt%* Pt/γ-Al_2O_3 as catalysts. The overall enhanced activity over micro-mesoporous K/LTL-MCM-41 composite was attributed to the cumulative effect of, 1) the higher basicity of micro-mesoporous K/LTL-MCM-41 composite, 2) the beneficial diffusion of open chain form xylose through the K/LTL zeolite channels, and 3) the accessibility of nano-sized Pt on Al_2O_3.

4.5 References

1. G. W. Huber and A. Corma, *Angewandte Chemie International Edition*, 2007, **46**, 7184-7201.
2. M. E. Davis, *Nature,* 2002, **417**, 813-821.
3. A. Corma, *Chemical Review*, 1997, **97**, 2373-2420.
4. M. Hartmann, *Angew. Chem., Int. Ed*, 2004, **43**, 5880-5882.
5. Y. Wei, T. E. Parmentier, K. P. de Jong, and J. Zecevic, *Chemical Society Reviews*, 2015, **44**, 7234-7261.
6. H. Xu, J. Guan, S. Wu and Q. Kan, *Journal of Colloid and Interface Science*, 2009, **329**, 346-350.
7. M. Banu, Y. H. Lee, G. Magesh, C.-M. Nam and J. S. Lee, *ChemCatChem*, 2015, **7**, 2354-2360.
8. S. C. G. Santos, A. M. G. Pedrosa, M. J. B. Souza, J. A. Cecilia and E. Rodríguez-Castellón, *Materials Research Bulletin*, 2015, **70**, 663-672.
9. C. Ji, L. Zhang, L. Li, F. Li, F. Xiao, N. Zhao, W. Wei, Y. Chen and F. Wu, *Industrial & Engineering Chemistry Research*, 2016, **55**, 7853-7859.

10. S. Habib, F. Launay, H. E. Zakhem, M. Mazaj, F. Guenneau, P. Beaunier, D. Brouri, N. N. Tušar, V. Kaučič, and A. Gédéon, *Materials Research Bulletin*, 2013, **48**, 1288-1295.
11. K. R. Kloetstra, H. W. Zandbergen, J. C. Jansen and H. van Bekkum, *Microporous Materials*, 1996, **6**, 287-293.
12. D. Kong, J. Zheng, X. Yuan, Y. Wang and D. Fang, *Microporous and Mesoporous Materials*, 2009, **119**, 91-96.
13. D. Van Vu, M. Miyamoto, N. Nishiyama, Y. Egashira and K. Ueyama, *Journal of Catalysis*, 2006, **243**, 389-394.
14. Y. Wang, D. Cui and Q. Li, *Microporous and Mesoporous Materials*, 2011, **142**, 503-510.
15. B. Xue, J. Xu, C. Xu, R. Wu, Y. Li and K. Zhang, *Catalysis Communications*, 2010, **12**, 95-99.
16. Q. Huo, Y. Gong, T. Dou, Z. Zhao, H. Pan, and F. Deng, *Energy and Fuels*, 2010, **24**, 3764-3771.
17. Y. Di, Y. Yu, Y. Sun, X. Yang, S. Lin, M. Zhang, L. Shougui and F.-S. Xiao, *Microporous and Mesoporous Materials*, 2003, **62**, 221-228.
18. S. D. Bhat, P. S. Niphadkar, T. R. Gaydhankar, S. V. Awate, A. A. Belhekar and P. N. Joshi, *Microporous and Mesoporous Materials*, 2004, **76**, 81-89.
19. Y.-S. Ooi, R. Zakaria, A. R. Mohamed and S. Bhatia, *Applied Catalysis A: General*, 2004, **274**, 15-23.
20. A. Tathod, T. Kane, E. S. Sanil and P. L. Dhepe, *Journal of Molecular Catalysis A: Chemical*, 2014, **388–389**, 90-99.
21. L. Wang, J. Zhang, F. Chen and M. Anpo, *The Journal of Physical Chemistry C*, 2007, **111**, 13648-13651.
22. H. Xiong, H. N. Pham, and A. K. Datye, *Green Chemistry*, 2014, **16**, 4627-4643.
23. N. P. Tangale, S. K. Sonar, P. S. Niphadkar, and P. N. Joshi, *Journal of Industrial and Engineering Chemistry*, 2016, **40**, 128-136.
24. B. Boukoussa, N. Aouad, R. Hamacha, and A. Bengueddach, *Journal of Physics and Chemistry of Solids*, 2015, **78**, 78-83.
25. J. Yu, J.-L. Shi, L.-Z. Wang, M.-L. Ruan and D.-S. Yan, *Materials Letters*, 2001, **48**, 112-116.

26. K. S. Hui and C. Y. H. Chao, *Journal of Hazardous Materials*, 2006, **137**, 1135-1148.

27. D. Barthomeuf, *Microporous, and Mesoporous Materials*, 2003, **66**, 1-14.

28. B. Veldurthy, J. M. Clacens, and F. Figueras, *Advanced Synthesis & Catalysis*, 2005, **347**, 767-771.

Chapter 5

Synthesis and characterization of zeolite K/LTL based micro-mesoporous composites by post-synthesis modification, seeding method, and two-step crystallization method, and their catalytic activity in the hydrogenation of xylose to sugar alcohols

5.1 Introduction

In the previous chapters, the zeolite K/LTL based micro-mesoporous composites synthesized by 1) post-synthesis modification with varying molar $Si_{(K/LTL\ zeolite)}/OH^-_{(aq.\ KOH)}$ ratio and 2) the seeding methods with the different SiO_2/Al_2O_3 ratio, were discussed independently. These materials were studied as a solid base for the noble metal-supported hydrogenation of xylose to sugar alcohols. It was observed that in a basic medium, more amount of sugar molecules were present in the open-chain form by undergoing isomerization reaction.[1] Hence, the open-chain sugar molecules were easily undergone catalytic hydrogenation in presence of external hydrogen. The presence of the solid bases enhances the open chain sugar molecules and showing the higher sugar alcohols yields.[2]

Reported literature was focused on the synthesis of zeolite-based micro-mesoporous composited with interconnected micro and mesopores by different methods of preparation and possesses unique characteristic properties and have their own advantages and disadvantages as summarized in Chapter 1. Different strategies such as dealumination by acid or steam treatment,[3-5] desilication by alkali treatment,[6-9] re-crystallization method,[10, 11] duel templating method[10, 12, 13] and microwave assisted method[14] were employed for the synthesis of micro-mesoporous composites.

The catalytic system with bimodal porosity, micro, and mesoporous system have been extensively studied after the synthesis of FAU/MCM-41 micro-mesoporous composites by one step method.[15] Literature was reported for the synthesis of micro-mesoporous composites with extensive use of BEA, ZSM-5, FAU, MOR etc. zeolites as a microporous phase with the combination of MCM-41 and SBA-15 as a mesoporous phase. In similar to above synthesis strategies, zeolite Beta based micro-mesoporous composites were prepared by desilication,[16] assembly of zeolite nanoclusters[17] and recrystallization method.[18]

Further, MCM-41 type of micro-mesoporous composite molecular sieve was prepared by using the zeolite L nanocrystals as a precursor. The catalysts exhibit good catalytic performance for hydro-upgrading of FCC gasoline.[19] Moreover, the ordered mesoporous aluminosilicates of MAS-3 and MAS-8 from L precursors were synthesized by using cetyltrimethylammonium bromide (CTMABr) and Pluronic P123 as templates.[20]

Recently, we have reported the synthesis of K/LTL micro-mesoporous composites by post-synthesis modification by alkali treatment.[21] However, due to limitations in the synthesis of K/LTL zeolite with a narrow range of molar Si/Al ratios, scanty literature are available showing the micro-mesoporous materials containing zeolite K/LTL. Therefore, the present chapter aims at the study of influence of methods of preparation of zeolite K/LTL based micro-mesoporous composites as a solid base for noble metal-supported hydrogenation of xylose to sugar alcohols (as thoroughly discussed in earlier Chapter 2 and Chapter 3) and as solid base catalysts in the transesterification reactions of soybean oil to biodiesel.

The catalytic transesterification of edible and non-edible oil (triglycerides) to biodiesel as an alternative fuel has attracted considerable attention in recent years. The recycling of used vegetable oil to the biodiesel fuel can be one of the vital applications in the domestic transportation as a non-conventional fossil fuel.[22] The transesterification of triglycerides into biodiesel (methyl esters of long-chain fatty acids) can be achieved by using low carbon alcohols such as methanol or ethanol, to nontoxic, renewable and biodegradable biodiesel in presence of sodium or potassium hydroxide catalyst,[23-25] producing mainly methyl ester and glycerol,[26] as shown in scheme 5.1.

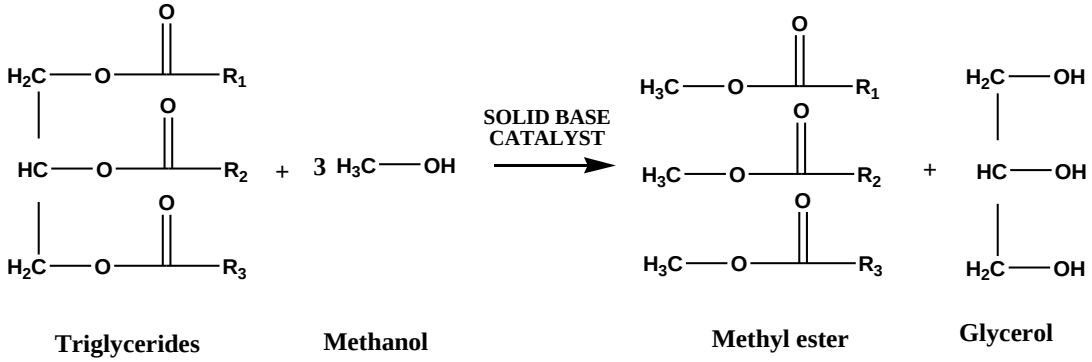

Scheme 5.1. Transesterification of triglycerides to biodiesel

The biodiesel originated from vegetable oil exhibited advantageous properties as compared to conventional petroleum-based diesel such as high flash point, lubricating properties and importantly, lower particulate matter and carbon monoxide emission which can lower the greenhouse effect.[23-25]

Oils and fats are chemically defined as the triglycerides, viz. the triester of fatty acids with glycerol as shown in Scheme 5.1. The chemical composition of the fatty acids mainly

determined the physical and chemical properties of oils or fats. Therefore, it is necessary to know about the fatty acid profile of the oils or fats.

Table 5.1. Composition of soybean oil in India[27, 28]

Fatty acid	Composition (*wt%*)
Palmitic (C16:0)	7-11
Stearic (C18:0)	2-6
Oleic (C18: 1)	22-34
Linolenic (C18:3)	5-10
Linoleic (C18:2)	43-56

Numbers in parenthesis signify the number of carbon atoms and the unsaturated centers (double bonds).

Soybean oil is one of the important edible oil and contributes to about 25% of total oil production in India.[29] In the year of 2016-2017, the total soybean oil production was estimated to 1.655 MMT, whereas in the year of 2017-2018, the soybean oil production was slightly decreased to 1.575 MMT.[30] Considering the several applications and the global market for soybean oil, the chemical composition of soybean oil should be known for its economics. The Table 5.1 documented the chemical composition of the soybean oil in India.[27, 28] The vegetable oil transesterification into biodiesel have been carried out industrially using homogeneous alkali catalyst.[31-33] Homogeneous base catalysts such as NaOH and KOH have been used widely because of a faster rate of reaction.[34] Moreover, the recycling and the neutralization of acid or basic homogeneous catalysts after the reactions need to be addressed systematically. However, the difficulties associated with the catalyst separation in homogeneous transesterification reaction can be overcome by using both, acid or basic heterogeneous catalysts.[35-40]

Several heterogeneous basic catalysts have been extensively studied for transesterification of vegetable oils such as alkali or alkaline metal doped metal oxides, alkali metal supported on alumina or zeolites, alkaline earth metal oxides, alkali metal exchanged zeolites, etc.[41-49] Among them, the basic modified zeolites with different alkali

cation exchange or alkali oxide have proved to be interesting candidates for transesterification reaction.[50, 51] Brito et al. have studied the transesterification of waste vegetable oil with methanol over Y zeolites with varying Si/Al ratio.[22] Suppes et al. has carried out the transesterification of soybean oil using NaX, FAU, ETS-10 zeolites.[50] The author used to exchange the counter ion by potassium and cesium. Among several series of catalysts, ETS-10 catalysts showed higher conversions as compared to the X type zeolite, which could be ascribed to the higher basicity of the catalyst and the ease of intra-particle diffusion due to large cavities. Another group has studied the transesterification of soybean oil over CaO supported NaY, KL and NaZSM-5 zeolites synthesized by microwave irradiation.[47] It was observed that the CaO/NaY catalysts showed higher catalytic performance due to the higher surface area, and the increase in the basic strength and the basicity. In a similar line, Pena et al. have reported the transesterification of sunflower oil using KNO_3/NaX catalyst.[52] Though, the biodiesel obtained under milder reaction conditions which satisfy the European norm EN-14214, the higher amount of KNO_3 on the zeolite (35 *wt%*) may affect the downstream processes. Further, Volli et al. have synthesized the zeolite X and A by an environmentally benign process utilizing the fly ash, and the counter ion exchanged to improve the basicity.[53] The zeolite ion-exchanged with potassium showing enhanced catalytic activity and showing the recyclability up to three runs with the marginal decrease in the crystallinity. A thorough experimental study on the deactivation of the K_2O/NaX and Na_2O/NaX catalysts was done by the Mucino et al. for the transesterification safflower oil.[54] It was observed that the deactivation constant of K_2O/NaX catalyst was higher as compared to the Na_2O/NaX catalyst and this could be attributed to the leaching of the active species and the poisoning of the catalyst surface.

In addition to the microporous zeolites as a support and/or the catalysts, literature reported the use of mesoporous material (eg. SBA-15) as catalysts or catalyst supports. Chen et al. have reported the Ti incorporated SBA-15 mesoporous catalysts as Lewis acid catalysts transesterification of Jatropha oil with methanol.[55] They have compared the catalytic activity with microporous TS-1 and commercial TiO_2 catalysts. The higher activity over Ti-SBA-15 mesoporous catalyst could be attributed to the accessible tetrahedral Ti^{4+} species present in the mesoporous framework. Another group of researchers reported, the Al-SBA-15 synthesized with varying molar Si/Al ratios (3, 22 and 73) and the catalytic

performance of the catalysts were studied for the acid-catalyzed transesterification of soybean oil and Jatropha oil.[56] In case of soybean oil, the higher catalytic activity was obtained over catalyst having higher aluminium content with Si/Al = 3 and the secondary reactions were also encountered. Meloni et al. have synthesized guanidine base 1,5,7-triazabicyclo[4.4.0]dec-5-ene for the functionalization of SBA-15 mesoporous material. The catalyst showed enhanced catalytic performance in the transesterification of soybean oil as compared to the commercial guanidine base 1,5,7-triazabicyclo[4.4.0]dec-5-ene grafted polymer.[57] Hou et al. have reported KOH/SBA-15 for solid base-catalyzed transesterification of soybean oil and methanol for biodiesel production, and the yield of biodiesel was reached to about 85 %.[58] Another literature reported the synthesis of 4-butyl-1,2,4-triazolium hydroxide grafted on the SBA-15 silica using 3-cholopropyltriethoxysilane.[59] This basic supported catalyst showed enhanced catalytic activity for transesterification of soybean oil with methanol. Aforementioned literature reports suggested that the microporous or mesoporous materials can be the implementation of as catalysts and/or catalyst supports. However, the literature is not available which report the use of micro-mesoporous composites prepared by different methods of preparation for the transesterification of vegetable oil.

The previous chapter showed that higher catalytic activity in the hydrogenation of xylose to sugar alcohols was achieved with the solid base having molar gel composition of $8SiO_2$: $1Al_2O_3$: $3.2K_2O$: $80H_2O$, as a consequence of higher aluminium content. Thus, in the present chapter, the zeolite K/LTL based micro-mesoporous composites were prepared with the molar gel composition of $8SiO_2$: $1Al_2O_3$: $3.2K_2O$: $80H_2O$ by different methods, namely, 1) post-synthesis modification, 2) seeding method and 3) two-step crystallization method. All the catalysts were thoroughly characterized by several analytical techniques. The basicity-porosity-activity correlation of zeolite K/LTL based micro-mesoporous material was studied as a solid base in the hydrogenation of xylose to sugar alcohols and as a catalyst in the transesterification of soybean oil with methanol under milder reaction conditions.

5.2 Experimental

5.2.1 Chemicals

The chemicals used for the synthesis of K/LTL zeolite based micro-mesoporous composites and the hydrogenation of xylose are described in Chapter 2, Section 2.2.1.1 and Section 2.5.1.1.

5.2.2 Synthesis of micro-mesoporous K/LTL composite by post-synthesis modification (8DSK/LTL)

The synthesis of K/LTL zeolite (molar Si/Al ratio = 2.6) with molar gel composition $8SiO_2$: $1Al_2O_3$: $3.2K_2O$: $80H_2O$ by following the similar procedure described in Chapter 2, Section 2.2.1.2 and designated as 8K/LTL. The micro-mesoporous K/LTL zeolite was prepared following post-synthesis modification by treating the K/LTL zeolite using 1.5 M aq. KOH solution at 70 ^oC for 1 h by following the procedure discussed in detail in Chapter 2, Section 2.2.1.3. The micro-mesoporous composite was designated as 8DSK/LTL.

5.2.3 Synthesis of micro-mesoporous K/LTL-MCM-41 composite by seeding method (K/LTL-MCM-41 Seed)

The micro-mesoporous K/LTL-MCM-41 composite was synthesized by seeding method with the molar gel composition of $8SiO_2$: $1Al_2O_3$: $3.2K_2O$: 1.9CTMABr: $256H_2O$ by following the experimental procedure described in Chapter 2, Section 2.2.1.4. The micro-mesoporous composite prepared by the seeding method was designated as K/LTL-MCM-41 Seed.

5.2.4 Synthesis of micro-mesoporous K/LTL-MCM-41 composite by two-step crystallization methods (K/LTL-MCM-41 Two-step)

The micro-mesoporous K/LTL-MCM-41 composite was synthesized by two-step crystallization methods with molar gel composition of $8SiO_2$: $1Al_2O_3$: $3.2K_2O$: 1.9CTMABr: $256H_2O$ by following the experimental procedure reported described in Chapter 2, Section 2.2.1.5.

5.2.5 Synthesis of 3.5 *wt%* Pt/γ-Al_2O_3 catalyst by wet impregnation method

3.5 *wt%* Pt/γ-Al_2O_3 catalyst used for the hydrogenation of xylose to sugar alcohols were synthesized by the wet impregnation method. The synthesis procedure is thoroughly described in Chapter 2, Section 2.2.1.6.

5.2.6 Hydrothermal stability

The hydrothermal stability of the zeolite-based micro-mesoporous composite was tested in boiling water for 8 h, as per the procedure is given in Chapter 2, Section 2.3.

5.2.7 Catalyst characterization

The synthesized materials were characterized by various analytical techniques such as ICP-OES, PXRD, N_2 adsorption-desorption measurement, CO_2-TPD, TEM, and HR-TEM analysis. The details of the analytical techniques and the sample preparation are described in Chapter 2, Section 2.4.

5.2.8 Catalytic activity

The catalytic activity of zeolite K/LTL based micro-mesoporous composites synthesized by different methods of preparations were tested as a solid base and 3.5 *wt%* Pt/γ-Al_2O_3 catalyst for hydrogenation of xylose to sugar alcohols. In addition, the porous and the basic properties of the micro-mesoporous composites were tested in the transesterification of soybean oil as model reaction with bulkier reactants and products molecules.

5.2.8.1 Hydrogenation of xylose to sugar alcohols

The detailed experimental procedure for hydrogenation of xylose to sugar alcohols, analysis of reactant and products and the calculation for the xylose conversion and sugar alcohol yield is described in Chapter 2, Section 2.5.1.

5.2.8.2 Transesterification of soybean oil as a model reaction

5.2.8.2.1 Experimental procedure

Transesterification reaction of soybean oil to biodiesel using solid base catalyst was studied as a model reaction to evaluate the micro-mesoporous composites by following the procedure in the reported literature.[60, 61] The transesterification reaction was carried out in 50 ml round bottom (RB) flask attached with the condenser. In the RB flask, 5 mL commercial edible grade soybean oil, 1.84 mL of methanol (99.8%, Loba Chemie, India) and 1 mL of n-hexane (99%, Loba Chemie, India) were charged. To this solution, 1 g of the micro-mesoporous composite as a catalyst was added. The molar ratio of methanol to soybean oil was 9:1 was kept constant. The RB flask was placed in the oil bath maintaining the temperature of 70 ^{o}C for 2 h under constant stirring at 500 rpm. After completion of the reaction, the RB flask was allowed to cool to room temperature and the sample was taken from the reaction mixture. The biodiesel proportion was separated from the catalyst by the centrifugation. The sample was then mixed with $CDCl_3$ (99.8%, Aldrich, USA) as solvent and biodiesel were analyzed by ^{1}H nuclear magnetic resonance spectroscopy (NMR).

5.2.8.2.2 Analysis of biodiesel by ^{1}H NMR method

The yield of biodiesel produced in the transesterification of soybean oil with methanol reaction was analyzed by ^{1}H NMR method reported by Gelbard *et al*.[61] For the analysis and calculation of yield of biodiesel, two types of ^{1}H NMR signals of biodiesel were considered for the integration (Figure 5.1).

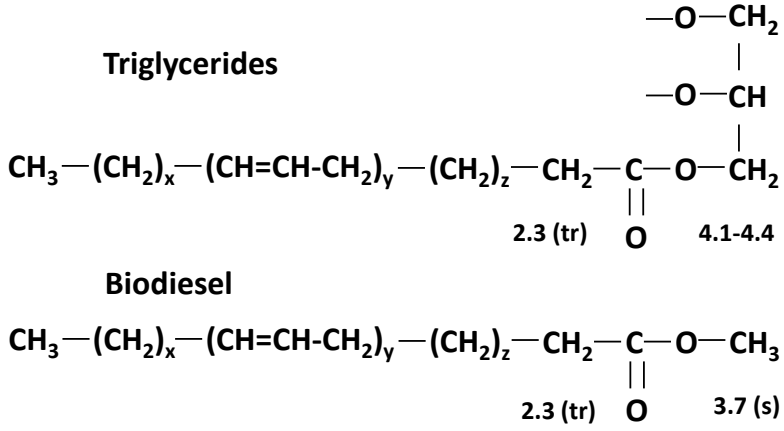

Figure 5.1. Assignment of chemical shifts of protons in triglycerides and biodiesel

In this method, 1) methoxy groups (OCH_3) in the methyl esters corresponding at 3.7 ppm appearing as a singlet, and 2) methylene group ($-CH_2-$) attached to the carbonyl carbon of ester group present in soybean oil appearing at 2.3 ppm as a triplet

The integrated areas of these signals were used for the calculation of the yield of transesterification reaction using the following formula as follows:

$$\textbf{\% Yield of biodiesel} = (2A_1/3A_2) \times 100$$

Where,

A_1= integrated value of the protons of the methyl esters (OCH_3 group)

A_2= integration value of the methylene protons ($-CH_2-$)

5.3 Results and discussions

5.3.1 Inductive coupled plasma-optical emission spectroscopy (ICP-OES)

In order to investigate the variation in the composition of K/LTL zeolite based micro-mesoporous composite synthesized with different methods of preparation, the composites were subjected to ICP-OES analysis. The molar Si/Al ratio of the K/LTL zeolite synthesized with molar composition $8SiO_2$: Al_2O_3: $3.2K_2O$: $80H_2O$ showed the value of 2.6 (Table 5.2). When the K/LTL was treated with 1.5 M aq. KOH solution at 70 ^oC for 1 h, the molar Si/Al ratio was found to decrease from 2.6 to 2.5. The reduction in molar Si/Al ratio with a marginal loss of crystallinity (94%) demonstrated the least extraction of Si atoms or dissolution of occluded amorphous matter from zeolite domain.[62] However, the preferential extraction of silicon from the zeolite framework was minimal. The primary reason for a small change in the molar Si/Al ratio could be the higher aluminum content may prevent the preferential silicon extraction against the attack of OH^- ions as discussed in Chapter 3. Further, micro-mesoporous K/LTL-MCM-41 composite prepared by seeding and two-step crystallization method was showed almost similar Si/Al ratio, 4.5 and 4.1, respectively, which matches with the initial molar gel composition.

Table 5.2. Physico-chemical properties of micro-mesoporous composites synthesized by different methods of preparation

Catalyst	**Si/Al ratio[a]**	**d_{100} (nm)**	**a_o (nm)**	**D_P (nm)**	**S_{BET} (m^2/g)**	**V_T (cm^3/g)**	**Basicity[b] (mmol/g)**	**CRY[c] (%)**
8K/LTL	2.6	-	-	-	274	0.16	0.558	100
8DSK/LTL	2.5	-	-	2.1	288	0.21	0.741	94*
Si-MCM-41	-	3.57	4.12	4.1	670	0.89	-	-
K/LTL-MCM-41 Seed	4.5	3.62	4.18	3.8	342	0.26	0.105	67
K/LTL-MCM-41 Two-step	4.1	4.15	4.79	3.9	458	0.38	0.098	55

a= ICP-OES, a_o = unit cell parameter = $2d_{100}/\sqrt{3}$, Dp = Average pore diameter, S_{BET} =BET surface area, V_T =Total pore volume, b= CO_2 TPD,
c= Crystalline matter by XRD, * = % relative crystallinity

5.3.2 Powder X-ray diffraction (PXRD)

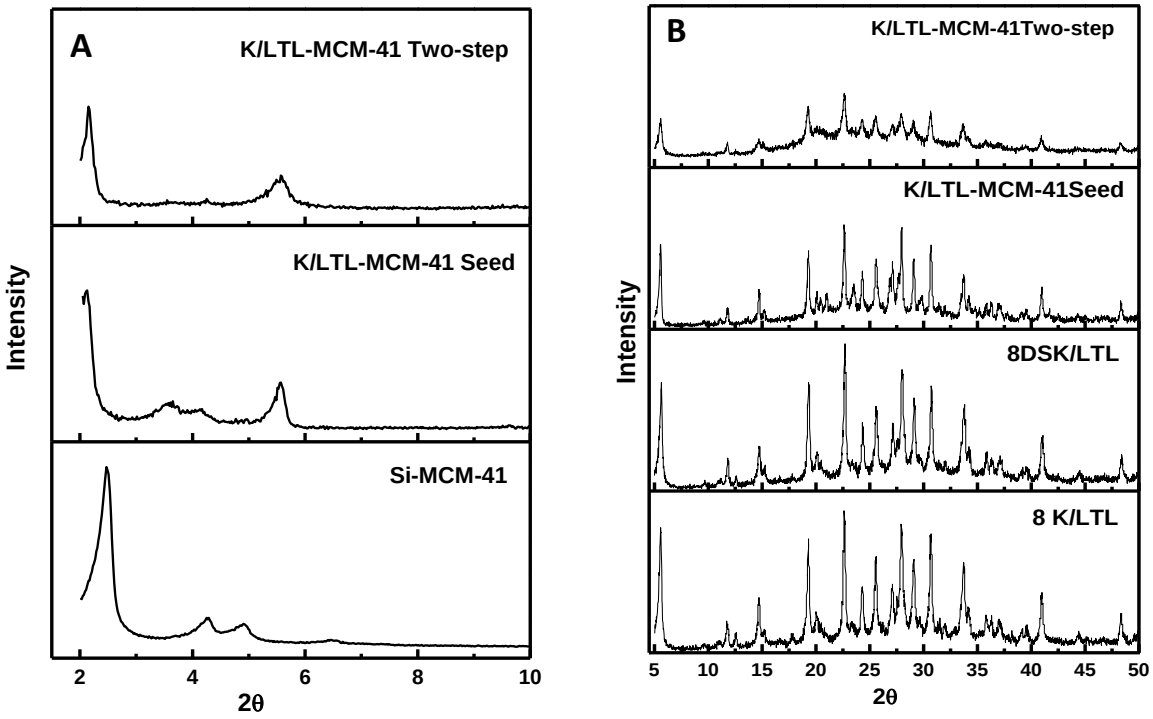

Figure 5.2. Low angle (A) and wide (B) PXRD patterns of micro-mesoporous composites

Figure 5.2 shows the powder XRD patterns of zeolite K/LTL based micro-mesoporous composites synthesized by the different method of preparation. The low angle XRD patterns (Figure 5.2 A) of Si-MCM-41, K/LTL-MCM-41 Seed and K/LTL-MCM-41 Two-step composites showed intense peak corresponds to (100) plane and the weak reflections corresponding to (110) and (200) planes. It revealed the presence of ordered 2D hexagonal symmetry of MCM-41 in composites and Si-MCM-41. The low angle PXRD also suggesting that the interplanar spacing d(100) and unit cell parameters (a_o) (Table 5.2) increased as compared to the siliceous MCM-41. It was also observed that K/LTL-MCM-41 Two-step composites showed a decrease in the intensity as a result of the development of K/LTL zeolite crystals embedded in or present on the surface of MCM-41 pore wall. Moreover, wide-angle PXRD patterns (Figure 5.2 B) evident all the micro-mesoporous composites demonstrated the characteristic peaks of K/LTL phase with no contribution due to another

crystalline phase.[21, 63] However, the variation in the PXRD patterns was accompanied by the changes in the structural features of the micro-mesoporous composite mainly depends upon the method of preparation. The 8DSK/LTL, after undergoing the post-synthesis treatment, showed a slight decrease in the intensity of diffraction peaks by treating the 8K/LTL zeolite with 1.5 M aq. KOH solution without a change in the peak position. The % crystallinity value of the sample is tabulated in Table 5.2. The 8DSK/LTL analogue has shown the minimal decrease in crystallinity indicating no perceptible structural damage. The extent of the drop in % crystallinity (94%) and the molar Si/Al ratio (2.5) was found to depend on the concentration of aqueous KOH solution used per gram of zeolite. It may introduce the mesoporosity on account of the removal of framework Si atoms from zeolite crystal domain.[64, 65] In case of K/LTL-MCM-41 seed and K/LTL-MCM-41 Two-step, the wide angle PXRD intensity was lower as compared to K/LTL zeolite, could be due to the presence of amorphous material (67% and 55%, respectively). Another reason for lowering in intensity in K/LTL-MCM-41 Two-step composite could be the hydrothermal crystallization time in the first step for synthesis of K/LTL zeolite was lower (10 h), which may generate secondary building units or nano-zeolite crystals only. It should be noted that in all the cases, the Al_2O_3/SiO_2, K_2O/SiO_2, and Al_2O_3/K_2O ratios were kept constant. Thus, PXRD patterns demonstrated that the methods of preparation played a crucial role in the structural regularity of micro-mesoporous composite.

5.3.3 N_2 adsorption-desorption measurement

The porous properties of zeolite K/LTL based micro-mesoporous composites were determined by N_2 adsorption-desorption analysis as shown in Figure 5.3, and corresponding values are tabulated in Table 5.2. The K/LTL zeolite has shown the BET surface area and total pore volume of the magnitude 274 m^2/g and 0.16 cm^3/g, respectively. The K/LTL zeolite showed very low total pore volume, which could be attributed to the microporous nature of zeolite crystals.

The N_2 adsorption-desorption isotherms showed that K/LTL zeolite exhibited type I isotherm which is the characteristic of microporous materials. The presence of hysteresis loop may be due to the aggregation of zeolite particles which is responsible for the intercrystalline mesoporosity. Moreover, 8DSK/LTL sample showed a combination of type

I and type IV isotherm with the appearance of a hysteresis loop indicating the development of mesoporosity in the microporous zeolite. Further, Si-MCM-41, K/LTL-MCM-41 Seed and K/LTL-MCM-41 Two-step exhibit type IV adsorption isotherms with hysteresis loop. The presence of hysteresis loop could be assigned to the capillary condensation as a result of the mesoporous nature of the composite.

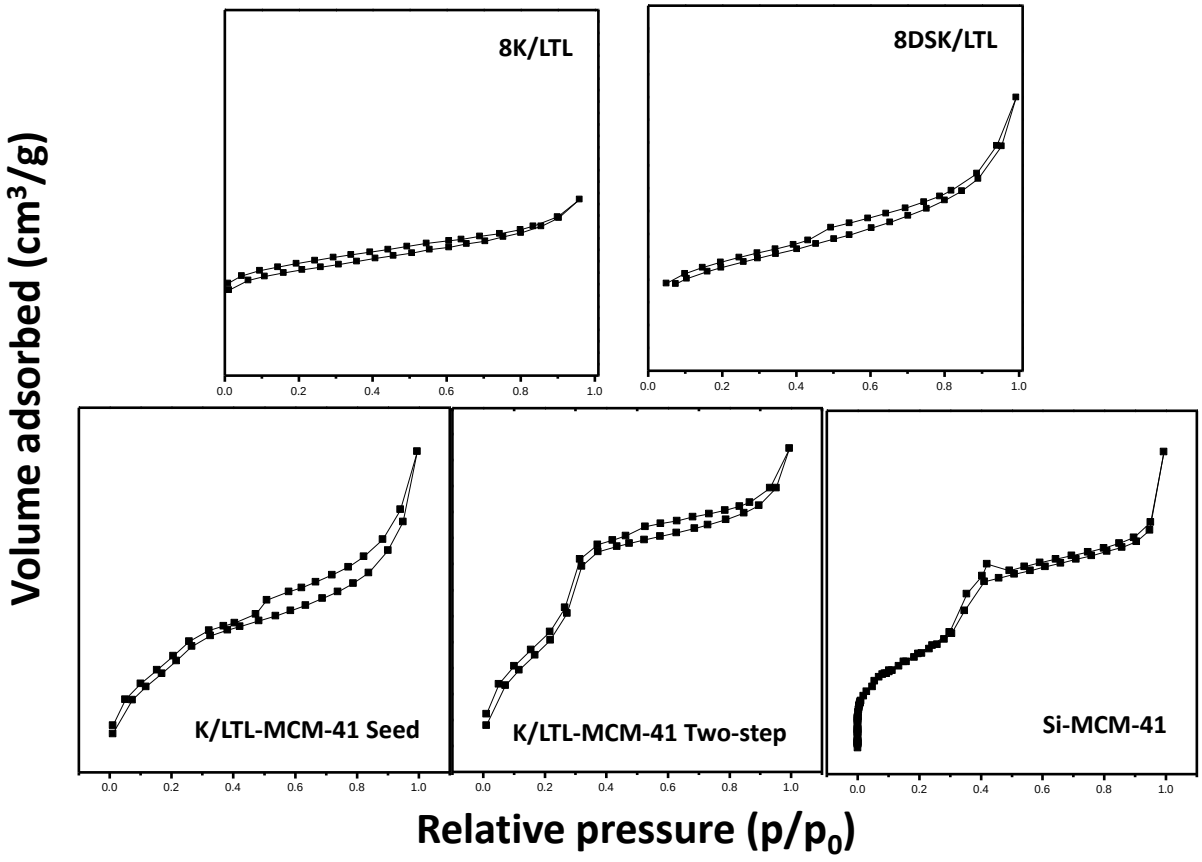

Figure 5.3. N_2 adsorption-desorption isotherms of micro-mesoporous composites

In comparison with 8K/LTL, alkali-treated 8DSK/LTL samples showed enhanced BET surface area (288 m^2/g) and total pore volume (0.21 cm^3/g), which could be due to the alkali treatment which may improve the mesoporosity in microporous zeolites by the extraction of framework Si atoms. As compared to the BET surface area (670 cm^2/g) and the total pore volume (0.89 cm^3/g) of Si-MCM-41, the K/LTL-MCM-41 Seed and K/LTL-MCM-41 Two-step synthesized by different methods of preparation showed lower BET surface area (342 cm^2/g and 458 cm^2/g, respectively) and the total pore volumes (0.26

cm^3/g and 0.38 cm^3/g, respectively). The surface area and the total pore volume of the micro-mesoporous composites increased in the order as follows: 8K/LTL < 8SK/LTL < K/LTL-MCM-41 Seed < K/LTL-MCM-41 Two step < Si-MCM-41. The average pore diameter of 8DSK/LTL was 2.1 nm due to the mesoporosity development. In the case of K/LTL-MCM-41 Seed (3.8 nm) and K/LTL-MCM-41 Two-step (3.9 nm), the average pore diameter was lower as compared with the Si-MCM-41 (4.1 nm). Considering the porous properties of all the composites, it was clear that the porous properties of the micro-mesoporous composites were depended mainly on methods of preparation.

5.3.4 Temperature programmed desorption of CO_2 (CO_2-TPD)

Basicity is one of the key factors which play a vital role in the catalytic performance. Therefore, the basicity of zeolite-based micro-mesoporous composites synthesized by the different method of preparation was estimated by temperature programmed desorption of CO_2 (CO_2-TPD) and the basicity values are tabulated in Table 5.2. The total basicity of 8K/LTL zeolite was found to be 0.558 mmol/g. The alkali treated zeolite 8DSK/LTL composite showed an increase in the basicity with a decrease in the molar Si/Al ratio due to aq. KOH solutions used for post-synthesis alkali treatment. It should be noted that after alkali treatment, the solid was washed several times till the pH of the filtrate was ~7. Thus, it seems that the post-synthesis alkali treatment resulted in the decrease in the framework Si/Al molar ratio (Table 5.2) by preferential removal of Si from zeolite framework and thereby increases the % tetrahedral aluminum content in the samples and not because of the occluded KOH. In addition to this, the basicity was found to be varied with a change in methods of preparation. Moreover, the K/LTL-MCM-41 Seed and K/LTL-MCM-41 Two-step showed much lower basicity, 0.105 mmol/g and 0.098 mmol/g, respectively, as compared to the parent 8K/LTL zeolite. The lowering in the basicity could be attributed to the presence of amorphous materials in the micro-mesoporous composite (Table 5.2). In case of K/LTL-MCM-41 Two-step, the secondary building units or partially formed zeolite nanocrystals with low crystallinity may responsible for the lowest basicity.

5.3.5 Transmission electron microscopy (TEM and HR-TEM)

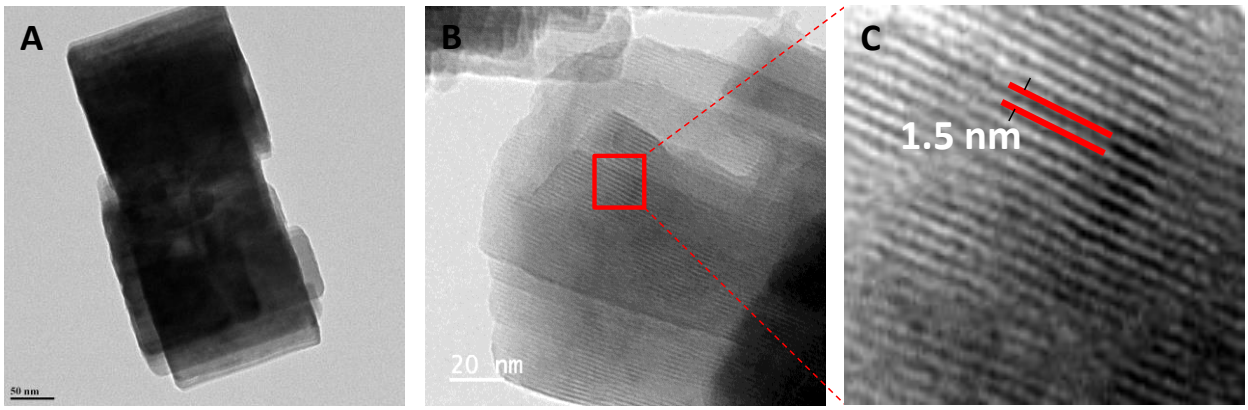

Figure 5.4. TEM image of 8K/LTL zeolite (A) and HR-TEM images of 8DSK/LTL micro-mesoporous composite

The porous nature and the morphology of the micro-mesoporous composites were studied by TEM and HR-TEM analysis. Figure 5.4 A showed the appearance of the fully crystalline cylindrical-rod shaped morphology of 8K/LTL zeolite crystals. The HR-TEM image of 8DSK/LTL micro-mesoporous composite (Figure 5.4B) illustrated the structural damage, especially at the edges of zeolite crystal, which was mainly attributed to the removal of Si atoms from the framework due to alkali post-synthesis modification. The increase in mesoporous volume and BET surface area, due to the generation of mesoporosity in the 8K/LTL zeolite, was supported by observations from the HR-TEM image of micro-mesoporous 8DSK/LTL composite. Figure 5.4 C clearly showed the lattice fringes of 8K/LTL zeolite corresponding to the d(100) spacing of 1.5 nm.

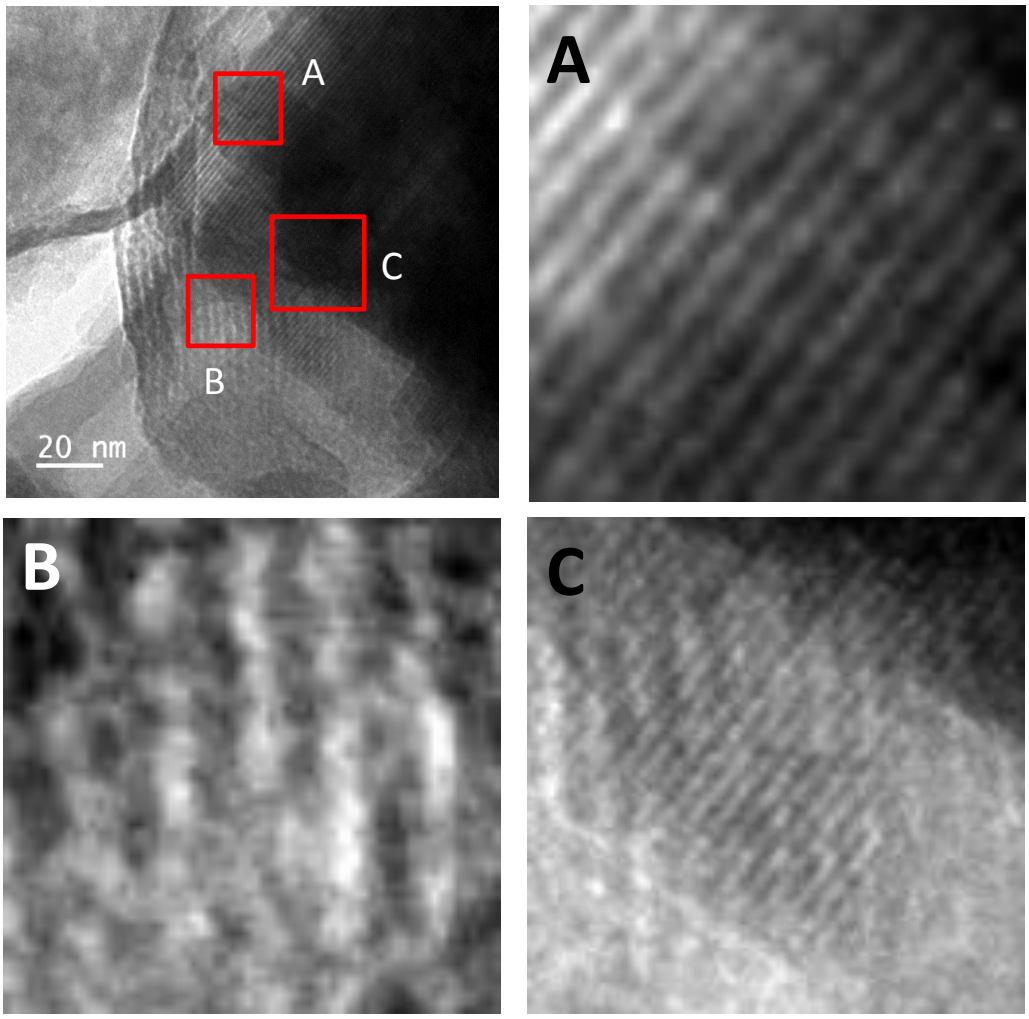

Figure 5.5. HR-TEM images of micro-mesoporous K/LTL-MCM-41 Seed composite, (Inverse FFT images A, B, and C were taken from different regions)

The HR-TEM image of calcined micro-mesoporous K/LTL-MCM-41 Seed composite and inverse FFT images of the composite at different regions are shown in Figure 5.5. One can see that micro-mesoporous K/LTL-MCM-41 Seed composite showed well-defined and ordered channels corresponding to the mesoporous structure of MCM-41 materials. The composite clearly showed the presence of microporous and mesoporous phases. The inverse FFT images gave clear information about the phases with d spacing. Inverse FFT region A, showed the presence of MCM-41 mesoporous channels, whereas, region B exhibits d spacing corresponding to the K/LTL zeolite crystals. The region C showed the

overlapping of the K/LTL zeolite crystals with MCM-41 mesophase, indicating the fully grown K/LTL crystals covered with MCM-41 materials.

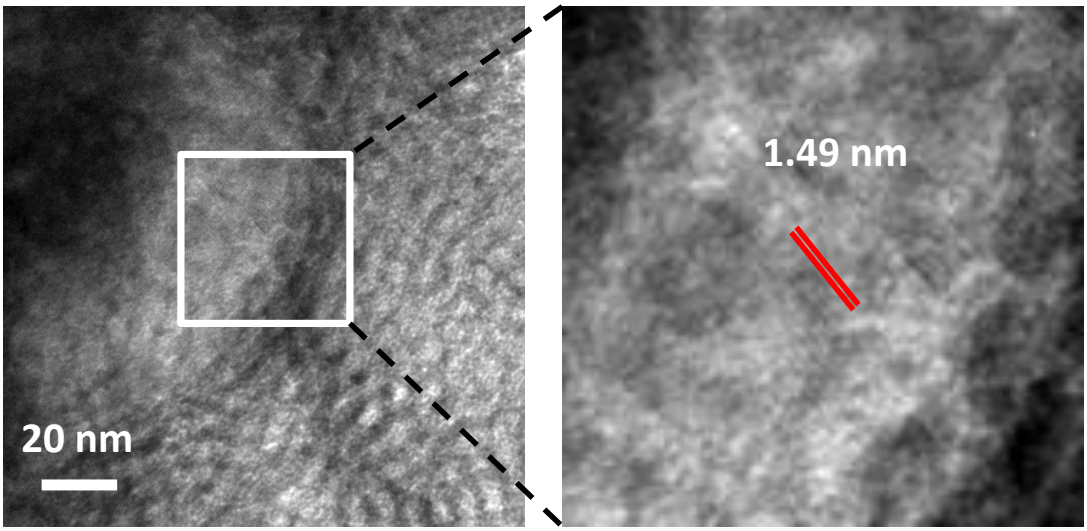

Figure 5.6 HR-TEM images of K/LTL-MCM-41 Two-step micro-mesoporous composite

The HR-TEM images of calcined micro-mesoporous K/LTL-MCM-41 Two-step composite are shown in Figure 5.6. The composite showed the presence lattice fringes corresponding to the MCM-41 mesoporous phase (d_{100}=4.1 nm). However, the inverse FFT image of the composite clearly indicated the presence of the lattice fringes corresponding to the zeolite nano-crystals (d_{100}=1.49 nm). This clearly envisioned that the zeolite nanocrystals were embedded in the mesopore walls of MCM-41 material. The presence of both, micro and mesoporous phases within the single composite suggested the interconnected micro and mesoporosity beneficial for catalytic performance. This micro-mesoporous structure with a crystalline MCM-41 wall constructed with zeolite nano-crystals may exhibit higher hydrothermal stability. Thus, from TEM and HR-TEM images of the micro-mesoporous composites, it is clear that the interconnected micro and mesoporosity depend mainly on the method of preparation.

5.3.6 Thermogravimetric analysis (TGA)

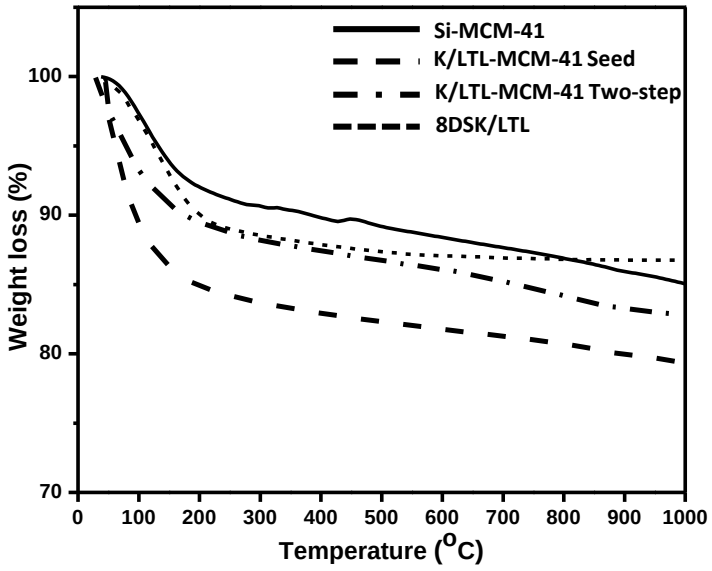

Figure 5.7. TGA of micro-mesoporous composites

Thermogravimetric analysis (TGA) technique is used to study the thermal stability of micro-mesoporous materials. It can also be used to predict the stability of composites based on the presence of zeolite building units in the wall of mesoporous materials.[66] The TGA curves of 8DSK/LTL and calcined SiMCM-41, K/LTL-MCM-41 Seed, and K/LTL-MCM-41 Two-step are shown in Figure 5.7. It can be seen that 15 *w%* weight losses were observed for Si-MCM-41. whereas, K/LTL-MCM-41 Seed, K/LTL-MCM-41 Two-step and 8DSK/LTL micro-mesoporous composites showed 20.8 *wt%*, 17.2 *wt%*, and 13.3 *wt%* mass loss below 1000 °C, respectively. All the samples showed the weight loss below 150 °C which could be ascribed to the mass loss of physically adsorbed water. Since all the material are calcined prior to analysis, the mass loss above 200 °C was noticed as a result of the loss of water due to dehydroxylation reactions.[67]

5.3.7 Hydrothermal stability

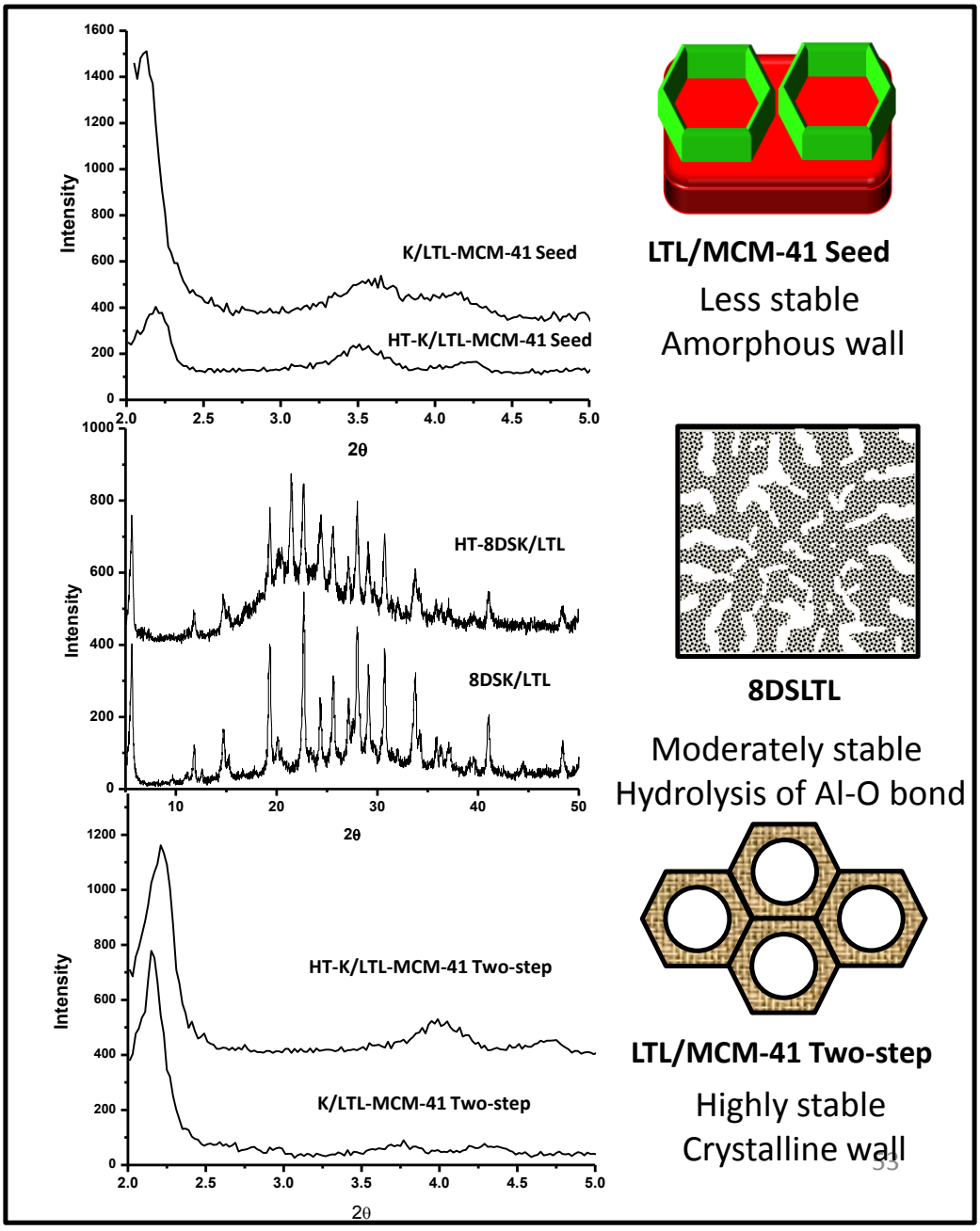

Figure 5.8. PXRD of hydrothermally treated micro-mesoporous composites

The hydrothermal stability of synthesized micro-mesoporous composites was evaluated in boiling water and the PXRD of hydrothermally treated composites are shown in Figure 5.8. The micro-mesoporous K/LTL-MCM-41 Seed composite prepared by the seeding method showed lowering in the intensity of the d100 plane after hydrothermal treatment. Further, 8DSK/LTL prepared by post-synthesis modification showed a slight decrease in peak intensity, whereas, K/LTL-MCM-41 Two-step synthesized by two-step crystallization is showing the slight decrease in the intensity and broadening of d100 peak corresponding to the MCM-41 phase. The hydrothermal stability increased in the order of: K/LTL-MCM-41 Seed < 8DSK/LTL < K/LTL-MCM-41 Two-step.

The hydrothermal stability trend can be explained on the basis of the structure and the treatment conditions. The hydrothermal stability of K/LTL-MCM-41 Seed was lower among all the composites as can be seen from low angle PXRD patterns. During the synthesis, first K/LTL zeolite crystals were fully grown and then MCM-41 was synthesized from the waste mother liquor without the addition of extra silica source. It means that amorphous MCM-41 was grown only on the crystals of K/LTL zeolite, as can be seen in the schematic diagram. Therefore, after hydrothermal treatment, the amorphous MCM-41 phase was a collapse, thereby showing lower stability. In the case of 8DSK/LTL analog showed retention in the LTL zeolite peak pattern but slight lowering in the peak intensity. This can be explaining on the basis of the dealumination phenomenon. It has been reported that the hydrothermal treatment by steaming at a higher temperature or in boiling water may cause structural collapse partially by the dealumination. Thus, in the present study, the lowering in the intensity of 8DSK/LTL micro-mesoporous composite after hydrothermal treatment could be due to the hydrolysis of the Si-O-Al bond. Finally, the K/LTL-MCM-41 Two-step showed a slight decrease in the intensity corresponding to the d100 peak because of the crystalline nature of the MCM-41 wall. In K/LTL-MCM-41 Two-step synthesis, the first step involves the formation of zeolite nanocrystals or secondary building units. These building units, in the second step, embedded into the MCM-41 mesoporous wall by hydrothermal treatment. Therefore, the micro-mesoporous K/LTL-MCM-41 Two-step composite showed higher hydrothermal stability in comparison to the K/LTL-MCM-41 Seed (as per the schematic diagram is shown in Figure 5.5).

5.4 Catalytic performance

The catalytic performance of the micro-mesoporous composites synthesized by different methods of preparation was tested, 1) for noble metal-supported hydrogenation of xylose to sugar alcohols as a solid base and, 2) transesterification of soybean oil as a catalyst.

5.4.1 Noble metal supported hydrogenation of xylose to sugar alcohols as a solid base

The influence of zeolite K/LTL based micro-mesoporous composites synthesized by different methods of preparation on noble metal-supported hydrogenation of xylose to sugar alcohols as a solid base is depicted in Figure 5.9. It showed that only 11 % xylose conversion and 4 % sugar alcohol yield was observed with 3.5 *wt%* Pt/γ-Al_2O_3 catalyst at 60 ^oC for 12 h. However, under the identical set of reaction conditions, by the addition of solid base 8K/LTL zeolite, three-fold enhancement catalytic activities was observed. The 8K/LTL zeolite showed 35% xylose conversion and 30.4% sugar alcohols yield was observed. Among various zeolite K/LTL based micro-mesoporous composites synthesized by different methods of preparation, 8DSK/LTL micro-mesoporous composite showed higher xylose conversion of 64% and sugar alcohols yield of 59%. MCM-41 did not show improvement in the catalytic activity which could be due to the absence of basic sites. Further, physical mixture (50/50 *wt%*) showed 17% xylose conversion and about 11% sugar alcohols yield. The higher sugar alcohols yield could arise as a result of basicity of the 8K/LTL zeolite. However, one can observe the catalytic performance of physical mixture was comparable with the MCM-41 mesophase. This could be explained on the basis of adsorption of xylose and products on the solid bases. In addition, micro-mesoporous composites, K/LTL-MCM-41 Two-step and K/LTL-MCM-41 Seed showed 53% and 48 % xylose conversion, respectively. Whereas it also showed 49 % and 45 % sugar alcohols yields over K/LTL-MCM-41 Two-step and K/LTL-MCM-41 Seed, respectively.

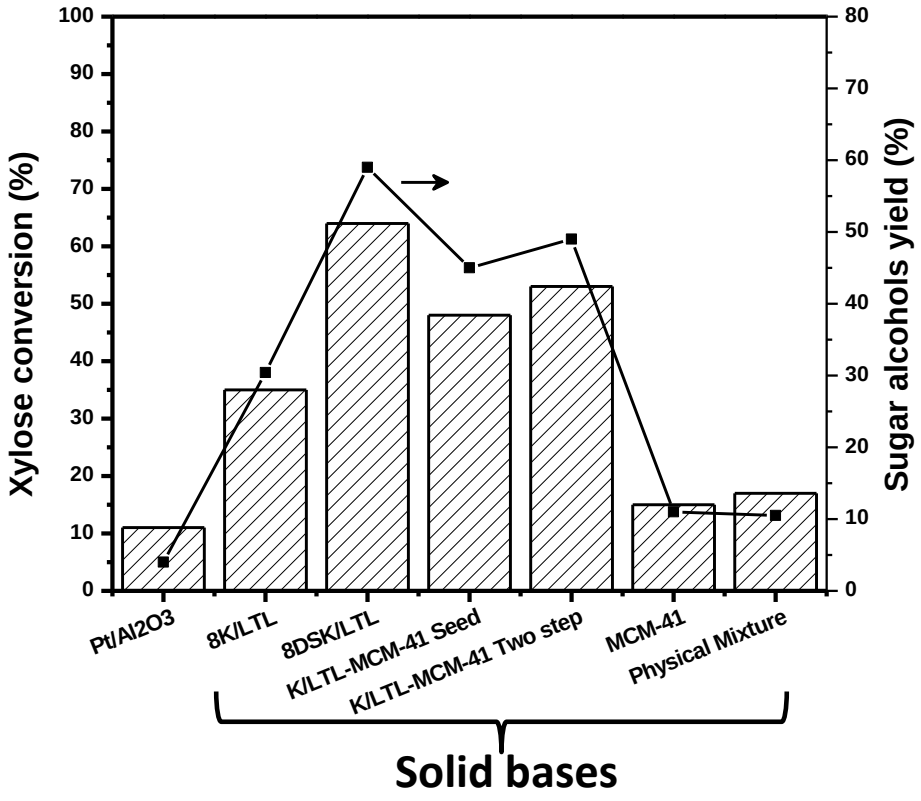

Figure 5.9 Catalytic activity of hydrogenation of xylose to sugar alcohols over micro-mesoporous composites as solid bases and 3.5 *wt%* Pt-Al_2O_3 catalyst (Reaction conditions: xylose: 0.15g, catalyst: 0.075g, solid base: 0.075g, water: 35ml, temperature: 60 ^oC, time 12 h, 16 bar H_2 pressure at R.T., 900RPM).

Overall increasing trend of the xylose conversion over solid bases was observed as: MCM-41 (15 %) < Physical Mixture (17 %) < 8K/LTL (35 %) < K/LTL-MCM-41 Seed (48 %) < K/LTL-MCM-41 Two-step (53 %) < 8DSK/LTL (64 %). Similarly, the sugar alcohols yield trend was increased as follows: MCM-41 (11 %) = Physical Mixture (11 %) < 8K/LTL (30.4 %) < K/LTL/MCM-41 Seed (45 %) < K/LTL/MCM-41 Two-step (49 %) < 8DSK/LTL (59 %). The catalytic performance of all the micro-mesoporous composites showed seems to be based on the methods of preparation of composites. 8DSK/LTL micro-mesoporous composite synthesized by post-synthesis modification using 1.5 M aq. KOH solution led to

the development of mesopores in the microporous zeolite (as evidenced by nitrogen sorption study). The xylose and xylitol with kinetic diameters of 6.55 Å and 6.58 Å, respectively, can easily pass through the mesopores without experiencing molecular restriction with more accessible basic sites. Further, the selective removal of the silicon from the zeolite matrix enhances the amount of alumina content per gram of the zeolite. As a result, the post-synthesis modified 8DSK/LTL showed improved basicity in comparison with without alkali treated 8K/LTL. It has been reported that in alkaline conditions, the concentration of xylose molecules present in the open chain is high which proceeds through Lobry de Bruyn-Albeda van Ekenstein transformation.[1, 2] Thus, hydrogenation of open chain xylose molecules was more efficient giving a higher catalytic performance. Therefore, the higher activity of 8DSK/LTL could be attributed to the pronounced effect of higher basicity, higher surface area, accessibility of active sites for reactants and efficient mass transfer through mesopores with preserved crystallinity.

The micro-mesoporous K/LTL-MCM-41 Two-step and K/LTL-MCM-41 Seed composites synthesized by the Two-step crystallization and the seeding method showed higher sugar alcohols yields as compared to the 8K/LTL. Though K/LTL-MCM-41 Two-step and K/LTL-MCM-41 Seed contains a lower amount of crystalline matter (55% and 67%, respectively) and lower basicity (Table 5.2), the higher catalytic performance could be attributed to the accessible basic sites in the composites. K/LTL-MCM-41 Seed composite prepared by seeding method showed higher surface area, a porous structure in micro and mesoporous region and the fully crystallized K/LTL zeolites. In K/LTL-MCM-41 Two step synthesized by two-step crystallization method, the secondary building units and/or zeolite nanocrystals were embedded in the walls of the MCM-41 mesophase. Moreover, it showed pore size distribution in the mesoporous region. Due to the lower amount of crystalline matter, K/LTL-MCM-41 Two step possesses lower basicity (Table 5.2). Despite lower crystalline matter and lower basicity, we can anticipate that the higher catalytic performance for hydrogenation of xylose to sugar alcohols not only depends on the basicity but also the composite with the higher surface area and the appearance of the mesopores also beneficial. Moreover, nano-sized Pt on alumina supports also aid in enhancement in the sugar alcohols yield.

5.4.2 Transesterification of soybean oil to biodiesel

In the present section, the transesterification of soybean oil with methanol to biodiesel using various zeolite K/LTL based micro-mesoporous composites were tested as solid basic heterogeneous catalysts. In previous section 5.4.1, the hydrogenation of xylose to sugar alcohols was studied over several zeolite K/LTL based micro-mesoporous composites. Though the catalytic activity of the synthesized materials was good, the advantageous diffusion of the reactant/product molecules would have essential to study. Because, as discussed in the previous sections, the kinetic diameter of the xylose and xylitol (main product) were 6.55 Å and 6.58 Å, respectively, whereas the one-dimensional pore dimension of K/LTL zeolite is 7.1 Å. Thus, the reactants and products molecules can pass through the zeolite pores. Therefore, in order to study the efficacy of synthesized micro-mesoporous materials, the reactants/products with larger molecular dimensions have chosen.

The aim of the aforementioned reaction was the study of transesterification of soybean oil having bigger molecular dimensions with methanol over various micro-mesoporous composites synthesized with different methods of preparation.

The catalytic performance of several zeolite K/LTL based micro-mesoporous composites were tested as a solid base catalyst for transesterification of soybean oil with methanol to biodiesel as depicted in Figure 5.10. The catalytic activity was correlated with the basicity as estimated by CO_2 TPD analysis (Table 5.2). The parent 8K/LTL zeolite as a solid base catalyst showed about 13% yield of biodiesel. The yield of biodiesel in the transesterification of soybean oil was calculated by ^{1}H NMR spectroscopy (Section 5.2.8.2.2) as shown in Figure 5.11. The assignments of ^{1}H NMR peaks of soybean oil and the biodiesel are tabulated in Table 5.3. In both the ^{1}H NMR spectra, all the signals match well. However, The ^{1}H NMR spectra of biodiesel consist of one extra peak at 3.68 ppm, corresponding to the methyl group of ester (-$COOCH_3$). The ^{1}H NMR studied indicating the transesterification of soybean oil carried out with methanol to form biodiesel.

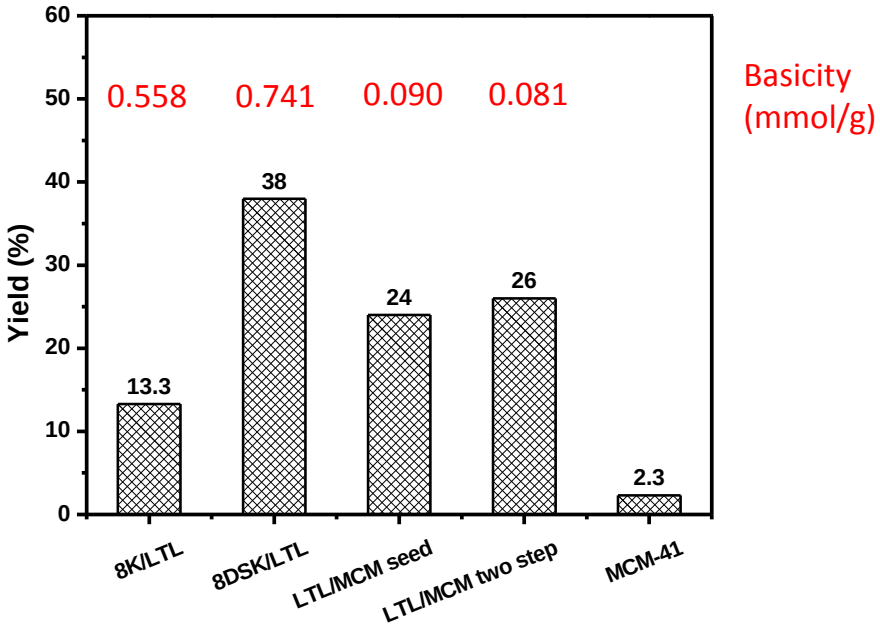

Figure 5.10. Transesterification of soybean oil to biodiesel over zeolite K/LTL based micro-mesoporous composites

(Reaction conditions: Soybean oil: 5 mL, catalyst: 0.1 g, MEOH 1.84 mL, n-hexane 1 mL, temperature 70 ^{o}C, time 1 h)

The increasing the order of biodiesel is as follows: MCM-41 (2.3%) < 8K/LTL (13.3%) < K/LTL/MCM-41 Seed (24 %) < K/LTL/MCM-41 Two-step (26 %) < 8DSK/LTL (38 %). Among all the catalysts, 8DSK/LTL synthesized by post synthesis treatment by aq. KOH treatment was found to be the most active catalyst under given conditions as a result of higher basicity, higher surface area, mesopore volume, and higher crystallinity. The higher yield (38%) of biodiesel over 8DSK/LTL could be attributed to the higher accessibility of basic sites to the bulkier reactant molecules located inside zeolite mesopores. In comparison to the 8K/LTL zeolite, it can be concluded that the bulkier reactant and products can easily be diffused through the mesopores without any steric constrain over 8DSK/LTL catalyst. However, the mass loss during the post-synthesis modification is the major issue.

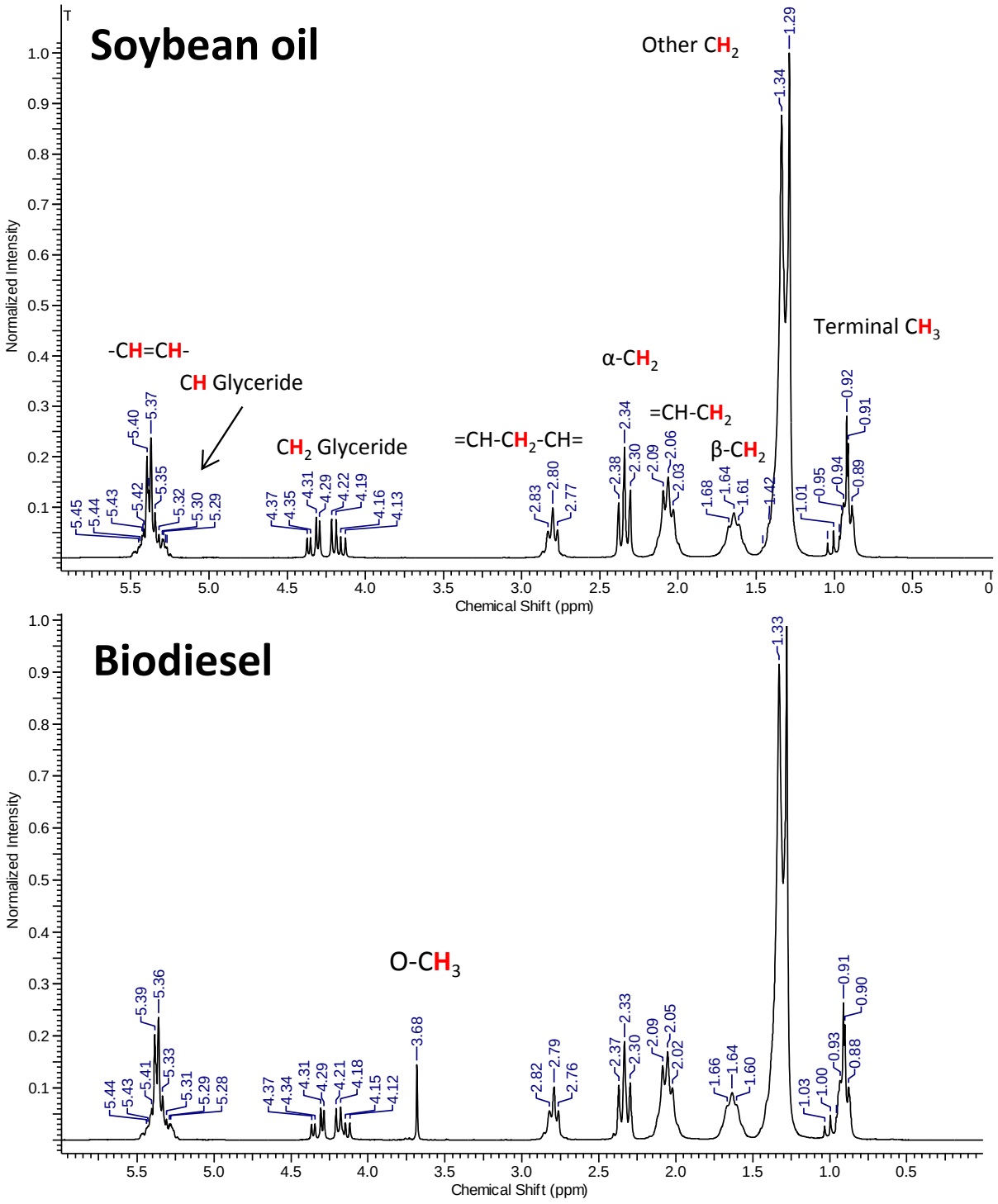

Figure 5.11 ^{1}H NMR spectra of soybean oil and biodiesel

Table 5.3 ^{1}H NMR spectra peak assignments of soybean oil and biodiesel

Proton(s)	Functional group	Compound / chemical shift, δ (ppm)	
		Soybean oil	**Biodiesel**
C**H**$_3$-C	Terminal methyl group	0.89-1.01	0.88-1.03
-(C**H**$_2$)n-	CH_2 Backbone	1.20-1.42	1.22-1.42
- C**H**$_2$CH$_2$COOH	Beta (β)-Methylene proton	1.61-1.68	1.60-1.66
=CH-C**H**$_2$-	Alfa (α)-Methylene group bonded to one double bond	2.03-2.09	2.02-2.09
-C**H**$_2$COOR	Alfa (α)-Methylene group bonded to an ester	2.30-2.38	2.30-2.37
=CH-C**H**$_2$-CH=	Alfa (α)-Methylene group bonded to two double bond	2.77-2.83	2.76-2.82
-COOC**H**$_3$	**Methyl group of ester**	-	**3.68**
- C**H**$_2$OCOR	Methylene group (C1 & C3) of glycerides	4.13-4.37	4.12-4.37
-C**H**OCOR	Methine proton at C2 of glycerides	5.29	5.28
-C**H**=C**H**-	Olefinic protons	5.32-5.45	5.31-5.44

Further, the maximum biodiesel production yield over K/LTL-MCM-41 Seed and K/LTL-MCM-41 Two step catalysts was found to be 24 % and 26 % yield, respectively at 70 ^{o}C for 1h. These values were higher than that of 8K/LTL zeolite, though the basicity values of micro-mesoporous composites were very low may be because of the higher surface area and mesopore volume. It clearly envisioned the dependency of the catalytic performance on the development of mesoporosity and catalytically active basic sites. As expected, both the catalyst showed lower yield as compared to 8DSK/LTL, most likely because of lower basic sites which are the primary requirement of the transesterification reaction. However, the development of micro-mesoporous composites could enhance the yield of biodiesel. In K/LTL-MCM-41 Seed have higher crystalline matter and accessible basic sites were observed. In case of K/LTL-MCM-41 Two-step, the zeolite nanocrystals were embedded into the walls of MCM-41 leading to the enhancement in the diffusion of reactants through the pores and the accessibility to basic sites of zeolites present in the pore wall.

5.5 Conclusions

Thus, the overall catalytic activity of a) Hydrogenation of xylose to sugar alcohols, and b) transesterification of soybean oil to biodiesel, mainly depended on, 1) methods of preparation and 2) higher porous properties such as BET surface area, mesopore volume, 3) the accessibility of the basic sites owing to the generation of mesopores, and 4) ease of diffusion of the reactants and products to and from the mesopores of micro-mesoporous composites. Among all, the K/LTL zeolite based micro-mesoporous composite prepared by the demetallation and the two-step crystallization showed enhancement in the catalytic activity and found to be the best heterogeneous catalysts for transesterification of biodiesel and the solid base for hydrogenation of xylose.

5.6 References

1. H. S. Singh, A. Gupta, A. K. Singh and B. Singh, *Transition Metal Chemistry*, 1998, **23**, 277-281.
2. A. Tathod, T. Kane, E. S. Sanil and P. L. Dhepe, *Journal of Molecular Catalysis A: Chemical*, 2014, **388–389**, 90-99.

3. A. Corma, V. Fornes, S. B. Pergher, T. L. M. Maesen and J. G. Buglass, *Nature*, 1998, **396**, 353.
4. S. Lopez-Orozco, A. Inayat, A. Schwab, T. Selvam, and W. Schwieger, *Advanced Materials*, 2011, **23**, 2602-2615.
5. D. Coster, A. L. Blumenfeld, and J. J. Fripiat, *The Journal of Physical Chemistry*, 1994, **98**, 6201-6211.
6. J. C. Groen, S. Abelló, L. A. Villaescusa and J. Pérez-Ramírez, *Microporous and Mesoporous Materials*, 2008, **114**, 93-102.
7. J. C. Groen, J. C. Jansen, J. A. Moulijn and J. Pérez-Ramírez, *The Journal of Physical Chemistry B*, 2004, **108**, 13062-13065.
8. J. C. Groen, W. Zhu, S. Brouwer, S. J. Huynink, F. Kapteijn, J. A. Moulijn, and J. Pérez-Ramírez, *Journal of the American Chemical Society*, 2007, **129**, 355-360.
9. J. Wang, J. C. Groen, W. Yue, W. Zhou, and M.-O. Coppens, *Journal of Materials Chemistry*, 2008, **18**, 468-474.
10. C. J. H. Jacobsen, C. Madsen, J. Houzvicka, I. Schmidt and A. Carlsson, *Journal of the American Chemical Society*, 2000, **122**, 7116-7117.
11. A. A. Campos, L. Dimitrov, C. R. da Silva, M. Wallau, and E. A. Urquieta-González, *Microporous and Mesoporous Materials*, 2006, **95**, 92-103.
12. A. H. Janssen, I. Schmidt, C. J. H. Jacobsen, A. J. Koster and K. P. de Jong, *Microporous and Mesoporous Materials*, 2003, **65**, 59-75.
13. I. Schmidt, A. Boisen, E. Gustavsson, K. Ståhl, S. Pehrson, S. Dahl, A. Carlsson, and C. J. H. Jacobsen, *Chemistry of Materials*, 2001, **13**, 4416-4418.
14. M. J. F. Costa, J. Marszewska, A. A. S. Gonçalves, L. K. C. de Souza, A. S. Araujo and M. Jaroniec, *RSC Advances*, 2016, **6**, 54956-54963.
15. U. Deforth, K. K. Unger and F. Schüth, *Microporous Materials*, 1997, **9**, 287-290.
16. C. R. Patil, P. S. Niphadkar, V. V. Bokade, and P. N. Joshi, *Catalysis Communications*, 2014, **43**, 188-191.
17. H. Xu, J. Guan, S. Wu and Q. Kan, *Journal of Colloid and Interface Science*, 2009, **329**, 346-350.

18. V. Ordomsky, V. Murzin, Y. V. Monakhova, Y. Zubavichus, E. Knyazeva, N. Nesterenko and I. Ivanova, *Nature, strength and accessibility of acid sites in micro/mesoporous catalysts obtained by recrystallization of zeolite BEA*, 2007.
19. Q. Huo, Y. Gong, T. Dou, Z. Zhao, H. Pan, and F. Deng, *Energy and Fuels*, 2010, **24**, 3764-3771.
20. Y. Di, Y. Yu, Y. Sun, X. Yang, S. Lin, M. Zhang, L. Shougui and F.-S. Xiao, *Microporous and Mesoporous Materials*, 2003, **62**, 221-228.
21. N. P. Tangale, S. K. Sonar, P. S. Niphadkar, and P. N. Joshi, *Journal of Industrial and Engineering Chemistry*, 2016, **40**, 128-136.
22. A. Brito, M. E. Borges, and N. Otero, *Energy & Fuels*, 2007, **21**, 3280-3283.
23. Z. Helwani, M. R. Othman, N. Aziz, W. J. N. Fernando, and J. Kim, *Fuel Processing Technology*, 2009, **90**, 1502-1514.
24. M. Di Serio, R. Tesser, M. Dimiccoli, F. Cammarota, M. Nastasi and E. Santacesaria, *Journal of Molecular Catalysis A: Chemical*, 2005, **239**, 111-115.
25. G. Nahar and K. Kendall, *Fuel Processing Technology*, 2011, **92**, 1345-1354.
26. S. Yamaguchi, M. Asamoto, S. Inoue, S. Kawahito, Y. Mieno, K. Ikushima, and H. Yahiro, *Transesterification of Triolein to Biodiesel Fuel over Mordenite-supported CaO Catalysts*, 2010.
27. A. Thomas, *https://www.chempro.in/fattyacid.htm, Chemistry*, 2000.
28. *http://onlinelibrary.wiley.com/doi/10.1002/14356007.a10_173/pdf*.
29. *http://ficci.in/spdocument/20539/SOYBEAN-Report.pdf*.
30. *http://www.sopa.org/world-soy-oil-production/?searchtype=search_by_year&years=2017 - 2018 &starting_year_value=&ending_year_value=&submit=Search*.
31. F. Ma and M. A. Hanna, *Bioresource Technology*, 1999, **70**, 1-15.
32. M. A. Dubé, A. Y. Tremblay and J. Liu, *Bioresource Technology*, 2007, **98**, 639-647.
33. L. B. Wen, Y. Wang, D. L. Lu, S. Y. Hu and H. Y. Han, *Fuel*, 2010, **89**, 2267-2271.
34. D. E. López, J. G. Goodwin, D. A. Bruce, and E. Lotero, *Applied Catalysis A: General*, 2005, **295**, 97-105.
35. V. G. Coteron A., Martinez M., Aracil J., *Pandalai, S.G. (Eds.), Recent Res. Developments in Oil Chemistry 1, Transworld Research Network, India*, 1997, 109-114.

36. E. Leclercq, A. Finiels and C. Moreau, *Journal of the American Oil Chemists' Society*, 2001, **78**, 1161-1165.
37. G. J. Suppes, K. Bockwinkel, S. Lucas, J. B. Botts, M. H. Mason, and J. A. Heppert, *Journal of the American Oil Chemists' Society*, 2001, **78**, 139-146.
38. B. M. Choudary, M. Lakshmi Kantam, C. Venkat Reddy, S. Aranganathan, P. Lakshmi Santhi and F. Figueras, *Journal of Molecular Catalysis A: Chemical*, 2000, **159**, 411-416.
39. H.-J. Kim, B.-S. Kang, M.-J. Kim, Y. M. Park, D.-K. Kim, J.-S. Lee, and K.-Y. Lee, *Catalysis Today*, 2004, **93-95**, 315-320.
40. S. Furuta, H. Matsuhashi and K. Arata, *Biomass and Bioenergy*, 2006, **30**, 870-873.
41. W. Xie, H. Peng, and L. Chen, *Applied Catalysis A: General*, 2006, **300**, 67-74.
42. W. Xie and H. Li, *Journal of Molecular Catalysis A: Chemical*, 2006, **255**, 1-9.
43. T. Ebiura, T. Echizen, A. Ishikawa, K. Murai, and T. Baba, *Applied Catalysis A: General*, 2005, **283**, 111-116.
44. X. Liu, H. He, Y. Wang and S. Zhu, *Catalysis Communications*, 2007, **8**, 1107-1111.
45. C. S. MacLeod, A. P. Harvey, A. F. Lee and K. Wilson, *Chemical Engineering Journal*, 2008, **135**, 63-70.
46. H. Zhu, Z. Wu, Y. Chen, P. Zhang, S. Duan, X. Liu and Z. Mao, *Chinese Journal of Catalysis*, 2006, **27**, 391-396.
47. H. Wu, J. Zhang, Q. Wei, J. Zheng, and J. Zhang, *Fuel Processing Technology*, 2013, **109**, 13-18.
48. C. C. C. M. Silva, N. F. P. Ribeiro, M. M. V. M. Souza, and D. A. G. Aranda, *Fuel Processing Technology*, 2010, **91**, 205-210.
49. F. Guo, Z.-G. Peng, J.-Y. Dai and Z.-L. Xiu, *Fuel Processing Technology*, 2010, **91**, 322-328.
50. G. J. Suppes, M. A. Dasari, E. J. Doskocil, P. J. Mankidy and M. J. Goff, *Applied Catalysis A: General*, 2004, **257**, 213-223.
51. W. Xie, X. Huang and H. Li, *Bioresource Technology*, 2007, **98**, 936-939.
52. R. Peña, R. Romero, S. L. Martinez Vargas, R. Natividad, and A. Ramírez, *Characterization of KNO3/NaX catalyst for sunflower oil transesterification*, 2013.
53. V. Volli and M. K. Purkait, *Journal of Hazardous Materials*, 2015, **297**, 101-111.

54. G. E. G. Muciño, R. Romero, I. García-Orozco, A. R. Serrano, R. B. Jiménez and R. Natividad, *Catalysis Today*, 2016, **271**, 220-226.

55. S.-Y. Chen, T. Mochizuki, Y. Abe, M. Toba, and Y. Yoshimura, *Ti-incorporated SBA-15 mesoporous silica as an efficient and robust Lewis solid acid catalyst for the production of high-quality biodiesel fuels*, 2014.

56. D. Meloni, D. Perra, R. Monaci, M. G. Cutrufello, E. Rombi, and I. Ferino, *Transesterification of Jatropha curcas oil and soybean oil on Al-SBA-15 catalysts*, 2016.

57. D. Meloni, R. Monaci, Z. Zedde, M. G. Cutrufello, S. Fiorilli and I. Ferino, *Applied Catalysis B: Environmental*, 2011, **102**, 505-514.

58. K. Hou and H. Li, *Preparation of biodiesel by transesterification of soybean oil over KOH/SBA-15 catalyst*, 2011.

59. W. Xie, L. Hu and X. Yang, *Industrial & Engineering Chemistry Research*, 2015, **54**, 1505-1512.

60. H.-J. Kim, B.-S. Kang, M.-J. Kim, Y. M. Park, D.-K. Kim, J.-S. Lee, and K.-Y. Lee, *Catalysis Today*, 2004, **93-95**, 315-320.

61. G. Gelbard, O. Brès, R. M. Vargas, F. Vielfaure and U. F. Schuchardt, *Journal of the American Oil Chemists' Society*, 1995, **72**, 1239-1241.

62. K. Sadowska, K. Góra-Marek, M. Drozdek, P. Kuśtrowski, J. Datka, J. Martinez Triguero, and F. Rey, *Microporous and Mesoporous Materials*, 2013, **168**, 195-205.

63. S. D. Bhat, P. S. Niphadkar, T. R. Gaydhankar, S. V. Awate, A. A. Belhekar and P. N. Joshi, *Microporous and Mesoporous Materials*, 2004, **76**, 81-89.

64. J. C. Groen, L. A. A. Peffer, J. A. Moulijn and J. Pérez-Ramírez, *Colloids and Surfaces A: Physico-chemical and Engineering Aspects*, 2004, **241**, 53-58.

65. X. Wei and P. G. Smirniotis, *Microporous and Mesoporous Materials*, 2006, **97**, 97-106.

66. P. Prokešová, S. Mintova, J. Čejka, and T. Bein, *Microporous and Mesoporous Materials*, 2003, **64**, 165-174.

67. T. Odedairo, R. J. Balasamy, and S. Al-Khattaf, *Catalysis Science & Technology*, 2012, **2**, 1275-1286.

Chapter 6

Dehydration of Fructose to 5-Hydroxymethylfurfural Over Micro-mesoporous H/BEA-SBA-15 Composite

6.1 Introduction

The conversion of lignocellulosic derived biomass into value-added chemicals e.g. 5-hydroxymethylfurfural (HMF), has gained paramount importance in recent years. The dehydration of fructose over dealuminated zeolite in MIBK and water biphasic system was firstly demonstrated high selectivity of HMF which could be due to the bidimensional structure and absence of cavities.[1, 2] Further, it has also been reported that the moderate acid sites help to enhance the HMF selectivity as compared to the strong acidic sites which favor parallel side reactions.[3]

Zeolite beta (BEA), belonging to the large pore family, can be used as a solid catalyst because of their advantageous catalytic properties (As discussed in Chapter 1). It is used as a catalyst for several reactions namely cracking,[4] isomerization,[5] alkylation,[6] and dehydration reactions. The aqueous phase dehydration of fructose to HMF over H/BEA zeolite and the rehydration of HMF to levulinic acid were studied with SiO_2/Al_2O_3 =18.[7] It demonstrated the role of external surface acid sites (Brønsted and Lewis) on the adsorption of reactants and products during the conversion of fructose to HMF and further continues to levulinic acid. The H/BEA zeolite showed better catalytic activity in fructose dehydration to HMF in presence of DMSO as solvent.[8, 9] Moreover, thermally stable H/BEA zeolite obtained by the dealumination as a catalyst exhibited consecutive reactions showing a moderate yield of HMF synthesized from carbohydrate.[10] The Fe exchanged BEA zeolite with varying Fe/Al ratios were applied as a catalyst for conversion of glucose into HMF under mild reaction conditions in the biphasic system.[11] They concluded that the synergetic effect of Lewis and Brønsted acid centers were demonstrated improvement in HMF yield. The kinetic study of tandem glucose to HMF dehydration reactions was also studied over bifunctional H/BEA zeolite in the aqueous phase.[12] In another study, three protonated zeolite, namely H/ZSM-5, H/Y, and H/BEA have been studied for the dehydration of glucose to HMF in a biphasic water/MIBK biphasic system and aqueous NaCl solution (20 *wt%*).[13] The selectivity and yield of the HMF obtained over H-zeolites were compared with mesoporous Al-MCM-41 type aluminosilicate with regards to structural and acidic properties of the zeolites.

However, the zeolite BEA often exhibited diffusion constraints for the molecules having kinetic diameter larger than the pore opening of zeolites and fast catalyst deactivation.[14, 15] Therefore, after successful implementation of two dimensional (2D) and three dimensional (3D) mesoporous systems with pore sizes of 1.5–50 nm, such as MCM-41, SBA-15, etc., several reviews were dedicated to explain the synthesis of zeolite-based interconnected micro-mesoporous composite materials to compensate diffusion limitation for bulkier molecules and accessibility of catalytically active sites.[16-19] Although Al incorporation into the mesoporous framework could exhibit the acidity, the amorphous nature of the mesopore wall resulted in the lower acidity than conventional zeolite.[20] Therefore, the hierarchical BEA zeolite with interconnected micro-mesoporosity has synthesized that showed better activity in cracking and esterification reactions.[21, 22] Further, the tin-beta zeolite has found to be an active catalyst for conversion of carbohydrates into HMF with water and THF solvent system.

The seeding method, where Brønsted/Lewis acidic sites can be introduced into mesoporous materials by the incorporation of zeolites seeds/zeolite building units into mesoporous walls have been studied[17, 23] and is showing enhanced hydrothermal and acidic properties than conventional zeolites.[24, 25] Various zeolite BEA based micro-mesoporous composites such as BEA-MCM-41,[26] BEA-KIT-6,[27] BEA-FDU-12[28] have been studied as a catalyst in which the BEA zeolite was served as acidic site for chemical reactions and mesopores resulted into the ease of diffusion of reactants as well as products molecules. In order to preserve the long-range atomic order zeolite framework and the acidic properties, the zeolite seeds with prolonging the crystallization time have been used during the mesoporous molecular assembly in micro-mesoporous composite.[29-32] In comparison with BEA-MCM-41, the micro-mesoporous BEA-SBA-15 with greater pore size and thicker wall enhanced the diffusion and stability of catalyst.[20, 27, 33, 34] With this regards, the ordered mesoporous titanosilicate were prepared from preformed TS precursors and assembled with the triblock copolymer (P123) showing excellent hydrothermal stability.[35] Therefore, the present study was aimed at the synthesis of highly ordered zeolite seeds assembled into the SBA-15 mesoporous wall under acidic conditions.

It is well known that the rehydration of HMF in aqueous acidic medium resulted into formation of side reaction products such as levulinic acid, formic acid, and polymeric by-

products, humins.[36] During the dehydration of fructose, the partially dehydrated intermediates formed undergo side reactions leading to the formation of condensation products such as polymers or humins.[37] The choice of proper solvent system for the fructose dehydration is one of the important aspects. Therefore, several attempts were focused on a biphasic system with water immiscible polar organic solvents such that the formed HMF can extract into the organic solvents and rehydration/condensation reactions of HMF are suppressed. The organic solvents such as methyl isobutyl ketone (MIBK),[38] dimethyl sulphoxide (DMSO,[39] tetrahydrofuran (THF),[40] toluene,[41] butan-2-ol,[41] ionic liquid,[42] etc. have demonstrated significant improvement in the HMF yield by selective extraction of HMF from the aqueous phase. The partitioning of HMF into organic phase prevents the formation of undesired dehydration byproducts. Therefore, the proper organic solvent has been chosen based on the partitioning coefficient of solvents. Among aforesaid organic solvents, the MIBK-water biphasic system was the suitable solvent system for the dehydration of fructose to HMF.[43] It has been reported that the strong Brønsted acid sites from the zeolite interact with MIBK during dehydration of fructose to HMF.[44]

The numerous literature is available that describe the zeolites as a solid acid catalyst for the dehydration of fructose to HMF in aqueous/organic solvents and several parameters such as the influence of acidity, surface area, pore volume, reaction temperature, time, solvents system have investigated. Therefore, the aim of the present study is to evaluate the influence of combined micro-mesoporosity on fructose dehydration to HMF. Herein, the zeolite-based H/BEA-SBA-15 micro-mesoporous composite was successfully synthesized by seeding method using Pluronic P123 triblock copolymer (EO20–PO70–EO20) in which pre-crystallized H/BEA zeolite seeds were subsequently assembled during the self-assembly of mesoporous materials as catalytically active sites. The physico-chemical properties of synthesized composites were characterized by several analytical techniques. The structure-property correlations between the interconnected micro and mesopores of H/BEA-SBA-15 and the catalytic performance for the dehydration of fructose to HMF in the biphasic system were discussed.

6.2 Experimental

6.2.1 Chemicals

The details for various chemicals used for the synthesis of micro-mesoporous H/BEA-SBA-15 composite and dehydration of fructose are given in Chapter 2, Section 2.2.2.1. In addition, the chemicals, as well as the standards used for fructose dehydration reactions, are given in Chapter 2, Section 2.5.2.1.

6.2.2 Synthesis of H/BEA zeolite

Beta zeolite (BEA) was prepared by following the literature reported elsewhere.[45] The Na/BEA zeolite was prepared by the hydrothermal crystallization from the aluminosilicate with the molar gel composition $6.0(TEA)_2O$: $2.4Na_2O$: $30.0SiO_2$: Al_2O_3: $840H_2O$. The detail experimental procedures for the synthesis of Na/BEA and its conversion to protonic form H/BEA are given in Chapter 2, Section 2.2.2.2 and Section 2.2.2.3, respectively. The protonic form of BEA zeolite was designated as H/BEA.

6.2.3 Synthesis of micro-mesoporous H/BEA-SBA-15 composite

The micro-mesoporous H/BEA-SBA-15 composite was synthesized by seeding method by following the reported literature with little modification.[33] A typical synthesis procedure for micro-mesoporous H/BEA-SBA-15 composite is given in Chapter 2, Section 2.2.2.4 and the catalyst was denoted as H/BEA-SBA-15. For comparison purpose, Si-SBA-15 and Al-SBA-15 were prepared with/without aluminium source by following the same procedure described above without addition of H/BEA zeolite under the same synthesis condition.

6.2.4 Characterization

The calcined H/BEA, micro-mesoporous H/BEA-SBA-15 composite, Si-SBA-15 and Al-SBA-15 materials were characterized by various analytical techniques, such as, inductive coupled plasma-optical emission spectroscopy (ICP-OES), powder X-ray diffraction (PXRD), nitrogen adsorption and desorption measurements, ^{29}Si and ^{27}Al magic angle spinning nuclear magnetic resonance spectroscopy (^{29}Si and ^{27}Al MAS NMR), temperature

programmed desorption of NH_3 (NH_3-TPD), infrared spectroscopy of adsorbed Pyridine (Py-IR), scanning electron microscope (SEM), transmission electron microscopy (TEM), high resolution transmission electron microscopic analysis (HR-TEM) and thermal gravimetric analysis (TGA) as described in Chapter 2, Section 2.4.

6.2.5 Catalytic activity

The catalytic activity of the synthesized materials was tested in the dehydration of fructose to HMF reactions in the biphasic system in the batch mode autoclaves and the reaction mixtures were analyzed by the HPLC and GC instruments. The detailed experimental set-up and the procedure are described in Chapter 2, Section 2.5.2.2. The typical experiments were carried out at a temperature range from 155 ^oC to 175 ^oC for the reaction period of 0.5 h to 2 h. The catalyst amount was varied from 0.07 g to 0.28 g in monophasic (water) and biphasic (water + MIBK) solvent system. In addition to this, the influence of stirring speed on the HMF yield was also studied in the range of 300 RPM to 900 RPM.

6.2.6 Analysis of the reaction mixture

The aqueous layer was analyzed using high-pressure liquid chromatography, HPLC maintained at a column temperature of 80 ^oC and refractor index detector. The organic layer was analyzed by gas chromatography (GC). The detailed procedure for sampling and the analysis conditions of columns and the detectors are given in Chapter 2, Section 2.5.2.3. All the samples were filtered through the 0.22 μm syringe filter before subjected for HPLC and GC analysis.

6.2.7 Calculations

Based on the assumption that the molecules involved in the reactions are spherical, the kinetic diameter of Fructose, glucose, and HMF was calculated based on their molecular weights as discussed in reported literature[46], as described in Chapter 2, Section 2.5.1.3.

The fructose conversion and HMF yield were calculated on mole basis by GC and HPLC by plotting the calibration curves using standards of definite concentrations. Details calculation methods are given in Chapter 2, Section 2.5.2.4. The turn over frequency (TOF)

was calculated based on the number of moles of the reactant converted and the moles of acidic sites present on the catalyst as described in Chapter 2, Section 2.5.2.4.

6.2.8 Hydrothermal stability test

The hydrothermal stability of calcined H/BEA-SBA-15 was studied by refluxing the composite in boiling water for 8 h as per the procedure described in Chapter 2, Section 2.3. The hydrothermal stability of the micro-mesoporous composite was tested by low angle and wide angle PXRD technique.

6.3 Results and discussion

6.3.1 Characterization of micro-mesoporous H/BEA-SBA-15 composite

6.3.1.1 Inductive coupled plasma-optical emission spectroscopy (ICP-OES)

The molar Si/Al ratio of H/BEA zeolite and micro-mesoporous H/BEA-SBA-15 composite was determined by ICP-OES analysis as tabulated in Table 6.1. The molar Si/Al ratio of H/BEA zeolite was found to be 14.8, whereas, the molar Si/Al ratio of micro-mesoporous H/BEA-SBA-15 composite was observed to be 57.8. The increase in molar Si/Al ratio of H/BEA-SBA-15 composite was attributed to the addition of silica during the synthesis of SBA-15 mesophase.

Table 6.1. Physico-chemical properties of H/BEA and micro-mesoporous H/BEA-SBA-15 composite

Catalysts	Si/Al ratio[a]	$d_{(100)}$[b] nm	a_0 nm	D nm	t nm	S_{BET} (m^2/g)	V_T (cm^3/g)	Cry (%)
H/BEA	14.8	-	-	-	-	470	0.381	100
H/BEA-SBA-15	57.8	10.3	11.8	7.6	4.2	594	0.601	52
Si-SBA-15	-	10.4	12.0	8.1	3.9	835	0.895	-

A= ICP-OES, b=PXRD, a_0 =Unit cell parameter, D= Mesopore Diameter, t= Wall thickness, S_{BET}= surface area, V_T=Total pore volume, Cry= Crystalline matter by PXRD

6.3.1.2 Powder X-ray diffraction (PXRD)

The low angle PXRD patterns of calcined H/BEA-SBA-15 synthesized by seeding method and Si-SBA-15 samples are shown Figure 6.1A. In the low 2θ region of 0.5-5°, three well-resolved peaks of (100), (110), and (200) reflections corresponding to hexagonal (p6mm) ordered mesoporous phase (SBA-15) were observed for H/BEA-SBA-15, and SBA-15 samples.[47] The H/BEA-SBA-15 composite possesses the relatively lower intensity of (100) reflection as compared to pristine SBA-15, indicating the structural disordering in the mesophase in the prior sample. The relative lowering in peak intensity may be due to the presence of BEA zeolite seed. The H/BEA zeolite seeds may be assembled in mesophase, which resulted in the structural disordering in the micro-mesoporous composite.[20] Moreover, the (100) diffraction peak was found to shift slightly towards lower 2θ angle, suggesting declining in the d100 spacing (Table 6.1). The decrease in d100 spacing of micro-mesoporous H/BEA-SBA-15 composite could be due to the presence of H/BEA zeolite seed which may present in the mesopores, on the surface or embedded in the wall of the composite. This can be explained on the basis of the interaction between the structural directing agent and silica precursor for mesophase with H/BEA zeolite seeds during hydrothermal treatment. In the synthesis gel, the size of H/BEA zeolite seed is larger than SiO_4 tetrahedra which may involve in the walls assembly of SBA-15 mesophase.

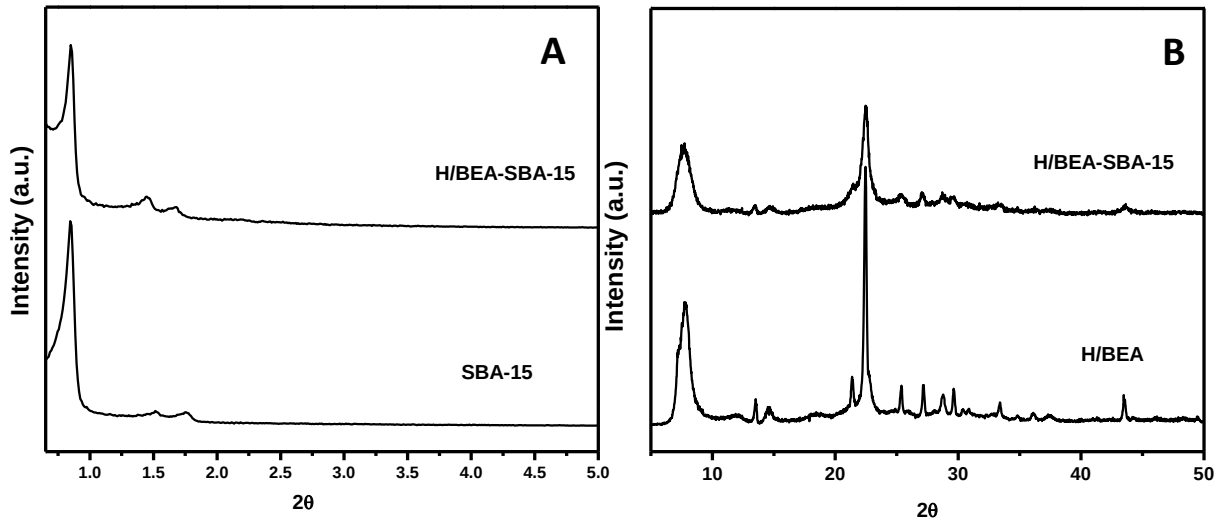

Figure 6.1. Low angle (A) and wide-angle (B) PXRD patterns of H/BEA and micro-mesoporous H/BEA-SBA-15 composite

Therefore, in comparison with siliceous Si-SBA-15, the low angle diffraction peaks were shifted to lower two-theta angles.[33] The wide angel PXRD patterns of H/BEA and H/BEA-SBA-15 composite are displayed in Figure 6.1B. It shows two prominent diffraction peaks at 7.3° and 22.4°, corresponding to the characteristic features of (101) and (302) planes of the microporous H/BEA zeolite phase.[33, 48] The micro-mesoporous H/BEA-SBA-15 composite also showed relatively lower intensity with broad peaks corresponding to the H/BEA zeolite seed, revealing that the crystallinity of BEA zeolite seeds in the composite was much lower than that of H/BEA zeolite.

6.3.1.3 N_2 adsorption-desorption analysis

The porous properties of H/BEA, H/BEA-SBA-15 and Si-SBA-15 samples are evaluated by low-temperature nitrogen adsorption-desorption isotherms which are shown in Figure 6.2. The H/BEA zeolite shows type I isotherm corresponding to the typical microporous nature of zeolite.[49] Moreover, Si-SBA-15 sample classified as type IV isotherm with the hysteresis loop due to capillary condensation at relative pressures P/P_0 of 0.4-0.8, which is the characteristic of ordered mesoporous materials.

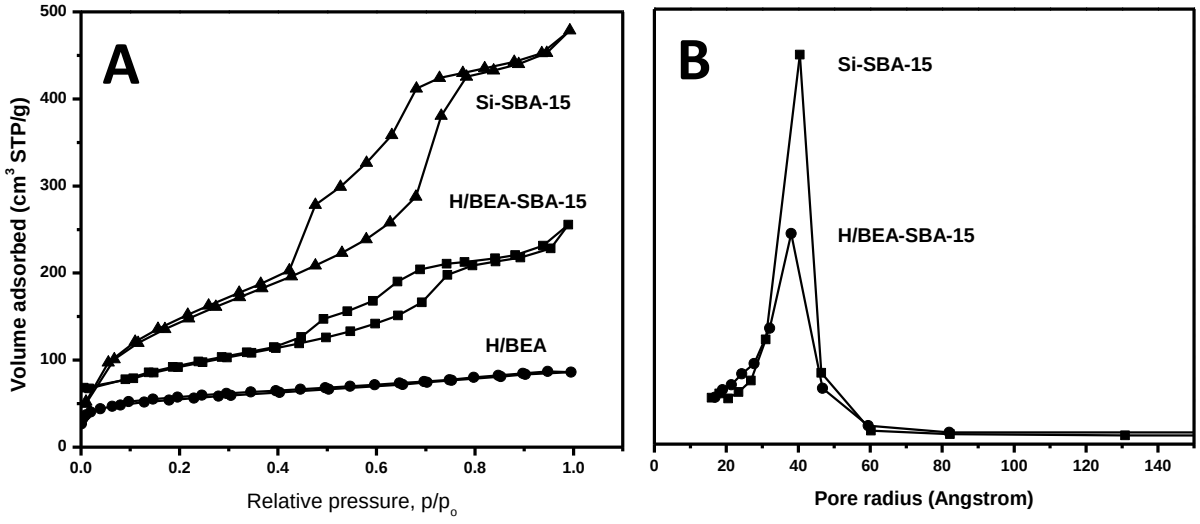

Figure 6.2. Nitrogen adsorption-desorption isotherms of micro-mesoporous H/BEA-SBA-15 composite and Si-SBA-15 (A) and mesopore size distribution (B)

As expected, the H/BEA-SBA-15 composite exhibited type IV adsorption isotherm with the hysteresis loop and narrow mesoporous distribution which accounts the presence of the micro and mesoporous structure. However, the volume uptake of nitrogen by H/BEA-SBA-15 composite was decreased which may be due to the reduction of pore volume as a consequence of zeolite assembly inside the mesopores.

The detailed porous properties of the calcined samples are shown in Table 6.1. The N_2 adsorption-desorption experiment also showed that the BET surface area of Si-SBA-15 and H/BEA were 835 m^2/g and 470 m^2/g, respectively, whereas, the BET surface area of micro-mesoporous H/BEA-SBA-15 composite was 507 m^2/g. In addition to this, H/BEA-SBA-15 composite showed a significant increase in the total pore volume of 0.601 cm^3/g as compared to pristine H/BEA, while H/BEA and Si-SBA-15 samples showed total pore volumes of 0.381 cm^3/g and 0.895 cm^3/g, respectively. This value was an intermediate between the pristine H/BEA zeolite and Si-SBA-15 mesoporous materials which is due to the presence of zeolite seeds in the micro-mesoporous H/BEA-SBA-15 composite. The BJH pore size distribution showed (Figure 6.2 B) the mesopore size of Si-SBA-15 and H/BEA-SBA-15 composite was centered at 8.1 nm and 7.6 nm, respectively. Further, H/BEA-SBA-15 composite exhibits a relatively thicker pore wall of 4.2 nm as compared to conventional Si-SBA-15 (3.9 nm). The lower mesopore size and the thicker mesopore wall could be attributed to the utilization of zeolite seed used as structural building units for the constructing the walls of the mesoporous material.[47, 50]

6.3.1.4 ^{29}Si and ^{27}Al Solid-state magic angle spinning nuclear magnetic resonance spectroscopy (^{29}Si and ^{27}Al MAS NMR)

The Si and Al coordination in H/BEA and micro-mesoporous H/BEA-SBA-15 composite were determined by ^{29}Si and ^{27}Al MAS NMR analysis as shown in Figure 6.3. However, it is very difficult to distinguish clearly the silicon species present in the microphase and mesophase. ^{29}Si MAS NMR spectra of H/BEA zeolite and micro-mesoporous H/BEA-SBA-15 composite showed two resonance peaks at -110 ppm and -114 ppm assigned to Si(OSi)4 units corresponding to crystallographically different sites present in H/BEA zeolite.[21, 51, 52] Another weak resonance peak observed at -102 ppm could be attributed to the (SiO)3Si(OAl) unit.[21, 52] However, one can noted that -113 ppm in micro-

mesoporous H/BEA-SBA-15 composite can also be assigned to the Q4 silicon species (Si(4Si)), whereas, weak and broad resonance peak at -95 to -105 ppm could be denoted as Q2, Si(2Si,2OH) and Q3, Si(3Si,1OH) silicon species.[21, 47] In comparison, a wide and low intense resonance peaks in composite could indicate the lesser amount of crystalline BEA domains present in the composite. Further, the population of Q4 and Q3 species were found to increase in micro-mesoporous H/BEA-SBA-15 composite, and another peak at -102 ppm was observed corresponding to the Q2 species, indicating the interaction between H/BEA zeolite seed and SBA-15 mesophase.

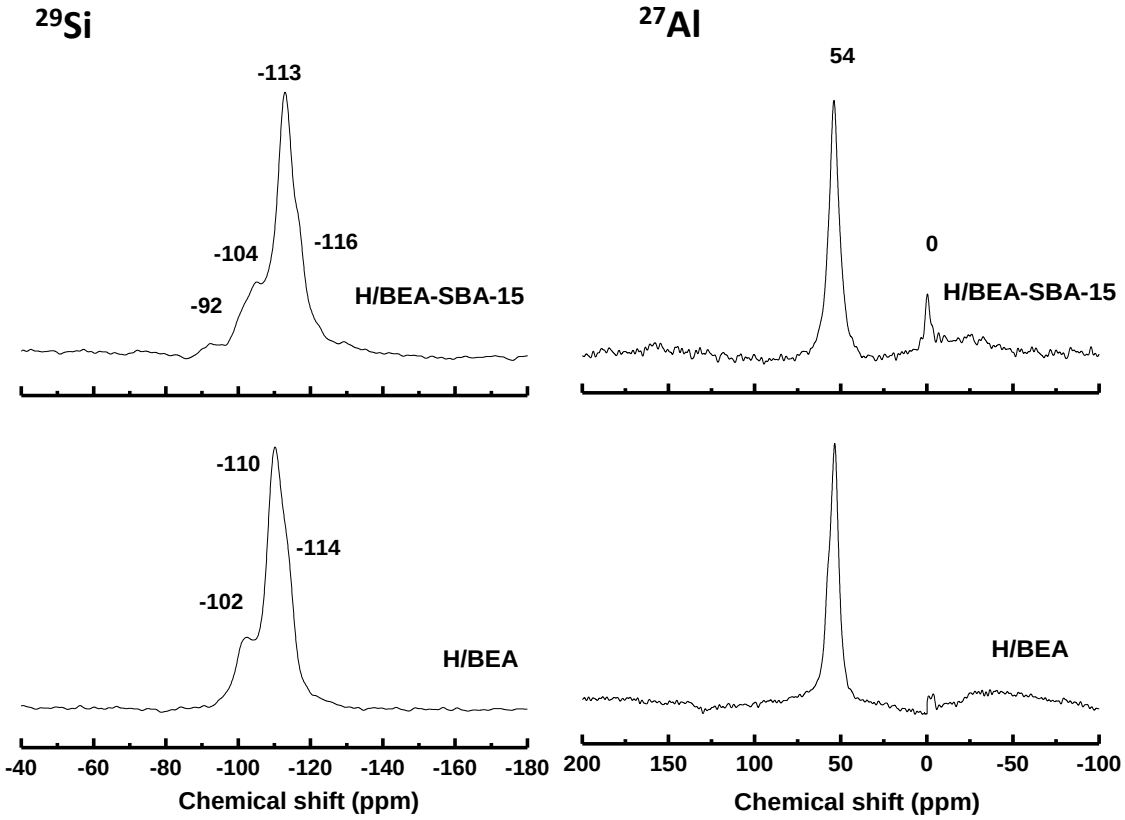

Figure 6.3 ^{29}Si and ^{27}Al MAS NMR spectra of H/BEA and micro-mesoporous H/BEA-SBA-15 composite

^{27}Al NMR spectra of H/BEA and micro-mesoporous H/BEA-SBA-15 composite are shown in Figure 6.3. It exhibits intense resonance peak at 54 ppm assigned to aluminium atom present in tetrahedral coordination (AlO_4 structural species) in H/BEA zeolite, whereas a very small resonance peak at 0 ppm corresponding to the octahedrally

coordinated (AlO_6 structural species) which was present as an extraframework aluminium. A similar phenomenon was also witnessed by the micro-mesoporous composite. These results inferred that the degree of tetrahedrally coordinated aluminium was higher as compared to the hexacoordinated aluminium in fully crystalline BEA zeolite. In micro-mesoporous H/BEA-SBA-15 composite, however, the intensity of resonance peak for extraframework aluminum was relatively high. Moreover, the relatively higher octahedral coordinated aluminium content in the micro-mesoporous H/BEA-SBA-15 composite might be produced during the synthesis of SBA-15 mesophase under acidic conditions via dealumination of beta zeolite seeds and/or primary building units in the BEA zeolite.[33] These octahedral Al species may responsible for the decrease in the contribution of Brønsted acidic sites of the microporous materials.

6.3.1.5 Acidity by temperature programmed desorption of NH_3 (NH_3-TPD) and Pyridine adsorbed IR (Pyridine-IR) analysis

The acidic properties of pristine H/BEA and micro-mesoporous H/BEA-SBA-15 composite (amount and strength of acidic sites) were investigated by NH_3-TPD analysis as shown in Figure 6.4 and the acidity of the composites are tabulated in Table 6.2. It showed that both H/BEA and H/BEA-SBA-15 composite displayed similar TPD profile and exhibited mainly two desorption peaks. A prominent peak appeared in the temperature range from 100 ^oC to 250 ^oC corresponded to weak acid sites, whereas, the broad peak observed ranging from 250 ^oC to 400 ^oC could be attributed to moderate acid sites. Further, it also showed that the weak desorption peak in both samples appeasers more pronounced, revealing that H/BEA and H/BEA-SBA-15 composite have a high amount of weak acidic sites.

Table 6.2 Acidity of H/BEA and H/BEA-SBA-15 composite

Catalysts	Total acidity mmol/g	weak acidity mmol/g	Moderate acidity mmol/g	B/L ratio
H/BEA	0.534	0.363 (68%)	0.171 (32%)	0.33
H/BEA-SBA-15	0.295	0.165 (56%)	0.130 (44%)	0.56

Values in the parenthesis indicating the percentage of acidic site

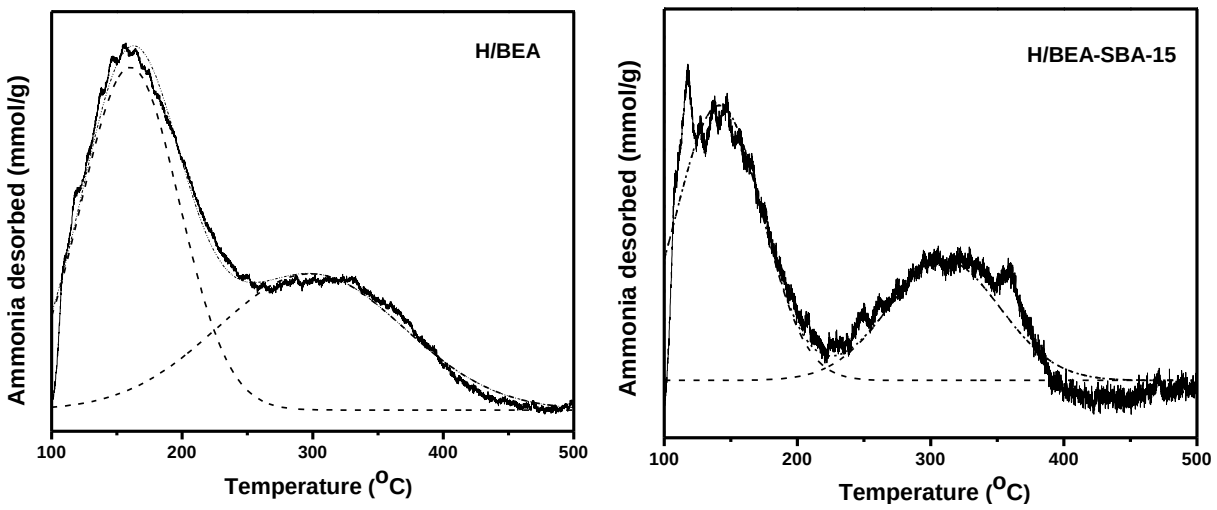

Figure 6.4. NH_3-TPD profiles of H/BEA and micro-mesoporous H/BEA-SBA-15 composite

The amount of total acidity of H/BEA-SBA-15 composite (0.295 mmol/g) was found to be significantly lower than pristine H/BEA zeolite (0.534 mmol/g). This could be attributed to the first, lowering in the Si/Al ratio and second, the presence of amorphous material used in the formation of SBA-15 mesophase that may cover the acidic sites of H/BEA zeolite seeds embedded in the mesoporous walls.

The Brønsted and Lewis acid sites in H/BEA and micro-mesoporous H/BEA-SBA-15 composites were differentiated by IR spectroscopy of adsorbed Pyridine (Pyridine-IR) as shown in Figure 6.5 and the B/L ratio was calculated according to the reported literature[53] as tabulated in Table 6.2. The pyridine-IR spectra of both the samples showed three distinguish peaks. The peak observed at 1443 /cm could be assigned to Lewis acid sites while the peak at 1540 /cm assigns to the Brønsted acid sites. In addition, the peak observed at about 1490 /cm was ascribed to the both Brønsted and Lewis acid sites.[53] Brønsted to Lewis acid site ratio (B/L) for H/BEA zeolite and H/BEA-SBA-15 was 0.33 and 0.56, respectively. It suggested that micro-mesoporous H/BEA-SBA-15 composite have higher Brønsted acidic sites as compared to the H/BEA zeolite.

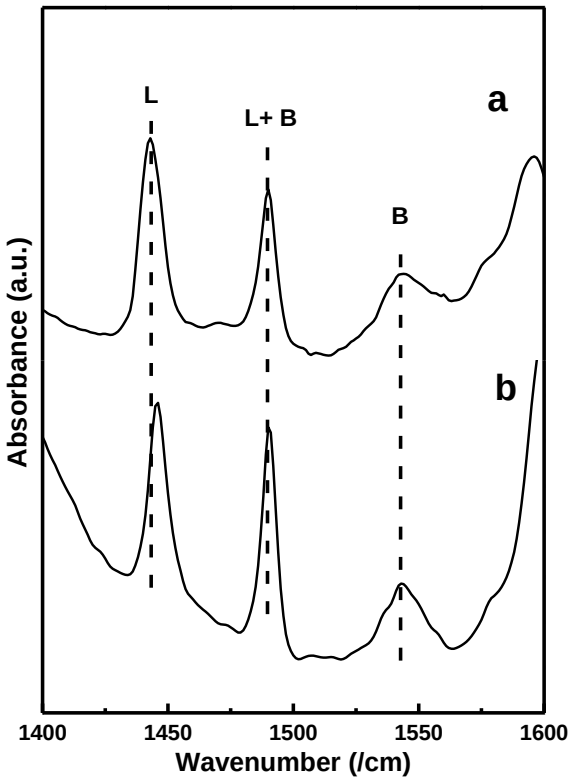

Figure 6.5. Pyridine-IR spectra of H/BEA (a) and micro-mesoporous H/BEA-SBA-15 composite (b)

However, ^{27}Al MAS NMR spectra showed that micro-mesoporous H/BEA-SBA-15 composite exhibit higher octahedral Al than that of H/BEA zeolite. It means that the micro-mesoporous H/BEA-SBA-15 composite should exhibit lower B/L ratio in comparison with H/BEA zeolite. This contradiction can be explained on the basis of the pore dimension of H/BEA zeolite, the kinetic diameter of adsorbed pyridine, the interaction of pyridine with catalytically active sites and importantly, the position of the Al in the catalysts. The Brønsted acid sites can be recognized by the interaction of pyridine with the Al present in the framework and from the terminal hydroxyl groups.[54] Moreover, the extra framework aluminium and defects in zeolite mainly responsible for the Lewis acid sites.[53] In H/BEA zeolite, the pyridine molecules with a kinetic diameter of 5.7 Å could interact with the entire acid sites present in the pores channels with dimensions 6.6 x 6.7 Å only or present at the channel intersections or entrance in consequence of H/BEA zeolite pore dimensions. In case of micro-mesoporous H/BEA-SBA-15 composite, with higher amount of extra-

framework Al, the pyridine molecules interact with the framework Al and higher amount of surface hydroxyl groups (due to SBA-15) exhibiting Brønsted acid sites. Whereas, the pyridine molecules interact with extra-framework Al present on the surface which exhibits Lewis acid sites. One of the possibilities of higher B/L ratio of micro-mesoporous H/BEA-SBA-15 composite could be some extra framework Al (Lewis acid sites) may not be accessible to the pyridine because of their position in the walls of SBA-15 mesophase.

6.3.1.6 Thermal analysis

The thermal stability of calcined micro-mesoporous H/BEA-SBA-15 composite was tested by TGA-DSC analysis and the experimental results are shown in Figure 6.6. The H/BEA-SBA-15 composite exhibited three mass losses with increasing temperature; first mass loss, below 150 ^{o}C, was primarily attributed to the loss of physically adsorbed water about 20 *wt*%. Whereas, second mass loss between the temperature range of 150–400 ^{o}C of about 2-3 *wt*%, may be attributed to the decomposition of residual structure directing agent. Further increase in the temperature ranging from 400–900 ^{o}C, the mass loss of about 2-3 *wt*% was apparently assigned to desorption of water by the dehydration and/or dehydroxylation owing to the condensation of silanol groups on the surface of mesoporous materials.[55]

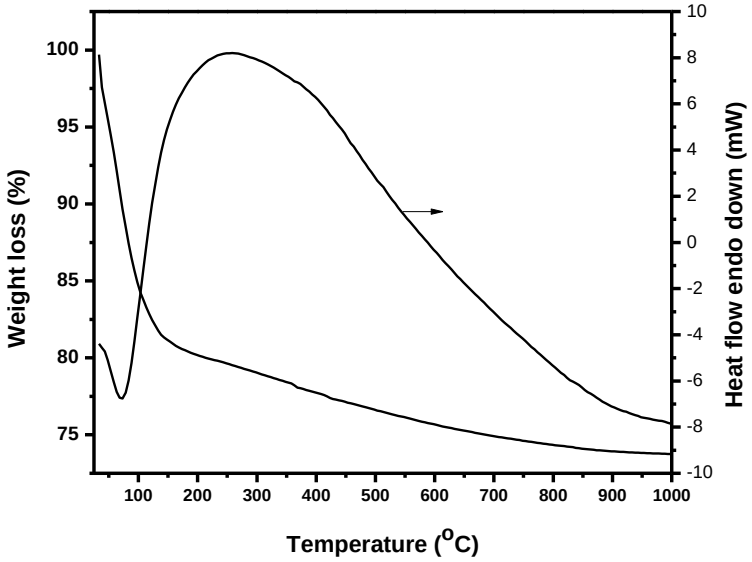

Figure 6.6. TGA-DSC curves of micro-mesoporous H/BEA-SBA-15 composite

6.3.1.7 Scanning electron microscopy (SEM)

The morphology of Si-SBA-15 (Figure 6.7A) and H/BEA-SBA-15 (Figure 6.7B) micro-mesoporous composite are investigated by SEM as shown in Figure 6.7. Both the samples clearly showed the aggregates of rode like particles indigenous to SBA-15 mesophase with a relatively uniform particle size of 1 μm. Further, micro-mesoporous H/BEA-SBA-15 composite (Figure 6.7B) did not show the appearance of separate mesoporous and microporous phases, though the presence of H/BEA zeolite seed was detected in PXRD. It envisioned that H/BEA zeolite seeds could be embedded in the pore walls of the SBA-15 structure. The hypothesis could be relevant only when the H/BEA zeolite seeds have a smaller size as compared to SBA-15 mesophase under a given set of conditions. Thus, in order to confirm this, the controlled experiment was performed where 3g H/BEA zeolite was treated with 130 mL of 0.29M HCl solution for 24 h, and the SEM image is shown in Figure 6.7 C. It clearly showed that aggregates of zeolite nanocrystals were formed with the average particle size of 50-100 nm. Therefore, it is envisioned that H/BEA zeolite seeds were embedded in SBA-15 mesopore wall.

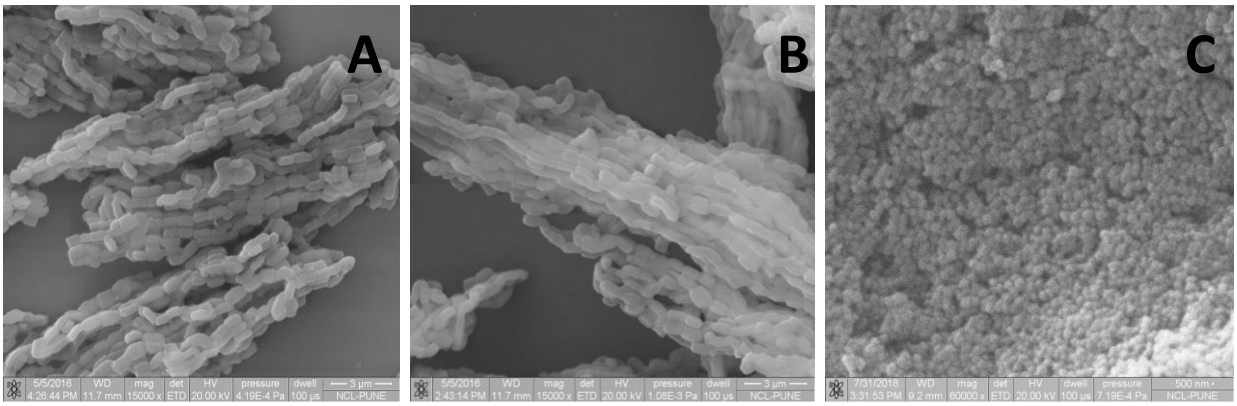

Figure 6.7. SEM images of Si-SBA-15 (A), micro-mesoporous H/BEA-SBA-15 composite (B), and acid treated H-BEA zeolite (C)

6.3.1.8 Transmission electron microscopy (TEM and HR-TEM)

The morphology of micro-mesoporous H/BEA-SBA-15 composite was also investigated by transmission electron microscopic (TEM) and high-resolution transmission electron microscopy (HR-TEM) technique as shown in Figure 6.8. The TEM image of

H/BEA-SBA-15 composite (Figure 6.8 A) clearly displayed well-ordered 2D hexagonal arrays of mesopores of SBA-15 mesophase.[27] These results are consistent with N_2 adsorption and PXRD results. Further, it is very difficult to see the morphology of microporous H/BEA zeolite, indicating that H/BEA zeolite seeds may embed in the wall during construction of the mesoporous structure of H/BEA-SBA-15 composite.

The high-resolution transmission electron microscopy (HR-TEM) displays a deep insight into the micro-mesoporous structure of H/BEA-SBA-15 composite (Figure 6.8 B-D). The composite envisioned the lattice fringes of micro and mesoporous channels. Further, HR-TEM image Figure 6.8D clearly evident the ordered BEA crystal lattices (d_{101}=1.1nm) oriented within the mesoporous matrix of SBA-15. It revealed that the composite proved to form interconnected micropores of H/BEA with mesoporous channels which are beneficial to improve the catalytic performance.

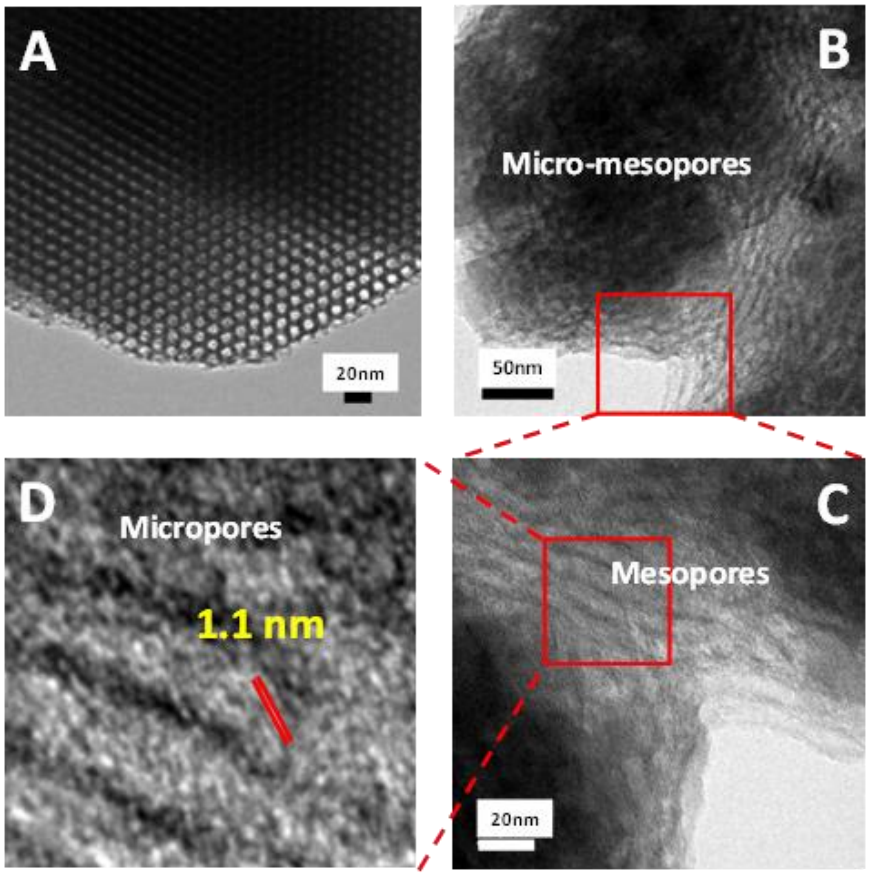

Figure 6.8. TEM (A) and HR-TEM images (B-D) of micro-mesoporous H/BEA-SBA-15 composite

6.3.2 Catalytic performance in dehydration of fructose to HMF

6.3.2.1 Initial screening of the catalyst

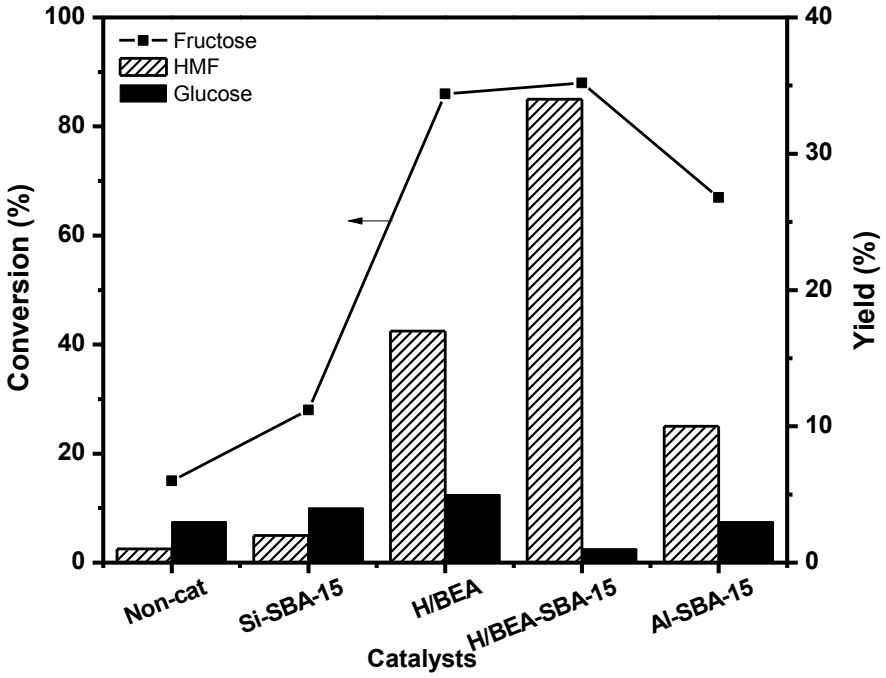

Figure 6.9. Catalytic performance in the dehydration of fructose to HMF (Reaction conditions: fructose: 0.5 g, catalyst: 0.14 g, water: MIBK 30 mL (1:5 *v/v*), time: 1 h, temperature: 165 ^{o}C, 500 RPM)

The dehydration of fructose to HMF (0.5 g in 5 mL water) reactions was carried out over various catalytic systems in 30 mL water: MIBK (1:5 *v/v*) solvent system for 1 h at 165 ^{o}C, and the results are presented in Figure 6.9. Initially, the silicious Si-SBA-15 catalyst was tested at 165 ^{o}C for 1 h, showed negligible activity because of the absence of acidic sites. The minor HMF yield over Si-SBA-15 could be attributed to the thermal reaction or very lower acidity of a surface hydroxyl group and/or physical adsorption of reactant and product. The H/BEA catalyst under given reaction conditions showed 86% fructose conversion with 16 % HMF yield and only 5% glucose yield. The mass balance in the reaction was about 80±5 %. The lower mass balance could ascribe to the formation of humins, polymerization products. The pore dimensions of H/BEA zeolite are 6.6 x 6.7 Å and 5.6 x 5.6 Å,[56] whereas, the kinetic diameters of fructose, glucose, and HMF are 6.96 Å, 6.96 Å and 6.18 Å, respectively. The pore dimensions of BEA zeolite and the kinetic diameters of

the reactant and products clearly envisioned that dehydration of fructose to HMF and the isomerization of fructose to glucose are carried out over the external surface of zeolite crystal. Moreover, the polymerization of HMF to humins may occur on zeolite surface or inside the pore.

It has been reported that the catalytic activity for the fructose to HMF dehydration was observed merely because of the Brønsted acidity of the catalyst. H/BEA zeolite with B/L ratio of 0.33 showed formation of HMF as a result of the presence of Brønsted acidic sites. In addition to this, Lewis acidic sites showed a prominent role in the isomerization of fructose to glucose. Further, fructose to glucose isomerization occurred as a result of Lewis acidity corresponding to the octahedral aluminium[7] present in the H/BEA zeolite as evidenced by ^{27}Al MAS NMR and Pyridine-IR technique. In the case of H/BEA-SBA-15 composite which exhibits B/L ratio of 0.56, showed higher HMF yield as a result of higher Brønsted acidic sites. It also showed lower glucose yield as a consequence of lower Lewis acidic sites. Thus, in the present case, the B/L ratio was a crucial parameter for fructose to HMF dehydration.

Among various Brønsted acidic catalysts, the micro-mesoporous H/BEA-SBA-15 composite exhibited higher fructose conversion of 88% and two-fold HMF yield of 34%. One can notice that the yield of glucose over H/BEA-SBA-15 composite was lower suggesting that the rate of fructose dehydration to HMF is faster as compared to the rate of isomerization of fructose to glucose at 165 ^{o}C. Although, H/BEA zeolite showed higher amount of total acidity (0.534 mmol/g) as compared with H/BEA-SBA-15 composite (0.295 mmol/g), the higher HMF yield over micro-mesoporous H/BEA-SBA-15 composite as a catalyst could be ascribed to the accessibility of reactant to the acidic sites of H/BEA zeolite seeds and the interconnection of micro and mesoporosity, which is discussed later. The higher activity could be ascribed to the higher amount of moderate acidity (44%) of H/BEA-SBA-15 composite in comparison with H/BEA zeolite (32%). Further, the reference mesoporous Al-SBA-15 catalyst demonstrated lower activity (10% HMF yield), as Al was present in the amorphous wall of Al-SBA-15 catalyst.

The catalytic performance was also correlated with the porous properties of the catalysts. The TOF values for fructose dehydration over H/BEA zeolite and micro-mesoporous H/BEA-SBA-15 composites were 20.5 /h and 61.7 /h, respectively, which

clearly indicate the effectiveness of interconnected micro and mesopores of H/BEA-SBA-15 composite. The kinetic diameters of reactant/products and the pore dimensions of catalysts clearly indicate that, in addition to Brønsted acidity, the porous properties such as total surface area, pore volume, and interconnected micro and mesoporosity have a crucial role in the catalytic performance. The H/BEA zeolite showed higher fructose conversion, but comparatively lower HMF yield. The maximum pore diameter of H/BEA zeolite is 6.7 Å showing comparatively lower surface area (470 m^2/g) and the total pore volume (0.381 cm^3/g). Therefore, fructose molecule with a molecular dimension of 6.96 Å, cannot be diffuse easily through the zeolite pores and experience accessibility of acidic sites in the zeolite pores.

It has been reported that fructose undergoes ring opening partly on the Lewis acid sites of zeolite.[57] The acyclic fructose, which is in equilibrium with the cyclic analogue, with the smaller dimensions can easily diffuse through the zeolite pores, where it interacts with the Brønsted acidic sites and undergoes dehydration to HMF. The cyclic form of the fructose having greater molecular dimension than the pore dimensions of zeolite, subjected for dehydration to HMF over the Brønsted acidic sites appeared on the external surface. In addition, strong acidic sites of H/BEA zeolite were responsible for the formation of high molecular weight humins by the rearrangement that decreased the HMF yield. In the case of micro-mesoporous H/BEA-SBA-15 composite, the H/BEA zeolite seeds were present in the mesoporous wall of SBA-15 showing the interconnected micro and mesoporosity (as evidence by characterization discussed above). In addition, the H/BEA-SBA-15 composite exhibited higher total surface area (507 m^2/g), total pore volume (0.601 cm^3/g) and display the mesopore size of 76 Å. Therefore, the cyclic form of fructose molecule with greater dimensions than maximum pore dimensions of H/BEA can rapidly be diffused through the higher cavities of SBA-15 mesophase. In micro-mesoporous H/BEA-SBA-15 composite with higher surface area and pore volume, fructose molecules have the accessibility of the Brønsted acidic sites of H/BEA zeolite seed situated in/on the pore walls of SBA-15 and dehydrated into HMF. The HMF molecules with kinetic diameter 6.18 Å can be diffused through the mesopores (pore dimension=76 Å) easily and extracted into the MIBK solvent. As a result, the catalytic active site could be available for more fructose molecules that would enhance HMF yield. Though micro-mesoporous H/BEA-SBA-15

composite consists of octahedral aluminium, due to smaller contact time of HMF with H/BEA zeolite seeds, it was less prone to rehydration and polymerization of HMF to unwanted byproducts. However, these Lewis acid sites may help in the isomerization of glucose to fructose again, as evidenced by the lower glucose yield. Another important factor that involved in the catalytic dehydration of fructose to HMF is the presence of an immiscible polar organic solvent, and the details on this are discussed in the later section.

Thus, the overall experimental results and discussion suggested that the catalytic performance for fructose to HMF dehydration was enhanced over bimodal micro-mesoporous H/BEA-SBA-15 composite as a result of 1) accessible Brønsted acidic sites, 2) higher surface area and total pore volume, 3) diffusion of bulky reactant and products from mesopores of SBA-15, and 4) interconnected micropores of H/BEA zeolite seeds embedded in mesopore wall and the mesopores of SBA-15 in biphasic solvent system.

6.3.2.2 Optimization of reaction parameters

6.3.2.2.1 Effect of organic solvents

The influence of the various biphasic solvent systems to achieve higher HMF yield was studied in dehydration of fructose to HMF reaction. In previous catalyst screening section, the micro-mesoporous H/BEA-SBA-15 composite showed good yield among various catalytic systems studied at 165 ^{o}C for 1 h. In order to achieve the best possible yield of HMF, the effect of the solvent system on the HMF yield was studied with water and biphasic solvent systems such as water+MIBK (1:5 *v/v*) and water+toluene (1:5 *v/v*) as shown in Figure 6.10. Under the given reaction conditions with water+MIBK (1:5 *v/v*) biphasic solvent system, maximum HMF yield of 34 % was achieved. In the case of the water+toluene solvent system, only 17 % HMF yield was observed whereas, with water as a solvent only 10 % HMF yield was observed. This indicates that the MIBK solvent was more effective in the extraction of HMF from water than toluene solvent, therefore, the higher yield was observed in the water+MIBK solvent system. This observation was consistent with the reported literature that the water and MIBK solvent system in the ratio of 1:5 (*v/v*) proved to be an effective solvent system to get higher HMF yield.[43] The observed results can be correlated with the solubility of the MIBK and Toluene in water, where MIBK showed higher solubility (1.19 g/100 mL at 20 °C) than that of Toluene (0.52

g/L at 20 °C).[58] Thus, due to the high solubility of MIBK in water, HMF was selectively extracted into the MIBK that prevented the condensation of HMF in water media.

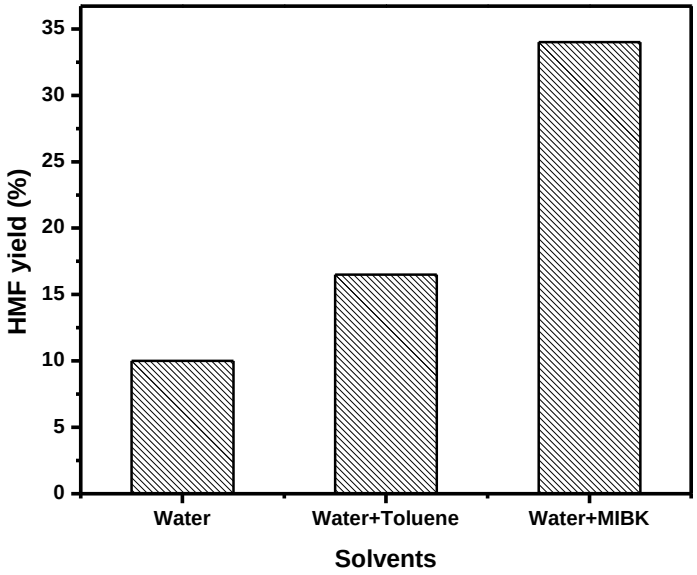

Figure 6.10. Effect of solvent on dehydration of fructose to HMF

(Reaction conditions: fructose: 0.5 g, catalyst: 0.14 g, time, 1 h, temperature: 165 ^{o}C, solvent 30 mL, for biphasic system water: organic solvent ratio = 1:5 *v/v*, 500 RPM)

Another reason for observing higher yield of HMF in water+MIBK biphasic solvent could be that the interaction of MIBK with hydrophobic nature of zeolites. It has been reported that the yield and selectivity of HMF was significantly enhanced in a biphasic water+MIBK solvent for dehydration of fructose to HMF using H/BEA zeolite with a lower acid strength which could be due to the suppression of humins formation by occupying the MIBK solvent in the zeolite pores.[59-61] The literature suggested that hydrophobic nature of zeolites causes adsorption of MIBK (σ= 5.7 Å) in the zeolite cavities resulting in the formation of strong hydrogen bonds between ketone group of MIBK and Brønsted acidic sites of zeolites.[61] As the kinetic diameter of HMF is lower than the maximum pore diameter of H/BEA zeolite, it can easily adsorb on the inner surface of hydrophobic zeolite pore. The MIBK solvent is expected to play a significant role in displacing the HMF produced inside zeolite pore and suppressed the oligomerization of HMF.

6.3.2.2.2 Effect of temperature

The influence of reaction temperature on dehydration of fructose to HMF over micro-mesoporous H/BEA-SBA-15 composite was investigated by varying the temperature between 155-175 °C as shown in Figure 6.11. Under the given reaction conditions, with increasing the reaction temperature from 155 to 165 °C, the HMF yield was increased from 17% to 34%. Moreover, the HMF yield was decreased to 23% with a further increase in the temperature to 175 °C. At the higher temperature of 175 °C, the lower HMF yield could be obtained as a result of the formation of unwanted products due to the side reactions. Further, the dark-colored reaction mixture was observed at a higher temperature which suggests the formation of soluble oligomers / humins. Therefore, 165 °C was considered as the optimum temperature for further reaction parameter study.

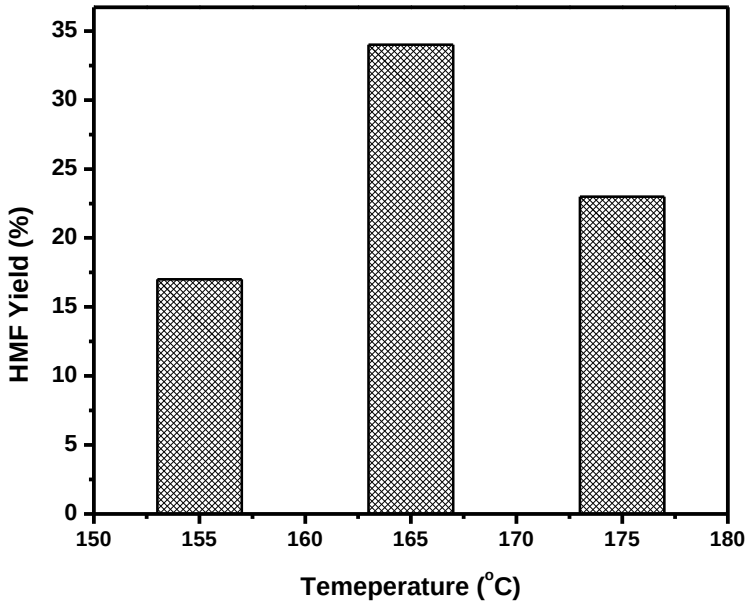

Figure 6.11. Effect of temperature on dehydration of fructose to HMF (Reaction conditions: fructose: 0.5 g, catalyst: 0.14 g, water: MIBK 30 mL (1:5 *v/v*), time: 1 h, 500 RPM)

6.3.2.2.3 Effect of amount of catalyst

The influence of the amount of catalyst was studied for fructose dehydration by varying the amount of catalyst from 0.075 to 0.28 g by keeping the amount of fructose constant (0.5 g in 5 mL water and 25 mL MIBK) and rest of the parameters were also kept constant as shown in Figure 6.12. The HMF yield was increased from 12.5 % to 34 % when the catalyst amount was increased from 0.075 g to 0.14 g after 1 h reaction time. It was observed that a further increase in the amount of catalyst from 0.14 g to 0.28 g, the HMF yield was decreased from 34% to 21%. At higher catalyst loading, the degradation of product/substrate to the humins formation was observed. Therefore, 0.14 g catalyst amount was found to be optimum catalyst loading for the dehydration of fructose to HMF (34%) over micro-mesoporous H/BEA-SBA-15 composite in a biphasic system.

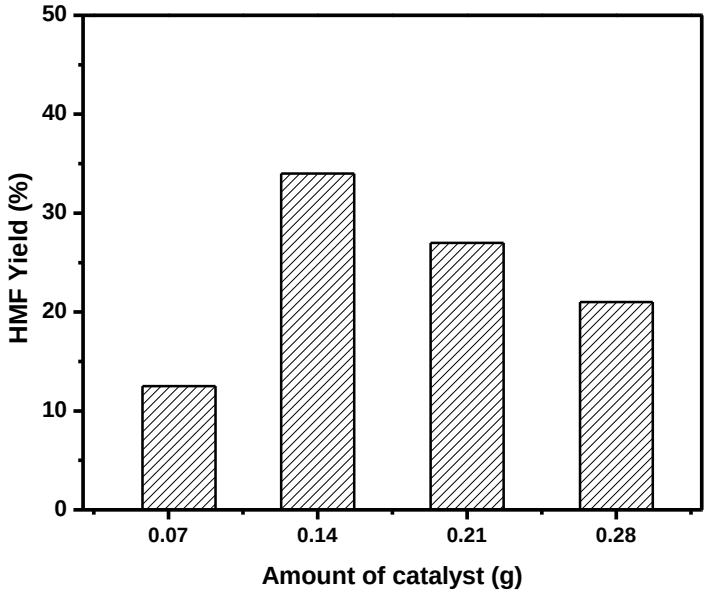

Figure 6.12. Effect of amount of catalyst on dehydration of fructose to HMF (Reaction conditions: fructose: 0.5 g, water: MIBK 30 mL (1:5 *v/v*), time: 1 h, temperature: 165 ^{o}C, 500 RPM)

6.3.2.2.4 Effect of reaction time

Since the micro-mesoporous H/BEA-SBA-15 composite was found to be showing best catalytic activity under given reaction conditions; to further enhance the HMF yield, the influence of the reaction time on the dehydration of fructose to HMF was investigated (Figure 6.13). It was shown that at 30 min of reaction time the higher HMF yield was achieved to 41 % at 165 ^{o}C. It also depicted that with the increase in the reaction time up to 2 h, the HMF yield was decreased to 29 % only. Thus, 30 min reaction time was considered as optimum reaction time for the dehydration of fructose. At shorter reaction time, the contact time of HMF to further acidic sites was lower, therefore side reactions were prevented. In case of longer reaction time, the contact of HMF with the acidic sites increases, which resulted in the formation of humins.

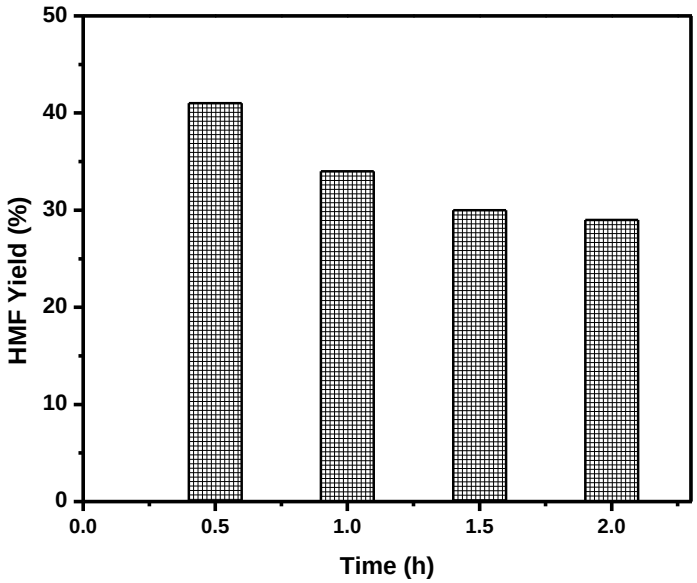

Figure 6.13. Effect of reaction time on dehydration of fructose to HMF (Reaction conditions: fructose: 0.5 g, catalyst: 0.14 g, water: MIBK 30 mL (1:5 *v/v*), temperature: 165 ^{o}C, 500 RPM)

6.3.2.2.5 Effect of stirring speed

In addition, the influence of stirring speed on the HMF yield was also studied by varying the stirring speed from 300 to 900 RPM, and the results are shown in Figure 6.14. Initially, at the stirring speed of 300 RPM, only 25% HMF yield was observed. The lower yield could be observed as a result of the polymerization of the reactants or products in at 165 ^{o}C. The increasing the stirring speed to 500 RPM, the HMF yield was increased to 41%. Further, with an increase in the stirring speed up to 900 RPM, the yield of HMF remains constant.

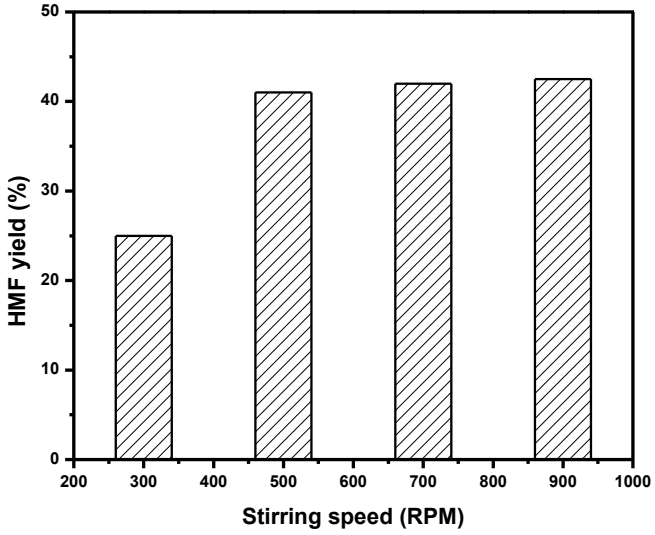

Figure 6.14. Effect of stirring speed on dehydration of fructose to HMF

(Reaction conditions: fructose: 0.5 g, catalyst: 0.14 g, water: MIBK 30 mL (1:5 *v/v*), time: 0.5 h, temperature: 165 ^{o}C,)

6.4 Conclusions

An efficient Brønsted acidic zeolite based micro-mesoporous H/BEA-SBA-15 composite was synthesized by seeding method to elucidate the fructose dehydration to HMF. The correlation between the HMF yields with respect to the molecular dimensions of reactant and products, acidity and porous nature of composite was delineated. It was found that, during the assembly of mesostructure SBA-15, the H/BEA zeolite seeds may assemble on the surface and/or embedded in the wall of the composite of SBA-15. The calcined

micro-mesoporous H/BEA-SBA-15 composite showed narrow pore size distribution in the mesoporous region and the thicker mesopore wall could be attributed to the utilization of zeolite seed used as structural building units for the constructing the walls of mesoporous SBA-15 material. The HR-TEM analysis revealed that composite formed with interconnected micropores of H/BEA with mesoporous channels. The solid acid micro-mesoporous H/BEA-SBA-15 composite was evaluated for dehydration of fructose to HMF yield in a biphasic system. The two-fold higher activity of thermally stable micro-mesoporous H/BEA-SBA-15 composite over H/BEA zeolite could be attributed to 1) accessible Brønsted acidic sites with higher B/L ratio, 2) higher surface area and total pore volume, 3) diffusion of bulky reactant and products from mesopores of SBA-15, and 4) interconnected micropores of H/BEA zeolite seeds embedded in mesopore wall and the mesopores of SBA-15 in biphasic solvent system. The higher TOF value showed the dehydration of fructose to HMF was carried out over Brønsted acidic sites of H/BEA zeolite seeds and passed out through mesoporous SBA-15. The higher yield could also be attributed to the water+MIBK biphasic system, where fructose dehydration occurred in the aqueous phase and rapidly extracted in MIBK solvent. The humins formation with lower HMF yield over H/BEA zeolite could be due to polymerization of HMF over strong acid sites.

6.5 References

1. C. Moreau, R. Durand, C. Pourcheron and S. Razigade, *Industrial Crops and Products*, 1994, **3**, 85-90.
2. C. Moreau, R. Durand, S. Razigade, J. Duhamet, P. Faugeras, P. Rivalier, P. Ros and G. Avignon, *Applied Catalysis A: General*, 1996, **145**, 211-224.
3. Y. Takeuchi, F. Jin, K. Tohji and H. Enomoto, *Journal of Materials Science*, 2008, **43**, 2472-2475.
4. K. Smith, M. D. Ajarim, G. A. El-Hiti, and C. Peters, *Topics in Catalysis*, 2009, **52**, 1696-1700.
5. K. Smith, M. D. Ajarim and G. A. El-Hiti, *Catalysis Letters*, 2010, **134**, 270-278.

6. B. M. Choudary, M. Sateesh, M. Lakshmi Kantam, K. Koteswara Rao, K. V. Ram Prasad, K. V. Raghavan, and J. A. R. P. Sarma, *Chemical Communications*, 2000, DOI: 10.1039/A908011B, 25-26.
7. J. S. Kruger, V. Choudhary, V. Nikolakis and D. G. Vlachos, *ACS Catalysis*, 2013, **3**, 1279-1291.
8. K.-i. Shimizu, R. Uozumi and A. Satsuma, *Catalysis Communications*, 2009, **10**, 1849-1853.
9. K. B. Sidhpuria, A. L. Daniel-da-Silva, T. Trindade and J. A. P. Coutinho, *Green Chemistry*, 2011, **13**, 340-349.
10. H. Li, S. Saravanamurugan, S. Yang and A. Riisager, *Green Chemistry*, 2016, **18**, 726-734.
11. H. Xia, H. Hu, S. Xu, K. Xiao, and S. Zuo, *Biomass and Bioenergy*, 2018, **108**, 426-432.
12. T. D. Swift, H. Nguyen, Z. Erdman, J. S. Kruger, V. Nikolakis and D. G. Vlachos, *Journal of Catalysis*, 2016, **333**, 149-161.
13. M. R. Mercedes, J. M. Ignacio, A. P. L., S. G. José, and M. T. Pedro, *ChemistrySelect*, 2017, **2**, 2444-2451.
14. M. E. Davis, *Nature*, 1993, **364**, 391.
15. C. H. Christensen, K. Johannsen, E. Törnqvist, I. Schmidt, H. Topsøe and C. H. Christensen, *Catalysis Today*, 2007, **128**, 117-122.
16. Y. Wei, T. E. Parmentier, K. P. de Jong, and J. Zecevic, *Chemical Society Reviews*, 2015, **44**, 7234-7261.
17. J. Č. a. S. Mintova, *Catalysis Reviews*, 2007, **49**, 457-509.
18. C. Robin, G. Corine, B. Metin and v. D. Sander, *ChemCatChem*, 2011, **3**, 67-81.
19. L.-H. Chen, X.-Y. Li, J. C. Rooke, Y.-H. Zhang, X.-Y. Yang, Y. Tang, F.-S. Xiao, and B.-L. Su, *Journal of Materials Chemistry*, 2012, **22**, 17381-17403.
20. Y. Han, F.-S. Xiao, S. Wu, Y. Sun, X. Meng, D. Li, S. Lin, F. Deng and X. Ai, *The Journal of Physical Chemistry B*, 2001, **105**, 7963-7966.
21. K. Tarach, K. Góra-Marek, J. Tekla, K. Brylewska, J. Datka, K. Mlekodaj, W. Makowski, M. C. Igualada López, J. Martínez Triguero and F. Rey, *Journal of Catalysis*, 2014, **312**, 46-57.

22. C. R. Patil, P. S. Niphadkar, V. V. Bokade, and P. N. Joshi, *Catalysis Communications*, 2014, **43**, 188-191.
23. Y. Liu and T. J. Pinnavaia, *Journal of Materials Chemistry*, 2002, **12**, 3179-3190.
24. L. Yu, Z. Wenzhong and P. T. J., *Angewandte Chemie International Edition*, 2001, **40**, 1255-1258.
25. Y. Han, S. Wu, Y. Sun, D. Li, F.-S. Xiao, J. Liu and X. Zhang, *Chemistry of Materials*, 2002, **14**, 1144-1148.
26. S. Zeng, J. Blanchard, M. Breysse, Y. Shi, X. Su, H. Nie and D. Li, *Applied Catalysis A: General*, 2006, **298**, 88-93.
27. D. Zhang, A. Duan, Z. Zhao and C. Xu, *Journal of Catalysis*, 2010, **274**, 273-286.
28. P. Du, P. Zheng, S. Song, X. Wang, M. Zhang, K. Chi, C. Xu, A. Duan, and Z. Zhao, *RSC Advances*, 2016, **6**, 1018-1026.
29. S. A. Bagshaw, N. I. Baxter, D. R. M. Brew, C. F. Hosie, N. Yuntong, S. Jaenicke and C. G. Khuan, *Journal of Materials Chemistry*, 2006, **16**, 2235-2244.
30. J. Wang, J. C. Groen, W. Yue, W. Zhou, and M.-O. Coppens, *Journal of Materials Chemistry*, 2008, **18**, 468-474.
31. Y. Xia and R. Mokaya, *Journal of Materials Chemistry*, 2004, **14**, 3427-3435.
32. X. H. Vu, N. Steinfeldt, U. Armbruster and A. Martin, *Microporous and Mesoporous Materials*, 2012, **164**, 120-126.
33. D. Zhang, A. Duan, Z. Zhao, X. Wang, G. Jiang, J. Liu, C. Wang and M. Jin, *Catalysis Today*, 2011, **175**, 477-484.
34. D. Gao, A. Duan, X. Zhang, K. Chi, Z. Zhao, J. Li, Y. Qin, X. Wang and C. Xu, *Journal of Materials Chemistry A*, 2015, **3**, 16501-16512.
35. F.-S. Xiao, Y. Han, Y. Yu, X. Meng, M. Yang and S. Wu, *Journal of the American Chemical Society*, 2002, **124**, 888-889.
36. S. Hu, Z. Zhang, Y. Zhou, B. Han, H. Fan, W. Li, J. Song, and Y. Xie, *Green Chemistry*, 2008, **10**, 1280-1283.
37. K. B. F. M., *Starch - Stärke*, 1990, **42**, 314-321.
38. B. M. Matsagar and P. L. Dhepe, *Catalysis Science & Technology*, 2015, **5**, 531-539.
39. J. N. Chheda, Y. Roman-Leshkov and J. A. Dumesic, *Green Chemistry*, 2007, **9**, 342-350.

40. C. J. Y. Gerentt and Z. Yugen, *ChemSusChem*, 2009, **2**, 731-734.
41. Y. Román-Leshkov, C. J. Barrett, Z. Y. Liu and J. A. Dumesic, *Nature*, 2007, **447**, 982.
42. C. Lansalot-Matras and C. Moreau, *Catalysis Communications*, 2003, **4**, 517-520.
43. B. M. Matsagar, M. K. Munshi, A. A. Kelkar and P. L. Dhepe, *Catalysis Science & Technology*, 2015, **5**, 5086-5090.
44. V. V. Ordomsky, J. van der Schaaf, J. C. Schouten, and T. A. Nijhuis, *Journal of Catalysis*, 2012, **287**, 68-75.
45. M. W. Kasture, P. S. Niphadkar, N. Sharanappa, S. P. Mirajkar, V. V. Bokade, and P. N. Joshi, *Journal of Catalysis*, 2004, **227**, 375-383.
46. P. Bhaumik and P. L. Dhepe, *Catalysis Today*, 2015, **251**, 66-72.
47. X. H. Vu, U. Bentrup, M. Hunger, R. Kraehnert, U. Armbruster and A. Martin, *Journal of Materials Science*, 2014, **49**, 5676-5689.
48. S.-P. Liu, L. Chen, and Y. M. Wang, *Solid State Sciences*, 2010, **12**, 1070-1075.
49. M. Rutkowska, L. Chmielarz, D. Macina, Z. Piwowarska, B. Dudek, A. Adamski, S. Witkowski, Z. Sojka, L. Obalová, C. J. Van Oers, and P. Cool, *Applied Catalysis B: Environmental*, 2014, **146**, 112-122.
50. V. S. P. Ganjala, C. K. P. Neeli, C. V. Pramod, M. Khagga, K. S. R. Rao and D. R. Burri, *Catalysis Communications*, 2014, **49**, 82-86.
51. W. Guo, C. Xiong, L. Huang and Q. Li, *Journal of Materials Chemistry*, 2001, **11**, 1886-1890.
52. J. Dijkmans, D. Gabriels, M. Dusselier, F. de Clippel, P. Vanelderen, K. Houthoofd, A. Malfliet, Y. Pontikes and B. F. Sels, *Green Chemistry*, 2013, **15**, 2777-2785.
53. N. A. S. Ramli and N. A. S. Amin, *Applied Catalysis B: Environmental*, 2015, **163**, 487-498.
54. P. Bräuer, P. L. Ng, O. Situmorang, I. Hitchcock and C. D'Agostino, *RSC Advances*, 2017, **7**, 52604-52613.
55. S. L. Burkett and M. E. Davis, *Chemistry of Materials*, 1995, **7**, 920-928.
56. *http://www.iza-online.org/*.
57. J. Jow, G. L. Rorrer, M. C. Hawley and D. T. A. Lamport, *Biomass*, 1987, **14**, 185-194.
58. S. Ramakanta and D. P. Laxmikant, *ChemSusChem*, 2012, **5**, 751-761.
59. D. Volkan, P. E. A., M. P. C. M. M. and H. E. J. M., *ChemCatChem*, 2011, **3**, 969-972.

60. M. Ohara, A. Takagaki, S. Nishimura and K. Ebitani, *Applied Catalysis A: General*, 2010, **383**, 149-155.

61. S. Dutta, *RSC Advances*, 2012, **2**, 12575-12593.

Chapter 7

Summary and conclusions

Summary and conclusions

Zeolites are the microporous, crystalline, hydrated, aluminosilicates which have a wide range of applications in fields of petroleum, clean energy storage, biomass conversion, etc. However, the zeolite is associated with the diffusion of reactants or products having molecular dimensions greater than the pore dimension of the zeolites are one of the challenging key problems. The accessibility of active sites of zeolites inside the pores and the diffusion problems can be overcome by the synthesis of micro-mesoporosity with combined micro and mesoporosity. Considering this key points, the thesis is aimed at the synthesis of zeolite (K/LTL and H/BEA) based micro-mesoporous composites with interconnected micropores and mesopores in order to enhance the catalytic performance for the valorization of sugars. Different syntheses strategies have applied to target at the enhancement of accessibility of reactants to the active sites of the zeolite, efficient mass transport and improved thermal and hydrothermal stability. It is envisaged that the preparation of compositionally/structurally different zeolite-based micro-mesoporous composites possessing combined advantages of both the mesoporous and the microporous (zeolites) molecular sieves would probably adopt a promising position in the solid catalysts due to their enhanced stability and ideal physico-chemical properties. They are conveniently synthesized by the implementation of the precise method of preparation such as post-synthesis modification and templating.

Considering the context of sustainability and green chemistry, I have focused on the development of new catalytic systems for the efficacious valorization of biomass-derived carbohydrates, sugars into value-added chemicals and provided insight into the interrelated structure-activity correlation. The thesis targeted an understanding to design a synthesis strategy for the application-driven micro-mesoporous composite with the interconnected well-organized micropores and mesopores. The Ph.D. thesis is divided into seven chapters of which chapters 2, 3, 4, 5 and 6 described the actual work carried out during my Ph.D. degree. The significant results and conclusions from each chapter are summarized in the present Chapter.

Chapter 1

Initially, Chapter 1 describes an overview of porous materials involving microporous, mesoporous and micro-mesoporous molecular sieves with regards to properties, structure, and mass transfer properties. It also enumerated that the conventional zeolites have various application in adsorption, separation, and catalysis owing to unique physico-chemical properties. However, the difficulties arise in molecular diffusion and the limited accessibility of the active sites of zeolites due to the pore constrain (< 1.5 nm) could captivate researchers attention in the synthesis of mesoporous materials. Though mesoporous materials resolve the diffusion problem owing to their large pores (2 < d < 50 nm), the lower acidic/basic sites and the hydrothermal stability due to the amorphous nature of the pore wall limit their industrial applications. Therefore, considering the advantages and disadvantages of the microporous/mesoporous materials, a new type of zeolite-based metallosilicates, viz. micro-mesoporous composite with the combined microporosity and mesoporosity has gained importance in the last few decades. It described the several strategies for the synthesis of micro-mesoporous materials and corresponding literature. Moreover, it also explains the brief introduction of renewable lignocellulosic biomass, their classification, composition, and structural features. The prime importance is concentrated on the hydrogenation of sugars to sugar alcohols (xylitol and arabitol) and dehydration of sugars to 5-hydroxymethylfurfural (HMF). The importance of sugar alcohols and HMF, conscious literature review and the advantages and drawbacks of the conventional catalytic system have been thoroughly evaluated.

Chapter 2

Chapter 2 describes the synthesis zeolite (K/LTL and H/BEA) based micro-mesoporous composites, important characterization techniques, and the experimental procedure to check the catalytic performance in the valorization of sugars.

- In the present chapter, mainly two types of micro-mesoporous composites were synthesized viz. 1) Basic micro-mesoporous composites and 2) acidic micro-mesoporous composites

1. Zeolite (K/LTL) based micro-mesoporous composites

   The solid basic micro-mesoporous composites using K/LTL zeolite were mainly synthesized by three synthesis strategies. 1) Post-synthesis modification (alkali

treatment), where effect of molar $Si_{(K/LTL\ zeolite)}/OH^-_{(aq.\ KOH)}$ ratio was studied (destructive strategy), 2) Seeding method, in which K/LTL-MCM-41 composites were synthesized with varying SiO_2/Al_2O_3 ratios (8, 10, 15, 20) by recycling of waste mother liquor (constructive strategy), and 3) Two-step crystallization method implemented for the synthesis of K/LTL-MCM-41 composite (constructive strategy). In the seeding method and two-step crystallization method, a soft template, CTMABr was used as a mesopore directing agent.

2. Zeolite (H/BEA) based micro-mesoporous composites

   The solid acidic zeolite H/BEA based micro-mesoporous composite (H/BEA-SBA-15) was prepared by the seeding method using Pluronic P123 as a soft template (constructive strategy).

3. Noble metal loaded on the γ-Al_2O_3 catalyst

   3.5 *wt%* Pt supported on the γ-Al_2O_3 catalyst was prepared by wet impregnation method.

- The physico-chemical properties of micro-mesoporous composites and the catalyst were assessed by various characterization techniques.
- The experimental setup, analysis of reaction mixtures and the conversion/yield/TOF calculation in the valorization of sugars are demonstrated. The chapter describes two chemical reactions namely, 1) Solid base promoted noble metal catalyzed hydrogenation of sugar to sugar alcohols using Pt/γ-Al_2O_3 catalyst and 2) Brønsted acid catalyzed dehydration of fructose to 5-hydroxymethylfurfural. The analysis of the reaction mixture was carried out by HPLC and GC techniques.

Chapter 3

In Chapter 3, the synthesis of zeolite K/LTL based micro-mesoporous composites by post synthesis modification by varying molar $Si_{(K/LTL\ zeolite)}/OH^-_{(aq.\ KOH)}$ ratio is discussed. It describes the application of micro-mesoporous composites as a solid base in the hydrogenation of xylose to sugar alcohols.

- Solid basic micro-mesoporous composites were synthesized following the post-synthesis modification (destructive strategy) by the treatment of K/LTL zeolite with varying aq. solution of alkali to get different molar $Si_{(K/LTL\ zeolite)}/OH^-_{(aq.\ KOH)}$ ratio (from1.328 to 0.148) at 70 ^oC for 1 h.

- The molar $(Si/Al)_{bulk}$ ratio and surface $(Si/Al)_{surf}$ ratio of the composite was decreased with decrease in the molar $Si_{(K/LTL\ zeolite)}/OH^-_{(aq.\ KOH)}$ ratio. This decrease in the molar Si/Al ratio in zeolite K/LTL based micro-mesoporous composites envisioned preferential extraction of silicon from the K/LTL zeolitic framework with the higher population of sites associated with the Al-species. The removal of silicon from the zeolite framework also confirmed by the FTIR technique as it showed shifting of absorption bands related to symmetric T-O stretching vibrations and double ring vibration to lower wavenumbers with decrease in the molar $Si_{(K/LTL\ zeolite)}/OH^-_{(aq.\ KOH)}$ ratio.
- The post-synthesis modification to K/LTL zeolite showed structural damage with the perceptible decrease in molar $Si_{(K/LTL\ zeolite)}/OH^-_{(aq.\ KOH)}$ ratio. However, the decrease in the % crystallinity was found to depend on the molar $Si_{(K/LTL\ zeolite)}/OH^-_{(aq.\ KOH)}$ ratio as it introduces the substantial mesoporosity on account of the preferential removal of framework (T= Si^{4+} and/or Al^{3+}) atoms from the zeolite crystal domain.
- The porous properties such as BET surface area, mesoporous surface area, mesopore volume, and total pore volume found to increase with a decrease in molar $Si_{(K/LTL\ zeolite)}/OH^-_{(aq.\ KOH)}$ ratio to a certain extent. It concluded the aqueous KOH treatment resulted in the development of secondary pores in the mesoporous region at the expense of micropores of zeolite. Further decline in the $Si_{(K/LTL\ zeolite)}/OH^-_{(aq.\ KOH)}$ ratio causes severe structural damage as indicated by a considerable drop in % relative crystallinity and lowering in the total surface area and pore volume. In conclusion, molar $Si_{(K/LTL\ zeolite)}/OH^-_{(aq.\ KOH)}$ ratio of 0.221 was found to be an optimum ratio for micro-mesoporous composites with improved textural properties without significant loss of pronounced crystallinity was achieved.
- The total basicity of micro-mesoporous composites was increased with the decrease in the molar $Si_{(K/LTL\ zeolite)}/OH^-_{(aq.\ KOH)}$ ratio, which could be associated with the decrease in molar Si/Al ratio and the higher aluminate anion content that are bounded to the potassium ions as charge compensating cations per gram of the sample.
- ^{29}Si MAS-NMR spectra suggested that removal of the silicon atoms from the zeolite framework could be affected by the attack of OH^- ions owing to the negatively

charged AlO^{4-} that prevents the hydrolysis of the Si-O-Al bond. Further, the ^{27}Al MAS-NMR spectra showed the presence of tetrahedrally coordinated aluminium sites (signal at 54.1 ppm), whereas the octahedrally coordinated Al (signal at 0 ppm) was found to be absent

- Further, SEM and TEM images of the micro-mesoporous composites witnessed the destruction of zeolite crystals particularly at the edges of the crystals. This confirmed the formation of intracrystalline mesoporosity in the zeolite crystals due to post-synthesis modification
- The catalytic performance of the synthesized micro-mesoporous composites was tested as a solid base in noble metal catalyzed hydrogenation of xylose to sugar alcohols (xylitol and arabitol) using Pt/γ-Al_2O_3 catalyst. Several reaction parameters were optimized such as temperature, hydrogen pressure, solid base to catalyst ratio and reaction time to achieve the higher sugar alcohols yield. The micro-mesoporous composite with molar $Si_{(K/LTL\ zeolite)}/OH^-_{(aq.\ KOH)}$ ratio of 0.265 was showed higher sugar alcohols yield of 50% with selectivity to sugar alcohols of 79% at 12 h at 60 ^oC.
- The higher catalytic activity in hydrogenation reaction could correspond to the formation of an open-chain form of the sugar molecules alkaline medium by Lobry de Bruyn-Alberda van Ekenstein transformation. These open-chain sugar molecules can easily undergo hydrogenation reaction under milder reaction conditions.
- In summary, the experimental results concluded that the catalytic performance of the zeolite K/LTL based micro-mesoporous composite as solid base was influenced by 1) the basicity of oxygen corresponding to the aluminate ions increased with decrease in molar $Si_{(K/LTL\ zeolite)}/OH^-_{(aq.\ KOH)}$ ratio, 2) the co-existence of micro-mesoporous structure, and 3) the nano-sized platinum on solid support.

Chapter 4

Chapter 4 focused on the synthesis of K/LTL-MCM-41 micro-mesoporous composites varying molar SiO_2/Al_2O_3 ratio utilizing mother liquor by efficient, economical and environmentally compatible route. Literature are available for the synthesis of micro-mesoporous composites involving BEA, MFI, MOR, etc. However, few literatures are available showing the micro-mesoporous materials containing K/LTL zeolite. One of the

reasons could be the difficulties arises in the synthesis of meso-microporous K/LTL molecular sieves with the marrow range of Si/Al ratio and stringent synthesis conditions. Moreover, the synthesis of K/LTL generates a considerable amount of waste which may create the environmental issues. After the completion of the process and the recovery of solid product, a large amount volume liquid filtrate (Mother Liquor, ML) is generated. It consists of unutilized sources and water, that cause adverse environmental effects, and makes the process nonprofitable. Therefore, the utilization of mother liquor containing unutilized precursors for the synthesis of value additional materials is challenging.

- In the present chapter, K/LTL-MCM-41 micro-mesoporous composites were synthesized varying molar SiO_2/Al_2O_3 ratio (8-10) by the utilizing siliceous mother liquor. In this process, the K/LTL zeolites were primarily synthesized by hydrothermal treatments at 170 ^oC for different treatment time and further the siliceous mother liquor was transformed into the mesoporous MCM-41 using cetyltrimethylammonium bromide as a structure directing agent (constructive strategy) at 110 ^oC for 24 h.
- Since the synthesis conditions for K/LTL zeolites with different molar SiO_2/Al_2O_3 ratios and Si-MCM-41 are different, several synthesis parameters such as molar gel composition, crystallization of time (aging time) of K/LTL zeolitic phase and MCM-41 mesophase, and the ratio of water of composite were studied to achieve optimum composites with the interconnected micropores and mesopores. In present work, the optimum crystallization period of 8, 12, 16 and 24 h for K/LTL zeolite phase (molar SiO_2/Al_2O_3 ratio = 8, 10, 5, 20, respectively), and the recrystallization period of 24 h for MCM-41 mesophase were chosen.
- The composites showed the presence of highly ordered 2-D hexagonal symmetry of MCM-41 mesophase irrespective of molar SiO_2/Al_2O_3 ratio. The results also summarized that the orderliness of the mesophase depended on the molar SiO_2/Al_2O_3 ratio and it decreased with decreasing the molar SiO_2/Al_2O_3 ratio.
- The PXRD analysis and the N_2 adsorption-desorption results accounted the following conclusions with decreasing SiO_2/Al_2O_3 molar ratio initial gel: 1) lowering orderliness of mesophase, 2) decreasing the wall thickness of mesopores, and 3) decreasing BET surface area and pore volume.

- 27Al MAS NMR revealed concluded that the acidic conditions (addition of H_2SO_4) during the preparation of MCM-41 did not result in the dealumination of K/LTL zeolite framework and the structure was retained. The basicity of the K/LTL-MCM-41 micro-mesoporous composites related to the aluminate ions of K/LTL zeolites decreased with enhancing SiO_2/Al_2O_3 ratio due to increasing overgrowth of siliceous MCM-41 phase.
- TEM and HR-TEM analysis showed the two-dimensional, well-defined and ordered a hexagonal array of uniform channels corresponding to the mesoporous structure of MCM-41 materials. The absence of K/LTL zeolite crystals in the composites indicating the fully grown K/LTL crystals overlapped with MCM-41 mesophase and the interconnected micro and mesopores.
- The K/LTL-MCM-41 micro-mesoporous composites showed a decrease in hydrothermal stability with decreasing molar SiO_2/Al_2O_3 ratio as a result of decreasing silica content.
- Finally, catalytic performance of K/LTL-MCM-41 micro-mesoporous composites tested as a solid base in hydrogenation of xylose over 3.5 *wt%* Pt/ γ-Al_2O_3 catalysts and higher activity for composite with molar SiO_2/Al_2O_3 ratio = 8 was attributed to the cumulative effect of, 1) the higher basicity of micro-mesoporous K/LTL-MCM-41 composite, 2) the beneficial diffusion of open chain form xylose through the mesopore channels with the accessibility of zeolite active sites, and 3) the presence of nano-sized Pt on Al_2O_3.

Chapter 5

In the present chapter, the influence of methods of preparation of zeolite K/LTL based micro-mesoporous composites was studied 1) as a solid base in the noble metal-supported hydrogenation of xylose to sugar alcohols and 2) as basic catalysts for the transesterification of soybean oil with methanol as model reaction with bulkier reactants and products molecules. For this purpose, three methods for the synthesis of micro-mesoporous composites, 1) post-synthesis modification (8DSK/LTL), 2) seeding method (K/LTL-MCM-41 Seed) and 3) two-step crystallization method (K/LTL-MCM-41 Two-step)

were selected keeping the molar gel composition of $8SiO_2$: $1Al_2O_3$: $3.2K_2O$: $80H_2O$ constant. The dependence of porous properties, interconnected micro-mesopores and the basicity on the methods of preparation are correlated with catalytic activity. The key points of the present chapter are summarized as follows.

- 8DSK/LTL synthesized by post-synthesis modification resulted into a reduction in molar Si/Al ratio with a marginal loss of crystallinity (94%) envisioned minimal extraction of Si atoms or dissolution of occluded amorphous matter. The primary reason for a minimal change in the molar Si/Al ratio could be the higher aluminum content may prevent the preferential silicon extraction against the attack of OH^- ions. Further, K/LTL-MCM-41 Seed and K/LTL-MCM-41 Two-step composites showed ordered 2-D hexagonal symmetry of MCM-41 in composites. However, the variation in the wide-angle PXRD patterns was accompanied by the changes in the structural features of the micro-mesoporous composite mainly depends upon the method of preparation.
- The 8DSK/LTL composite showed higher BET surface area and total pore volume in comparison with parent 8K/LTL as a result of the development of intracrystalline mesoporosity. The surface area and the total pore volume of the micro-mesoporous composites increased in the order as follows: 8K/LTL < 8SK/LTL < K/LTL-MCM-41 Seed < K/LTL-MCM-41 Two step < Si-MCM-41.
- In addition, the basicity trend was also found to depend on the method of preparation following the order of 8DSK/LTL < K/LTL-MCM-41 Seed < K/LTL-MCM-41 Two-step. The higher basicity of 8DSK/LTL could be attributed to the lower Si/Al ratio, whereas the lower basicity of K/LTL-MCM-41 Seed and K/LTL-MCM-41 Two-step could be ascribed to the presence of amorphous materials in the micro-mesoporous composite
- HR-TEM image of 8DSK/LTL micro-mesoporous composite illustrated the structural damage, especially at the edges of zeolite crystal due to alkali post-synthesis modification. It showed clear evidence of formation of intracrystalline mesoporosity. The K/LTL-MCM-41 Seed and K/LTL-MCM-41 Two-step micro-mesoporous composite showed well-defined and ordered channels corresponding

to the mesoporous structure of MCM-41 materials. Moreover, K/LTL-MCM-41 Two-step envisioned that the zeolite nanocrystals were embedded in the mesopore walls of MCM-41 material.

- The hydrothermal stability micro-mesoporous composites were evaluated in boiling water and showing an increasing trend as K/LTL-MCM-41 Seed < 8DSK/LTL < K/LTL-MCM-41 Two-step. The higher hydrothermal stability of K/LTL-MCM-41 Two-step attributed to the fact that zeolite nanocrystals or secondary building units may be embedded into the MCM-41 mesoporous wall. Further, 8DSK/LTL showed a slight lowering in hydrothermal stability may be due to the hydrolysis of the Si-O-Si bond by water. The lowest hydrothermal stability of K/LTL-MCM-41 Seed ascribed to the amorphous wall of MCM-41.
- The overall catalytic activity of zeolite K/LTL based micro-mesoporous composites for a) Hydrogenation of xylose to sugar alcohols, and b) transesterification of soybean oil to biodiesel, mainly depended on, 1) methods of preparation and 2) higher porous properties such as BET surface area, mesopore volume, 3) the accessibility of the basic sites owing to the interconnected micropores and mesopores, and 4) ease of diffusion of the reactants and products to and from the mesopores of micro-mesoporous composites. Among all, the K/LTL zeolite based micro-mesoporous composite prepared by the demetallation and the two-step crystallization showed enhancement in the catalytic activity and found to be the best heterogeneous catalysts for transesterification of biodiesel and the solid base for hydrogenation of xylose.

Chapter 6

In Chapter 6, the zeolite H/BEA based H/BEA-SBA-15 micro-mesoporous composite was evaluated in the Brønsted acid catalyzed dehydration of fructose to 5-hydroxymethylfurfural (HMF) in a biphasic solvent. Herein, the zeolite-based H/BEA-SBA-15 micro-mesoporous composite was successfully synthesized by seeding method using Pluronic P123 triblock copolymer in which pre-crystallized H/BEA zeolite seeds were subsequently assembled during the self-assembly of mesoporous materials as catalytically active sites (constructive strategy). The physico-chemical properties of synthesized composites were characterized by several analytical techniques. The structure-property

correlations between the interconnected micropores and mesopores of H/BEA-SBA-15 and the catalytic performance for the dehydration of fructose to 5-hydroxymethylfurfural in the biphasic system were discussed.

- The H/BEA-SBA-15 micro-mesoporous composite showed the development of a hexagonal array of mesoporous phase (p6mm) of SBA-15. However, as compared to the siliceous SBA-15, the peak intensity of composite in wide angle PXRD was lower indicating H/BEA zeolite may present in the mesopores, on the surface or embedded in the wall of the composite causes structural disordering in the mesophase.
- The H/BEA-SBA-15 composite showed lower BET surface area and total pore volume as a consequence of zeolite assembly inside the mesopores. The lower mesopore size (7.6 nm) and the thicker mesopore wall (4.2 nm) as compared to conventional Si-SBA-15 (3.9 nm) could be attributed to the utilization of zeolite seed used as structural building units for the constructing the walls of the mesoporous material.
- The population of Q4 and Q3 species were found to increase in micro-mesoporous H/BEA-SBA-15 composite, and another resonance peak corresponding to the Q2 species, indicating the interaction between H/BEA zeolite seed and SBA-15 mesophase. In micro-mesoporous H/BEA-SBA-15 composite, tetrahedral and octahedral coordinated Al-species were observed, which envisioning extra-framework aluminium was formed during the synthesis of SBA-15 mesophase under acidic conditions via dealumination of beta zeolite seeds and/or primary building units in the H/BEA zeolite.
- The amount of total acidity of micro-mesoporous H/BEA-SBA-15 composite (0.295 mmol/g) was found to be significantly lower than pristine H/BEA zeolite (0.534 mmol/g), as a result of lowering in the Si/Al ratio and presence of amorphous material used in the formation of SBA-15 mesophase. The IR spectroscopy of adsorbed Pyridine (Pyridine-IR) clearly distinguished the Brønsted and Lewis acid sites indicating that the micro-mesoporous H/BEA-SBA-15 composite has higher Brønsted acidic sites as compared to the H/BEA zeolite.
- The morphology of micro-mesoporous H/BEA-SBA-15 composite did not show the appearance of separate mesoporous and microporous phases as H/BEA zeolite

seeds could be embedded in the pore walls of the SBA-15 structure. Further, TEM and HR-TEM analysis of H/BEA-SBA-15 composite displayed well-ordered 2D hexagonal arrays of mesopores of SBA-15 mesophase and interconnected micropores of H/BEA with mesoporous channels of SBA-15.

- The catalytic performance of micro-mesoporous H/BEA-SBA-15 composite in Brønsted acid catalyzed dehydration of fructose to HMF in a biphasic solvent. Several reaction parameters such as the influence of temperature, time, amount of catalysts, stirring speed and solvents system have investigated. Under optimum conditions, H/BEA-SBA-15 composite showed a 41 % yield of HMF at 165 ^{o}C at 0.5 h, which was many folds higher than parent H/BEA zeolite.
- The overall experimental results and discussion suggested that the catalytic performance for dehydration of fructose to HMF was enhanced over bimodal micro-mesoporous H/BEA-SBA-15 composite as a result of 1) accessible Brønsted acidic sites, 2) higher surface area and total pore volume, 3) diffusion of reactant and products from mesopores of SBA-15, and 4) interconnected micropores of H/BEA zeolite seeds embedded in mesopore wall and the mesopores of SBA-15 in biphasic solvent system.

List of Publications

1. **N.P. Tangale**, P.S. Niphadkar, S.S. Deshpande, P.N. Joshi, "Dehydrogenation of cyclohexanol over Cu/Al_2O_3 catalysts prepared with different precipitating agents", *Applied Catalysis A: General*, 467, 421–429 (2013).

2. P.S. Niphadkar, **N.P. Tangale**, P.N. Joshi, S.V. Awate, "Crystallization kinetics of Sn-MFI molecular sieve formation by dry gel conversion method", *Microporous and Mesoporous Materials*, 182, 73–80 (2013).

3. **N.P. Tangale**, A.A. Belhekar, K.B. Kale, Shobha V. Awate, "Enhanced Mineralization of Gaseous Organic Pollutant by Photo-Oxidation Using Au-Doped TiO_2/MCM-41", *Water Air Soil Pollution*, 225, 1847, 1-13 (2014).

4. **N.P. Tangale**, P.S. Niphadkar, V. Samuel, S.S. Deshpande, P.N. Joshi, S.V. Awate, "Synthesis of Sn-containing anatase (TiO_2) by sol-gel method and their performance in catalytic water splitting under visible light as a function of tin content", *Materials letters*, 171, 50-54, (2016),

5. **N.P. Tangale**, S.K. Sonar, P.S. Niphadkar, P.N. Joshi, "Hierarchical K/LTL zeolites: Synthesis by alkali treatment, characterization and catalytic performance in Knoevenagel condensation reaction", *Journal of Industrial and Engineering Chemistry*, 40, 128-136, (2016).

6. **N.P. Tangale**, P.S. Niphadkar, P.N. Joshi, P.L. Dhepe, "K/LTL-MCM-41 micro-mesoporous composite as solid base for the hydrogenation of sugars", *Catalysis Science & Technology*, 8, 6429-6440, (2018).

7. **N.P. Tangale**, P.S. Niphadkar, P.N. Joshi, P.L. Dhepe, "Hierarchical K/LTL zeolite as solid base for aqueous phase hydrogenation of xylose to xylitol", Microporous & Mesoporous Materials, 278, 70-80, (2019).

8. **N.P. Tangale**, P.S. Niphadkar, P.N. Joshi, P.L. Dhepe, "The dehydration of fructose to 5-hydroxymethylfurfural over micro-mesoporous H/BEA-SBA-15 composite", Manuscript under preparation.

9. **N.P. Tangale**, P.S. Niphadkar, P.N. Joshi, P.L. Dhepe, **"**Synthesis and characterization of zeolite K/LTL based micro-mesoporous composites by post-synthesis modification, seeding method and two-step crystallization method, and their catalytic activity in hydrogenation of xylose to sugar alcohols", Manuscript under preparation.

Contributions to Symposia and Conferences

- Best poster award: Entitled “Hierarchical K/LTL zeolite as solid base for aqueous phase hydrogenation of xylose to xylitol” National Science Day 2018 Celebration” held at CSIR-National Chemical Laboratory, India (2018).
- Poster presented entitled “Hierarchical K/LTL zeolite as solid base for aqueous phase hydrogenation of xylose to xylitol” during 23rd national symposium on catalysis (CATSYMP-23) held at Bengaluru, India (2018).
- Poster presented entitled “Synthesis characterization and catalytic activity of rice husk derived porous silica and carbon for hydrogenation of sugar to sugar alcohols” National Science Day 2018 Celebration” held at CSIR-National Chemical Laboratory, India (2017).
- Poster presented entitled A synergetic effect of Lewis and Brønsted acidity on the “One-Pot” synthesis of 5-hydroxymethylfurfural from glucose in biphasic system National Science Day 2016 Celebration” held at CSIR-National Chemical Laboratory, India (2016).
- Poster presented entitled “An assessment of post-synthesis modification strategy towards the synthesis of bimodal micro-mesoporous K/LTL zeolites” National Science Day 2018 Celebration” held at CSIR-National Chemical Laboratory, India (2015).
- Poster presented entitled “Molecular sieves” Foundation day Celebration” held at CSIR-National Chemical Laboratory, India (2015).
- Attending conference on "Sustainable Catalytic Technologies" organized at CSIR-National Chemical Laboratory, India (2017).
- Attending the 2nd international symposium on ionic liquids entitled “Ionic liquids-Alternative benign materials for renewable energy and its applications” held at National chemical laboratory, Pune, India (2013).

Notes

Notes

Notes

Notes

Notes